Phenanthracene Nanotubes for Template-designed Organic Electronics

Dissertation

zur

Erlangung des Doktorgrades (Dr. rer. nat.)

der

Mathematisch-Naturwissenschaftlichen Fakultät

der

Rheinischen Friedrich-Wilhelms-Universität Bonn

vorgelegt von

Simon Christian Rickert

aus Bonn

Bonn, 2024

Angefertigt mit Genehmigung der Mathematisch-Naturwissenschaftlichen Fakultät der Rheinischen Friedrich-Wilhelms-Universität Bonn

1. Gutachter/Betreuer: Prof. Dr. Sigurd Höger

2. Gutachter: Prof. Dr. Andreas Gansäuer

Tag der Promotion: 14.06.24

Erscheinungsjahr: 2024

Die vorliegende Arbeit wurde am Kekulé-Institut für Organische Chemie und Biochemie der Rheinischen Friedrich-Wilhelms-Universität Bonn in der Zeit von November 2020 bis März 2024 unter der Leitung von Prof. Dr. Sigurd Höger angefertigt.

“Research is for nations and mankind, not for researchers themselves.”

Ryōji Noyori

Danksagung

Zuallererst möchte ich mich bei Herrn Prof. Dr. Sigurd Höger für die freundlicher Aufnahme in den Arbeitskreis, das mir entgegengebrachte Vertrauen und die Vergabe des interessanten Themas bedanken. Besonders die Unterstützung und Freiheit in den Entscheidungen im Rahmen der Forschung und die Ermöglichung einiger Reisen zu Konferenzen weiß ich sehr zu schätzen.

Herrn Prof. Dr. Andreas Gansäuer danke ich für die Übernahme des Zweitgutachtens und die Betreuung und das Feedback als Mentor im Rahmen der BIGS-Chemistry. Ich danke außerdem Herrn Prof. Dr. Stefan Grimme und Herrn Prof. Dr. Lukas Schreiber für die Teilnahme an der Prüfungskommission.

Herrn Prof. Dr. Grimme und Dr. Andreas Hansen danke ich des Weiteren für die Betreuung als Mentoren im Rahmen des TIDE-Graduiertenkollegs. Julia Kohn danke ich hierbei für die Organisation meiner *lab rotation* im AK Grimme, sowie die Unterstützung mit quantenchemischen Rechnungen.

Generell danke ich allen Beteiligten im TIDE-Graduiertenkolleg für die Ermöglichung vieler interessanter Kollaborationen, Retreats, und Workshops. Insbesondere möchte ich mich für die finanzielle Unterstützung für meinen Forschungsaufenthalt in den USA bedanken. Dort bedanke ich mich bei Herrn Prof. Dr. Timothy M. Swager für die sehr herzliche Aufnahme in seine Gruppe und dem Team dort für die kollegiale Atmosphäre. Besonders nennen möchte ich hierbei Jessica Beard und Lennon Shao-Xiong Luo, auch für das Mentoring bei den Sensor-Messungen.

Ich danke allen Mitarbeiterinnen und Mitarbeitern der zentralen Einrichtungen der chemischen Institute, die die Forschung erst ermöglichen. Hierbei danke ich besonders Frau Dr. Engeser für die zahlreichen Sondermessungen im Bereich der Massenspektrometrie. Ulrike Blank und Dr. Gabriele Richardt danke ich für sämtliche organisatorische Unterstützung vor allem bezüglich meines Forschungsaufenthalts und dem damit verbundenen Versand der Moleküle in die USA.

Herrn Prof. Dr. Lupton danke ich für die photophysikalischen Messungen an meinen Molekülen in seiner Gruppe.

Ich danke dem AK um Dr. Stevan-Sven Jester für die STM-Aufnahmen. Vorallem danke ich Joshua Bahr für die viele Messzeit um die anspruchsvollen Moleküle abbilden zu können.

Tristan J. Keller, danke ich für das Interesse an meiner Arbeit und für seine Einblicke in das TIDE-Graduiertenkolleg, ohne die ich mich nie dafür beworben hätte und damit ein Großteil meiner Forschung so nicht möglich gewesen wäre.

Allen aktuellen und ehemaligen Mitarbeiterinnen und Mitarbeitern im AK Höger danke ich für die entspannte Atmosphäre und die schöne Zeit, egal ob beim Kickern, Grillen, Spieleabenden, Karnevalspartys oder einem Pubquiz. Vorallem auch an die Konferenzen, wie die KOPO oder die ISMSC in Island denke ich gerne zurück. Ich danke auch meinen Laborkolleginnen Christin Henschke, Martha Trubel und Johanna Maria Wollenweber für die gemeinsame Zeit, die stets gute Stimmung und den eher entspannten Musikgeschmack im Labor, sowie die immer erfrischend andere Polymersicht bei aufkommenden synthetischen Problemen. Lucas Rothe danke ich für die Einführung in die MPLC um schwierige Trennprobleme zu lösen, so wie den interessanten Austausch über synthetische Fragestellungen, aber auch XRD und Rechnungen.

Philipp Krämer, ohne den ich wohl heute noch auf meine Filtrationen mit Papierfiltern warten würde, danke ich für das sorgfältige Korrekturlesen dieser Arbeit und die hilfreichen Verbesserungsvorschläge, sowie die humorvolle Zeit im Labor neben der Synthese.

Zu guter Letzt möchte ich meiner Familie und Freunden danken, die mich immer auf verschiedenste Art und Weise auf meinem Weg unterstützt haben und mich in wenig erfolgversprechenden Phasen der Arbeit immer davon auf das Leben außerhalb des Labors ablenken konnten.

Ganz Besonders danke ich meinen Eltern für die langjährige Unterstützung in jeglicher Hinsicht, die mir die Freiheit gegeben hat, mein Studium und die Promotion bis hierhin befreit von anderen Sorgen abschließen zu können.

Abbreviations

δ	chemical shift (NMR)
λ	(electromagnetic) wavelength
2D	two-dimensional
3D	three-dimensional
AcOH	acetic acid
APCI (MS)	atmosphere pressure chemical ionization
aq.	aqueous
Au(111)	gold surface material used for STM
bs	broad singlet (NMR)
CH	cyclohexane
conc.	concentrated
CPDMS-	(3-cyanopropyl)dimethylsilyl-
d	doublet (NMR)
Da	*Dalton* (unified atomic mass unit)
DCM	dichloromethane
dd	doublet of doublets (NMR)
ddt	doublet of doublet triplets (NMR)
DFT	density-functional theory
DIPA	diisopropylamine
DMF	dimethylformamide
DOSY	diffusion ordered spectroscopy (NMR)
dt	doublet of triplets (NMR)
EI (MS)	electron ionization
eq.	equivalents
ESI (MS)	electrospray ionization
et al.	et alii (latin; “and others”)
EtOH	ethanol
EtMgBr	ethylmagensium bromide
Et_2O	diethyl ether
FET	field effect transistor

GFET	graphene field effect transistor
GPC	gel permeation chromatography
recGPC	recycling gel permeation chromatography
h	hour(s)
HOMO	highest occupied molecular orbital
HOPG	highly oriented pyrolytic graphite
J	coupling constant (NMR)
LOD	limit of detection
LUMO	lowest unoccupied molecular orbital
M or M	molarity in mol/l
M	molecule (mass spectrometry)
m	multiplet (NMR)
MALDI (MS)	matrix-assisted laser desorption/ionization
min	minute(s)
MS	mass spectrometry
m/z	mass-to-charge ratio in Dalton (MS)
NBS	*N*-bromosuccinimide
NIS	*N*-iodosuccinimide
NMR	nuclear magnetic resonance
norm.	normalized
o-DCB	*ortho*-dichlorobenzene
OLED	organic light emitting diode
OSC	organic solar cell
P3HT	poly(3-hexylthiophene)
PCBM	phenyl-C61-butyric acid methyl ester
PNT	phenanthracene nanotube
ppb	parts per billion
ppm	parts per million
p-SWCNT	pristine single-walled carbon nanotube
QCMB	quartz crystal microbalance
R_f	retardation factor (TLC)
r.t.	room temperature

s	singlet (NMR)
SPM	shape-persistent macrocycle
STM	scanning tunnelling microscopy
SWCNT	single-walled carbon nanotubes
t	triplet (NMR)
TBAF	tetrabutylammonium fluoride
TCB	1,2,4-trichlorobenzene
THF	tetrahydrofuran
TIPS-	triisopropylsilyl-
TLC	thin-layer chromatography
TMS-	trimethylsilyl-
TNT	2,4,6-trinitrotoluene
TOF (MS)	time-of-flight
Tol	toluene
UV	ultraviolet electromagnetic radiation
UV/Vis	ultraviolet and visible electromagnetic radiation
VOC	volatile organic compound
XPhos	Dicyclohexyl[2′,4′,6′-tris(propan-2-yl)[1,1′-biphenyl]-2-yl]phosphane

Contents

1. Abstract

The overall increasing energy consumption worldwide demands for new fundamental research that can contribute to mitigate its negative ecological effects. One such valuable field of research is the area of organic electronics. Materials used in organic electronics offer a variety of advantages over established inorganic materials, such as easy solution processability, but also low power-consumption and flexibility of the resulting devices. However, to this date the efficiency of such devices is also lower than that of their inorganic counterparts. One prominent approach to overcome this challenge is to use supramolecular self-assembly of the active materials on a template to generate ordered structures, mimicking those in crystalline silicon-based devices, e.g. solar cells, to increase the efficiency of the resulting devices while retaining the intrinsic advantages of organic materials.

This work in particular focuses on the synthesis and fundamental investigation of materials relevant for such applications. A new class of materials, i.e. the phenanthracene nanotubes (short: PNTs) are presented and it is demonstrated how a reliable bottom-up approach towards these molecules was realised. For this the established synthetic approaches towards shape-persistent macrocycles and the synthesis of H-shaped molecules for ladder-polymers were combined. The modularity of this method was then used to obtain PNTs of different shapes (cylindrical, pyramidal and bowl-shape). After the successful synthesis of these compounds, they were investigated regarding the formation of self-assembled monolayers on a carbon-based substrate (highly oriented pyrolytic graphite) using scanning tunnelling microscopy. Together with quantum chemical models it was shown that the cylindrical PNTs are less rigid than their molecular formulae suggest and can collapse into a more compressed form. The flexibility in shape of the cylindrical PNTs was then utilized to demonstrate the potential of PNTs in the field of template-designed organic electronics by manufacturing a single-walled carbon nanotube chemiresistor (i.e. a sensing device). This sensor performed well for explosive detection (i.e. 2-nitrotoluene as marker for 2,4,6-trinitrotoluene) in terms of selectivity, stability, and humidity tolerance. In this way a low-power consumption device that is portable and can also be used for large area monitoring was made, displaying the advantages of organic electronics compared to the here usually used stationary and energy-intensive gas chromatographs. Moreover, regarding its sensitivity the limit of

detection lies at 11 ppb, which is among the best results for single-walled carbon nanotube chemiresistors obtained to this date.

2. Introduction

Over the last decades it was clearly observable that the world-wide energy consumption is sharply rising. Moreover, global electricity consumption as an energy subgroup is increasing at an even higher rate (cp. Figure 1a).[1] Setting this into the context of challenges arising from climate change and developing countries aiming at raising the standard of living for their population concurrently, it becomes apparent that the rate of electricity consumption will rise even faster in the near future. However, since the discovery and development of conductive polymers in the early 1970s,[2] for which the *Nobel* prize in chemistry was awarded to *A. Heeger*, *A. MacDiarmid*, and *H. Shirakawa*, the use of organic materials to provide solutions for the challenges stated above became a highly investigated topic of research and the emerging field of organic electronics is today not only of interest for research purposes, but already a growing market (Figure 1b). Displays in consumer products and chemiresistive sensors for industry applications being only two representatives, showing the versatility of products made available by the use of organic materials with distinct optoelectronic properties.[3] The growth of this market is based on the many advantages organic materials provide in electronic applications over their inorganic counterparts, such as easy processability using low-cost techniques, scalability, as well as facilitating the manufacturing of devices, which are lightweight and have a lower energy consumption compared to similar devices utilizing inorganic materials.[4]

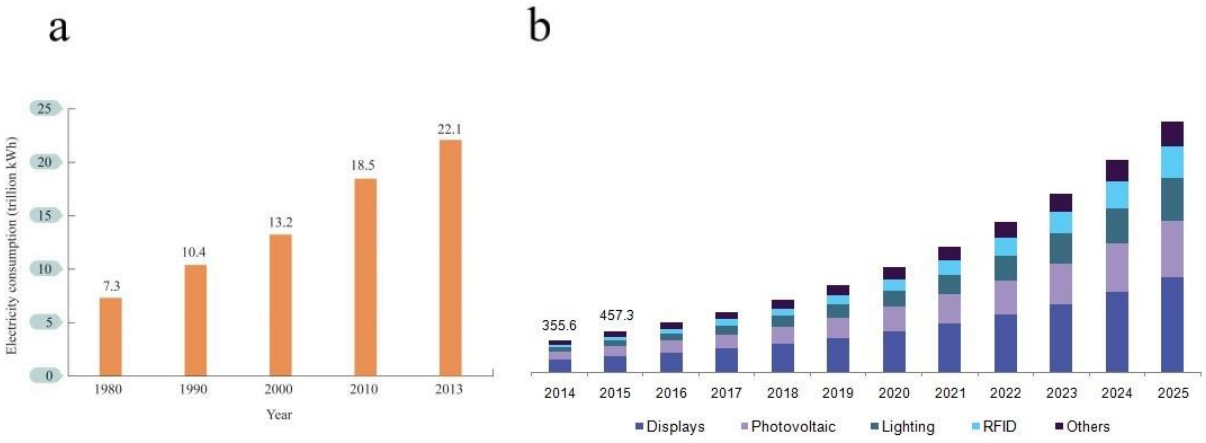

Figure 1: a) Annual global electric energy consumption in million kWh; b) China's annual market revenue (and prognosis) of printable organic electronics by device in million USD.[3,4]

Whilst applications in organic light emitting diode (short: OLED) displays are already realized, there are still limitations in the practical use of organic materials for example as active layers in organic solar cells (short: OSCs), owing to their degradability by UV-radiation, or low performance due to non-radiative voltage losses.[5] The research conducted in this work is embedded in the *Research Training Group 2591* by the German research foundation *DFG*, which focusses on the investigation of the influence of templates to order organic molecules via self-assembly, thus imitating the ordered crystalline structure of inorganic materials in electronic applications, e.g. silicon-wafers in solar cells. Within this research framework it is studied to what extent this approach can contribute to an increase in performance of organic materials in such applications, while retaining their intrinsic properties like flexibility and facile processability.

This work specifically focuses on phenanthracene nanotubes (short: PNTs), i.e. 3D-structures on the nanometre scale containing a cavity and having an aromatic phenanthracene backbone incorporated into their structure. The relevance of this research shall be shown in the following by introducing organic solar cells (short: OSCs) and chemiresistive sensors as two very different electronic applications, describing how the molecules synthesized in this work can contribute to improve the performance of such devices. Furthermore, scanning tunnelling microscopy (short: STM) will be introduced as a powerful tool to investigate the formation of self-assembled monolayers on templating surfaces, which will be a relevant analytical part of this work. In addition, synthetic pathways towards shape-persistent macrocycles (short: SPMs) will be presented, as they are an integral part of the PNT synthesis.

3. Organic Electronics

3.1 Silicon-based Solar Cells

Since the sun is the largest continuous source of energy in our solar system, it is no surprise that harnessing its energy for the generation of electricity is a prominent field of research in the wake of an ever growing need for electrical energy over the last decades.[1] The first steps towards the development of solar cells were taken in 1883 with the development of the first photovoltaic cell by *C. E. Fritts* consisting of selenium on a thin layer of gold and giving an efficiency, i.e. the fraction of energy in form of sunlight that is actually converted into electricity, below 1%.[6] Then, after *Einstein* was able to explain the photoelectric effect on a quantum basis and nearly a century of further research on this topic, the first practical solar cell was developed in the *Bell laboratories* in 1954. It was a silicon *p-n* junction photocell with an efficiency of 6%.[7] Recently, efficiencies as high as 47% could be achieved with a multi-junction solar cell.[8] An overview on the basic types of silicon-solar cells available today shall be given in the following.

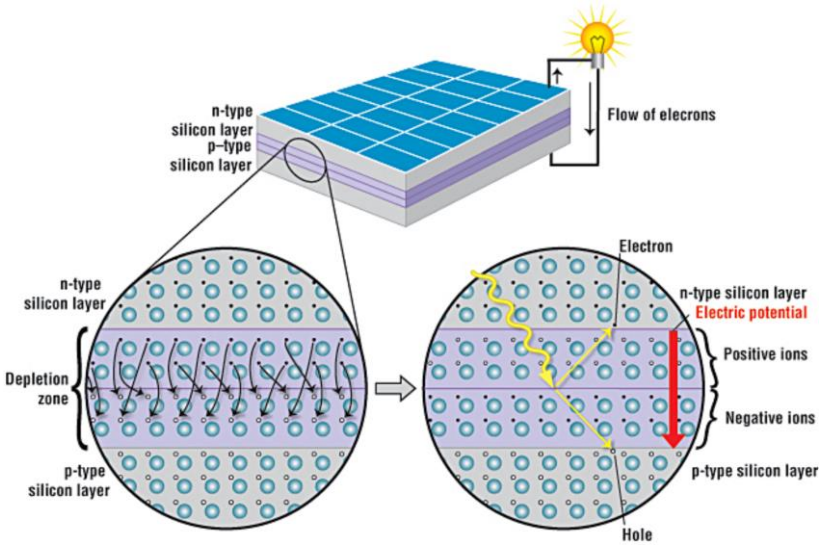

Figure 2: Schematic representation of a *p-n* junction solar cell with a close-up view on the depletion zone.[9]

Regarding the general composition, a simple solar cell consists of a bottom electrode, followed by a *p*-type (hole-conductor) and a *n*-type (electron-conductor) silicon layer and a transparent top electrode, which allows for transition of the sunlight. Depending on the morphology of the silicon layers one can differentiate three distinct types of solar cells namely monocrystalline, polycrystalline, or amorphous. While monocrystalline solar cells

have the highest efficiency, they need precise and high temperature manufacturing processes which are costly. This can be mitigated by mixing smaller crystals in a polycrystalline solar cell which, however, comes at the cost of lower efficiency. Amorphous solar cells can be produced by coating low-cost polymers without the need of high temperature, but only yield efficiencies of 6-9%.[10]

However, the overall mechanism of electricity generation for these distinct types of solar cells is the same. The *p*-type silicon layer is generated by doping with electron-deficient atoms like boron or gallium leading to the generation of electron holes (i.e. the absence of an electron at a position where one could exist in an atomic lattice) in the layer, whereas the *n*-type silicon layer is doped with phosphorus or arsenic and thus leading to mobile electrons. At the junction of both silicon layers electrons and holes can combine. This generates an electrical field due to the residual positive ions in the *n*-type layer and negative ions in the *p*-type layer respectively. Hence, a depletion region around the *p*-*n* junction is formed and charge transfer through the junction is hindered (cp. Figure 2). When light shines on the device and if the energy of the incident photons is larger than the band-gap of the semiconducting layers, electrons are excited from the valence band into the conduction band and form approximately free electron-hole-pairs. Due to the continuous nature of the energy band levels, which in addition are only bound by weak *Coulomb*-interactions,[11] these can then separate by two main motions. One is diffusion from zones with high charge carrier concentration to zones with lower concentration. The other is drift of carriers, due to the electrical field induced by the depletion region. Both these forces can oppose each other, and their influence is different depending on which region of the solar cell is considered. This can be understood easiest when imagining the generation of an electron-hole-pair in the depletion region. Here the electric field is very strong compared to the gradient of charge carrier concentration and thus the electron will be pushed to the *n*-type silicon layer and the hole to the *p*-type silicon layer, separating the electron-hole-pair. Thereby, a voltage is generated and connection of the electrodes of the solar cell to an electrical circuit leads to the flow of a current.

Additionally, photons hitting the surface of the solar cell can either be reflected or pass through without any effect. The energy loss by reflection can be lowered using anti-reflective coatings.[12] Moreover, transmission can be reduced by adding a layer for up-conversion of photons with a lower energy than the band gap.[13] Conversely, layers for down-conversions can be added to reduce the amount of thermal energy generated by high-energy photons via

non-radiative recombination and hence, increase the efficiency of the solar cell, which is dependent on the temperature and also by increasing the amount of photons from the spectrum of light emitted by the sun, which can be utilized for the generation of an electrical current in the solar cell.[14,15]

In recent years further advances have been made leading to the so-called “third generation of solar cells” including the use of nanocrystals or perovskites in the active semiconducting layer. While this has led to the possibility of manufacturing solar cells at lower prices and still retaining a relatively high efficiency, the general challenges of solution processability and manufacturing of lightweight and flexible devices to provide cost-effective energy remain.[10,11,15]

3.2 Organic Solar Cells

Compared to established silicon-based solar cells organic solar cells (short: OSCs) have intrinsic advantages, such as mechanical flexibility and easy processing techniques, including printing, spin-coating and spray deposition, which leads to the possibility of manufacturing devices at a high efficiency per unit cost ratio. This can lead to relevant new applications like semi-transparent solar cells in windows or polymer-based flexible OSCs that can be coated on various available surfaces to enable low-cost electricity generation.[11,16] But, OSCs also suffer from easy degradability, due to structural changes to the morphology of the donor molecules over time and diffusion of water and oxygen into the device, which is problematic for the air and moisture sensitive organic materials.[5,17] Furthermore, they generally have a lower efficiency than their silicon-based counterparts. This is mainly rooted in the different mechanism of current generation in OSCs, which shall be discussed in the following.

As depicted below, the composition of an OSC resembles that of a silicon-based solar cell with the main difference being, that the active layer consists of electron-donors and -acceptors in the form of either small molecules or polymers, instead of doped semiconductors. The electron-hole pairs generated in the donor-molecules upon exposure of the OSC to light are tightly-bound by *Coulomb*-interactions, unlike those in their silicon-based counterparts.[11] These so-called “excitons” can then be separated via charge-transfer at a donor/acceptor-interface. The donor highest occupied molecular orbital (short: HOMO) and lowest unoccupied molecular orbital (short: LUMO) are higher in energy than those of the

acceptor. Therefore, the electron which is photo-excited to the LUMO of the donor can be transferred to the LUMO of the acceptor, whereas the hole cannot be transferred to the HOMO of the acceptor being lower in energy than that of the donor (cp. Figure 3c). This way, dissociation of the exciton is achieved, leading to holes and electrons diffusing to the anode and cathode respectively, generating a voltage.[11,18]

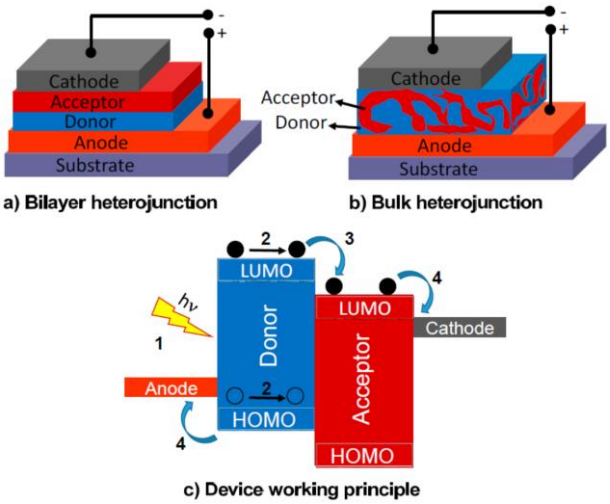

Figure 3: Device structures and working principle of organic solar cells electrons and holes depicted as full spheres and empty spheres, respectively.[18]

The traditional approach to manufacturing an OSC is the bilayer heterojunction device with a separated donor and acceptor layer similar to the *p*- and *n*-type layers in silicon-based solar cells. However, since the excitons in OSCs are tightly-bound their diffusion length before recombination is much smaller (on the order of nanometres compared to micrometres for the silicon-based analogues).[11] Hence, even though improvements regarding the efficiency are possible by tuning the electronic properties of the donor and acceptor to gain a larger energy difference between their LUMOs, and improving the crystal structure by thermal annealing after deposition on the substrate, the device architecture is limited to thin films of the active layers.[11] Another approach, is the bulk heterojunction device, where donor and acceptor are forming a blend in solution and phase-separate after being applied on the surface of the device. Employing this approach, nanojunctions are introduced in the active layer, which increase the probability of an exciton being able to diffuse to a donor/acceptor-interface and dissociate there before recombining, even for active layers thicker than the diffusion length of the exciton.[11,19] This concept to improve the efficiency of OSCs can be utilized for donors and acceptors comprising polymers and small molecules alike.

Further developments include the introduction of electron- and hole-blocking layers between the active layer and the respective electrode to prevent elements from the electrode to diffuse into the active layer, which would lead to increasing device degradation.[11,17] Concerning the organic donor- and acceptor-molecules used for the active layer of the OSCs, some commonly used solution processable donors and acceptors are depicted below.

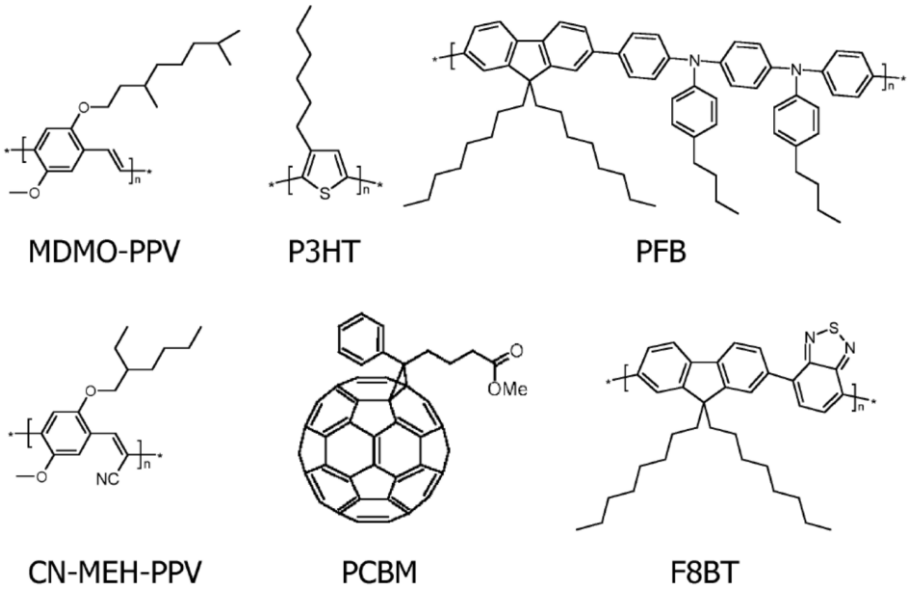

Figure 4: Illustration of commonly used donor- and acceptor-materials (first- and second-row) in OSCs.[19]

Their solution processability is ensured by the alkyl-side chains increasing the solubility of the compounds. Additionally, the active layer for the OSC can be generated by formation of a blend or by block-copolymerisation of donors and acceptors, leading to the desired structure-motif with nanojunctions between donor and acceptor moieties. Since the exciton diffusion length in the organic active layer is short, the efficiency of the OSC largely depends on the nanoscale morphology of the active layer and small changes in the structure of donor or acceptor can have a large effect. It is obvious that different compositions of donor/acceptor block-copolymers would lead to different morphologies after microphase separation of the different blocks, due to different volume fractions. However, even the regioregularity of a polymer, i.e. if each repeating unit is derived from the same isomer of the monomer, can have a significant influence on the morphology of the active layer. This was investigated for the poly(3-hexylthiophene) (short: P3HT) and phenyl-C61-butyric acid methyl ester (short: PCBM) (cp. Figure 4) donor/acceptor system, showing that increased regioregularity of the P3HT leads to an increase in OSC efficiency.[20] Implementing these and further

improvements in the OSC device architectures led to the optimization of their efficiency from 0.001% in 1975 to 18% reached in 2021.[11,21]

Recent advances in this field of research employ a supramolecular approach to generate desired morphologies in the active layer of OSCs using self-assembly of small donor- and acceptor-molecules via different non-covalent interactions like π-π-stacking, as was shown for hexabenzocoronene and perylenediimide.[22] Further examples are squaraine dyes or fused ring electron acceptors.[23] It can be observed that the use of self-assembly to obtain tubular structures of donors and acceptors which are segregated and have a defined distance to each other, is a promising approach to improve the efficiency of OSCs. Here, the morphology of the active layer is controlled by carefully designed donor- and acceptor-molecules suitable for self-assembly. Therefore, it is important to perform further studies in this area. This work will focus on the self-assembly of PNTs at the solid-liquid interface on highly oriented pyrolytic graphite (short: HOPG) as suitable template, investigating the template directed formation of monolayers via scanning tunnelling microscopy (short: STM). Moreover, co-adsorption of these molecules serving as donor-hosts for acceptor molecules like PCBM, will be attempted to generate ordered structures with defined donor/acceptor distances. Additionally, stacking of the tubular structures shall be studied, to gain information on how far the HOPG template exerts an influence on the self-assembly, i.e. expanding the concept from monolayers of the tubular structures to bilayers and further. The basic insights gained from this research can contribute to enhance molecular design of donors and acceptors to improve the efficiency of OSCs via good control over the morphology of the active layer through template-assisted self-assembly.

3.3 Chemiresistive Sensors

Another application in organic electronics, apart from the mechanistically very similar organic solar cells and their organic light-emitting diode counterparts, for which the PNTs investigated in this work can be used, are chemiresistive sensors. The first chemiresistors have been in commercial use since the 1970s, with a prominent example being the carbon monoxide sensor.[24] In the following decades further chemiresistors were developed for other toxic gases such as nitrogen oxide, nitrogen dioxide and hydrogen sulfide.[24] However, the improvement of selectivity of these sensors has limits based on the mechanism by which they

function. Generally, a metal oxide film as semiconducting material is placed in a gap between two electrodes. Moreover, the surface of the metal oxide is saturated with oxygen under ambient conditions, which extracts electrons from the surface, leading to the formation of a depletion region (cp. 3.1 Silicon-based Solar Cells). This, in turn, lowers the conductivity of the metal-oxide film. Upon exposure to a reducing gas, the oxygen on the surface of the metal oxide is reduced, decreasing the area of the depletion region and increasing the conductivity, which can be detected as an electrical response towards the analyte, i.e. the reducing gas. A variety of metal oxides have been used to manufacture such chemiresistors and tune their selectivity towards toxic gases, that are desired to be detected.[24]

More recently, networks of single-walled carbon nanotubes (short: SWCNTs) have been employed as semiconductors, instead of metal oxides. This is due to several factors. On the one hand, the increasing availability of SWCNTs with satisfactory consistent properties, like chirality or polydispersity.[25] On the other hand, they may offer the same advantages that OSCs have over their silicon-based counterparts, as enabling the production of low-cost, lightweight and flexible devices by the use of polymer substrates and solution processes, e.g. drop casting or spin-coating.[26] This has led to applications like hazard badges in clothing for work environments, where one might get exposed to toxic substances.[27] Furthermore, the ability to increase the sensitivity of SWCNT chemiresistors is enhanced, compared to the use of metal oxides, which emerges from their different mechanism of interaction to analytes. Since the SWCNTs are *p*-type materials by doping with the abundant oxygen under ambient conditions, and thus hole-conductors (cp. 3.1 Silicon-based Solar Cells), no depletion region is formed at the surface. They interact with detectable analytes directly and, unlike metal oxides, are not reliant on the interaction of reducing agents with ambient oxygen on their surface for a signal response via increased conductivity. This also broadens the scope of discernible substances to any compound, which might either be *n*- or *p*-doping, i.e. electron-donating or -withdrawing, and hence would either decrease or further increase the hole-conducting properties of the SWCNTs.[25] This leads to an increase or decrease in resistivity when detecting *n*- or *p*-doping analytes respectively, which can be measured. The advantage of SWCNT-based chemiresistors is reflected in the infinite possibilities of modulation of the pristine SWCNTs via covalent modification and non-covalent interactions to gain sensors, which are highly selective and sensitive to a specific analyte. This ranges from covalent modification of SWCNTs with pyridinol to sense HCl-gas, to the detection of

the carcinogenic ethyl acrylate via the change in oxidation state of palladium in an oxidative *Heck*-coupling at the SWCNT surface.[28]

Moreover, for cases where a high specificity is difficult to attain, due to chemical similarity, e.g. benzene and toluene, it is possible to manufacture sensor arrays.[25] These consist of multiple sensors with differently modified SWCNTs and can identify such similar analytes not by one absolute signal response, but via a "fingerprint recognition", based on different affinities of each sensor of the array towards the similar analytes in question.

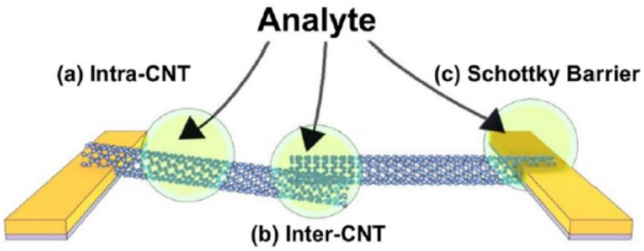

Figure 5: Illustration of a CNT-based chemiresistor and its sensing mechanisms: a) at the CNT surface (intra-CNT); b) at the interface of two CNTs (inter-CNT); c) at the CNT electrode interface (*Schottky*-barrier).[25]

Additionally, the interface between SWCNT and electrode and between two SWCNTs have also shown to have a significant influence on the electronic properties of the device and thus can be used as a way of detection for suitable analytes.[25] The latter can be used directly when adding polymers that can swell upon selective interaction with an analyte and thus weaken the inter-SWCNT interactions, leading to a signal response due to increased resistivity (cp. Figure 5).[25]

An example shall be given in the following, where it has been demonstrated that this can largely improve the signal response and thus lower the limit of detection (short: LOD; the smallest amount of analyte that gives a mean signal larger than three times the standard deviation of the baseline) to detect explosives. When using pristine SWCNTs as semiconductors in a chemiresistor to detect 2,4,6-trinitrotoluene (short: TNT), a signal response in form of lowered resistivity was observed via *p*-doping of the electron-deficient analyte. However, when utilizing a dispersion of SWCNTs with a carbazole-derived oligomer, an increased resistivity was detected via the mechanism explained above.[29] Due to the larger signal response via the swelling-mechanism an LOD in the range of few ppb could be achieved.[29] Based on these results, it shall be investigated if the differently sized PNTs synthesized in this work, can exert a size exclusion effect and hence can be utilized as

selectors in SWCNT based chemiresistors. Because of their polycyclic aromatic backbone, they should be able to attract electron-deficient nitroaromatics, like TNT via π-π-stacking. This way, it should be possible to manufacture lightweight, transportable explosive detecting sensors, demonstrating the impact of this fundamental research for very different applications in the field of organic electronics.

3.4 Scanning Tunnelling Microscopy as a Tool to Investigate Surface Morphologies

Scanning tunnelling microscopy enables the investigation of the morphology of a surface and because of that, it can also be used to study the self-assembly of molecules on a templating surface. The in this work synthesized PNTs shall be utilized to generate mono- and multilayers on HOPG, to gain fundamental insights on the template's influence on the ordering of molecules with interesting optoelectronic properties. This can contribute to the optimization of various organic electronic applications and the use of STM as a method of investigation is crucial to this research. Therefore, the basic principles of this method are presented in the following.

The scanning tunnelling microscope was developed in 1979 by *G. Binning* and *H. Rohrer*[30], for which both were awarded with the Nobel Prize in Physics in 1986. It is based on the quantum mechanical phenomenon of tunnelling, i.e. the ability of subatomic particles to pass through a potential barrier that they cannot surmount by classical means due to a lack of potential energy.[31]

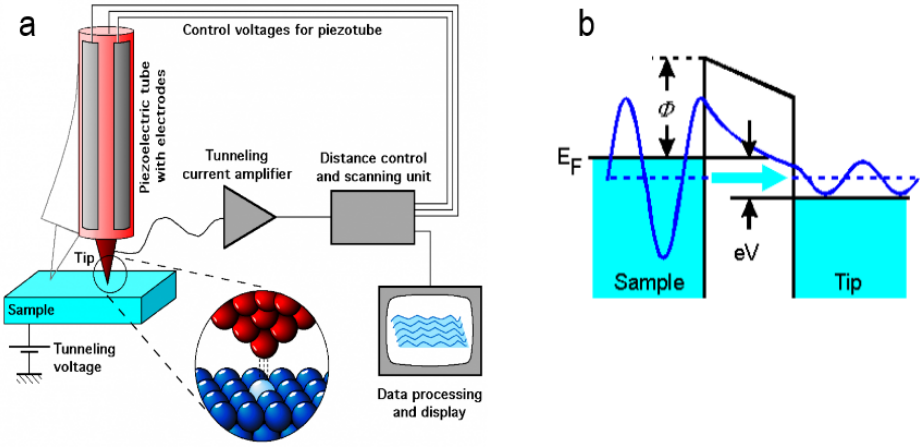

Figure 6: a) Schematic representation of a scanning tunnelling microscope; b) Tunnelling effect between sample and tip displaying the "tunnelling region" $e*V$ between the two *Fermi* energies E_F, the electron wave (blue) and the average work function of sample and tip Φ.[32,33]

When the tip of the microscope is approached to molecules that are adsorbed on a surface sample (cp. Figure 6b), e.g. HOPG, the wave-functions of the tip and sample overlap in a way that there is a finite probability of finding an electron in the barrier region or on the other side of the potential barrier.[33] Therefore, a tunnelling current can be measured when a voltage difference -bias voltage- is applied. For the electron to tunnel from the sample via the molecule to the tip, the HOMO of the molecule must be in the so-called "tunnelling regime" *e*V*, which lies between the *Fermi* energies of the sample and the tip (cp. Figure 6b). Scanning an area of the surface sample leads to the creation of a topographical map showing the adsorbed molecules on the surface, providing insights into the surface morphology.[31]
Piezoelectric ceramics are used for the fine positioning of the tip near the sample, which are polarised under mechanical stress and vice versa.[34] Due to the sensitivity of this process piezoelectric ceramics are suitable materials for the purpose of height regulation on Ångström scale to maintain a constant tunnelling current. In order to obtain high resolution images, the STM-tips must have a low curvature (i.e. be very sharp), so that the coarse surface structures can be resolved. Depending on the tip material, electrochemical etching as well as cutting and grinding are used to sharpen the tips.[35] Platinum-iridium tips are frequently used, as they do not form oxide layers under ambient conditions, that would block the tunnelling current. Typical surface materials used for the STM investigation of organic molecules are HOPG or Au(111).[34]

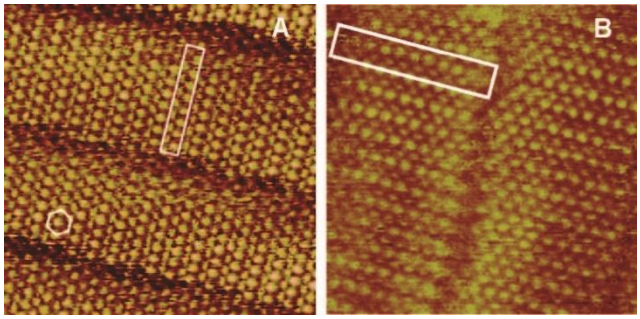

Figure 7: Scanning tunnelling microscopy images of nonadecane (A) and 1-bromoeicosane(B) at the solution/solid interface between HOPG and a solution of the respective compound. Image parameters: (A) 7.5 × 7.5 nm², V_S = –1.5 V, I_t = 300 pA; (B) 6 × 6 nm², V_S = –1.5 V, I_t = 250 pA. The white boxes indicate the approximate location of a single molecule. Each solution was prepared at half-saturation in 1-phenyloctane for nonadecane and octanoic acid for 1-bromoeicosane.[36]

The deposition of molecules on a surface can be done in ultra-high vacuum or from solution, allowing for the formation of self-assembled monolayers. Long alkyl-chains on the target

molecules are helpful, as they lead to a uniform alignment of the molecules on a HOPG surface (cp. Figure 7). They also enhance the adsorption of the molecules on the surface by providing a large contact area for *Van-der-Waals* forces.[31,36–41]

In general, two operating modes for scanning are available. The first method is the constant height mode, where the height of the tip remains unchanged, and the surface topography can be measured by the change in current. This mode enables fast scanning frequencies. However, it can only be applied to perfectly flat samples, as otherwise the tip would eventually collide with the surface. The other, more commonly used method is the constant current mode. Here, the current is maintained constant, so that the tip follows the contour of the samples. This enables the measurement of non-flat samples, but the scanning frequencies are lower in this mode. In addition, defects in the non-ideal structures of the respective surface material, such as step-edges or simply non-planar surfaces are problematic for STM measurements. However, the quality of the resulting STM images of the investigated molecules or monolayers thereof can be increased by a force field calculation with the surface as interaction partner (e.g. graphene in the case of HOPG)[42], yielding idealized structures of the observed self-assembled monolayers for the design of a fitting supramolecular model. Further problems, innate to measurements under ambient conditions like temperature drifts and moisture can be avoided by thermal annealing of the surface and internal calibration. Sound insulation is also essential to avoid vibrations during the measurement, since the tunnelling current is very sensitive towards the distance between the tip and the sample. Either magnetic levitation, or simple mechanical spring systems are used for this purpose.[31,33]

STM can be used not only to analyse but also to manipulate samples, as has been shown in various publications[43], the most prominent example being the controlled diffusion of fullerenes.[44] Moreover, it was possible to navigate fullerene molecules through carbon nanotubes and study the interactions with STM.[45] These achievements highlight the potential of STM as a tool in the analysis and manipulation of monolayers formed from nanoscale compounds. Based on these results, this work does not only aim at studying self-assembled monolayers formed by phenanthracene nanotubes via template-assistance, but also stacking behaviour of these molecules and host-guest chemistry on the surface using acceptor molecules, like fullerenes. This way the ability of generating defined segregated donor-acceptor interfaces by templated self-assembly and host-guest chemistry of organic molecules shall be studied.

4. Shape-Persistent Macrocycles

4.1 State of the Art

Since from a synthetic point of view the PNTs, investigated in this work are based on shape-persistent macrocycles (short: SPMs), it is essential to introduce this class of molecules, as well as explaining ways of accessing it. Shape-persistent macrocycles in general are a subcategory of macrocycles, which are molecular compounds whose atoms are arranged in a way that they form a ring.[46] SPMs are defined as cyclic molecules, whose average diameter <*d*> is equal to their circumference *l* divided by π (cp. Figure 8; $< d > = \frac{l}{\pi}$). In contrast to flexible macrocycles, they consist of repeating units which only possess few degrees of freedom. The rigid backbones of SPMs generate large molecular surfaces, which can undergo self-organization into ordered structures.[31,47]

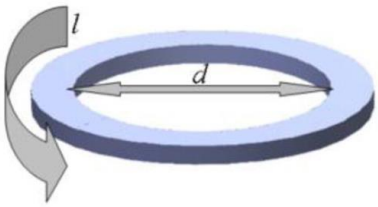

Figure 8: Geometric description of SPMs: For the average diameter the following applies.[48]

Since the publication of the first syntheses of phenylene-acetylene based SPMs by *Staab et al.* in 1974[49], the synthesis of such structures on nanometre scale has been in the focus of intensive research not least because of their versatility in the field of materials science. *Staab et al.* also developed purely phenylene based macrocycles with an increased rigidity (cp. Figure 9).[31,50]

In addition, this area of research benefited from the concurrent advances made in transition metal catalysis with the development of the *Negishi* and *Sonogashira* cross-coupling reactions in the late 1970s, as well as more modern advancements like the alkyne metathesis. These cross-coupling reactions allow a selective bond formation between sp^2- and/or sp-hybridized carbon centres and lead to viable synthetic routes for SPMs, which will be presented in the following chapter.[31]

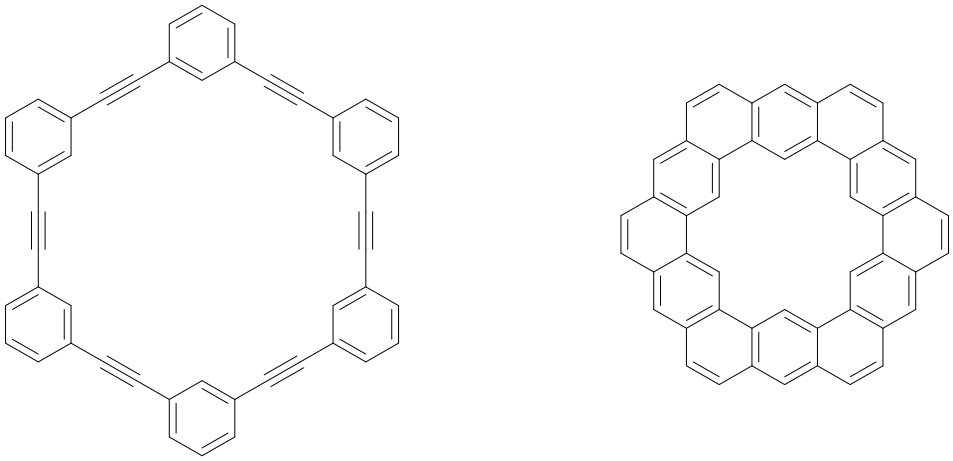

phenylene-acetylene based SPM Kekulen

Figure 9: Shape-persistent macrocycles by *Staab et al.*[49,50]

One major function of SPMs is the formation of nanoporous solids, which have a wide range of usage in technological applications, such as sensors, optical and electronical devices or in energy storage and conversion.[51] In the following, SPMs that meet the requirements of these applications are presented. In general, a high degree of stability of the utilized compound is required for use as nanoporous solid. However, it was observed that large SPMs are often not very shape-persistent, but flexible due to the limited persistence length (a quantification of stiffness, defined as the length over which correlations in the direction of the tangent of a chain are lost) of their phenylene or phenylene-ethynylene backbone.[52] To circumvent this challenge the rigidity of SPMs can be increased by introducing spokes and thus creating molecular spoked wheels.

Characteristic for SPMs is their ability to form self-assembled monolayers at the solid/liquid interface and therewith generate differently shaped and functionalized nano-patterned structure motifs, whose appearance and functionalization is directly linked to the SPMs used and their respective functional groups. Recent developments in this field of research include the synthesis of 2D-SPM polygons (cp. Figure 10) and the observation of various nano-patterned structures via STM when combining these polygons on HOPG.[53] To this end, the SPMs contain outward-facing long alkyl-chains, that enable structured deposition on HOPG.[37] Basic concepts for this are, on the one hand, the preferred alignment of the alkyl-chains along the HOPG main axes and, on the other hand, a strong interdigitation tendency of oppositely-oriented alkyl-chains.[31,38–41,54] In this way, multi-component assemblies are formed, that can be detected by STM, which lays the foundation for extending

this approach to the third dimension to obtain monolayers of the PNTs synthesized in this work and therewith obtain functionalization above the surface, as well as an enhanced possibility for host-guest chemistry.

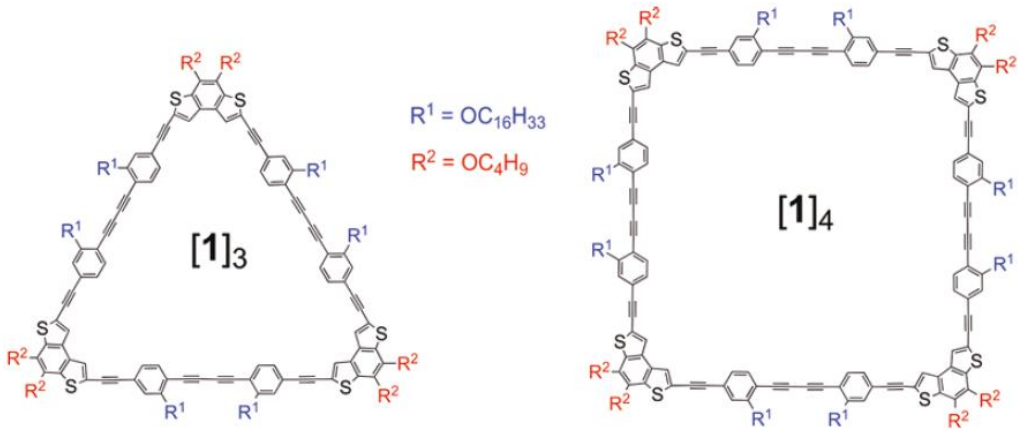

Figure 10: Molecular structures of cyclooligomeric polygons $[1]_n$, n = 3-4.[53]

Furthermore, for the application of SPMs in chemical sensing it was found, that the main influence on the host-guest chemistry of SPMs (apart from functional groups for the formation of non-covalent interactions) is the size of the cavity inside them.[55] Therefore, *Höger et al.* synthesized an amphiphilic SPM containing both H-donating hydroxy-groups and hydrophobic alkoxy-groups and designed a guest containing H-accepting amine-groups matching the size of the host-cavity. It was observed that the hydroxy-groups facing outward in polar solvents pointed inward upon addition of the guest molecule. This is due to a conformational change in the SPM caused by association of the guest molecule in the host cavity via hydrogen-bonding.[31,56] In this way the potential of SPMs as sensor molecules was explored. Functionalizing the vacant cavities of the PNTs synthesized in this work, which are prone to undergo host-guest chemistry with matching molecules, or the exploitation of non-covalent interactions they might exert, could lead to similar applications in chemical sensing, while adding an enhanced size exclusion effect due to the three-dimensional structure.

Another important application for SPMs emerged already few years after the synthesis of *Staab's* SPM when *Chandrasekhar et al.* discovered the columnar phase of liquid crystals.[57] It was shown that columnar structures formed from disc-like molecules via supramolecular assemblies, e.g. using π-π-interactions, can form mesophases when flexible side chains lower their melting points below isotropisation temperature.[57]

These π-π-interactions can also be utilized to form tubular structures via π-π-interactions from SPMs for other applications. In order to obtain such a structure with a channel in its centre the utilized SPMs must favour face-stacking over off-centre parallel stacking, which would not allow for larger tubes, due to the parallel-displacement of the SPM rims ending the tube after only few SPMs stacking on top of each other (Figure 11). However, to tune SPMs for eclipsed face-stacking several conditions must be met.

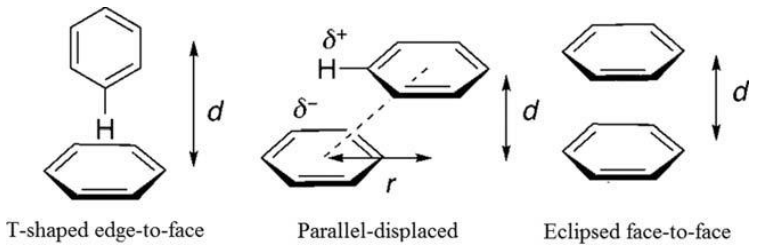

Figure 11: Illustration of the different types of π-π-stacking of aromatic rings, by representative conformations of the benzene dimer.[58]

As *Hunter et al.* noted two electron-deficient aromatic systems are more likely to stack in a face-to-face fashion than any other combination of electron-rich and electron-deficient systems, because π-stacking is stabilized by the effects of polarization.[59] Moreover, *W. Zhang* and *J. S. Moore* discovered that these general observations also apply for the formation of π-stacks from SPMs.[60] Furthermore, π-π-interactions are strengthened by a planar and rigid framework of the SPM and by *exo*-annular alkoxy groups.[61] Although this results in a set of rules, that has to be taken into consideration when designing an SPM with optimized aggregation behaviour in solution by choosing the right functional groups, π-π-interactions still remain relatively weak. To circumvent the problem of instable structures due to the weak π-π-interactions and to be able to synthesize stable channel-like structures a covalent approach can be chosen. Such an approach was successfully applied by *Höger et al.* to synthesize macrocycle encapsulated rod-like molecules, which are interesting for application in photovoltaics and as photochemical sensors.[62] However, the synthesized channel-like structure is a priori filled with a host molecule connecting the SPMs and therefore no further host-guest chemistry is possible. Nevertheless, this is a first step towards the synthesis of stable channel-like structures. A different approach, which will be used to synthesize the desired PNTs in this work, is to covalently connect SPMs via their periphery, resulting in hollow tubes. This way stable channel-like structures can be generated using

covalent connections, while concurrently preserving the cavity of the SPM and this way allowing for host-guest chemistry. However, this approach requires the choice of an effective method to synthesize and connect the targeted SPMs. In the following several of such methods will be presented and discussed in terms of their innate advantages and disadvantages.[31]

4.2 Synthetic Challenges

In general, four major synthetic approaches towards SPMs can be distinguished.

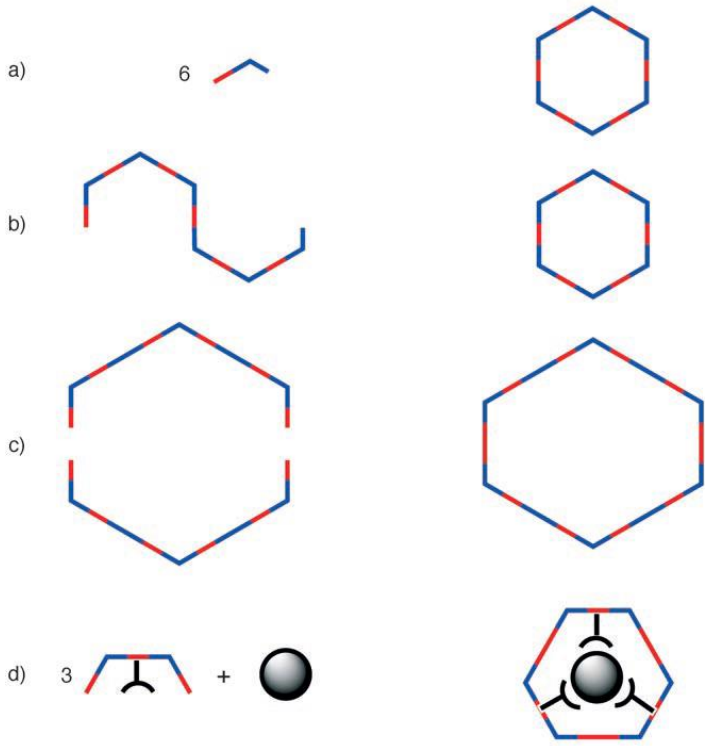

Figure 12: Illustration of synthetic strategies towards SPMs: a) cyclooligomerisation, b) intramolecular cyclization, c) bimolecular coupling/intramolecular cyclization, d) templated cyclization.[47]

The first one is the cyclooligomerisation (cp. Figure 12a). It was used by *Staab et al.* for the synthesis of the first SPMs[49] and is a very straightforward approach, as it only requires the synthesis of small molecules, which then form the SPM in a one-pot reaction. However, a major disadvantage of this approach is the problem of "overshooting". Since usually irreversible reactions like homo- or cross-couplings are used, the formation of undesired bonds cannot be corrected and the product distribution is kinetically determined.[47] In other terms, if an oligomer in the reaction solution grows only one monomer larger than intended,

ring-closure to the desired SPM is no longer possible. This leads to low yields, but on the other hand the SPMs can be synthesized quickly from readily available substrates. In addition, different ring sizes are available in one reaction. Therefore, the suitability of this method depends on availability and price of the starting material, as well as the necessary effort for the product separation. Often the monomers contain ethynylene units, which are attractive building blocks due to their simple linear geometry, their potential for extended π-conjugation as well as their accessibility by a wide range of syntheses.[31,63]

Diametrically opposed is the approach of intramolecular ring closure of a large precursor (cp. Figure 12b), which already contains all atoms of the ring. Here, a highly pre-organized substrate is synthesized, which enables the formation of the SPM in an intramolecular manner and thus eliminates the problem of "overshooting". Regardless, the yields obtained by this approach are often still low, because of the multistep synthesis required to gain the precursor.[64] In addition, this synthesis is often tedious and time consuming. However, it allows the selective interior and exterior introduction of functional groups into the precursor and therefore facilitates the synthesis of carefully designed SPMs, which then can be used e.g. for host-guest chemistry via polar groups.[31,65]

Another synthetic approach, that combines the advantages of the two strategies presented above, is the intermolecular coupling of monomers followed by intramolecular cyclization (cp. Figure 12c). It provides moderate yields, inasmuch as the one-pot reaction of coupling and cyclization gives lower yields than the intramolecular ring closure of a large precursor already containing all atoms of the ring. However, the precursor monomers can be synthesized using fewer synthetic steps and thereby are obtained in higher yields.[47] The crucial step of this approach is the coupling of the monomers, which should be carried out under high dilution conditions and should not be designed to couple more than two monomers per formed SPM to give appreciable yields.[66] Nevertheless, it is unavoidable to receive a product mixture of differently sized SPMs, since the product distribution is kinetically determined. This approach was successfully applied by *Höger et al.*[67] in the synthesis of the first shape-persistent macrocyclic amphiphile. Due to the advantages mentioned above, it is also used in this work to form the desired phenanthracene nanotubes by connection of precursors to SPMs. However, for economical and ecological reasons the synthesis will be modified by the use of pseudo-high-dilution conditions, i.e. the slow addition of the monomer over several hours instead of using large amounts of solvents.[31]

An even more successful synthetic approach towards SPMs – in terms of overall yield – is the template directed cyclization of monomers (cp. Figure 12d). The underlying concept of this approach is the use of high dilution conditions to minimize the formation of larger open-chain oligomers combined with a template leading to a locally high concentration of reactive monomer end-groups and consequently facilitating the formation of the cyclic SPMs in high yields (cp. Figure 13).[47] This way, the intramolecular ring-closure is faster than the intermolecular formation of open-chain oligomers. The utilized templates can be covalently bound to the precursor and removed after cyclization, or act via non-covalent interactions, such as metal-coordination.[68,69] Moreover, different templates can be utilized to selectively synthesize SPMs of different sizes.[31,47] Despite the advantages of the template directed cyclization it can prove difficult to find a matching template. Furthermore, for the template to work, specific functional groups for covalent linkage or non-covalent interactions must be incorporated into the monomer structure, which requires additional synthetic steps.[31]

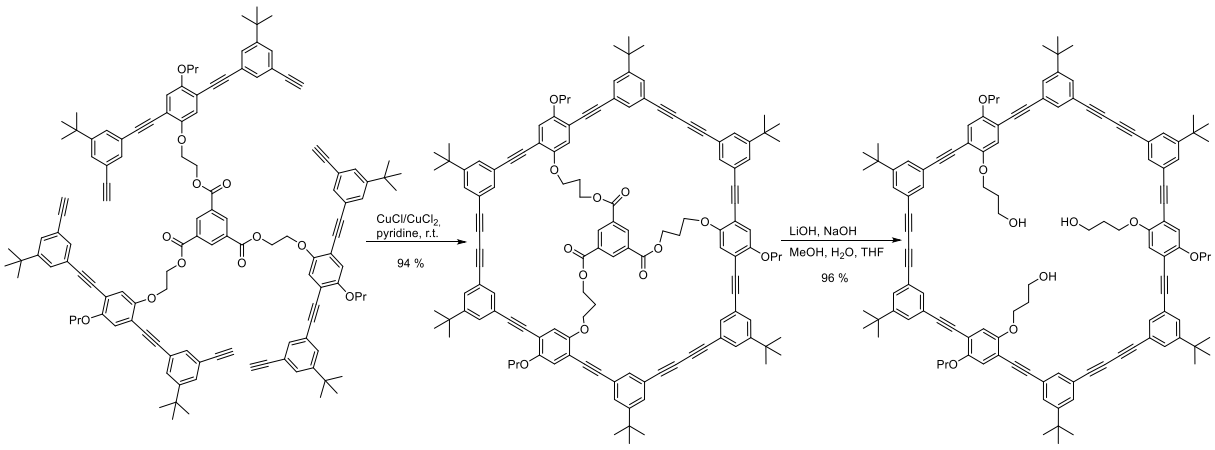

Figure 13: Synthesis of an SPM using a covalently bound template.[68]

All the above-described synthetic routes are kinetic approaches utilizing irreversible coupling-reactions. Another route to synthesize SPMs is to use a thermodynamic approach employing reversible reactions known as dynamic covalent chemistry. One exemplary reaction, that can be used for the synthesis of SPMs is the alkyne-metathesis. In general, the main two influences on any thermodynamically driven process are enthalpy and entropy. While the change in enthalpy during a reaction mainly depends on the number of interactions and the sum of their individual binding energies, the change in entropy depends on the degrees of freedom of the whole system. For this reason, cyclic structures are preferred

enthalpically, as they have a higher number of interactions than their open-chain counterparts. On the other hand, open-chain structures are entropically preferred, as they have more degrees of freedom. Therefore, the influence of temperature can be utilized to control the reaction by adjusting the entropic influence, which is temperature dependent.[31]

Furthermore, at a certain size of oligomers, the difference in the number of interactions between cyclic and open-chain structures becomes relatively small, and the influence of enthalpy is overcompensated by the entropy gain for open-chain structures. This induces the formation of polymers or large open-chain oligomers instead of cyclic structures at high concentrations and explains the need of high-dilution conditions. In addition, small macrocycles, which would be entropically favoured over large macrocycles, are often unfavourable in the case of SPMs due to the high angular strain, which allows the synthesis of large SPMs under thermodynamic control.[31,47]

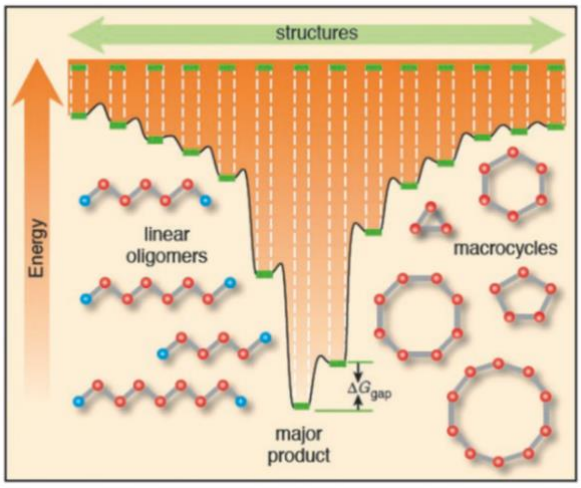

Figure 14: The cyclooligomerisation landscape.[47]

Taking these thermodynamic principles into account, it is possible to synthesize one unique structure from a multitude of probable products, provided that it is thermodynamically the most stable product and the energy gap between it and the next stable structure is large enough (cp. Figure 14).[47] However, the energy difference between several available products is usually too small to tune the reaction conditions towards one specific product, so that a distribution of different oligomers is obtained. The amount of each individual oligomer is then determined by its thermodynamic stability under the respective reaction conditions in relation to the other oligomers. Thus, the most stable oligomer will be the main product, but not the

only one as it should ideally be, according to theoretical expectations. This results in the need for an efficient separation method to isolate the desired product from a multitude of similar compounds in terms of their chemical properties such as polarity.[31]

In addition, this approach has several drawbacks, the most considerable one being that the synthesis of strained molecular structures is not possible, as they are enthalpically unfavourable. Furthermore, the growing oligomers must remain soluble, otherwise they will no longer participate in the reversible reaction and reduce the yield in the same way "overshooting" does when using kinetic approaches.[47] Therefore, the thermodynamic approach for the synthesis of SPMs can only be used efficiently in a few specific cases, where the above-mentioned limitations do not hinder the formation of the desired product.[31]

4.3 Analytical and Recycling Gel Permeation Chromatography

After the discussion of synthetic pathways towards SPMs, in the following a short introduction to gel permeation chromatography (short: GPC) as analytical tool will be given to facilitate retracing of the choices made regarding the oligomerisation reactions to gain the PNTs in this work. Moreover, the use of recycling GPC (short: recGPC) as preparative separation method for oligomers will be presented.

Gel permeation chromatography is a separation method based on the hydrodynamic radius of the respective molecules, that shall be separated.[70] The GPC separation mechanism utilizes pores of different sizes within polystyrene beads packed in a column. Molecules fitting into more pores have a longer retention time on the column than molecules fitting into less pores, hence leading to a separation of molecules with a different hydrodynamic radius. This means, that the separation is ideally based on size-exclusion only and not on physical or chemical interactions of the molecules with the stationary phase of the column, like it is the case for the column chromatography e.g. using silica gel.[71]

The column of a GPC-system usually consists of a crosslinked polystyrene stationary phase, that swells to a gel in the mobile phase, i.e. an organic solvent which is often THF or DMF. The pore size distribution designates the selective permeation region (cp. Figure 15b). This is the particle size of the molecules that can be separated using this specific column. Molecules that are larger do not fit into any of the pores and molecules smaller fit into all the pores and hence elute from the column -not separated- after the same time, for each case respectively. In

turn molecules with a size in the selective permeation region fit only into a fraction of the pores, i.e. depending on their hydrodynamic radius a different internal volume of the gel is available to them, and thereby they elute from the column after different times (cp. Figure 15a).

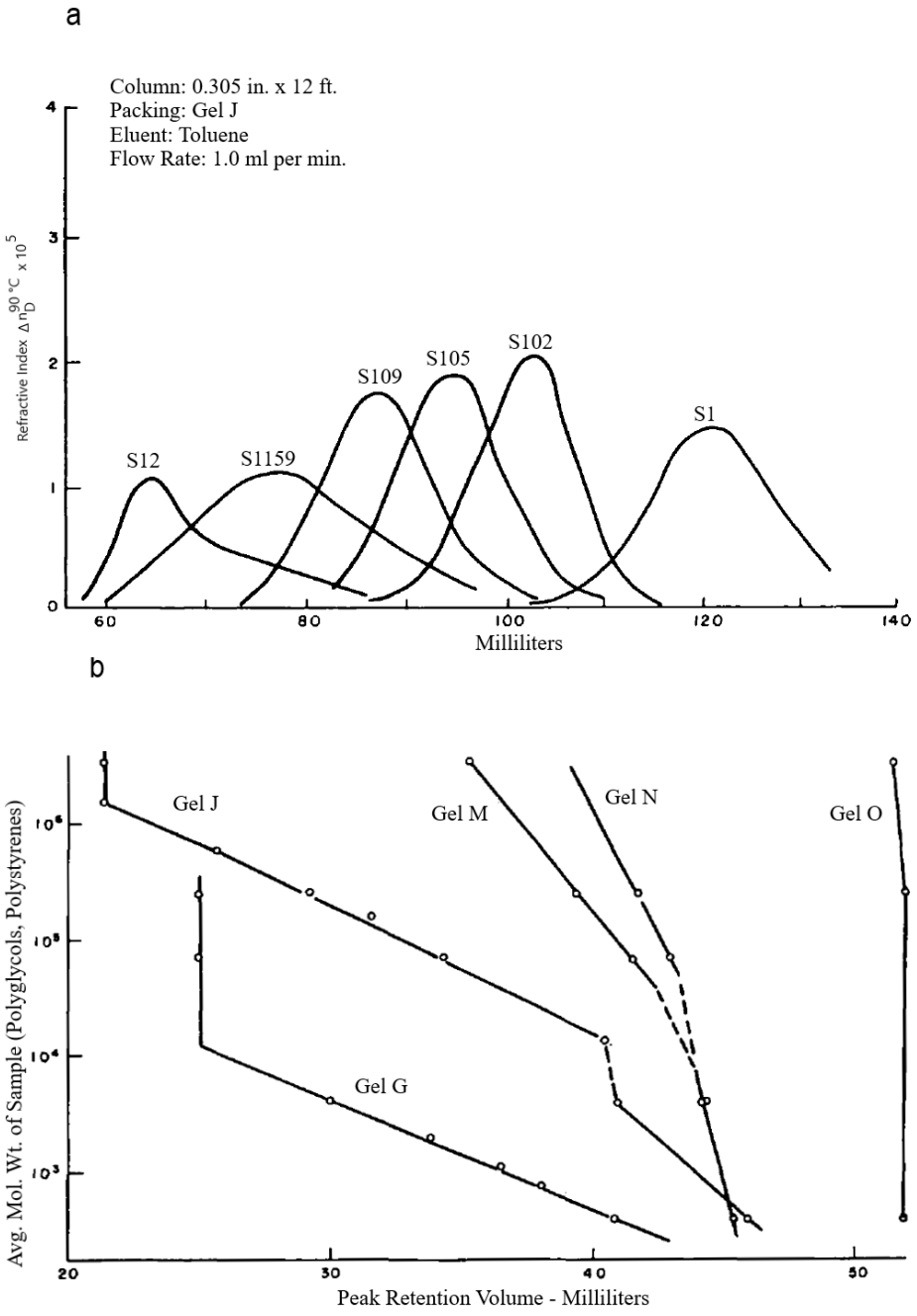

Figure 15: Illustration of the first published GPC-experiment: a) elution diagram for different polystyrene samples on gel "J"; b) representative permeability curves for different gels, showing a distinct permeability region for gel "J" (second from the left).[71]

GPC is often used to analyse (analytical GPC) and separate (recGPC) oligomers and polymers, as their size corresponds well to their molecular weight and separation via polarity is often not possible for them due to their similarity with respect to functionalization. However, a GPC is generally calibrated to polystyrene, a coiled polymer. Hence, when analysing rigid-rod molecules with a larger persistence length, the correlation of molar mass to elution time is different, since a rigid-rod polymer of the same molecular weight as a styrene polymer has a larger hydrodynamic radius.[72] This is why the molar mass obtained from such a GPC analysis, also for the in this work synthesized rigid H-shaped monomers and PNTs, is overestimated. This can be seen when comparing to the actual molar mass obtained from MALDI(+) mass spectrometry. However, plotting the molar mass distribution obtained from GPC analysis, still can give a qualitative insight into the molecules formed during the oligomerisations performed in this work, as well as their relative proportions. Fundamentally, both GPC methods are based on the same principles presented above. However, recGPC distinguishes itself from analytical GPC by a row of separation columns, that allow for injection of larger sample amounts, as well as higher flow rates. In addition, after elution from the columns a sample can be "recycled", i.e. be submitted to the separation columns again. Hence, several separation cycles are available, until satisfactory separation of the injected compound mixture is achieved.

Since simple analysis of a reaction solution is possible, analytical GPC is a powerful tool for reaction progress tracking for oligomerisations. It is used in this work on the one hand, to determine and compare the outcomes when screening different oligomerisation procedures, and on the other hand recGPC is then utilized to separate the respective oligomers from the reaction mixtures.

4.4 Preliminary Work

In recent years, a variety of shape-persistent macrocycles have been synthesized in the *Höger*-group and self-assembled monolayers of these on HOPG have been studied via STM by the *Jester*-group. Most prominently mentioned should be the work of *E. Sigmund*, who synthesized differently shaped polygons by oligomerisation of a monomer. Mixtures of these polygons with different compositions enable the formation of various nanopatterned structures upon self-assembly on HOPG (Figure 16).[53] Additionally, the formation of a

two-dimensional supramolecular structure by co-deposition of an SPM and phenyl-C61-butyric acid methyl ester (PCBM) on HOPG was shown by *Pan et al.*[73] However, it was also recognized that some corners of such SPM polygons can point-inwards after formation of the self-assembled monolayer, leading to the conclusion that these SPMs are not as shape-persistent as previously assumed and can in fact collapse.

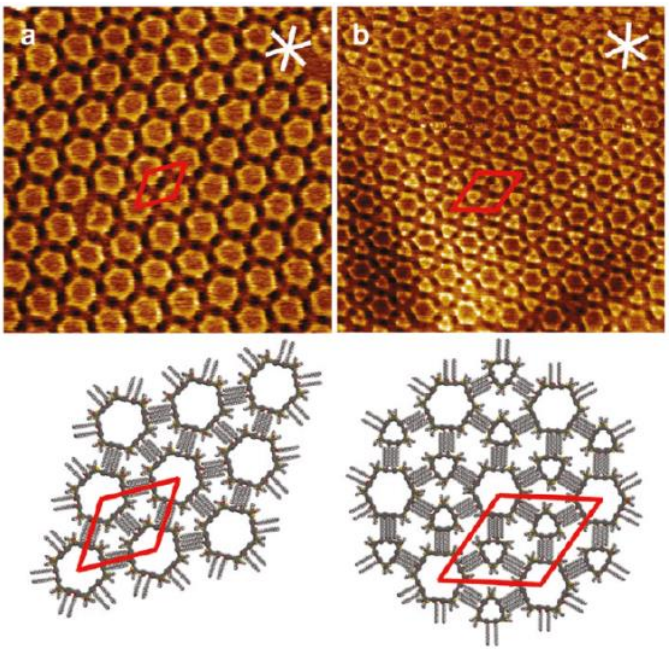

Figure 16: STM images and molecular models of the patterns of (a) $[1]_6$ (c = 2 x 10^{-6} M, 62.8 x 62.8 nm^2, V_S = -1.0 V, I_t = 6 pA, thermally annealed for 1 min at 60 °C; *p6mm*, *a* = 7.5 ± 0.1 nm, *b* = 7.5 ± 0.1 nm, $\gamma(a,b)$ = 60 ± 2°) and (b) a binary mixture of $[1]_3$ and $[1]_6$ ($c([1]_3)$ = 10^{-5} M; $c([1]_6)$ = 10^{-7} M; $c([1]_3)/c([1]_6)$ = 100:1), 79.9 x 79.9 nm^2, V_S = -0.8 V, I_t = 9 pA; *p6mm*, *a* = 9.8 ± 0.2 nm, *b* = 10.1 ± 0.2 nm, $\gamma(a,b)$ = 60 ± 2°) at the TCB/HOPG interface. The unit cells and substrate main axis directions are indicated in red and white color, respectively.[53]

This led to the development of molecular spoked wheels and subsequently to platform molecules, where e.g. fullerenes (PCBMs) are connected covalently to the SPM, which in turn is stabilized by internal spokes (cp. Figure 17).[74] Based on these results it can be assumed that if the SPMs were not stabilized by spokes but by connection at their rims to form phenanthracene nanotubes, a cavity for host-guest chemistry with fullerenes would be available upon formation of a self-assembled monolayer. Hence, this approach gives rise to ordered structures with defined donor/acceptor distances, relevant for the improvement of OSCs.

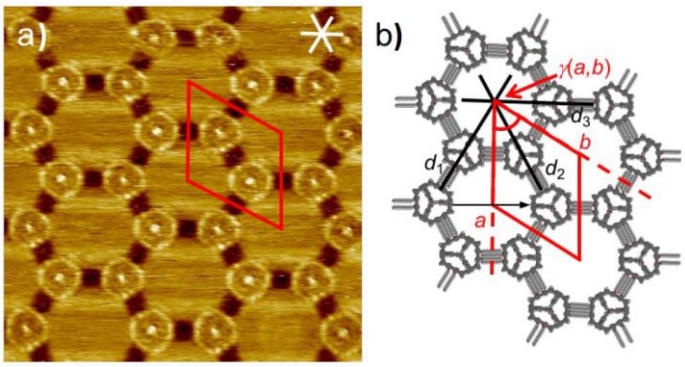

Figure 17: a) STM image of a platform molecule with covalently attached PCBM, c = 10^{-7} M, thermally annealed for 20 s at 80 °C, Vs = -0.8 V, I_t = 14 pA, at the TCB/HOPG interface, image size 33.6 × 33.6 nm^2; b) molecular model of the respective molecule, lattice constants $a = b$ = (10.4 ± 0.2) nm, $\gamma(a,b)$ = (60 ± 2) °. The unit cells and substrate main axis directions are indicated in red and white color, respectively.[75]

As far as preliminary work from a synthetic point of view is concerned, *S. Meißner* developed a synthesis for nanoscale ladder polymers in the *Höger* group.[76] The synthetic approach is based on the work by *Kador et al.*[77] and uses H-shaped monomers with protected ends at one rigid-rod, so that they can initially be polymerised on one side selectively and the ladder polymer is formed in a polymer analogous "zipping-reaction" (i.e. an intramolecular reaction in which the reactive partners are predetermined by the preorganization of the on one side connected ladder precursor) after deprotection of the second rigid-rod. The use of end-caps in the synthesis of such ladder polymers opens the possibility of synthesizing well-defined oligomers. These are of interest as model systems for the corresponding polymers, since physical properties such as the persistence length can be effectively extrapolated from the oligomers to the polymers, for which it is often much more difficult to obtain such data.[31,72]

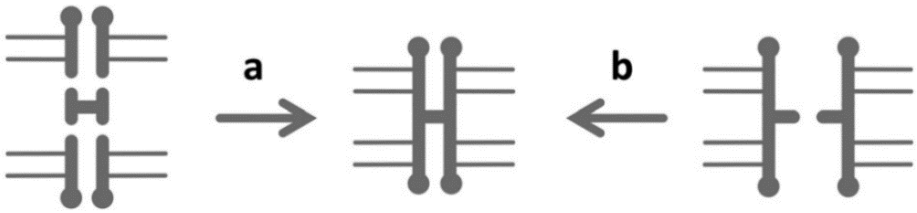

Figure 18: Illustration of synthetic strategies towards H-shaped rod-spacer-rod molecules, displaying central spacer and rigid rods (bold lines), long alkyl chains (thin lines) and silyl-protecting groups (bold filled circles).[78]

There are two main synthetic strategies towards the H-shaped monomers. Either a spacer is coupled with four rigid-rods via e.g. a *Glaser* or *Sonogashira* coupling (cp. Figure 18a), or two rigid rods are coupled with a smaller spacer to form an I-shaped molecule. Two I-shaped

molecules can then be connected by previously installed functional groups at the spacer (cp. Figure 18b). In order to obtain a degree of shape-persistence of the ladder oligomer, that would support a nanotubular structure and thus make this a feasible strategy for synthesising PNTs, the spacer of the H-shaped monomer must be very rigid. Potential rigid spacers are based on polycyclic aromatic hydrocarbons like pyrene, or the in this work utilized phenanthrene.[31]

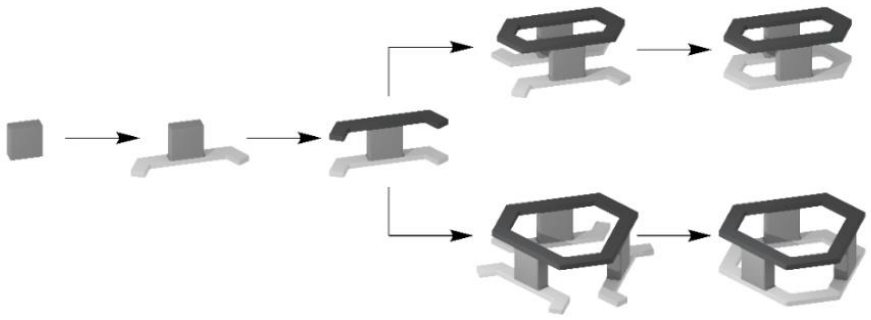

Figure 19: Illustration of the synthetic strategy towards the desired phenanthracene nanotubes. (top: cyclodimer **D_{1c}**; bottom: cyclotrimer **T_{1c}**).

Based on such rigid H-shaped molecules, which can yield defined oligomers, it is conceivable that if the utilized rigid-rods were not linear but angled, it should be possible to gain cyclic oligomers (i.e. SPMs). These are then connected at their rims via the rigid spacer and should give non-collapsible tubes on the nanometre scale. In this work the H-analogous monomers will be synthesized by a similar approach, as for the synthesis of an H-shaped monomer (cp. Figure 19).

Therefore, angled rigid-rods with protected ends (light grey; Figure 19) are connected to one half of a spacer molecule. Then, the other half of the spacer molecule is coupled followed by another set of differently protected angled rigid-rods (dark grey; Figure 19). This allows then for selective deprotection of the angled rigid rods and cyclic structures are obtained via an oligomerisation reaction. After separation of the different products, each of the cyclic structures (cp. dimer and trimer in Figure 19) can then be closed analogous to the "zipping-reaction" presented before, to give the respective PNTs.

5. Aim of this Work

As discussed before, template-assisted self-assembly of organic molecules can optimize the performance of organic electronic devices, contributing to mitigate the worldwide increasing energy consumption and the undesirable effects resulting thereof. In this work fundamental insights on template-assisted self-assembly of organic molecules shall be gained by the synthesis of phenanthracene nanotubes (e.g. Figure 20), based on SPMs. The formation of self-assembled monolayers of these PNTs will then be investigated via STM at the solid/liquid-interface using HOPG as template.

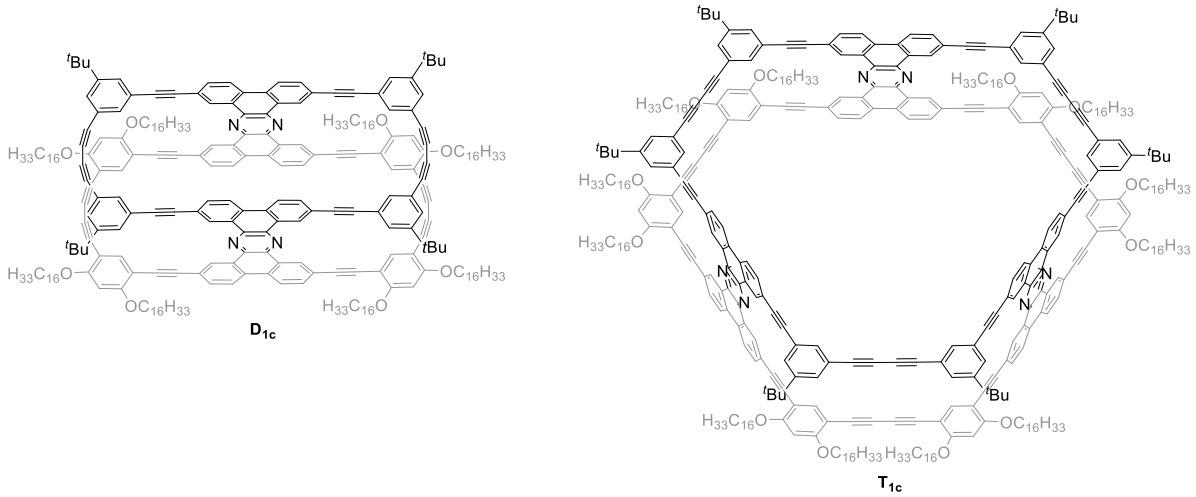

Figure 20: Schematic representation of the envisioned structure of phenanthracene nanotubes **D$_{1c}$** and **T$_{1c}$**.

Differently shaped PNTs shall be gained using a modular synthetic approach inspired by preliminary work regarding the oligomerisation of H-shaped molecules, performed in the *Höger* group.[76] These can also be perceived as expansion to the third dimension of the molecular polygons investigated before.[53] They shall have distinct properties on the surface based on their shape and give rise to different functions, including host-guest chemistry of these molecules acting as donor-hosts for PCBM acceptors. Their potential as donors will be evoked by a large aromatic backbone connecting two SPMs to gain the desired tubular structure. The aromatic backbone itself will consist of polycyclic aromatic hydrocarbons, connected via phenazine units, to gain rigid cylindrical structures (cp. Scheme 1). Such structural units are also used in donor molecules for OSCs.[79] Hence, segregated

donor/acceptor nanostructures with defined distances, guided by the nanopatterned surface of the self-assembled molecules shall be generated and investigated using STM.

Moreover, the application of PNTs as selectors in SWCNT-based chemiresistors via non-covalent interactions will be tested to demonstrate the potential of these molecules to be utilized in different areas of application in organic electronics. Furthermore, the molecules will be investigated concerning their optoelectronic and photophysical properties.

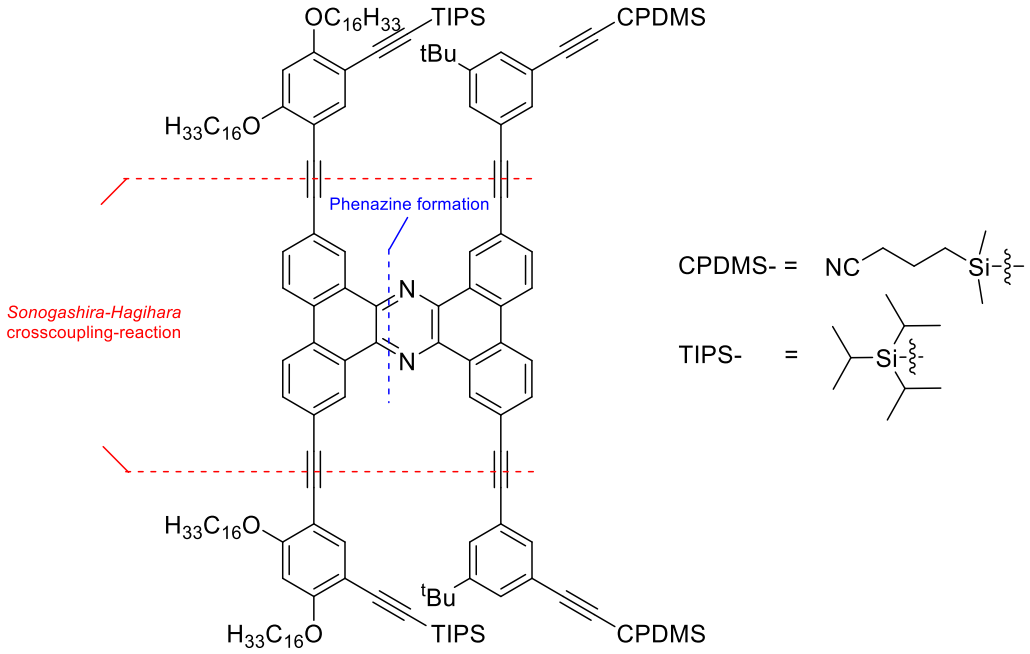

I

Scheme 1: Retrosynthetic approach to the H-shaped precursor **I**.

For the formation of PNTs from H-shaped monomers it is of utmost importance, that each monomer bears two TIPS-protected acetylenes at the rigid rod on one side of the spacer and two CPDMS-protected acetylenes on the other side (cp. Scheme 1). Only in this way, is a controlled two-step oligomerisation analogous to the synthesis of the ladder polymers feasible, yielding PNTs with a preferred side for adsorption on HOPG, which is given by alkyl-chains that are previously incorporated into the TIPS-protected angled rigid rods. The potential for orientation-controlled deposition on a surface in turn preserves access to the cavity of the PNTs and hence enables the selective adsorption of complementary guest molecules at the solid/liquid or solid/gas interface. This distinguishes the target molecules from other recent advances in the bottom-up synthesis of nanotubular structures, like

nanobelts.[80,81,82], that are symmetrical and have no side preference for the adsorption on a surface.[80,82] Based on these insights, it becomes obvious, that the formation of self-assembled monolayers from phenanthracene nanotubes via template assistance is enabled only by a carefully planned synthetic approach.

The synthetic strategy to gain the aimed channel-like structures (i.e. dimers, trimers, tetramers, …) of H-shaped monomers, will be elucidated using the example of H-shaped monomer **I**. For the purpose of oligomerisation via a *Glaser* coupling, **I** is equipped with differently protected acetylene groups (cp. Scheme 1). These silyl-protecting groups make selective deprotection possible, due to their gradual stability towards deprotection conditions. Hence, in a first reaction step an intermolecular coupling followed by intramolecular cyclization (cp. 4.2 Synthetic Challenges) is performed under pseudo-high-dilution conditions to deliver variously sized SPMs, whilst one half of the acetylenes of **I** still remains protected. After separation of these differently sized cyclic oligomers via recGPC and deprotection of the remaining TIPS-protecting groups, the second SPMs are formed in another *Glaser* coupling yielding a cylindrical structure of two same-sized SPMs connected via an imine bond at their phenanthrene spacer (cp. Figure 20).

Regarding the synthetic strategy towards **I** itself, first an angled I-shaped molecule is synthesized from two triisopropylsilyl- (short: TIPS-) protected angled rigid-rods and a phenanthrene spacer. The I-shaped molecule is then connected to a second spacer via phenazine formation. Finally, two (3-cyanopropyl)dimethylsilyl- (short: CPDMS-) protected angled rigid-rods are coupled to the second spacer. This adaptation of the synthetic approach compared to “strategy b” towards H-shaped monomers (cp. Figure 18b; 4.4 Preliminary Work) is required, to prevent cleavage of the relatively labile CPDMS-protecting groups during the acidic reaction conditions, when coupling the two phenanthrene spacers. Moreover, if all four angled rigid rods were coupled to the spacer in one step, a statistical mixture of products bearing different numbers and arrangements of CPDMS- and TIPS-protected angled rigid rods, which were difficult to separate, would be obtained.

As is depicted above, the H-shaped monomers consist of two different types of angled rigid rods and central spacers respectively (cp. Scheme 1). Hence, it is conceivable that a combination of different rod- and spacer-molecules, using the same coupling reactions in a modular approach, gives access to a variety of H-shaped monomers. That is to say, that the synthetic strategy towards the H-shaped molecules needs to be optimized only once and can

then be utilized to give reliable access to the desired structures. This leaves only the need to devise efficient syntheses to different small molecules, rather than for the whole nanotubular structures, which would be much more costly and time consuming. This way distinct shapes of the cyclic oligomers shall be attained (bowl-, pyramidal-, cylindrical-shape). These terms reflect the expected molecular form after alignment on HOPG in an orientation-controlled manner, where the ring functionalized with the alkoxy side-chains adsorbs on the graphite respectively (cp. Figure 21, Figure 50).

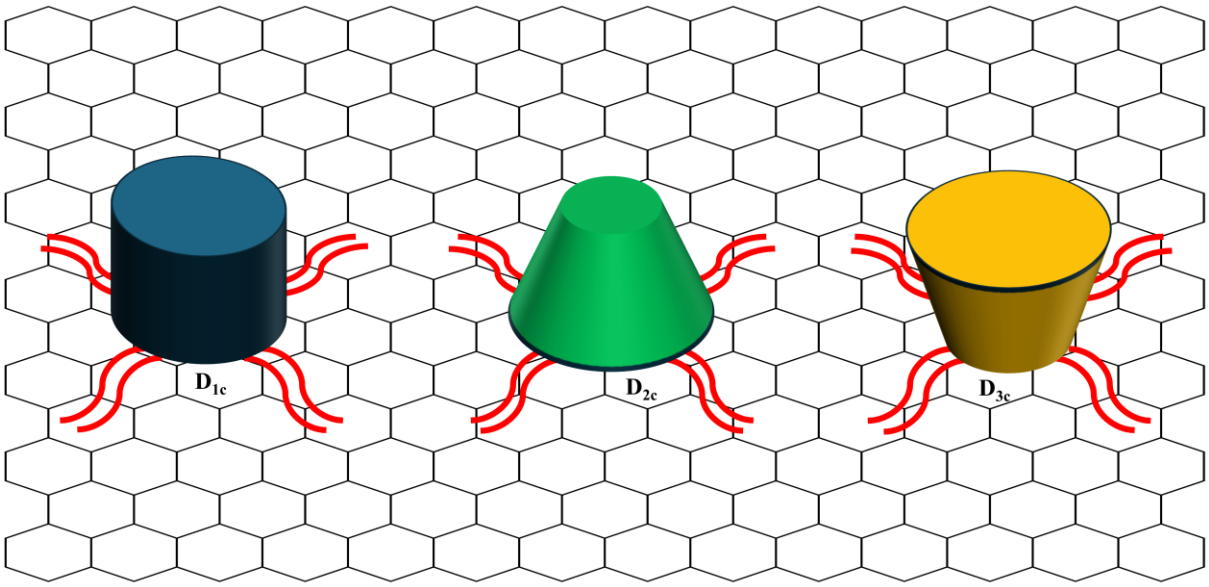

Figure 21: Illustration of the differently shaped target molecules adsorbed on a graphene sheet: Shown are the cylindrical dimer **D1c** (blue), the pyramidal dimer **D2c** (green) and the bowl-shaped dimer **D3c** (yellow); the alkoxy side-chains are depicted in red.

6. Synthesis of the Phenanthracene Nanotubes

6.1 Synthesis of the H-shaped Monomers

6.1.1 Synthesis of the Central Spacer Building Blocks

The synthesis of the first central spacer building block starts from the commercially available phenanthrenequinone (**1**), which was iodinated with *N*-iodosuccinimide in conc. H_2SO_4 (95%) at room temperature for 24 hours. Gratifyingly, the desired 2,7-substitution pattern is preferred by the mesomeric- and inductive-effects of the ketone- and phenyl-substituent for each of the two electrophilic aromatic substitutions respectively.

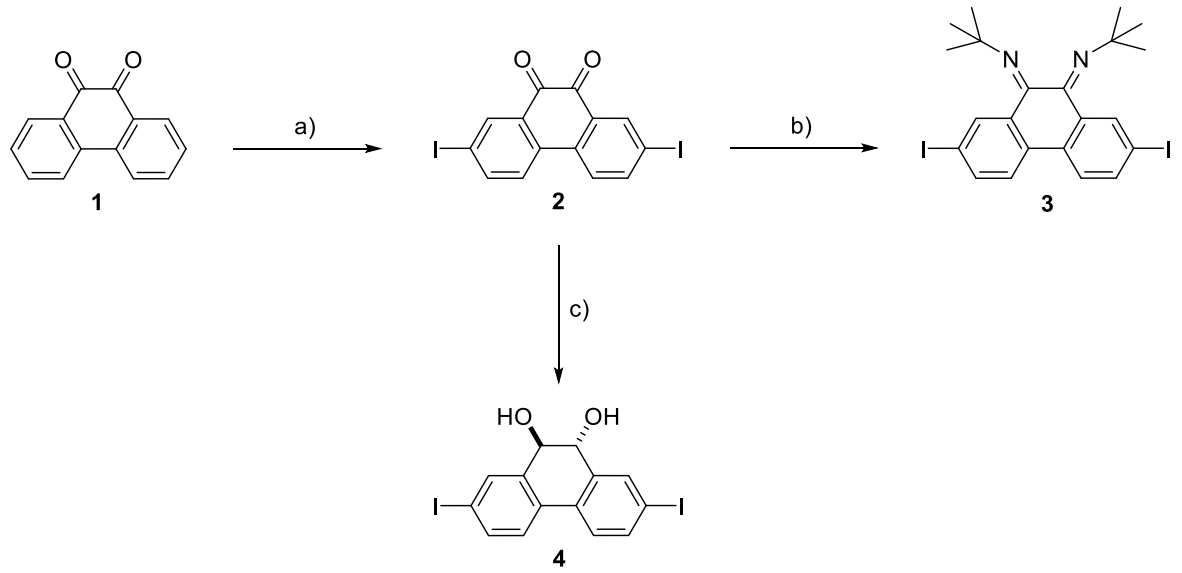

Scheme 2: Synthesis of phenanthrenediimine **3**: a) NIS, conc. H_2SO_4 (95%), 24 h, r.t., 95%; b) *tert*-butylamine, $TiCl_4$, toluene, r.t., 23 h, 70%; c) $NaBH_4$, EtOH:H_2O (7:1), r.t., 23 h, then aq. HCl (10%), 91%.

Additionally, an improvement of the yield of 2,7-diiodophenanthrenequinone (**2**) from 54% to 95% was achieved by optimization of the reaction quenching with water. For this, the reaction solution was added dropwise to the ice-cold water to minimize inclusion of impurities in the precipitating product. Hence, the crude product of quinone **2** was received pure and further recrystallization of the poorly soluble compound was no longer necessary, leading to the increase in yield. Moreover, quinone **2** was then further reacted to an imine to achieve higher yields at the subsequent *Sonogashira* cross-coupling with the angled-rigid rods. The reasons for this will be explained when discussing the coupling of the building blocks (cp. 6.1.3 Coupling of the Building Blocks to the H-shaped Monomers). The formation of

phenanthrenediimine **3** was performed by stirring quinone **2** with $TiCl_4$ as *Lewis*-acid catalyst and *tert*-butylamine in toluene at room temperature for 23 hours. After recrystallization from acetonitrile the product was obtained as mixture of *E/Z*-isomers in 70% yield. Moreover, for the same purpose quinone **2** was reduced to the alcohol by stirring with $NaBH_4$ in EtOH:H_2O (7:1) at room temperature for 23 hours. Acidic workup and filtering-off the precipitate yielded 91% of *trans*-2,7-diiodophenanthrene-9,10-diol (**4**). These building blocks were then further substituted with angled rigid-rods via *Sonogashira* cross-couplings before being coupled with different central spacer building blocks bearing diamine-units, enabling the formation of various PNTs from differently sized SPMs.

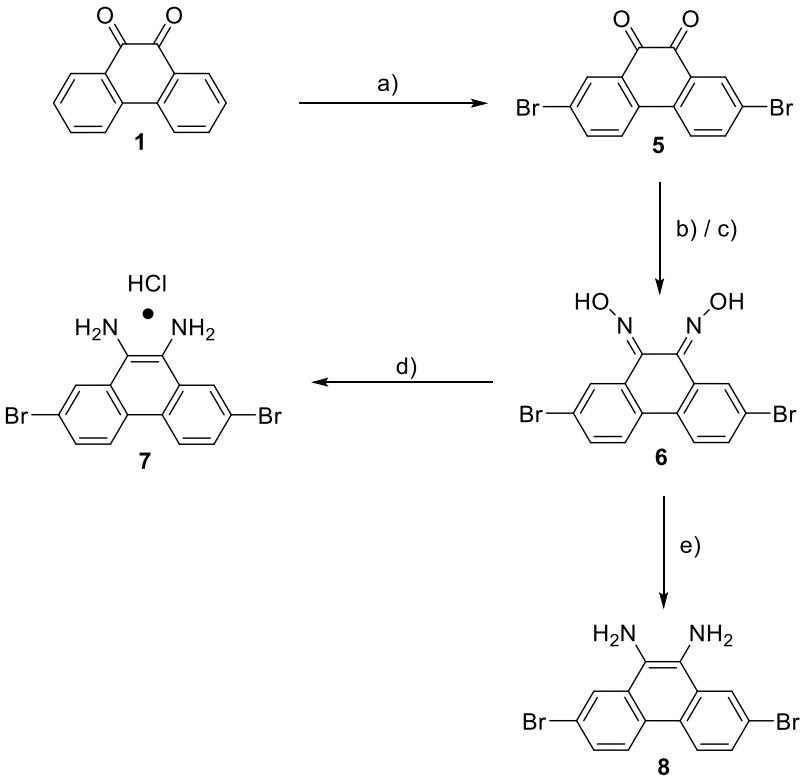

Scheme 3: Synthesis of phenanthrenediamine **8**: a) NBS, conc. H_2SO_4 (95%), r.t., 24 h, 59%; b) NH_2OH*HCl, NaOAc, EtOH, reflux, 12 h, 20%; c) NH_2OH*HCl, pyridine, EtOH, reflux, 40 h, 80%; d) $SnCl_2$*2 H_2O, conc. HCl (37%), EtOH, 70 °C, 3 h, 56%; e) $SnCl_2$, conc. HCl (37%), EtOH, reflux, 3 h, then NaOH (2 M), 15 min, 45%.

The second building block is structurally related to the first one and thus can also be synthesized starting from phenanthrenequinone (**1**). In a first reaction **1** was brominated by a procedure analogous to that described above, stirring with *N*-bromosuccinimide in conc. H_2SO_4 overnight. However, it was not possible to increase the yield substantially in the same

way as for the iodination since the crude product could not be obtained in a pure form. Hence, recrystallization from toluene was necessary giving 2,7-dibromophenanthrenequinone (**5**) in 59% yield. The small increase in yield compared to the initial 54% can be attributed to the strict use of 95% H_2SO_4 over 97% H_2SO_4, which has a lower viscosity and allows for vigorous stirring of the reaction mixture. Then, the transformation of the diketone-unit into the desired diamine-unit was performed over two steps. First 2,7-dibromophenanthrene-9,10-dione dioxime (**6**) was synthesized by refluxing quinone **5** in EtOH with hydroxylammonium chloride and sodium acetate for 24 hours. After recrystallization from acetone dioxime **6** was obtained in 20% yield. This reaction was then optimized using pyridine as a stronger base and elongation of the reaction time to 40 hours. The yield gained by this second approach was 80%. Secondly, dioxime **6** was reduced to the diamine hydrochloride **7** by stirring at 70 °C for three hours in EtOH after addition of tin(II) chloride dihydrate dissolved in conc. HCl (37%). Filtering-off the precipitate, yielded **7** in 56% yield. The synthesis of diamine hydrochloride **7** as stable salt was chosen in a first approach due to the known issues of decomposition of similar aromatic 1,2-diamines upon exposure to air.[83,84] However, as will be discussed when presenting the coupling of the building blocks (cp. 6.1.3 Coupling of the Building Blocks to the H-shaped Monomers), the coupling of **7** with a derivative of diketone **2** only gave low to moderate yields due to its poor solubility in the used solvents for the phenazine formation. Hence, also 2,7-dibromophenanthrene-9,10-diamine (**8**) was synthesized by a similar reaction procedure. Therefore, dioxime **6** was suspended in EtOH at 0 °C and anhydrous tin(II) chloride dissolved in conc. HCl (37%) was added. After refluxing for three hours, the precipitate was filtered-off and suspended in a saturated $NaHCO_3$-solution. After subsequent extraction with dichloromethane the product was received in 28% yield. The yield could be increased by use of a stronger base for the generation of the free diamine from the hydrochloride salt. Hence, when utilizing an aqueous NaOH-solution (2 M) the product was received in 45% yield. Since the yield seemed to be limited by the surface of the insoluble dioxime hydrochloride **7** formed in the first step of the reaction, it was attempted to dissolve **7** under reflux and then adding it dropwise to the aqueous base-solution. For this a procedure by *S. Claus* for the synthesis of 1,2,4,5-tetraaminobenzene from its respective hydrochloride was used.[85] However, **7** could not be dissolved in water even under reflux and using this reaction procedure no product could be isolated.

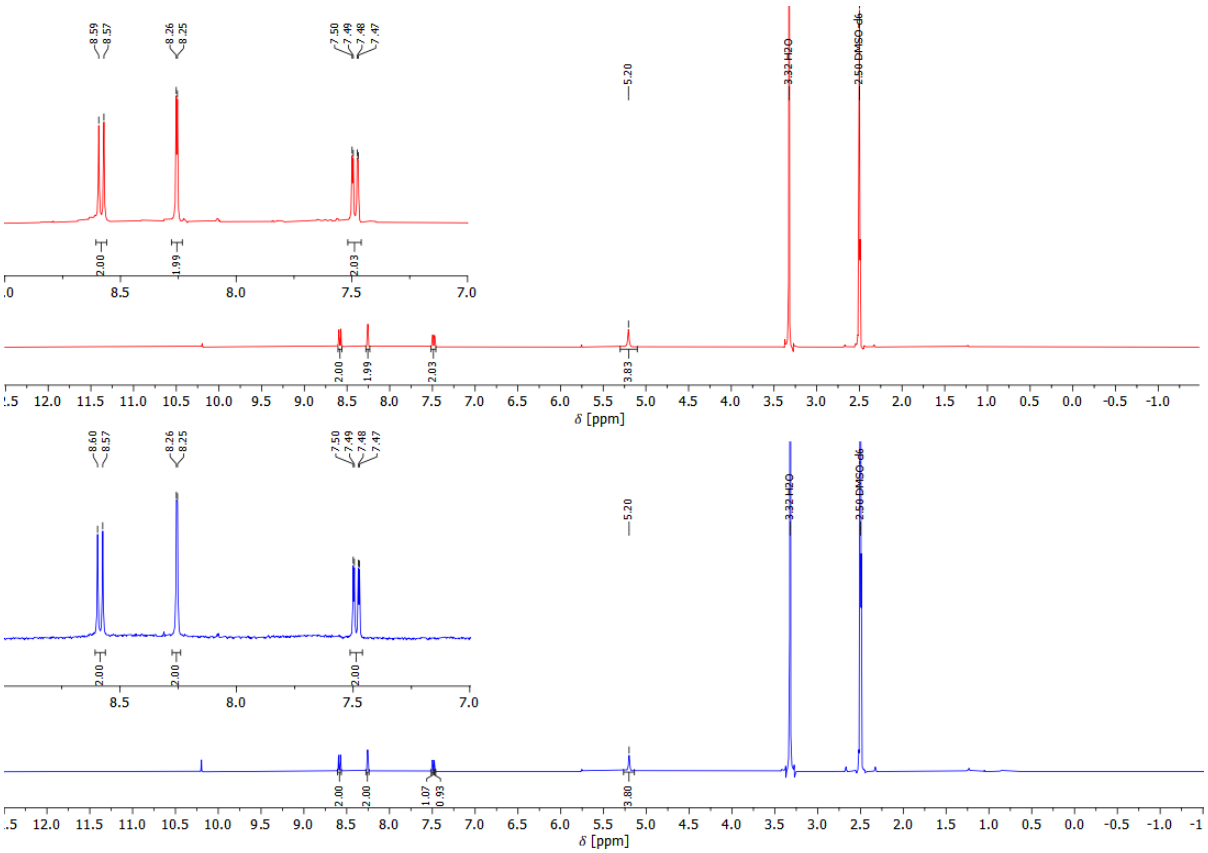

Figure 22: ^{1}H-NMR spectra of diamine **6** (400 MHz, DMSO-d6, 298 K) directly after the synthesis (upper spectrum/red) and after three months (lower spectrum/blue).

Moreover, it was found that diamine **8** was not as prone to undergo decomposition, as was first assumed. This can be seen when comparing the ^{1}H-NMR spectra for the compound directly after the synthesis and 3 months later after storing under ambient conditions (cp. Figure 22). The spectra were recorded in DMSO-d6, which is a good solvent for various organic substances, to ensure that any decomposed fragments of **8** would be observed in the NMR-spectrum. Both spectra are identical and no lowered reactivity of the compound was found after three months, i.e. the subsequent coupling reactions to the imine still gave the expected yields. Furthermore, for diamine **8** bromine had to be utilized as substituent allowing for the coupling with the angled rigid-rods via a *Sonogashira* cross-coupling, instead of iodine. This is due to the instability of iodine at the phenanthrene during the reduction of the respective dioxime to the 1,2-diamine leading to a mixture of one- and twofold de-iodinated species, which was observed during preliminary work performed for a Master's Thesis.[31] Hence, it is necessary for the *Sonogashira* cross-coupling to be carried out at elevated temperature (i.e. 80 °C) instead of room temperature and lower yields are to be expected,

because of the stronger carbon-bromine bond ($D°_{298}$[C-Br] = 285.0 ± 8 kJ/mol; $D°_{298}$[C-I] = 232.2 ± 13 kJ/mol).[86]

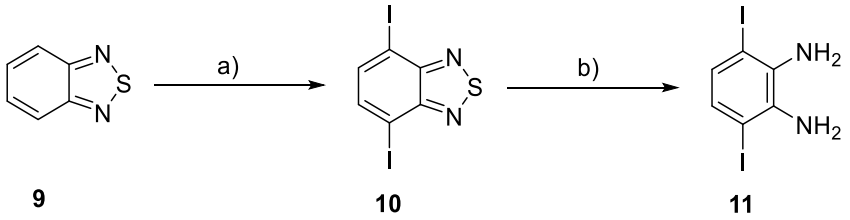

Scheme 4: Synthesis of benzenediamine **11**: a) I_2, Ag_2SO_4, conc. H_2SO_4 (95%), 70 °C, 18 h, 44%; b) $NaBH_4$, $CoCl_2$*$6H_2O$, THF:EtOH (1:3), reflux, 3 h, 33%.

Lastly, a smaller 1,2-diamine building block was synthesized from 2,1,3-benzothiadiazole (**9**) based on procedures by *S. Meißner*.[76,87] The chinoide character of the molecule allows for the selective two-fold iodination in position 4 and 7. This reaction was performed by stirring for 18 hours at 70 °C with iodine and Ag_2SO_4, yielding the product **10** in 44% after filtering off and washing with EtOH and toluene. This molecule could then be stored and directly before phenazine formation with a diketone, the 1,2-diamine could be deprotected by reductive sulfur extrusion. Since, this way the 1,2-diamine was freshly prepared before this condensation, lowered yields due to the known decomposition of the compound under air were mitigated.[87,88] For the deprotection, 4,7-diiodo-2,1,3-benzothiadiazole (**10**) was refluxed with $NaBH_4$ and cobalt(II) chloride hexahydrate in a mixture of THF:EtOH (1:3) for three hours. As was shown by *S. Meißner* only about 30% of the substrate is deprotected this way.[87] A separation of the remaining substrate, however, was possible using a flash-chromatography. This way, the amount of time for which the compound is under air compared to a column chromatography could be reduced, and therefore also reducing the proportion of the product **11**, that undergoes decomposition before being added to the condensation reaction with a derivative of diketone **2**. Moreover, the separation is facilitated by the pressure of the flash-chromatography system decreasing the tailing, i.e. the broadening of the back-half of a peak in an elugram of a separation method due to additional interactions exceeding the expected separation-mechanism. In this case the tailing is based on the secondary interactions of the polar amine-groups with the polar silicic acid groups of the stationary phase, i.e. the silica gel.

Mechanistically the deprotection of benzothiadiazole **10** is not yet fully clarified, but it is assumed that the 2,1,3-benzothiadiazole is adsorbed on the surface of an *in situ* formed

Co_2B-catalyst, increasing the electrophilicity of the imin-carbon. This facilitates the hydride-transfer from $NaBH_4$ followed by re-aromatisation and a hydride-mediated reductive splitting of the thiadiazole-ring.[88]

6.1.2 Synthesis of the angled Rigid-Rod Building Blocks

The first angled rigid-rod building block was already synthesized up to molecule **16** during preliminary work performed for a Master's Thesis and the synthesis was not further optimized in the scope of this work.[31] However, it shall be presented here for the sake of completeness. Its synthesis starts from the commercially available *tert*-butylaniline (**12**), which was twofold iodinated, by slow addition of iodine monochloride dissolved in conc. HCl (37%) to a solution of **12** at room temperature over one hour, subsequently stirring for another hour. After aqueous workup and purification via column chromatography, 2,6-diiodo-4-*tert*-butylaniline (**13**) was received in 88% yield.

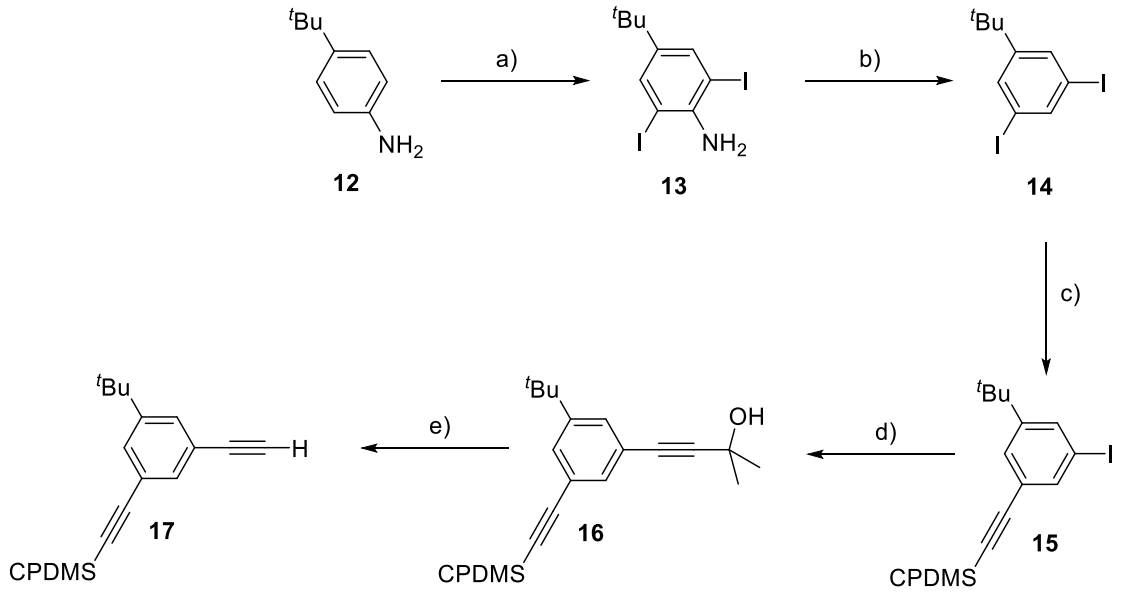

Scheme 5: Synthesis of the angled rigid-rod **17**: a) ICl, conc. HCl (37%), H_2O, r.t. 2 h, 88%; b) $NaNO_2$, conc. H_2SO_4 (95%), EtOH, reflux, 21 h, 61%; c) $PdCl_2(PPh_3)_2$ (cat.), PPh_3, CuI (cat.), CPDMS-acetylene, piperidine:THF (2:1), r.t., 18 h, 49%; d) $PdCl_2(PPh_3)_2$ (cat.), PPh_3, CuI (cat.), 2-methylbut-3-yn-2-ol, piperidine:THF (2:1), r.t., 18 h, 93%; e) NaOH (dry), toluene, reflux, 30 min, 61%.

A de-amination was then performed via generation of the diazonium-ion followed by a nitrogen extrusion. For this, **13** was refluxed in EtOH with $NaNO_2$ and conc. H_2SO_4 for 21 hours, whereby the extrusion of nitrogen could be observed as foam, forming in the

reaction mixture. After aqueous workup and purification via column chromatography 1-*tert*-butyl-3,5-diiodobenzene (**14**) was received in 61% yield. Since **14** is bearing two iodine substituents and the aimed molecule **16** shall be substituted by two different acetylenes, a statistical *Sonogashira* cross-coupling was necessary. Hence, upon coupling **14** with exactly one equivalent of an acetylene a product distribution ratio of 1:2:1 (substrate:product:twofold-byproduct) would be expected. When **14** was coupled with CPDMS-acetylene employing a catalyst system of $PdCl_2(PPh_3)_2$, CuI and PPh_3, as well as using piperidine as base, onefold-coupled product **15** was received in 49% (after acidic workup and purification via column chromatography, as for all following cross-coupling reactions). This result corresponded well to the expected maximal yield of 50%. Higher yields could have been achieved using a substrate bearing one bromine and one iodine substituent. Due to the lower reactivity of the bromine under *Sonogashira* cross-coupling conditions, as explained before, a selectivity towards the iodine is observed when performing such reactions at room temperature. However, since such a substrate analogous to **14** could only be attained by a longer synthetic route it was reasoned that the potential of increasing the total yield over all steps, compared to the work-effort, is minimal and thus this approach was not pursued further. **15** was then coupled with 2-methyl-but-3-yn-2-ol (formally an acetone protected alkyne, hence often named acetonide-protecting group) under the same conditions, giving the acetonide-protected angled rigid-rod **16** in 93% yield. These gradual protecting groups now allowed for a selective deprotection and this way refluxing **16** in dry toluene with dry NaOH for 30 minutes gave the final deprotected angled rigid-rod **17** in 61% yield. As was shown before by *S. Meißner*, when using these conditions to selectively deprotect the acetonide protecting-group in the presence of CPDMS- or trimethylsilyl- (short: TMS) protecting groups, the dryness of the reagents is of utmost importance.[87] This is due to the fact, that water will lead to the formation of hydrated OH^-, that can cleave the CPDMS- or TMS-protecting groups, thus reducing the yield of the selectively deprotected product **17**, while generating a byproduct with two deprotected acetylenes. This, however, is not observed when using TIPS-protecting groups as will be presented later in this work, since they exert a higher stability under these basic conditions.

The second angled rigid-rod synthesized, is structurally very similar to the first one, the only difference being the missing *tert*-butyl group. This synthesis was started from the commercially available 1-bromo-3-iodobenzene (**18**). Utilizing the bromo-iodo-selectivity in

Sonogashira cross-couplings, as mentioned above, the protected angled rigid-rod **19** was accessible in only one reaction. $PdCl_2(PPh_3)$, CuI and PPh3 were used as catalyst-system and piperidine and THF as base and solvent respectively. One equivalent of CPDMS-acetylene was added and the reaction mixture was stirred for 20 hours. Completion of the reaction was verified via thin-layer chromatography (short: TLC). Subsequently, two equivalents of 2-methyl-but-3-yn-2-ol were added and the reaction mixture was stirred at room temperature for another 22 hours. This way the protected angled rigid-rod **19** was received in 31% yield. This yield is lower than the 46% yield in which the first angled rigid-rod **16** was received over two steps, however the work-effort is minimized. Increasing the reaction temperature during the second step might increase the yield, however, due to the instability of the acetonide-protecting group under basic conditions and heat this was not attempted in the first approach.

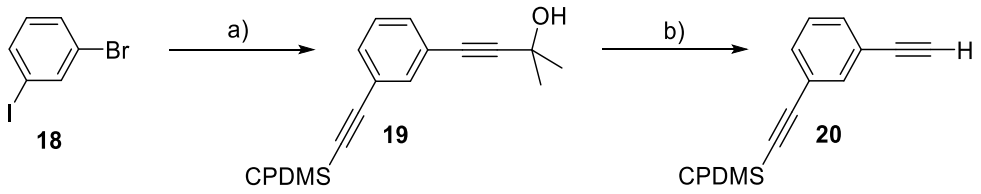

Scheme 6: Synthesis of angled rigid-rod **20**: a) $PdCl_2(PPh_3)_2$ (cat.), PPh_3, CuI (cat.), CPDMS-acetylene, piperidine:THF (2:1), r.t., 20 h, then 2-methylbut-3-yn-2-ol, r.t., 22 h, 31%; b) NaOH (dry), toluene, reflux, 30 min, 45%.

19 was deprotected using the same reaction conditions as before, yielding the deprotected angled rigid-rod **20** in 45%. To increase the yield of the selective deprotection of **16** and **19**, implementing an alternative to the acetonide-protecting group that provides a more complete orthogonality could be attempted in the future for similar reaction sequences. That could be realised using a trimethylgermanium-protected acetylene. This acetylene can be deprotected via a protodegermylation using 10-mol% CuBr in a mixture of THF and MeOH (1:1), while leaving TMS-protecting groups and their CPDMS-analogues intact.[89] However, also the cost of utilized reagents should be taken into consideration and this is why this alternative germanium-containing protecting-group was not applied in this work.

The third and last angled rigid-rod is bearing the alkyl-chains necessary for the adsorption of the desired PNTs on the HOPG surface. These are introduced as hexadecyloxy-chains via etherification. The first approach towards angled rigid-rod **30** was made starting with the twofold iodination of commercially available resorcinol **21**. Hence, iodine monochloride was

slowly added to **21** in Et_2O at 0 °C and then stirred for one hour at room temperature, giving 4,6-diiodoresorcinol (**22**) in 87% yield after aqueous workup and trituration in water for 30 minutes. Cooling and slow addition of the iodine monochloride were necessary due to its high reactivity. If the addition was performed to fast, lowered yields due to the formation of trifold iodinated byproduct was the consequence.

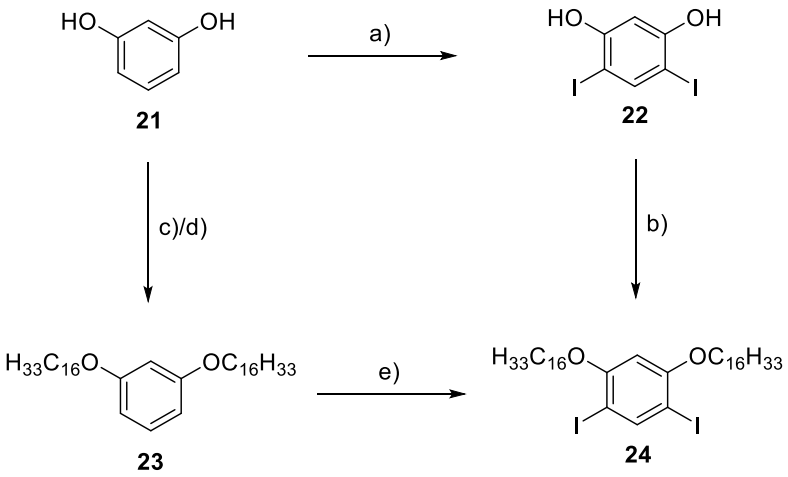

Scheme 7: Synthesis of alkoxylated diiodoresorcinol **24**: a) ICl, Et_2O, 0 °C, then r.t., 1 h, 87%; b) see Table 1; c) K_2CO_3 (anhydr.), KI (cat.), $BrC_{16}H_{33}$, acetone, reflux, 47 h, 66%; d) Cs_2CO_3, KI (cat.), $BrC_{16}H_{33}$, acetone, reflux, 46 h, 98%; e) NIS, DCM, 67 h, 91%.

For the following etherification to gain compound **24** several different procedures were performed to gain the product in higher yields (Table 1). First, a *Williamson*-etherification was performed refluxing **22** with 1-bromohexadecane, potassium carbonate and catalytic amounts of potassium iodide in acetone for 43 hours. Here, the more active and also more costly 1-iodohexadecane is generated *in situ* via a *Finkelstein*-reaction leading to the precipitation of the in acetone less soluble potassium bromide. In addition, the direct use of 1-iodohexadecane as a highly viscous substance is more difficult to handle because it has a melting point close to room temperature (21-23 °C). This way, product **24** was obtained in only 8% yield.

To increase this yield several different attempts were made. First, an excess of the more active 1-iodohexadecane was directly used instead of *in situ* generation, combined with the use of caesium carbonate instead of potassium carbonate, due to its higher solubility in organic solvents. This led to an increase in yield to 39%. Elongation of the reaction time to 3 days, however, led to no further significant increase giving **24** in 40% yield. When letting the

reaction reflux even further for five days, only 2% yield were isolated, due to de-iodination of the compound. The use of DMF as solvent to be able to increase the reflux temperature did not give a desired increase in yield either and only 10% of **24** could be obtained. Furthermore, other approaches like the use of tetra-*n*-butylammonium bromide as phase transfer catalyst in combination with potassium hydroxide as a stronger base, or the use of sodium hydride with 15-crown-5 to increase the nucleophilicity at the oxygen-atoms of resorcinol by full deprotonation and the formation of a solvent separated ion-pair with the counter-ion, did not lead to the expected increase in yield for this nucleophilic substitution reaction. In fact, no product could be isolated from these attempts.

Table 1: Different reaction conditions for the etherification of **22** and their respective yields.

Reagents	Solvent	Reaction Time	Yield [%]
$BrC_{16}H_{33}$, KI (cat.) K_2CO_3 (anhydr.)	acetone	43 h	8
$IC_{16}H_{33}$, Cs_2CO_3	acetone	44 h	39
$IC_{16}H_{33}$, Cs_2CO_3	acetone	3 days	40
$IC_{16}H_{33}$, Cs_2CO_3	acetone	5 days	2
$IC_{16}H_{33}$, Cs_2CO_3	DMF	3 days	10
$IC_{16}H_{33}$, NaH, 15-crown-5	THF	21 hours	- -
$IC_{16}H_{33}$, $^nBu_4^+Br^-$, KOH	Acetone/H_2O	3 days	- -

Since this rigid-rod was essential for all PNTs synthesized in this work to enable the adsorption on the HOPG surface and increase the solubility of the large rigid structures, a reliable large-scale synthesis was necessary. Because 40% yield in the second step of the synthesis hindered this aim, a different path to compound **24** was chosen. Hence, the order of the first reaction steps, i.e. iodination and etherification, was inverted. This approach was not chosen initially, due to the possibility of iodination of the alkoxy-chains. These byproducts would have been difficult to remove and thus a mild method for the iodination needed to be found. First, however, the etherification of resorcinol (**21**) was performed under the standard *Williamson*-etherification conditions, i.e. refluxing with 1-bromohexadecane, potassium carbonate and catalytical amounts of potassium iodide in acetone for 47 hours. This way, 1,3-bis(hexadecyloxy)benzene (**23**) was obtained in 66% yield. This result could then be

improved further to receive **23** in 98% yield by the use of caesium carbonate as base. Here, no column chromatography was necessary, since due to the high turnover only small amounts of the at room temperature liquid 1-bromohexadecane remained. These could then be removed together with the base and potassium salts by filtering off the product, which precipitated upon addition of cold water. Subsequent washing with water and acetone gave pure **23**, which then needed to be iodinated. A first attempt was the use of a protocol by *L. Emmanuvel et al.* for the *in situ* generation of iodine monochloride, by a system of sodium periodate, potassium iodide and sodium chloride.[90] This would be milder than its direct addition to the reaction mixture. Even though the formation of the dark red iodine monochloride was visible in the reaction mixture, no turnover could be observed via TLC and no product could be obtained. Hence another approach was taken inspired by a procedure by *L. Assies et al.* for the bromination of 1,3-bis(octadecyloxy)benzene.[91] Utilizing this procedure, **23** was stirred with *N*-iodosuccinimide at room temperature in DCM for 67 hours. After removing residual *N*-iodosuccinimide by trituration with MeOH for 15 minutes, the twofold iodinated product **24** was obtained in 91% yield. Upon upscaling of the synthesis, it was observed, that the use of larger amounts of DCM until the substrate was dissolved completely would lead to the formation of onefold iodinated product exclusively in a yield of 95%. This, in turn, could then be converted into **24** in 97% yield using it as a substrate under the same reaction conditions with a smaller amount of DCM as solvent. Henceforth, in larger scale **23** was then only suspended in DCM to retain the high concentration of the *N*-iodosuccinimide, that seemed to be essential and this way **24** was obtained in 91% when reacting 10 g of the substrate **23**. In conclusion, the improvements that were achieved by the different approaches presented above led to an increase of yield over these two steps from initially 7%, to 89% enabling a reliable upscalable synthetic basis for the synthesis of angled rigid-rod **30**.

Based on that, two acetylenes bearing different protecting groups, that allow for selective deprotection were coupled with the twofold iodinated species **24**. For this, a mostly statistically driven *Sonogashira* cross-coupling with TIPS acetylene was performed analogous to the one for the synthesis of angled rigid-rod **17**, presented before. Hence, **24** was reacted with TIPS-acetylene employing a catalyst system of $PdCl_2(PPh_3)_2$, CuI and PPh_3, as well as using piperidine as base. After acidic workup and purification via column chromatography, onefold coupled product **25** was received in 49% yield and also twofold product **26** could be obtained in 33% yield. The isolation of the twofold coupled product here was possible since

the TIPS-protecting group is not polar, whereas the CPDMS-protecting group used for the angled rigid-rod **17** is polar and due to its strong interaction with the stationary silica gel phase during the column chromatographic purification of the compound, the twofold coupled product could not be isolated there. But this also means that it is more difficult and time-consuming to separate the two products **25** and **26**. However, since here the isolation of twofold coupled product **26** was possible, this reaction gave a usable yield of 82%, because not only the 49% of the desired product **25**, but also the 33% of the side-product **26** could further be used to gain angled rigid-rod **30** over two steps (cp. Scheme 8).

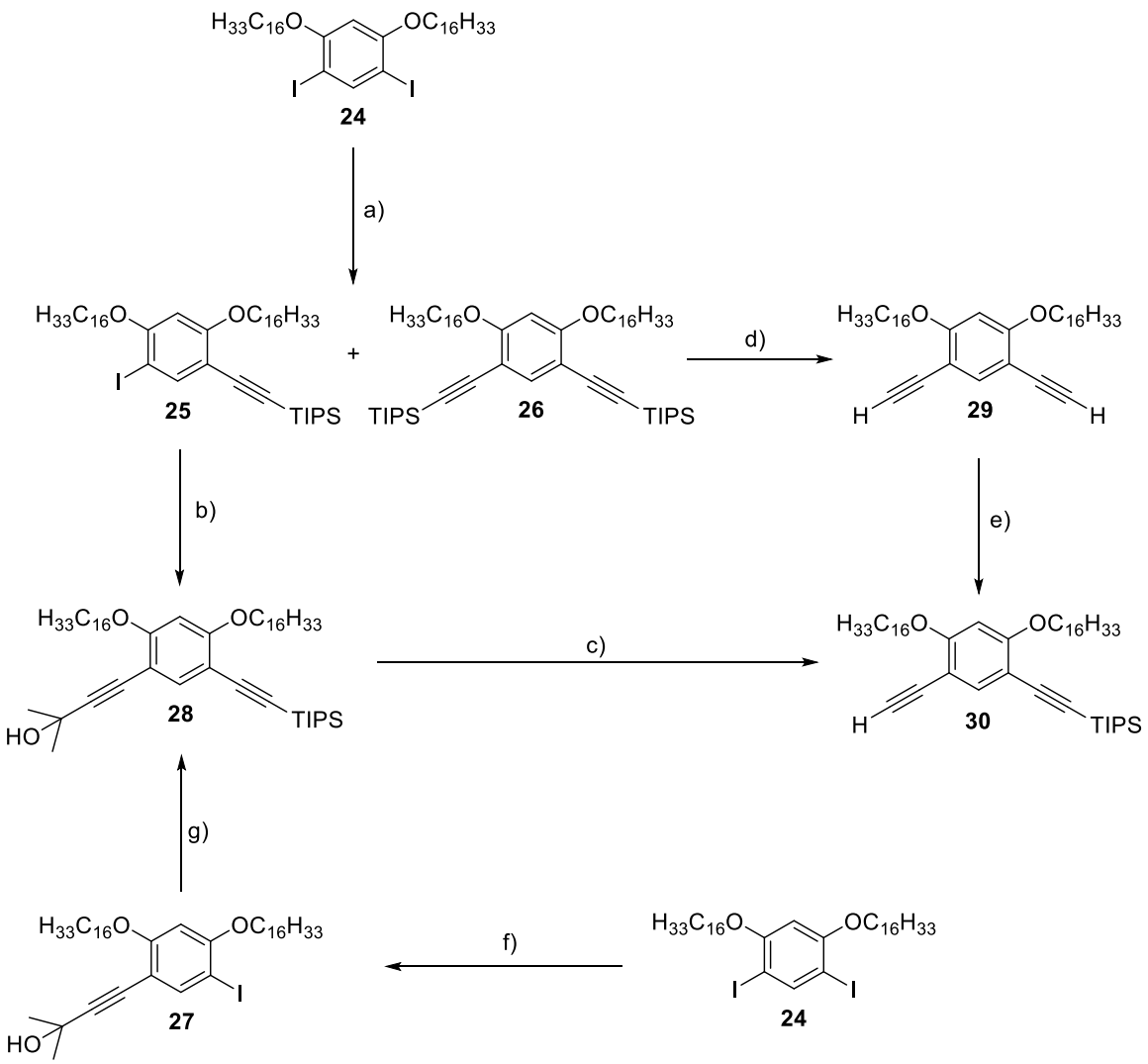

Scheme 8: Synthesis of angled rigid-rod **30**: a) $PdCl_2(PPh_3)_2$ (cat.), PPh_3, CuI (cat.),TIPS-acetylene, piperidine:THF (2:1), 35 °C, 20 h, 49% **25** and 33% **26**; b) like a), but with 2-methyl-but-3-yn-2-ol, r.t., 21 h, 77%; c) NaOH, toluene, reflux, 1 h, 96%; d) TBAF (1M in THF), THF, 35 °C, 3 h, 84%; e) EtMgBr (1M in THF), THF, TIPS chloride, 66 h, 40 °C, 30%; f) like a) but with 2-methyl-but-3-yn-2-ol, 40 °C, 23 h, 49%; g) like a) but 40 °C, 69 h, >99%.

For this purpose, **26** was fully deprotected by stirring with a tetrabutylammonium fluoride solution (1 M in THF) in THF at 35 °C for three hours, since a previous attempt of statistical deprotection with tetrabutylammonium fluoride and water also only yielded the completely deprotected product **29**. After termination of the reaction by addition of water and purification via column chromatography the deprotected species **29** was obtained in 84% yield. **29** was then reacted with ethylmagnesium bromide and TIPS chloride, stirring in dry THF at room temperature for 19 hours to give deprotected angled rigid-rod **30** in 30%. Using *n*-butyllithium instead to activate the acetylene gave **30** in only 8% yield.

Furthermore, onefold coupled product **25** was coupled with 2-methyl-but-3-yn-2-ol via a *Sonogashira* cross-coupling under the same conditions as presented above, giving the acetonide-protected angled rigid-rod **28** in 77% yield. Subsequently, **28** was refluxed with NaOH in toluene for three hours followed by column chromatographic purification. This led to the isolation of deprotected angled rigid-rod **30** in 96% yield. As explained before, in this case the reagents and solvent were not required to be dry due to the stability of the TIPS-protecting group under these conditions. Moreover, this explains the high yield of 96% over the lower yields of 61% and 45% for the other rigid rods bearing CPDMS-protecting groups, since there residual water leads to the formation of a completely deprotected byproduct. These CPDMS-protecting groups, however, are necessary at some angled rigid-rods to provide the ability of selective deprotection, i.e. of CPDMS-protecting groups in the presence of TIPS-protecting groups, at the stage of the completed respective H-shaped monomer (cp. 4.4 Preliminary Work).

Since the usefulness of being able to isolate **26** was reduced by the fact that the yields over two steps to gain **30** were only 25% and the separation of **25** and **26** was tedious and time consuming, another approach towards deprotected angled rigid-rod **30** was chosen by inversion of the order in which the two acetylenes are coupled to **24**. This way a twofold coupled product would not be isolatable, due to reasons explained above. However, the easy purification outweighed the inability to gain the twofold product with its limited usefulness. Hence, **24** was coupled statistically via a *Sonogashira* cross-coupling with 2-methyl-but-3-yn-2-ol using the same catalyst system as described above giving the onefold coupled product **27** in the expected 49% yield. Then, **27** was coupled in another *Sonogashira* cross-coupling and **28** was obtained in >99% yield. Comparing this approach with the first one (including the additional yield of **30** obtained from the twofold coupled

product **26**), the yield over the three steps was slightly increased from 44% to 47%, whilst simultaneously increasing time efficiency and lowering the work-effort. Considering the whole synthesis of angled rigid-rod **30** all improvements and changes to the synthetic route led to an increase of the overall yield starting from 3%, to 42% over 5 steps. This is close to the maximally achievable yield of 50%, taking into consideration that a statistical reaction is part of this sequence.

6.1.3 Coupling of the Building Blocks to the H-shaped Monomers

Based on the reliable syntheses developed for the building blocks, several different H-shaped monomers, that lead to different PNTs were attainable. The first couplings of the building blocks were performed with the aim of synthesizing an H-shaped monomer, that would give cylindrical structures upon oligomerisation.

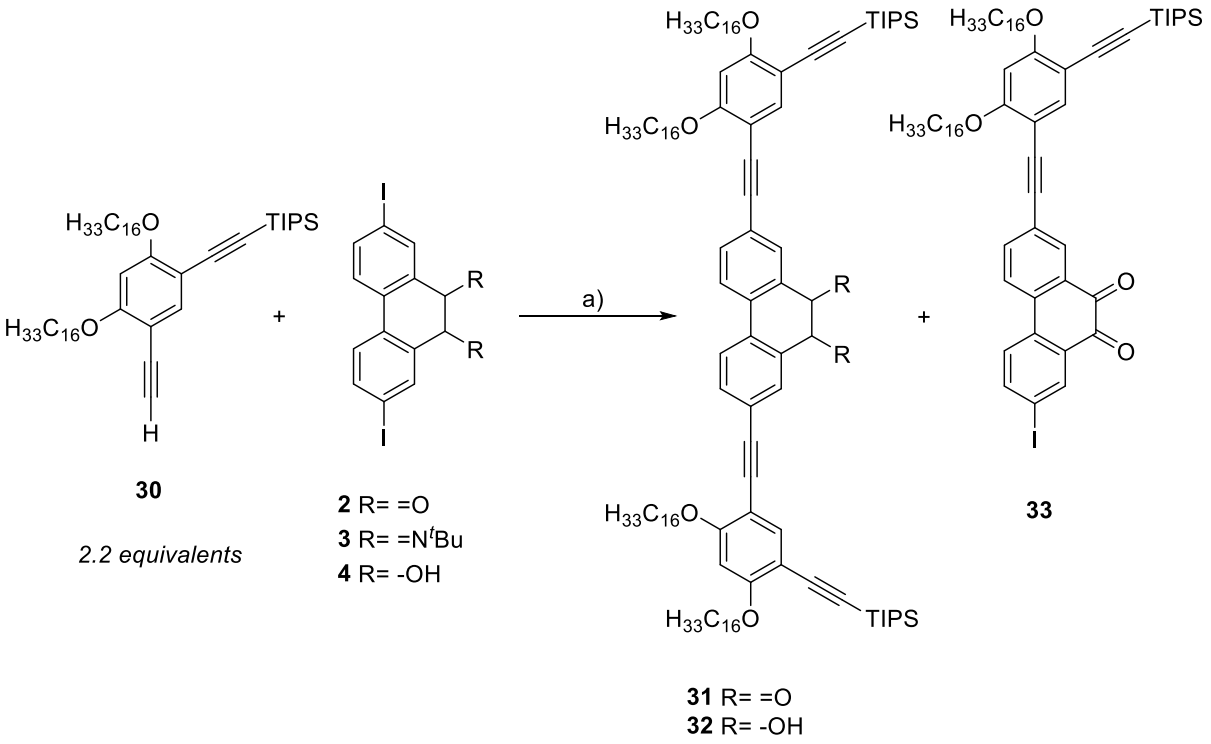

Scheme 9: Synthesis of the U-shaped diketone **31** and the U-shaped diol **32**: a) see Table 2.

The synthesis of this H-shaped monomer **I** was started by coupling 2,7-diiodophenanthrenequinone (**2**) with deprotected angled rigid-rod **30** via a *Sonogashira* cross-coupling performed under the same conditions as during the synthesis of

30. However, only 15% of the desired twofold coupled U-shaped diketone **31** together with 29% of the onefold coupled byproduct **33** could be obtained. In a second attempt the reaction was performed at 80 °C to increase the reactivity of the substrate, facilitating the insertion of palladium into the carbon-iodide bonds. However, this resulted in no isolatable product or substrate, due to de-iodination of the substrate. Additionally, employing onefold coupled byproduct **33** in another *Sonogashira* cross-coupling with 2.5 equivalents of deprotected angled rigid-rod **30**, U-shaped diketone **31** was obtained in 50% yield. The remaining unreacted rigid-rod **33** could be isolated as *Glaser*-byproduct in every attempt, i.e. coupled with itself by a *Glaser* reaction probably due to residual oxygen (which is often observed to some extent for *Sonogashira* cross-couplings, even though they are performed under an inert-gas atmosphere). It was reasoned from this, that the *Sonogashira* cross-coupling was inhibited in some way that would lead to the faster formation of *Glaser*-byproduct, than coupling of the components.

Table 2: Reaction conditions for the *Sonogashira* cross-couplings leading to the U-shaped diketone **31** and the U-shaped diol **32**.

Substrate	Catalyst-System	Reaction Time / Temperature	Product	Yield [%]
2	$Pd(PPh_3)_4$, CuI	18 h / r.t.	**31**	15%
			33	29%
2	$PdCl_2(PPh_3)_2$, PPh_3, CuI	17 h / 80 °C	**31**	- -
			33	- -
2	$Pd(OAc)_2$, *XPhos*, CuI	19 h / r.t.	**31**	12%
			33	26%
4	$Pd(OAc)_2$, *XPhos*, CuI	20 h / 40 °C	**31**	7%
			32	- -
3	$PdCl_2(PPh_3)_2$, PPh_3, CuI	20 h / 40 °C	**31**	62%
			33	29%

Hence, in a next attempt, a more reactive catalyst system was chosen with $Pd(OAc)_2$ and the *XPhos* ligand. This choice was based on reactivity studies for *Sonogashira* cross-couplings, that have shown the increase of reactivity with increasing *Tolman* cone angle, i.e. the angle swept by a cone that encloses all ligand groups with the vertex at the metal-centre as a

measure for the steric bulk of a ligand.[92] The higher reactivity of this catalyst system compared to the PPh_3 ligand is hence based on the larger *Tolman* cone angle of 256 ° for *XPhos*, compared to 145 ° (these values were determined in a (Ligand)AuCl model system).[93] Moreover, *XPhos* is also air-stable and comparably low-priced with regard to other highly reactive phosphine ligands. $Pd(OAc)_2$ was chosen as palladium source via *in situ* reduction of Pd(II) to Pd(0), because other methods of formation of an active $(XPhos)_2Pd(0)$-complex have severe deficiencies.[94] The use of the air-stable palladium(0) $Pd_2(dba)_3$ catalyst for example, fails to deliver the aimed at active complex, due to the strong coordination of the disbenzylideneacetone (short: dba) ligand, hence leading to a lowered reactivity.[94,95] Though, this approach, utilizing a more reactive catalyst system did also not lead to an improvement in yield for this reaction, it will be employed at a later stage of the synthesis when performing the *Sonogashira* cross-couplings with the aryl-bromide substrates, which are innately less activated.

It has to be mentioned that low yields for *Sonogashira* cross-couplings with phenanthrenequinones like **2** and related 1,2-dikteones are known and the low reactivity can be mitigated by adding a large excess of the acetylene compound, i.e. six equivalents or more compared to the 2.2 equivalents used here.[85] This, however, was not possible, because no commercially available acetylenes like TIPS-acetylene were used, but costly acetylenes, that had to be synthesized over multiple steps. Furthermore, masking the 1,2-diketone unit before the *Sonogashira* cross-coupling and regaining the groups afterwards via deprotection has shown to increase the yield.[96,97] One possible issue causing the low yield could be the low solubility of quinone **2**. So, it was envisioned, that reduction to the alcohol before the *Sonogashira* cross-coupling and re-oxidation afterwards in a mild fashion tolerating the alkynes, e.g. by the use of the *Dess-Martin* periodinane would be possible. This should result in a higher overall yield, if reduction and oxidation could be performed efficiently, even though two synthetic steps were added. After reduction to the alcohol in 91% (cp. 6.1.1 Synthesis of the Central Spacer Building Blocks), **4** was coupled under the optimized *Sonogashira* cross-coupling conditions. However, even though **4** showed good solubility, the yields were still poor. Additionally, instead of the expected U-shaped diol **32** only 7% of the oxidized product U-shaped diketone **31** were isolated, making the re-oxidation obsolete, and no higher total yield was attainable by this approach.

This way, it became obvious that solubility was not the only factor contributing to the inhibition of the *Sonogashira* cross-coupling and leading to the formation of the *Glaser*-byproduct in large quantities. It was assumed in the literature, that the oxidative-addition in the *Sonogashira* cross-coupling mechanism can be hindered by coordination of a 1,2-diketone unit as a good ligand for the palladium(0)-catalyst.[97] Hence, 1,2-diketone **2** was protected as a ketal using 1,2-ethandiole. It was shown by *S. Claus* before utilizing such ketals to increase the yield obtained in *Sonogashira* cross-couplings of the related 4,5,9,10-pyrenetetrone, that the ketal formation under standard conditions using an inverse *Dean-Stark*-apparatus gave only low yields and a mixture of products bearing different amounts of ketals and ketones was isolated.[85] Because of this, a more recent procedure was used, heating both components with (1*S*)-(+)-camphorsulfonic acid in MeOH in a microwave reactor at 120 °C for three hours. After aqueous workup and purification via column chromatography, the pure twofold ketal **34** was still only gained in 9% yield.[98]

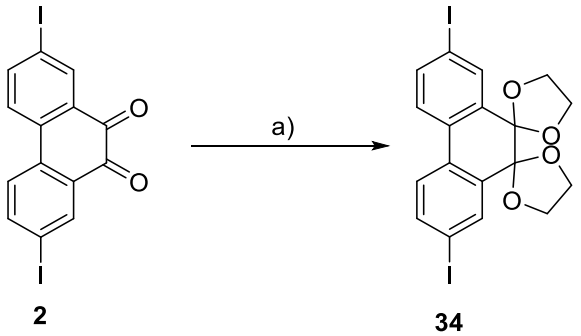

2 **34**

Scheme 10: Synthesis of 1,2-diketal **34**: a) 1,2-ethanediol, (1*S*)-(+)-camphorsulfonic acid, *microwave*, 120 °C, 3 h, 9%.

Based on this, another approach was chosen, using an imine to protect the 1,2-diketone group. Since an imine-bond formation was planned to connect the two central-spacer building blocks at a later stage, it was of general interest for this work to obtain such imines in high yields. Additionally, other known protecting groups, like the formation of a *tert*-butyl-dimethylsilyl ether, would not allow for selective deprotection with respect to the TIPS-protected acetylene-groups at angled rigid rod **30**.[96] The synthesis of a *tert*-butylimine was chosen, since on the one hand it would increase the molecules solubility and also the steric bulk lowering its ability to act as a ligand for the palladium. On the other hand, it should not be as difficult to cleave after the *Sonogashira* cross-coupling compared to the stable

aromatic amines, that would be used to form the phenazine-unit connecting the central-spacer building blocks at a later stage.

After phenanthrenediimine **3** was successfully synthesized and gave a mixture of *E/Z*-isomers in 70% yield, it was coupled under the initially used *Sonogashira* cross-coupling conditions. This way 62% of the desired twofold coupled U-shaped diketone **31** together with 29% of the onefold coupled byproduct **33** could be obtained directly, since the imine was easily cleaved during the acidic workup of the reaction. This could also be tracked by the colour change of the reaction solution from orange to violet (cp. Figure 23). Hence, no further deprotection step was necessary for the imine-cleavage, directly increasing the yield of U-shaped diketone **31** by 47% compared to the coupling with the diketone **2**, with substrate **3** being readily available in two steps from the commercially available phenanthrenequinone (**1**).

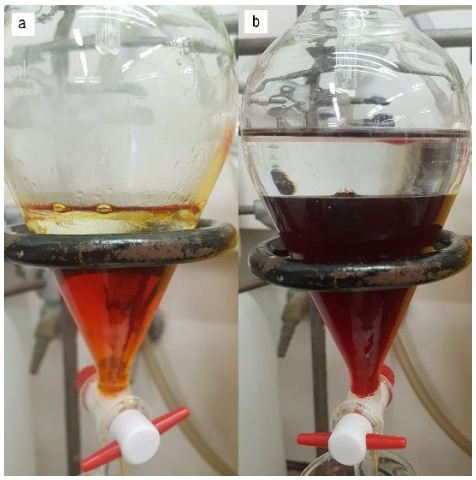

Figure 23: Coloured reaction solution in DCM, under colourless aq. HCl (10%): a) before shaking the separatory funnel; b) after shaking the separatory funnel; the colour change is caused by the cleavage of the imine generating U-shaped diketone **31**.

In a first attempt the U-shaped diketone **31** should then be coupled with 2,7-dibromophenanthrene-9,10-diamine hydrochloride (**7**) to generate the U-shaped phenazine **35**. Utilizing a standard procedure for this, **31** was refluxed with **7** in EtOH together with acetic acid as catalyst for 20 hours. However, this way no product could be isolated, but gratifyingly 84% of **31** were obtained after aqueous workup and purification via column chromatography. Since during the reaction, it was observed that **7** did not dissolve, in a second attempt $CHCl_3$ was used instead of EtOH in an effort to maintain similar reaction temperatures, while concurrently improving the solubility of **7** in the reaction mixture. However, again only the substrate **31** was isolated after refluxing for 24 hours. The coupling

conditions were then changed from acid- to base-catalysis using Et_3N instead of AcOH. So, when refluxing **31** and **7** with Et_3N in THF for 23 hours, the desired product U-shaped phenazine **35** was obtained in 28%. During this reaction it was observed, that **7** completely dissolved in the reaction mixture. Hence, the success of the procedure was attributed to the release of the free 1,2-diamine **8** from the hydrochloride salt via the Et_3N base.

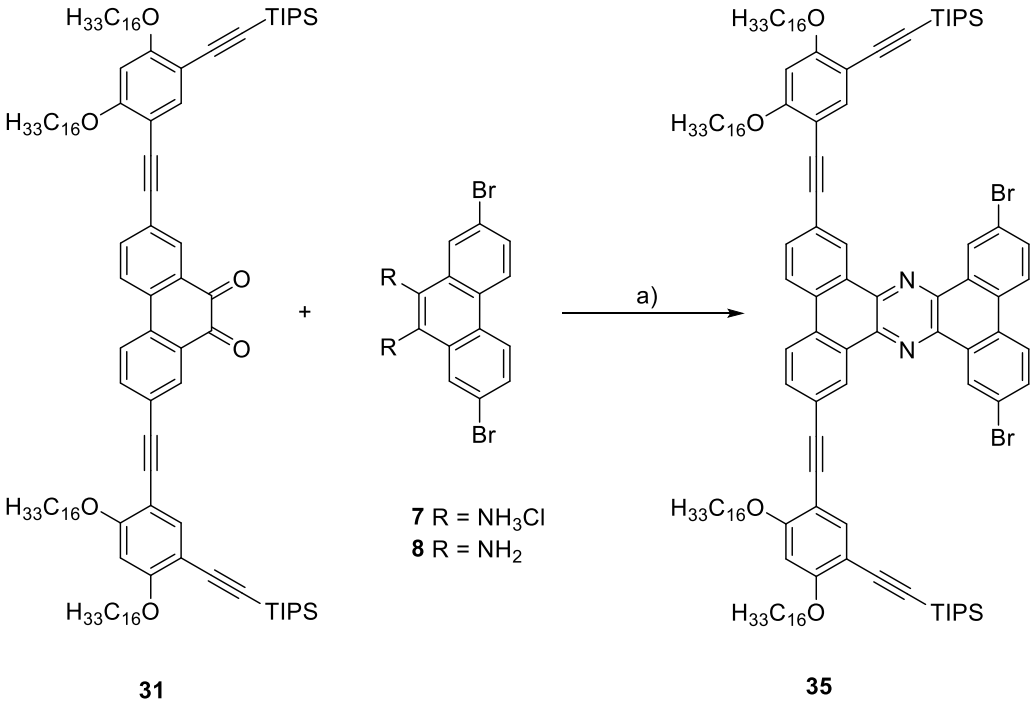

Scheme 11: Synthesis of U-shaped phenazine **35**: a) see Table 3, reflux, 24 h.

Additionally, preliminary work on the formation of aromatic imines, i.e. phenazines, from related structures by *S. Claus* showed, that acidic coupling conditions usually gave higher yields.[85]

Table 3: Reaction conditions for the condensation of U-shaped diketone **31** to U-shaped phenazine **35**.

Substrate	Solvent	Catalyst	Yield [%]
7	EtOH	AcOH	- -
7	$CHCl_3$	AcOH	- -
7	THF	Et_3N	28
8	$CHCl_3$	AcOH	58
8 (2 eq.)	$CHCl_3$	AcOH	92

Based on this, it was envisioned that deliberately synthesizing 2,7-dibromophenanthrene-9,10-diamine (**8**), which should have a better solubility than **7**, and then performing the phenazine formation via acid catalysis should give higher yields. Indeed, this way **35** was obtained in 58%.

Furthermore, when using two equivalents of 1,2-diamine **8** to compensate for decomposition of the compound under acidic conditions at the elevated temperatures the yield was increased to 92%. The excess use of the 1,2-diamine **8** posed no challenge during separation from the product via column chromatography, due to its high polarity compared to the relatively unpolar phenazine **35**, bearing four hexadecyloxy-chains. Hence, this crucial coupling step in the synthesis of H-shaped monomer **I** could now be performed without a large loss of material allowing to obtain **I** on the semi gram scale after two further steps. Moreover, due to the unexpected stability of **8** (cp. 6.1.1 Synthesis of the Central Spacer Building Blocks), long-term storage was possible without posing further challenges.

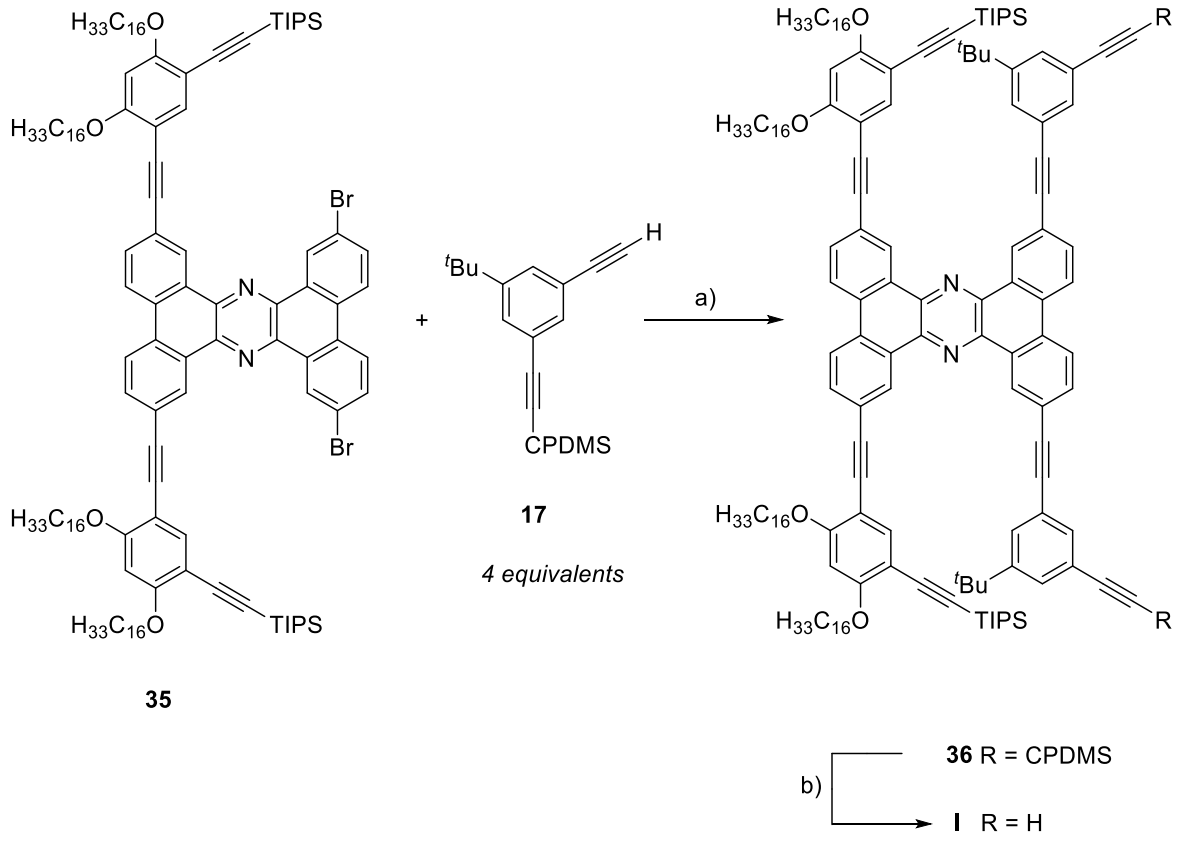

Scheme 12: Synthesis of the H-shaped monomer **I**: a) $Pd(OAc)_2$ (cat.), *XPhos*, CuI (cat.), piperidine:THF (2:1), 80 °C, 20 h, 67%; b) K_2CO_3 (anhydr.), MeOH:THF (1:2), r.t., 24 h, >99%.

Phenazine **35** was then coupled with **17** via a *Sonogashira* cross-coupling employing the $Pd(OAc)_2$, *XPhos* catalyst system, due to its advantages explained before. A highly reactive catalyst system was necessary for this reaction on the one hand due to the sterically demanding substrate **35** and on the other hand, since an aryl bromide was used, which is lower in reactivity compared to an aryl iodide (cp. 6.1.1 Synthesis of the Central Spacer Building Blocks). Additionally, this is why the reaction also had to be performed at elevated temperature, i.e. 80 °C. Furthermore, four equivalents of alkyne **17** were used, to compensate for the expected increase in formation of *Glaser*-byproduct based on the high reaction temperature, as well as the lowered reactivity of **35**. This way the protected H-shaped monomer **36** was obtained in 67% yield after acidic workup and purification via column chromatography, which was a satisfactory result in the context of the challenges this reaction posed. **36** was then stirred with anhydrous K_2CO_3 in MeOH:THF (1:2) at room temperature for 24 hours. Hereby, the CPDMS-protecting groups were cleaved selectively and the final product H-shaped monomer **I** was received in >99% yield after aqueous workup and column chromatographic purification, demonstrating the effectiveness of this modular approach towards new H-shaped molecules (cp. 4.4 Preliminary Work).

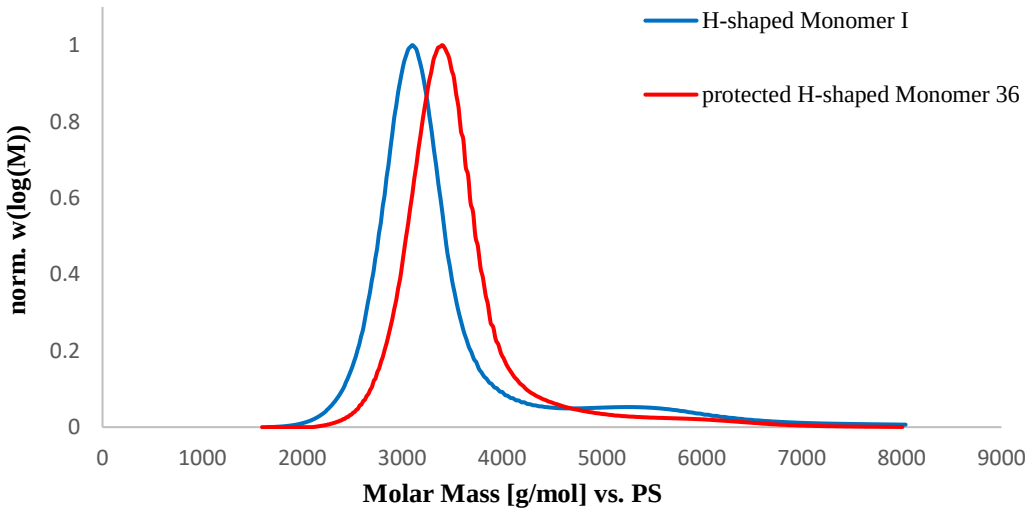

Figure 24: Molar mass distribution of the GPC-analysis of protected H-shaped monomer **36** (red) and H-shaped monomer **I** (blue); calibrated against a polystyrene standard.

The purification of **36** and **I** was greatly facilitated due to the large change in polarity of the molecules during these last two reactions, based on the use of the CPDMS-protecting group.

This group can be seen as a polar analogue to the TMS-protecting group regarding its stability and by utilizing it **I** was gained in a pure form, which is important to get reliable results during the following oligomerisation to the nanotubular structures. Hence no further time-consuming purification via recGPC was necessary.

After the successful synthesis of the first H-shaped monomer **I**, a second one was synthesized, which should give rise to pyramidal structures after oligomerisation and adsorption of the structures to HOPG (cp. 5 Aim of this Work; Figure 21). For the synthesis of this H-shaped monomer **II**, previously synthesized U-shaped diketone **31** was coupled by condensation with benzenediamine **11** to give U-shaped phenazine **37**. Due to **11** being prone to undergo decomposition under ambient conditions, it was freshly prepared and immediately used after purification. Hence, employing the optimized reaction procedure for the formation of the phenazine, gained by the experiments performed during the synthesis of H-shaped monomer **I**, both compounds were refluxed in $CHCl_3$ with AcOH as acid catalyst for 20 hours. This way, U-shaped phenazine **37** was obtained in 94% yield.

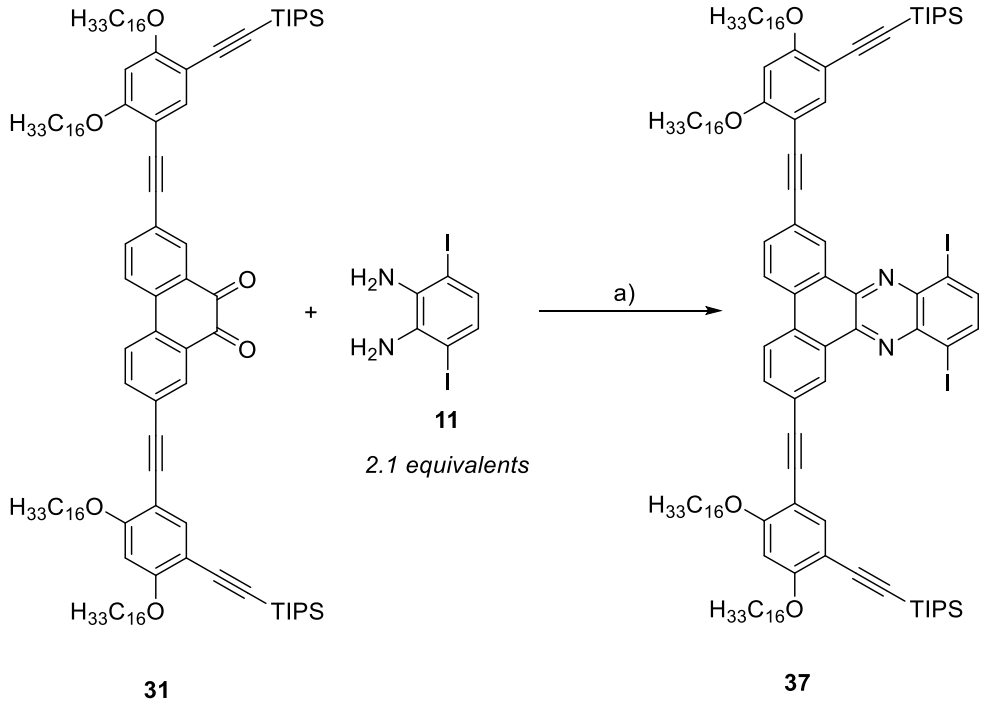

31 **37**

Scheme 13: Synthesis of the U-shaped phenazine **37**: a) AcOH, $CHCl_3$, reflux, 20 h, 94%.

Afterwards, U-shaped phenazine **37** was coupled with angled rigid-rod **20** via a *Sonogashira* cross-coupling. The only difference in structure of **20** compared to the

previously used angled rigid-rod **17** is the omitted *tert*-butyl group. This change was made, since it was envisioned, that the pyramidal PNTs formed from H-shaped monomer **II** might be able to form molecular stacks via self-assembly on the HOPG surface and the *tert*-butyl group would increase steric hinderance regarding this stacking possibility. Moreover, the *tert*-butyl group was initially introduced to increase the solubility of the rigid monomer. However, it was assumed that the increased solubility provided by the four hexadecyloxy-chains should be sufficient, as H-shaped monomer **I** showed even good solubility in polar protic solvents like MeOH, despite its nonpolar nature.

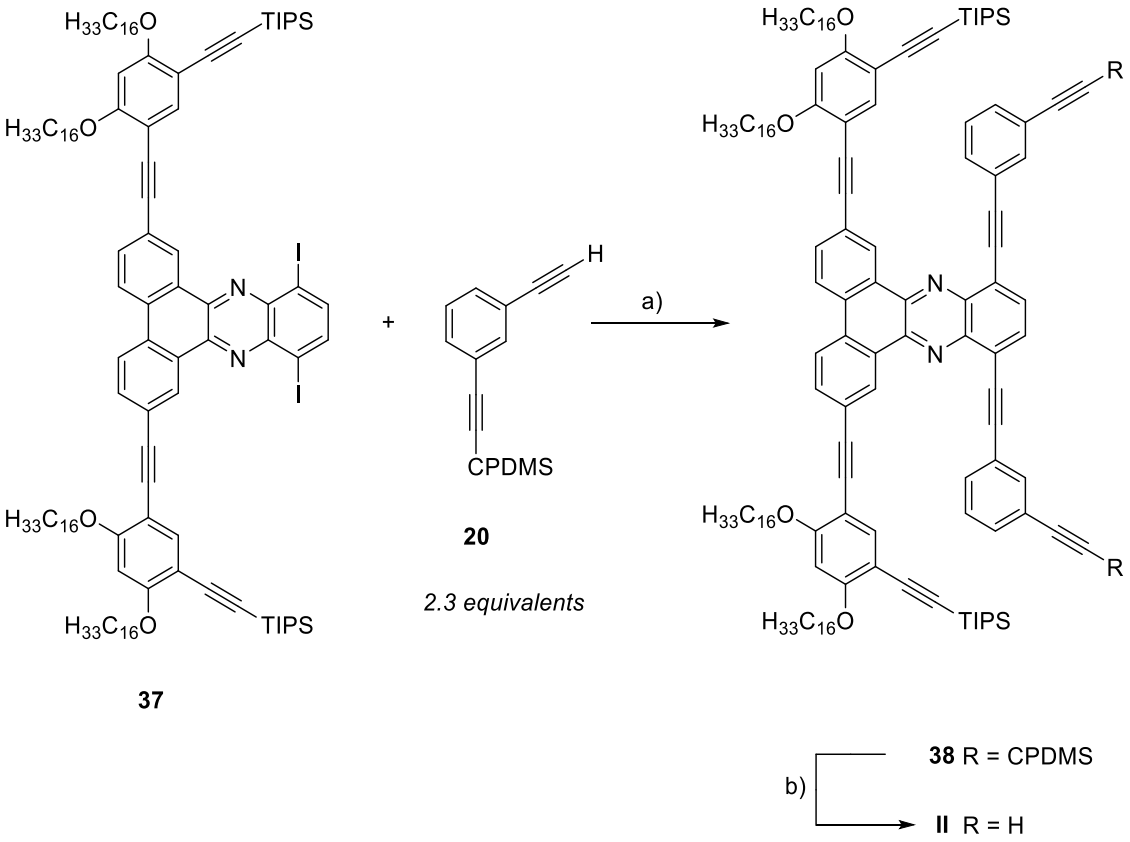

Scheme 14: Synthesis of the H-shaped monomer **II**: a) $Pd(OAc)_2$ (cat.), *XPhos*, CuI (cat.), piperidine:THF (2:1), 40 °C, 68 h, 57%; b) K_2CO_3 (anhydr.), MeOH:THF (1:2), r.t., 24 h, >99%.

Hence, **37** and **20** were stirred with $Pd(OAc)_2$, *XPhos* and CuI in piperidine:THF (2:1) at 40 °C for 68 hours, giving protected H-shaped monomer **38** in 57% yield. This yield is slightly lower than that achieved for protected H-shaped monomer **36**, even though here a more reactive aryl iodide was used. This contrary observation might be the result of steric hindrance, as the pairs of angled rigid-rods are closer to one another, due to the smaller

1,2-diamine unit. However, since no elevated temperatures were necessary here, it was also decided to only use 2.3 equivalents of **20** instead of the four equivalents used in the synthesis of **36**, which might have contributed to the lowered yield. The CPDMS-protecting groups of **38** were then selectively cleaved analogously to the synthesis of H-shaped monomer **I**, giving **II** in the same yield at comparable scales. Like for **I**, no further purification via recGPC was necessary (cp. 11 Appendix; Figure 71).

The synthesis of the last H-shaped monomer **III**, to gain bowl-shaped structures after oligomerisation and adsorption to HOPG starts with the coupling of phenanthrenediimine **3** and angled rigid-rod **17** via a *Sonogashira* cross-coupling using the standard catalyst system of $PdCl_2(PPh_3)_2$, PPh_3 and CuI, that was also previously utilized for the synthesis of U-shaped diketone **31**. Hence, when stirring the compounds in piperidine:THF (2:1) at 40 °C for 24 hours, U-shaped diketone **39** was formed. As observed before, the *tert*-butylimine was cleaved during the acidic workup and the product was isolated in 51% yield after purification via column chromatography.

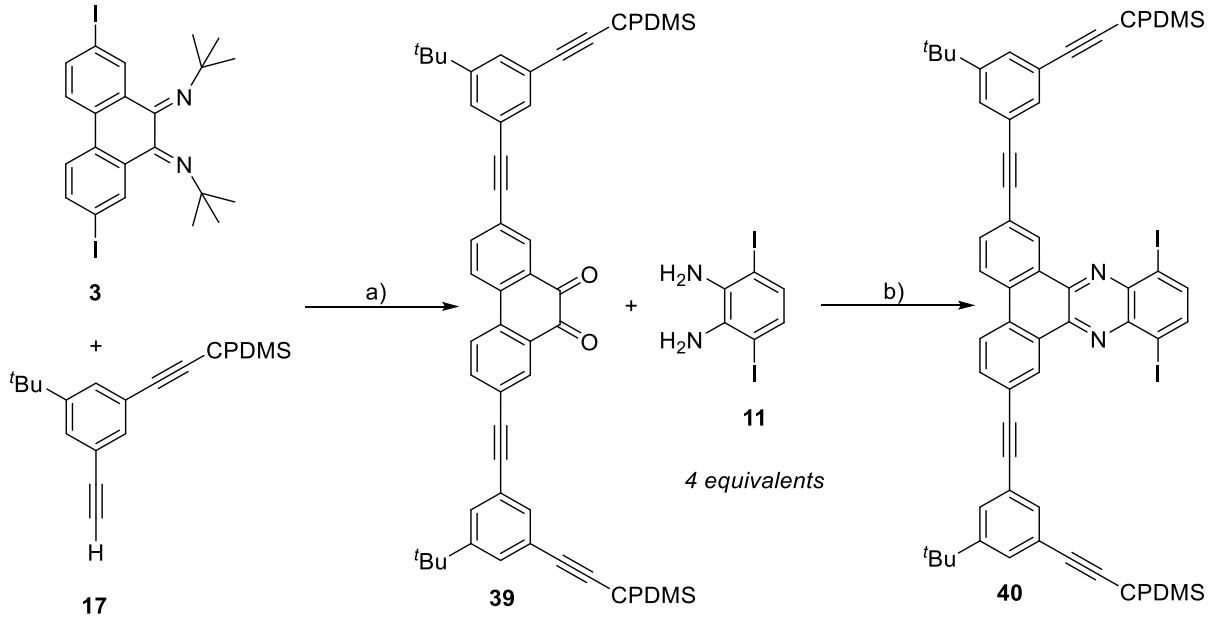

Scheme 15: Synthesis of U-shaped phenazine **40**: a) $PdCl_2(PPh_3)_2$ (cat.), PPh_3, CuI (cat.), piperidine:THF (2:1), 40 °C, 21 h, 51%; b) AcOH, $CHCl_3$, reflux, 23 h, >99%.

The lower yield compared to the synthesis of **31** is most likely due to the high polarity of this compound bearing two CPDMS-protecting groups and no nonpolar and solubility promoting

hexadecyloxy-chains, which made it difficult to obtain all of **39**, due to the strong interaction with the polar SiO_2-stationary phase used for column chromatography. Moreover, no onefold coupled product could be isolated. Angled rigid-rod **17** was chosen instead of angled rigid-rod **20**, since here the increased solubility from the *tert*-butyl group is important, since no hexadecyloxy chains are yet installed at the central spacer. Additionally, the bowl-shaped nanotubular structures gained from H-shaped monomer **III** were not designed to stack on the HOPG surface, but to serve as host-molecules for fullerene-guests. Hence, sterically hindering stacking of the bowl-shaped PNTs by the presence of the *tert*-butyl group was desirable. Diketone **39** was then coupled with 1,2-diamine **11** under conditions analogous to the phenazine formations previously presented. However, here four equivalents of the 1,2-diamine were used, to test, if that would increase the yield even further. Indeed, after refluxing both substrates in $CHCl_3$ with an AcOH acid catalyst for 23 hours, U-shaped phenazine **40** was isolated in >99% yield.

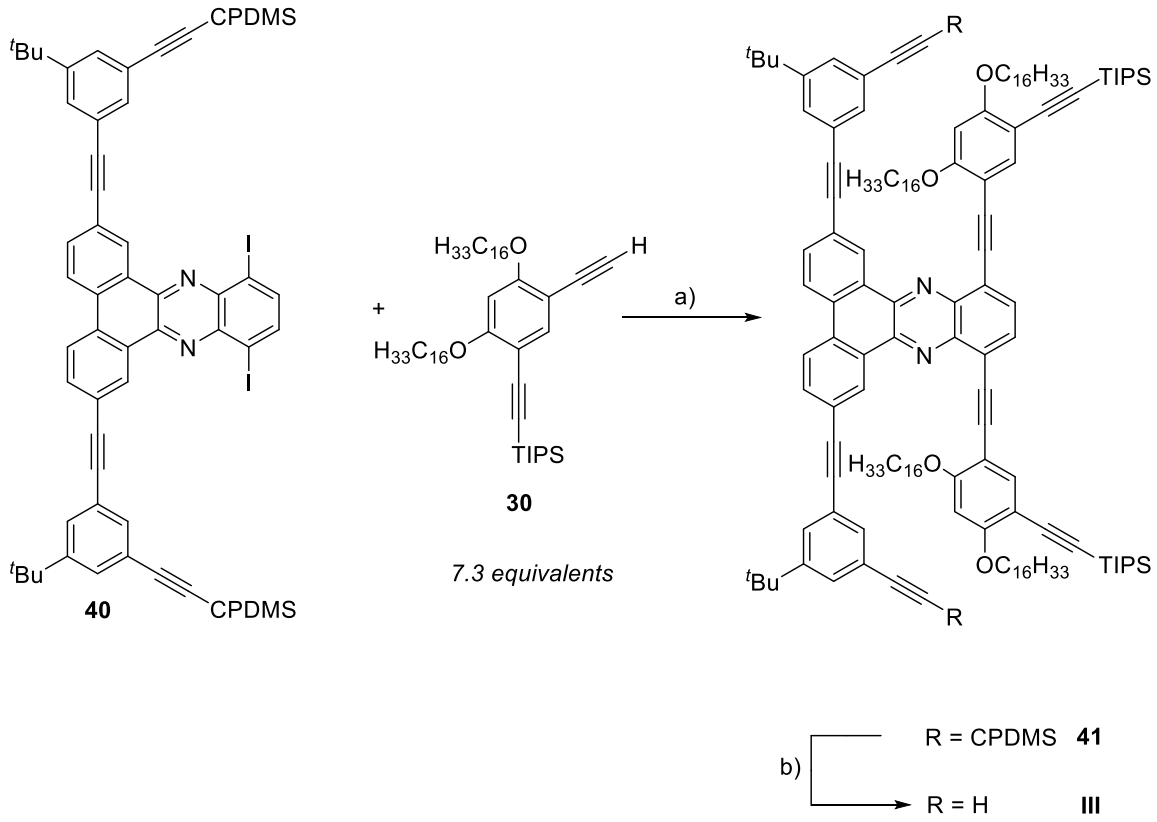

Scheme 16: Synthesis of the H-shaped monomer **III**: a) $Pd(OAc)_2$ (cat.), *XPhos*, CuI (cat.), piperidine:THF (2:1), 40 °C, 45 h, 66%; b) K_2CO_3 (anhydr.), MeOH:THF (1:2), r.t., 23 h, >99%.

Afterwards, **40** was coupled with angled rigid-rod **30** in a similar fashion as for the previous H-shaped monomers. Thereby, using $Pd(OAc)_2$, *XPhos* and CuI as catalyst system and stirring the substrates in piperidine:THF (2:1) at 40 °C for 45 hours, protected H-shaped monomer **41** was received in 66% yield. The yield is comparable to the previous couplings to the other protected H-shaped monomers. However, in this reaction the angled rigid-rod **30** was used in an excess (7.3 eq.), to mitigate the expected lowered yield due to the steric hinderance of the hexadecyloxy-chains of **30**. This hinderance resulted from the close spatial proximity of the aryl iodide to the already attached angled rigid-rods at **40**. The CPDMS-protecting groups of protected H-shaped monomer **41** were then cleaved under the same conditions discussed for the other H-shaped monomers, giving **III** in the same yield on comparable scales. Like for **I** and **II**, no further purification via recGPC was necessary (cp. 11 Appendix; Figure 72). In contrast to the other H-shaped monomers, in this case the deprotected alkynes are located at the angled rigid-rod, that will form the larger SPM of the nanotubular structures in the *Glaser* coupling. In how far the size of the SPM coupled first during the *Glaser* coupling affected the yield of the different possible oligomers will be discussed in the following chapter. Additionally, the alkylated angled-rigid-rods, which shall adsorb on the HOPG surface for the STM measurements, are located at the smaller SPM obtained from H-shaped monomer **III**. Hence, the PNTs have a bowl-shape, which should enable them for host-guest chemistry with suitable guests like PCBM.

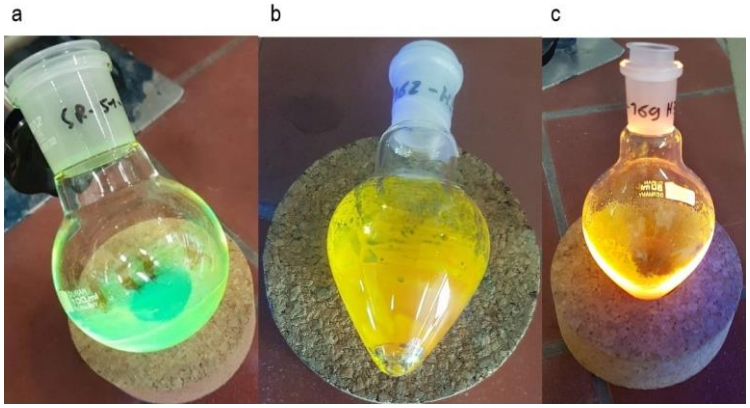

Figure 25: Visible differently coloured fluorescence of the H-shaped monomers by irradiation with a UV-lamp (λ = 366 nm): a) H-shaped monomer **I** (green fluorescence); b) H-shaped monomer **II** (orange fluorescence); c) H-shaped monomer **III** (orange fluorescence).

Furthermore, for all three H-shaped monomers, strong fluorescence was observed even in the solid state by irradiation with a UV-lamp (λ = 366 nm). Based on this, further investigations

of the photophysical properties of these molecules and their respective PNTs were performed and will be presented later on (cp. 7.1 Photophysical Measurements).

6.2 Oligomerisation of the H-shaped Monomers

Using GPC analysis (4.3 Analytical and Recycling Gel Permeation Chromatography) different *Glaser* coupling reaction conditions were tested for the oligomerisation of H-shaped monomer **I** (cp. Figure 26).

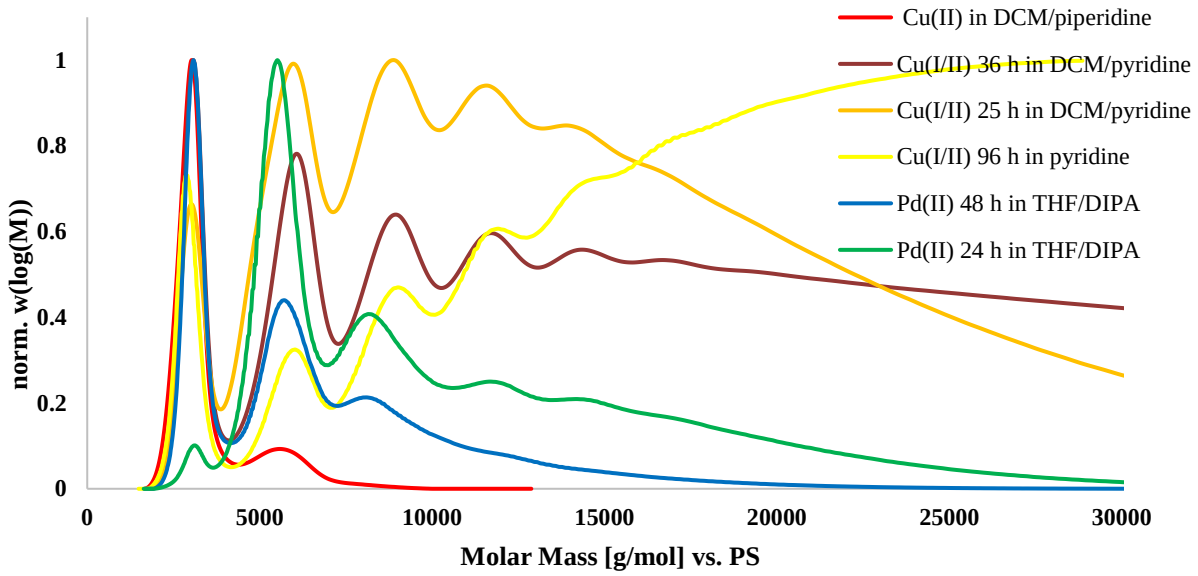

Figure 26: Molar mass distribution of the GPC-analysis of crude products from *Glaser* oligomerisations of H-shaped monomer **I** using Cu (shades of yellow to red) and Pd (green, blue) as catalyst; calibrated against a polystyrene standard.

As explained before (cp. 4.2 Synthetic Challenges), the oligomerisations were performed under pseudo-high-dilution conditions to preferably form the desired small cyclic oligomers over large linear oligomers and polymers. However, to achieve this the substrate had to be injected into the catalyst-solution over the course of several days, due to the high turnover rate of the Cu-catalysed reactions. It was observed that efficient combination of adding the substrate dissolved in DCM instead of the pure base and shorter substrate-injection times led to the formation of the desired cyclic dimers and trimers in higher quantities, but a large amount of substrate was nonetheless converted to linear oligomers. Moreover performing an *Eglinton*-variant of the reaction only using Cu(II) in stoichiometric amounts did not lead to the formation of any product except for traces of the dimer (cp. Figure 26, red curve).[99]

Another variant would have been the *Glaser-Hay* reaction, which was not tested in this work since it is known to give chlorinated alkynes as byproducts.[100] These not entirely closed cyclic structures would have been difficult to separate via recGPC from the desired products. As can be seen from the molar mass distributions above, a modern Pd(II)-catalysed *Glaser* coupling reaction by *Li et al.* was the most suitable for the purpose of generating small cyclic oligomers (cp. Figure 26, blue/green curves), compared to the classical Cu-catalysed variants.[101] Here, instead of bond formation via two alkynylide anions, a transmetalation of the alkynylides to a Pd(II)-centre from a Cu-co-catalyst occurs. The product is then released via a reductive elimination. The mechanism is very similar to that of the *Sonogashira* cross-coupling, however, the resulting Pd(0) is not undergoing oxidative addition to an arene-halide bond, but is re-oxidized by an additional oxidant e.g. trimethylamine *N*-oxide or iodine.

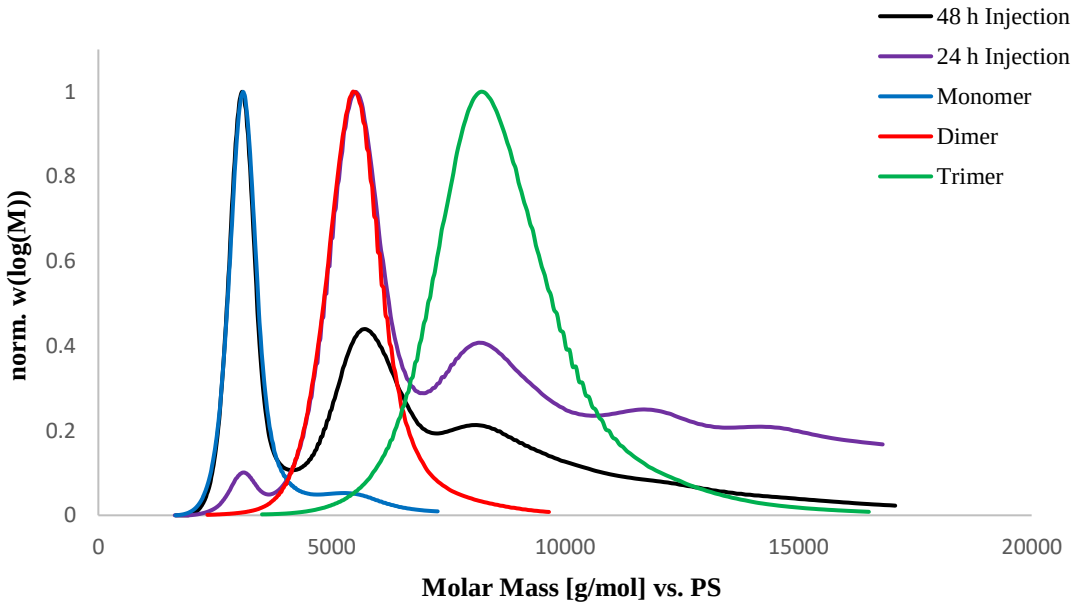

Figure 27: Molar mass distribution of the GPC-analysis of *Glaser* oligomerisations of H-shaped monomer **I**. Shown are crude products (black,violet), as well as the pure cyclic oligomers (red,green) and the monomer (blue) after recGPC; calibrated against a polystyrene standard.

This reaction proceeds much faster than the Cu-catalysed variants and hence allows for a higher selectivity for the intramolecular bond formation to attain cyclic structures even using faster injection times. When comparing different injection times of 24 and 48 hours for this reaction, it is recognizable that faster injection of the substrate leads to higher amounts of larger oligomers (cp. Figure 27). But, because of a nearly complete consumption of the

substrate, still more of the cyclic dimer and trimer can be obtained. This good combination of fast reaction procedure and gratifying yields made gaining the cyclic dimers and trimers in pure form and larger quantities feasible. Hence, this Pd-catalysed oligomerisation reaction was chosen for all further oligomerisations of the different H-shaped monomers in this work.
Additionally, in the products obtained from the Cu-catalysed oligomerisations impurities always remained, which could not be separated via recGPC, compared to the pure products obtained by the Pd-catalysed reactions, as can be seen from the comparison of the MALDI(+) mass spectra below.

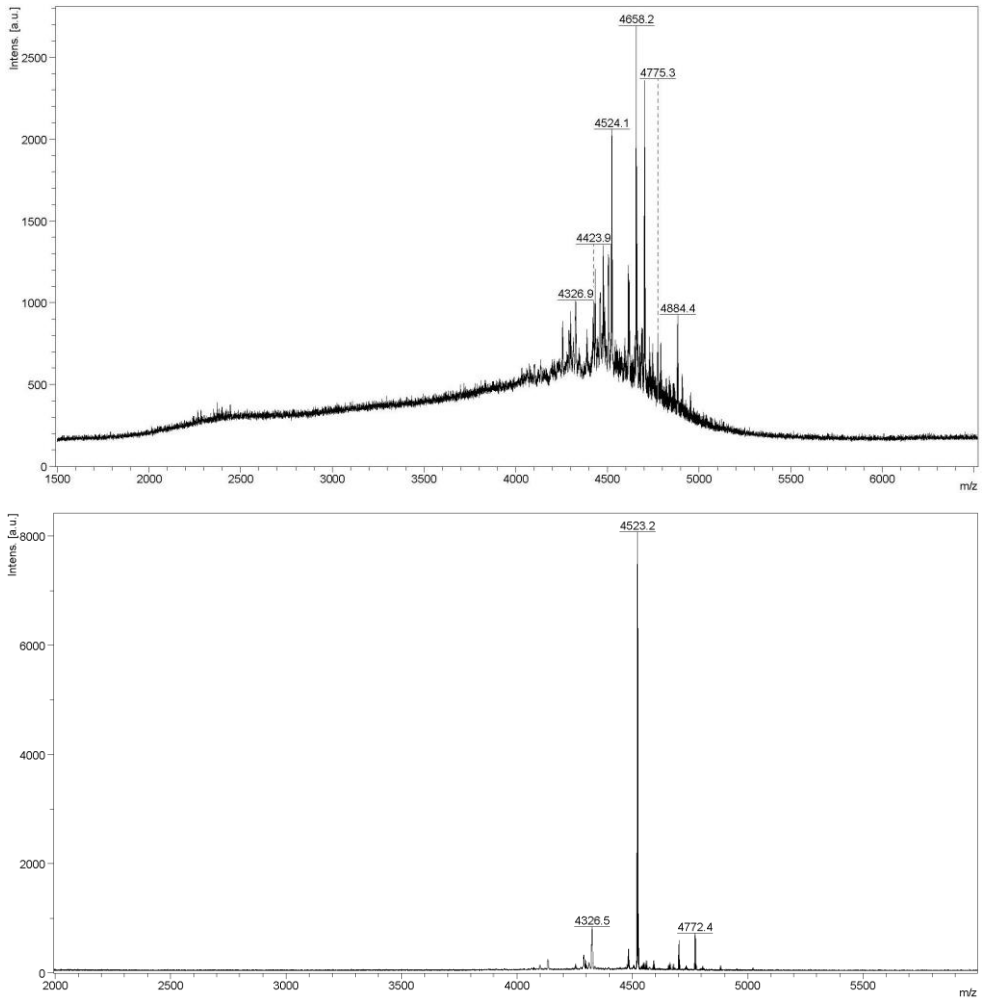

Figure 28: Comparison of the MALDI(+) mass spectra of cyclic dimer **D$_1$**, obtained by a Cu-catalysed reaction (top) and by a Pd-catalysed reaction (bottom); Matrix: DCTB.[102]

Moreover, it was generally not possible to isolate cyclic tetramers by any of the oligomerisation reaction conditions towards the PNTs that were tested. The tetramers obtained were always linear (also in the oligomerisations of **II** and **III**), probably due to the

angle of the rigid-rods at the monomers being too small. Hence, a cyclic tetramer would be strained and did not form during the oligomerisations since it would enthalpically not be favourable in addition to the general entropic disfavourment of larger cyclic oligomers. Using the synthetic approach presented above with injection of the substrate over 24 hours and a Pd-catalyst, the cyclic dimer **D₁** and the cyclic trimer **T₁** of the H-shaped monomer **I** were obtained in 31% and 9% yield respectively, after isolation via recGPC. Comparing this to the first attempt with a 48-hour injection time, an increase in yield of **D₁** by 10% was achieved, but also a slight decrease in yield of **T₁** by 3% occurred, even though there was a larger peak for **T₁** visible in the GPC-analysis (cp. Figure 27). This was attributed to the larger amounts of tetramer which were also generated, making separation via recGPC more difficult. This separation problem is predominantly seen for larger cyclic structures, since their size does not increase proportionally with each additional monomer.

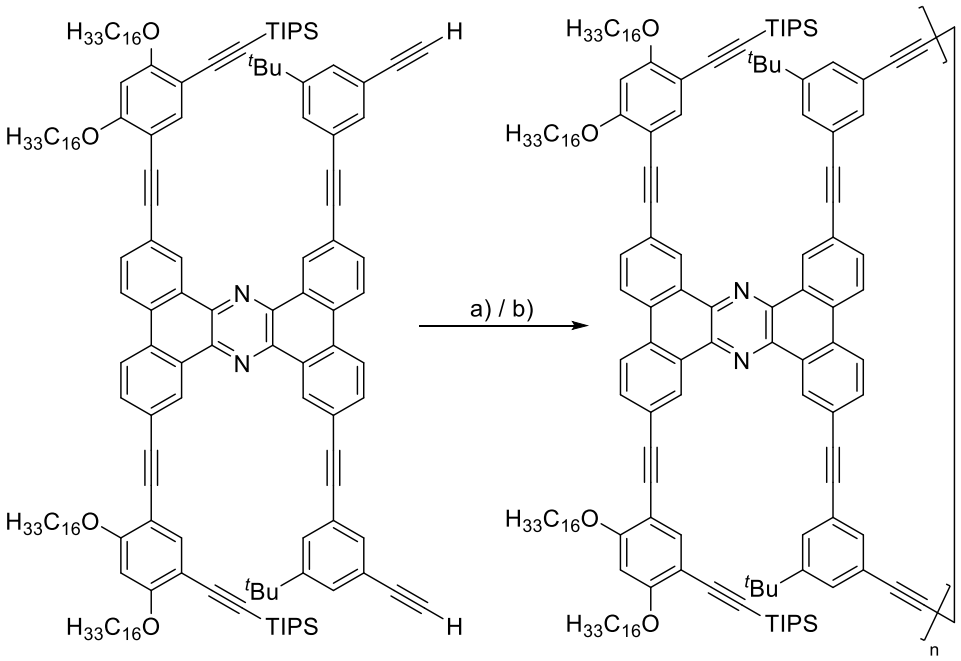

I **D₁** n=2 **T₁** n=3

Scheme 17: Palladium-catalysed oligomerisation of the H-shaped monomer **I**: a) $PdCl_2(PPh_3)_2$ (cat.), CuI (cat.), I_2, THF:DIPA (1:1), 50 °C, injection over 48 h, 21% **D₁** and 12% **T₁**; b) $PdCl_2(PPh_3)_2$ (cat.), CuI (cat.), I_2, THF:DIPA (1:1), 50 °C, injection over 24 h, 31% **D₁** and 9% **T₁**.

These reaction steps can also be tracked easily using ^{1}H-NMR spectroscopy. As is illustrated below, specifically the region around a chemical shift of 3 ppm (cp. Figure 29, blue box) is

useful for this purpose, since only alkyne-H signals are found there. Hence, it could be utilized to determine if the isolated cyclic products of the oligomerisation reactions were closed completely. This was observed for the dimer and trimer spectra, where the alkyne-H signal fully vanished. Additionally, the detected appearance of this signal, combined with the disappearing CPDMS-protecting group signals (cp. Figure 29, green box left and right edge) gave insight into the success of the deprotection reaction towards H-shaped monomer **I**. Furthermore, the other parts of the spectrum (cp. Figure 29, orange box) remained unchanged throughout the reactions. This was expected, as the cyclic oligomers are fully symmetrical and thus should give no other observable signals than those of the monomer. That is why NMR-spectroscopy could be utilized to determine the outcome of the oligomerisations, but not to differentiate the dimer **D₁** from the trimer **T₁**. Distinguishing these oligomers was achieved using MALDI(+) mass spectrometry and GPC-analysis.

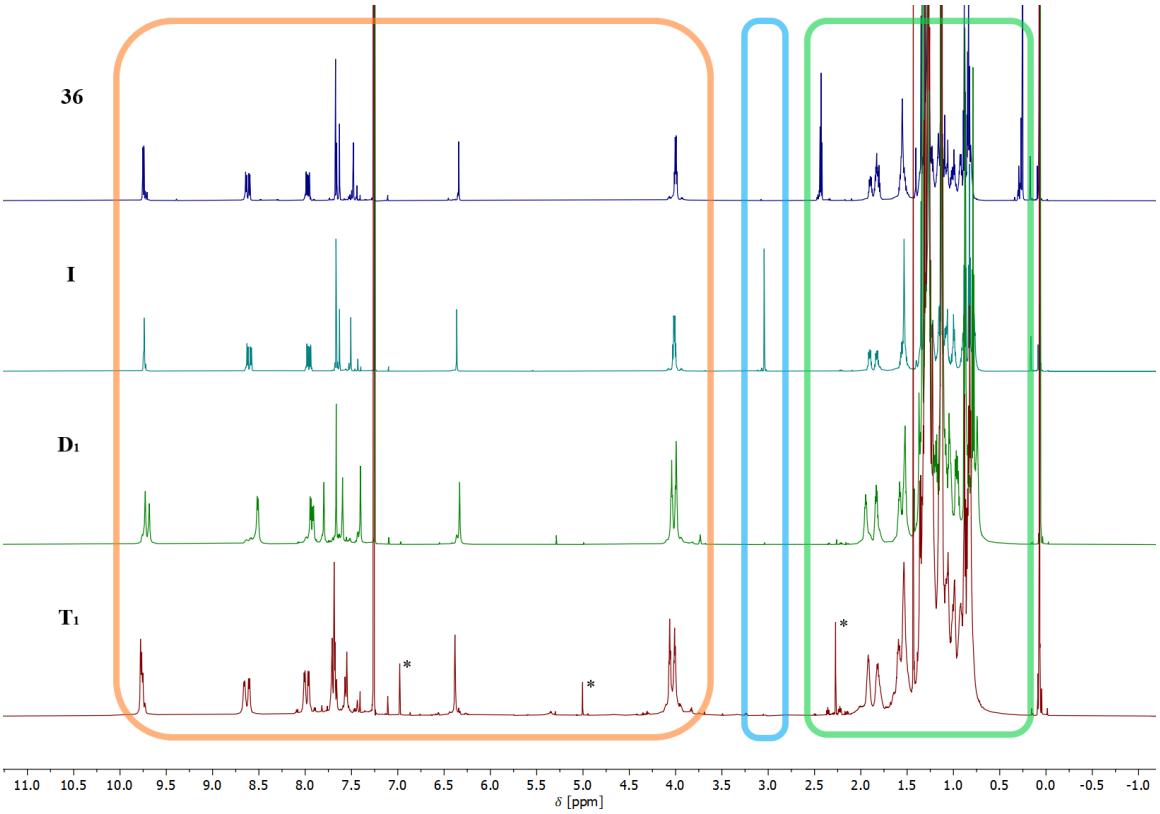

Figure 29: Stacked ^{1}H-NMR spectra (700 MHz, $CDCl_3$, 298 K) of the protected and deprotected H-shaped monomer **36** and **I** (blue and turquoise), as well as the dimer **D₁** (green) and trimer **T₁** (red); asterisks denominate impurities.

After successfully isolating **D₁** and **T₁** in pure form the remaining TIPS-protecting groups at the not-yet coupled alkynes were cleaved for the dimer and trimer individually. For this, they

were stirred with tetrabutylammonium fluoride in THF for three hours at 35 °C. The respective products, i.e. the deprotected dimer **D$_{1d}$** and the deprotected trimer **T$_{1d}$** could not be isolated in a pure form after a filtering column chromatography using silica gel. Furthermore, additional purification via column chromatography resulted only in the loss of material and the impurities remained.

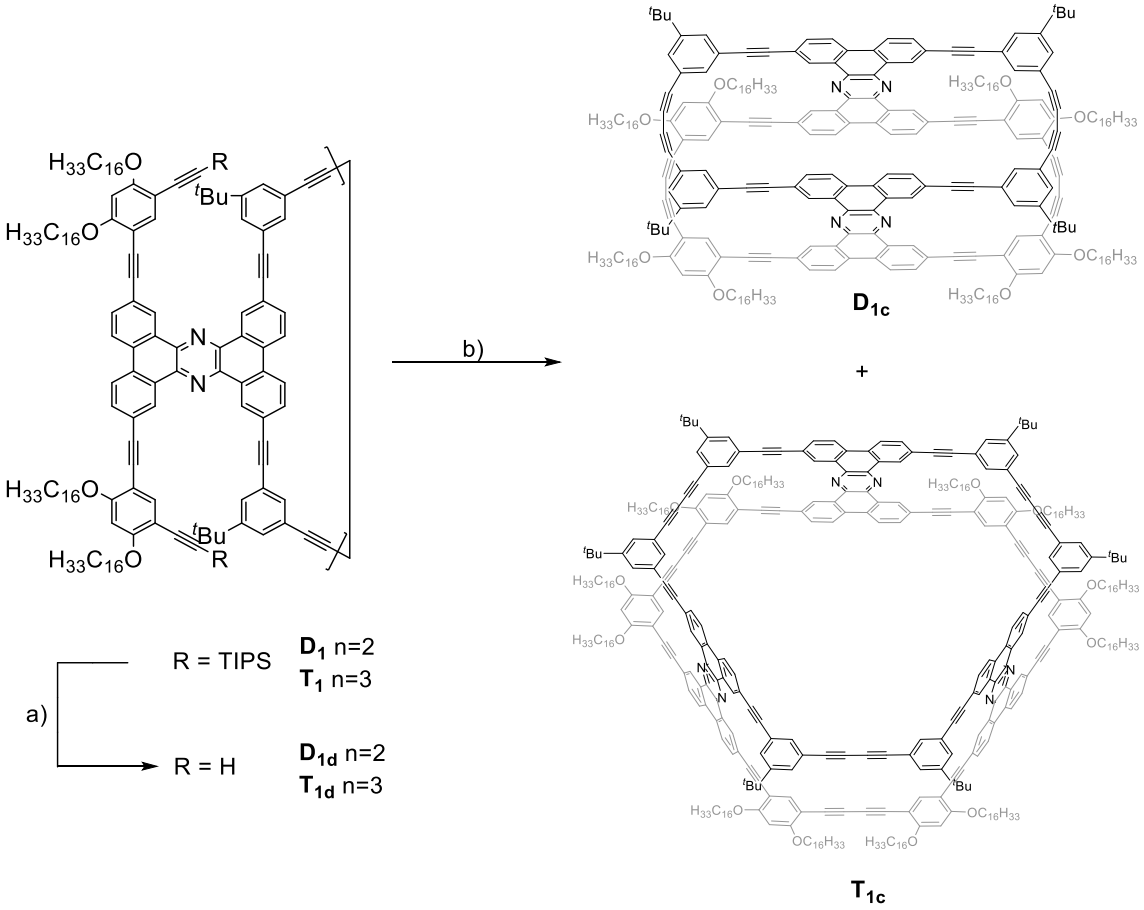

Scheme 18: Synthesis of the cylindrical target molecules: a) TBAF (1 M in THF), THF, 35 °C, 3 h; b) $PdCl_2(PPh_3)_2$ (cat.), CuI (cat.), I_2, THF:DIPA (1:1), 50 °C, injection over 48 h, 25% **D$_{1c}$** and 7% **T$_{1c}$**, over two steps respectively.

However, in the recorded ^{1}H- and ^{13}C-NMR spectra the signal of the TIPS protecting group had vanished and the alkyne-H signal around 3 ppm was visible. Moreover, in the MALDI(+) mass spectrum the product was observed as main peak, leading to the conclusion of a successful and complete cleavage of the TIPS-protecting group (cp. Figure 30). It was refrained from additional purification via recGPC, since due to the length of the process and the elevated temperature the deprotected alkynes could have coupled in an uncontrolled fashion, yielding undesired larger oligomeric structures instead of the intramolecular reaction

to close the second SPM to form the aimed at cylindrical structures. Hence, the deprotected products were used as obtained in the next reaction.

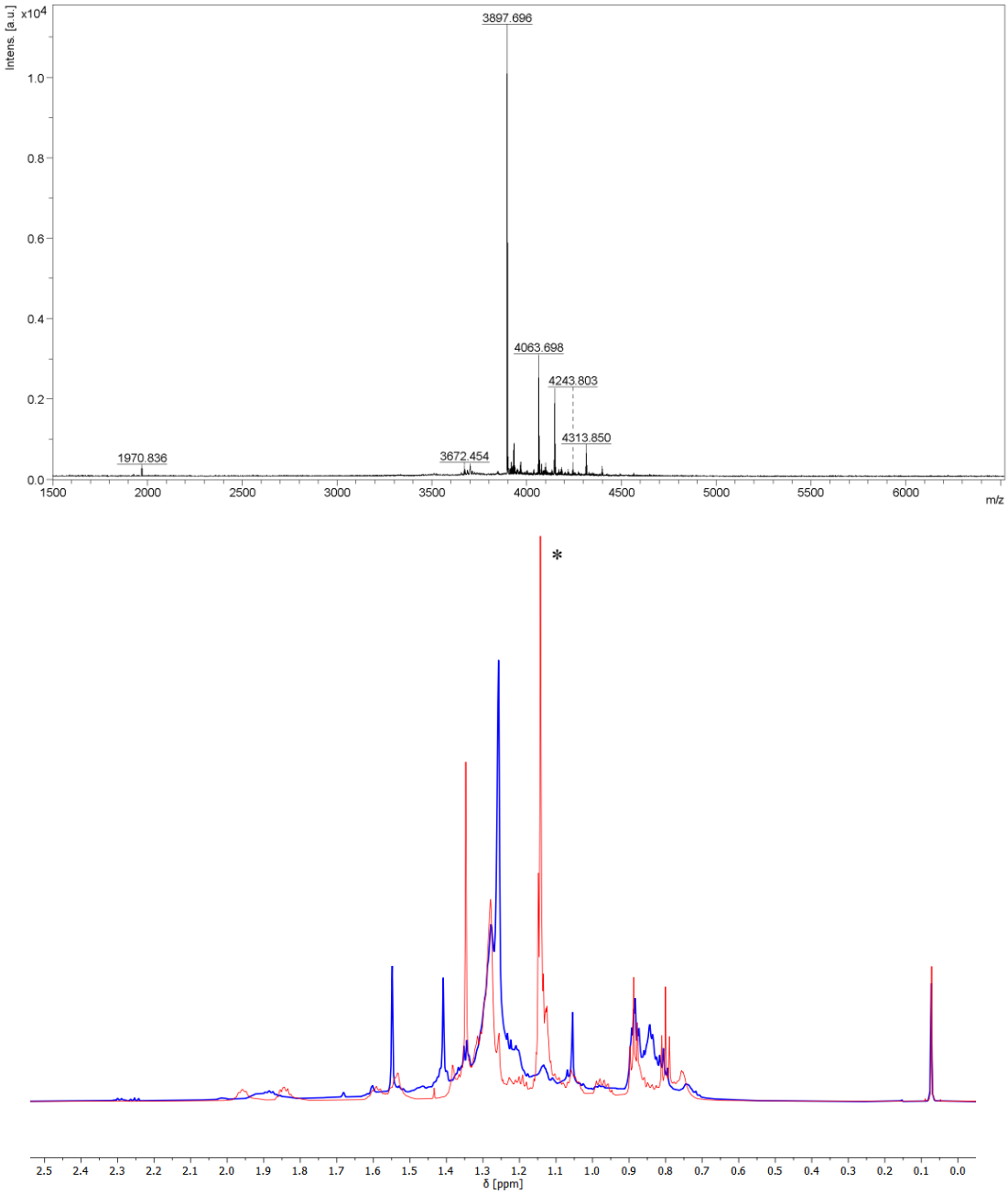

Figure 30: MALDI(+) mass spectrum of deprotected cyclic Dimer **D$_{1d}$** showing the desired product as main peak, as well as residual impurities and matrix adducts; Matrix: DCTB (top) and superimposed ^{1}H-NMR spectra of **D$_1$** (red) and **D$_{1d}$** (blue); asterisk denominates the TIPS-protecting group signal (bottom).[102]

D$_{1d}$ and **T$_{1d}$** were then closed to the cylindrical target molecules via a *Glaser* coupling reaction utilizing the conditions described above. However, the injection time of the respective deprotected oligomers was elongated to 48 hours, effectively lowering the

concentration of substrate in the catalyst solution at any given time. This was to ensure the preference of the substrate to undergo the intramolecular reaction over intermolecular couplings. Hence, after purification via recGPC the aimed at molecules **D$_{1c}$** and **T$_{1c}$** could be obtained in 25% and 7% yield over two steps, respectively. As can be seen from the MALDI(+) mass spectra given below, both compounds were isolated in pure form and their isotope pattern was fitting to the calculated one.

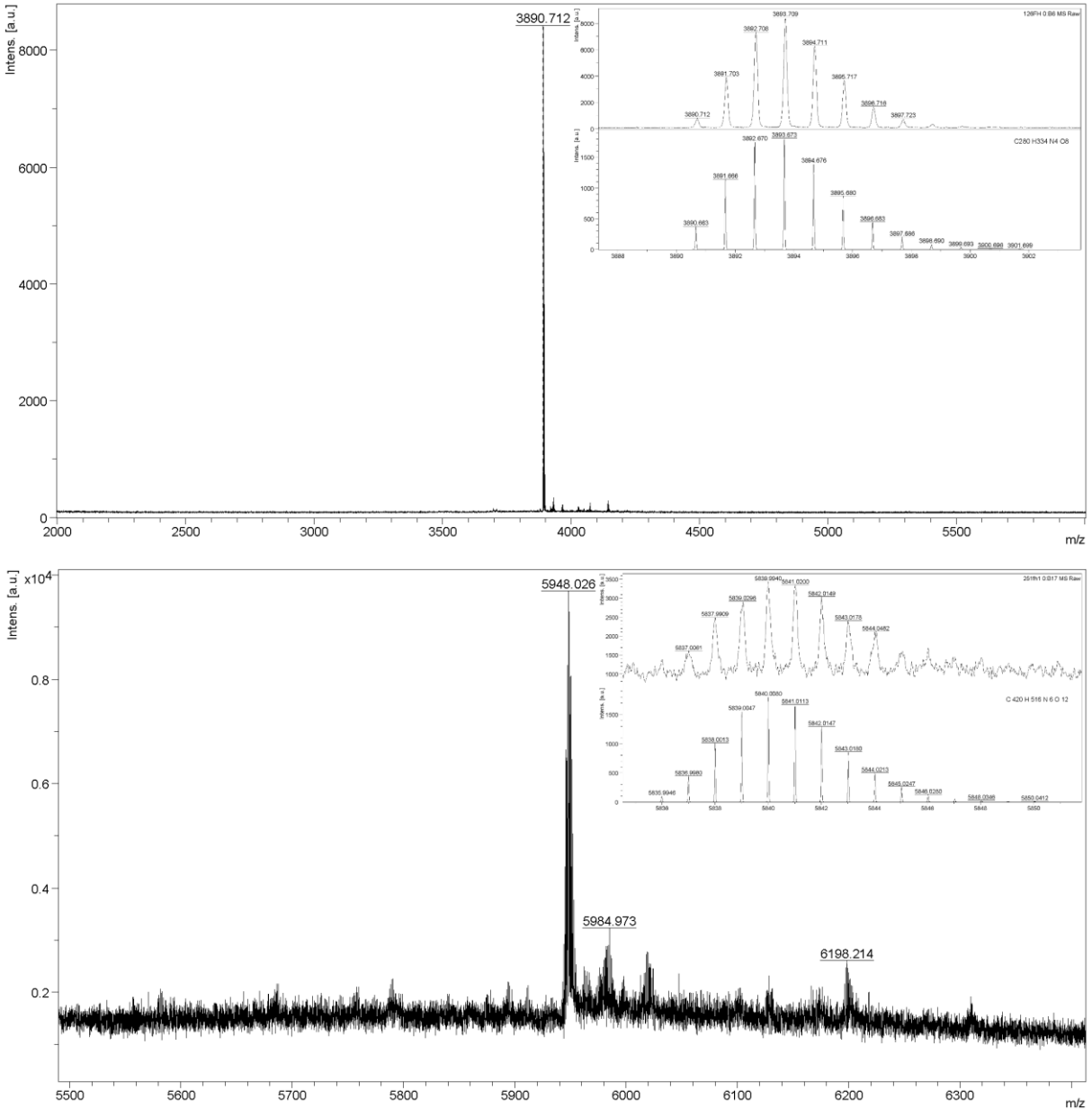

Figure 31: MALDI(+) mass spectra of the cylindrical target structures dimer **D$_{1c}$** (top) and trimer **T$_{1c}$** (bottom; added Ag^+-salts); Matrix: DCTB.[102]

However, the respective NMR-spectra could only be analysed qualitatively, showing signals resembling those of the monomer, since a large broadening of the signals made integration impossible (cp. Figure 32).

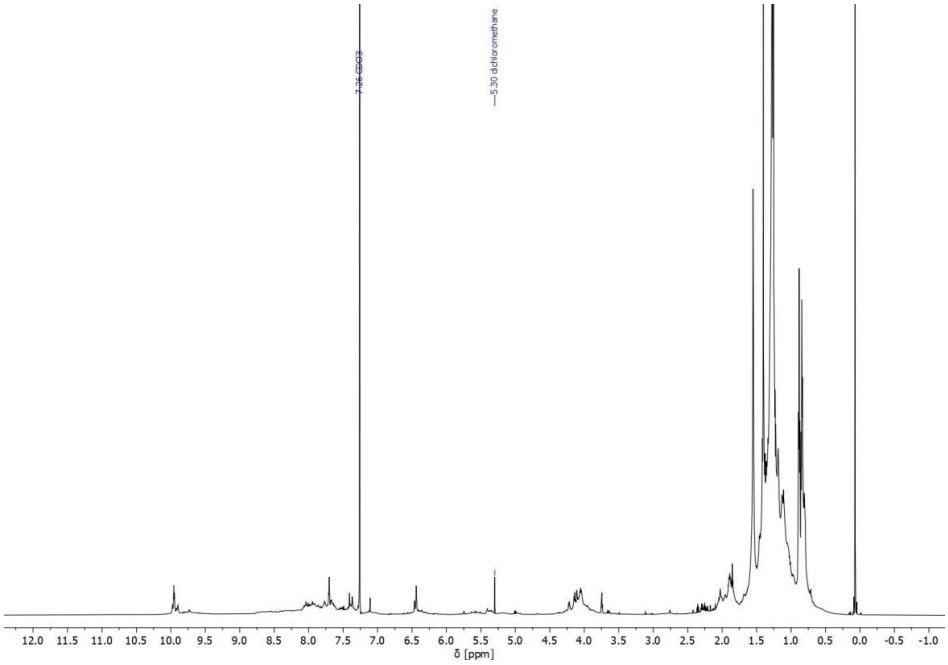

Figure 32: ^{1}H-NMR spectrum of **D$_{1c}$** (700 MHz, $CDCl_3$, 298 K) @ 4 mg/ml.

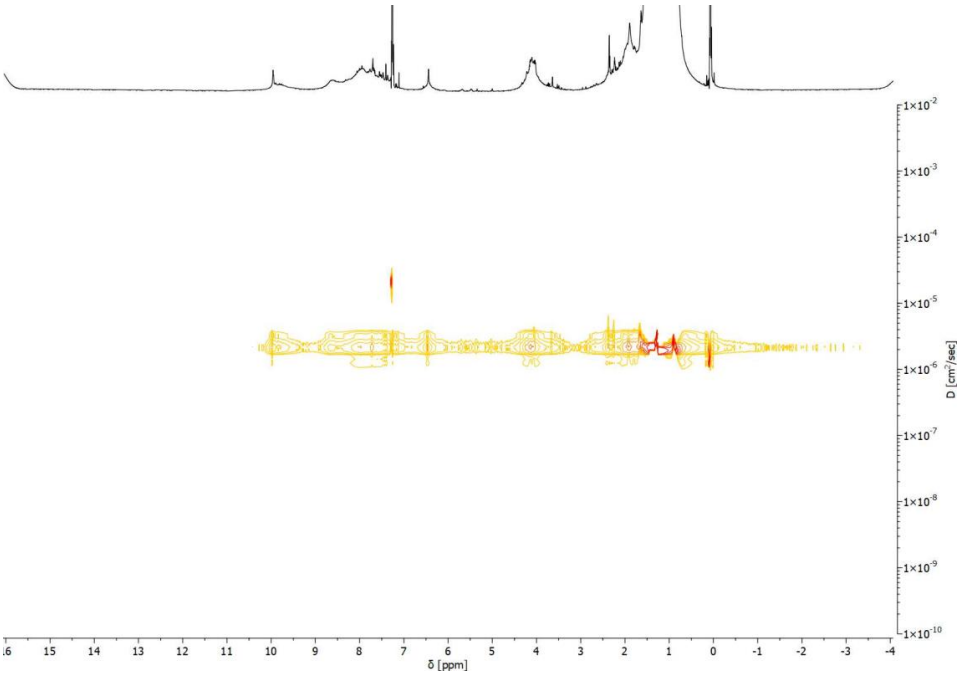

Figure 33: DOSY-NMR spectrum of **D$_{1c}$** (700 MHz, $CDCl_3$, 298 K).[102]

Measurements of the ^{1}H-NMR spectra at -40 °C and 80 °C gave no improvement in quality of the data, nor did a change in the utilized solvent and increase in the substance concentration.[102] Still, the absence of any terminal-acetylene peaks in the region around 3 ppm in the ^{1}H-NMR-spectra serves as additional evidence for the complete closure of the butadiynes. Moreover, in a DOSY-NMR experiment for **D$_{1c}$** only one distinct species in solution was observed (cp. Figure 33).

Furthermore, analytical GPC showed signals without impurities for **D$_{1c}$** and **T$_{1c}$**, at a lower molar mass than their respective precursors **D$_{1d}$** and **T$_{1d}$**. This is expected due to the final structures being smaller, as they no-longer have outward pointing H-shaped monomer arms after closure of the second rim compared to their open-counterparts.

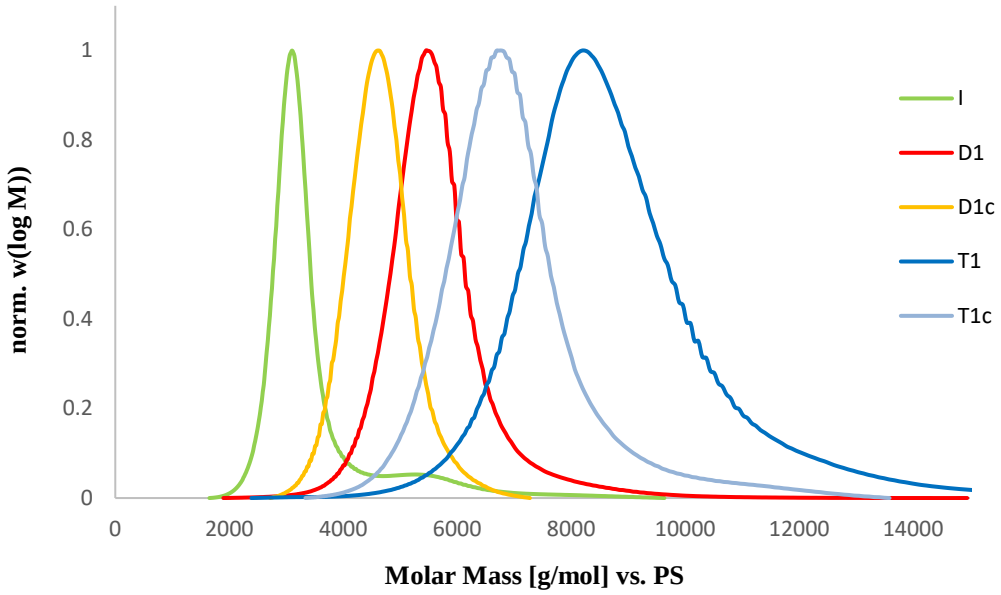

Figure 34: Molar mass distribution of the GPC-analysis of monomer **I** (bright green), dimer **D$_1$** (red) and trimer **T$_1$** (blue), as well as the respective cylindrical structures **D$_{1c}$** (orange) and **T$_{1c}$** (bright blue) (all calibrated against a polystyrene standard).[102]

The unobtainability of meaningful NMR-spectra was also the case for **D$_{2c}$** and **T$_{2c}$**, which additionally were only obtained in small amount, as well as **D$_{3c}$** and **T$_{3c}$**, even though here the open precursors **D$_{3d}$** and **T$_{3d}$** were received completely pure, as will be presented in the following. Like for the **D$_{1c}$** and **T$_{1c}$**, also here MALDI(+) mass spectrometry and analytical GPC were the methods of choice to characterise the compounds (cp. 11 Appendix).

Regarding the oligomerisation of the H-shaped monomers **II** and **III** in general, the dimers and trimers were obtained in more comparable amounts, whereas for **I** more dimer than trimer was obtained. This behaviour might be connected to the smaller ring-size of one of the rings of **II** and **III** respectively and is more pronounced for **III**. It can be surmised that the higher ring-strain resulting from that leads to the increased formation of trimer.

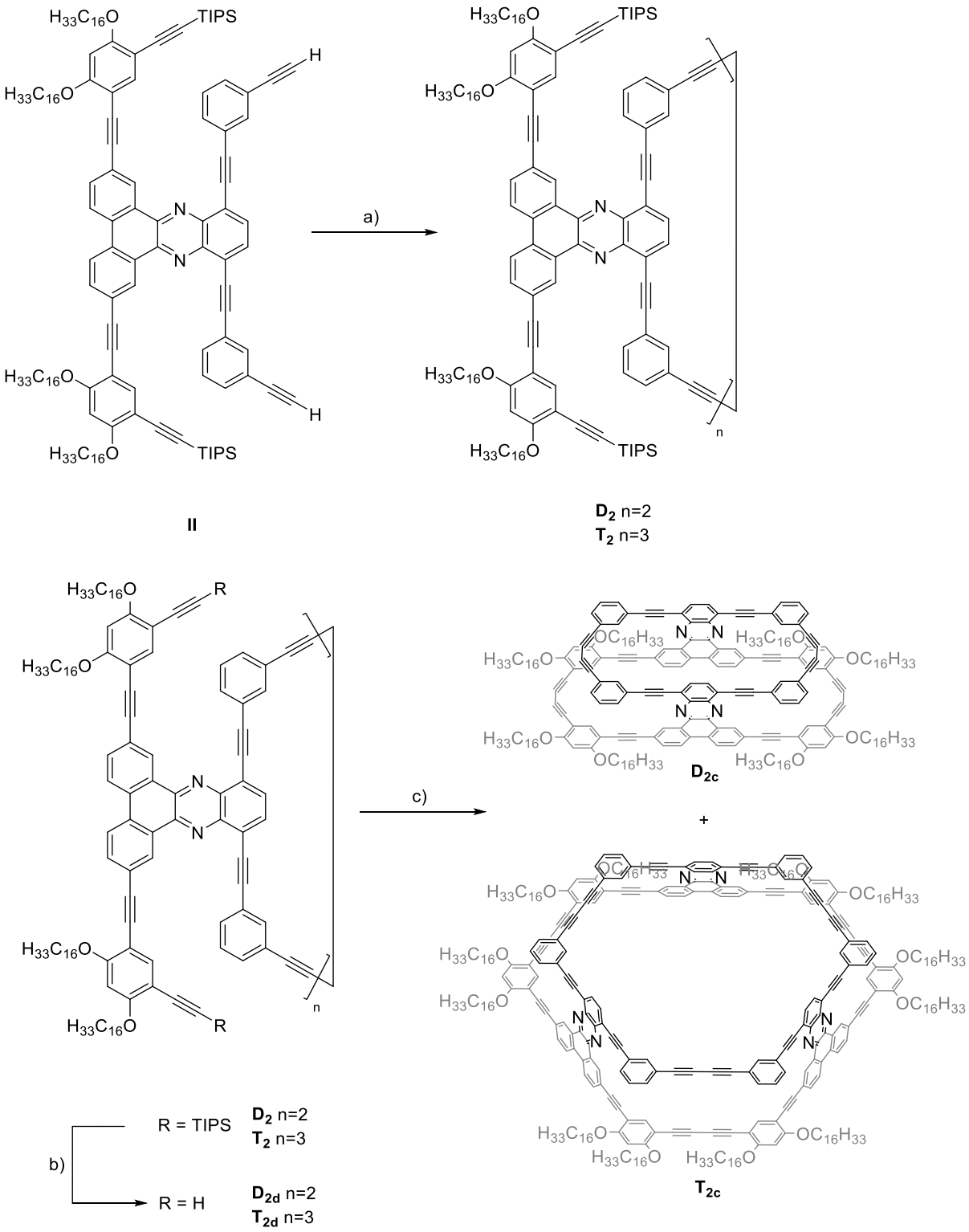

Scheme 19: Palladium-catalysed oligomerisation of the H-shaped monomer **II** and subsequent closure to the pyramidal target structures: a) $PdCl_2(PPh_3)_2$ (cat.), CuI (cat.), I_2, THF:DIPA (1:1), 50 °C, injection over 24 h, 22% **D₂** and 13% **T₂**; b) TBAF (1 M in THF), THF, 35 °C, 3 h; c) $PdCl_2(PPh_3)_2$ (cat.), CuI (cat.), I_2, THF:DIPA (1:1), 50 °C, injection over 48 h, 2% **D₂c** and 3% **T₂c**, over two steps respectively.

Using the synthetic methods presented for **I** above, H-shaped monomer **II** was oligomerised yielding $\mathbf{D_2}$ in 22% and $\mathbf{T_2}$ in 13% yield after separation via recGPC. Deprotection with TBAF and subsequent cyclization yielded the pyramidal dimer $\mathbf{D_{2c}}$ and trimer $\mathbf{T_{2c}}$ in only 2% and 3%, respectively. The low yield might be explained by the molecules design to exert stacking behaviour by their shape and the missing steric bulk from the ^{t}*Bu*-groups at one rim compared to the oligomers generated from **I** and **III**. The stacking then leads to intermolecular reactions even under the chosen high-dilution conditions in the final cyclization.

While MALDI(+) mass spectra confirmed the successful synthesis of $\mathbf{D_{2c}}$, for $\mathbf{T_{2c}}$ the largest observable signals were that of a $[2M+H]^+$ peak and its matrix adducts (cp. 11 Appendix; Figure 127). However, a small $[M]^+$ peak of $\mathbf{T_{2c}}$ was visible as well (cp. Figure 35; red arrow). In general, aggregate formation of molecules based on SPMs (when not sterically hindered) is known and can be detected in MALDI-TOF mass spectra, as has been shown by *Höger et al.* in the case of an amphiphilic SPM.[103]

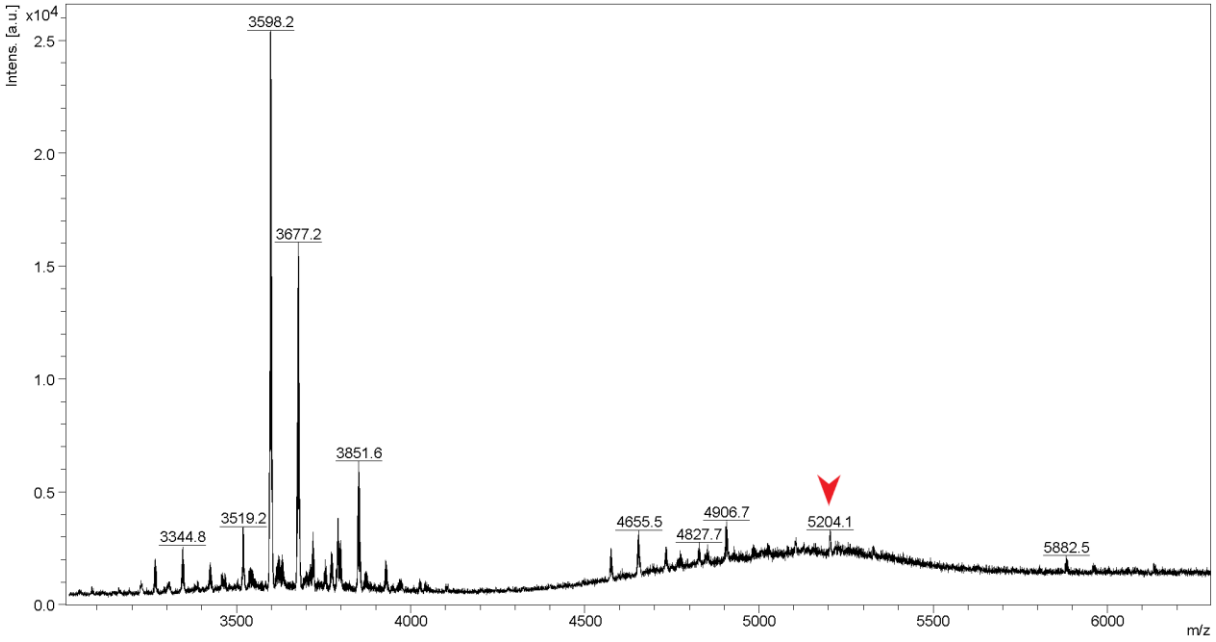

Figure 35: MALDI-TOF mass spectrum of $\mathbf{T_{2c}}$ (matrix: DCTB); red arrow denominates the $[M]^+$ peak of $\mathbf{T_{2c}}$.

Furthermore, in the analytical GPC the closed structure was not observed as smaller, i.e. lower molar mass (cp. Figure 36). That would have been expected due to the no-longer outward pointing H-shaped monomer arms after closure of the second rim compared to the open-counterpart $\mathbf{T_2}$ (and was observed for all other PNTs synthesized in this work;

cp. 11 Appendix; Figure 70 and Figure 72). However, $\mathbf{T_{2c}}$ was slightly larger, which could be attributed to the desired stacking behaviour of the pyramidal structures. For a covalent inter-molecular coupling of two open trimer-molecules in the last cyclization a larger increase giving the size of a hexamer would be expected, which is not observed by analytical GPC. While these results hint at a self-aggregation behaviour of $\mathbf{T_{2c}}$, STM is the method of choice to fully elucidate the structure. There, 3D stacks of $\mathbf{T_{2c}}$ can be distinguished from covalently connected trimer rings, that should give flat structures on the HOPG surface.

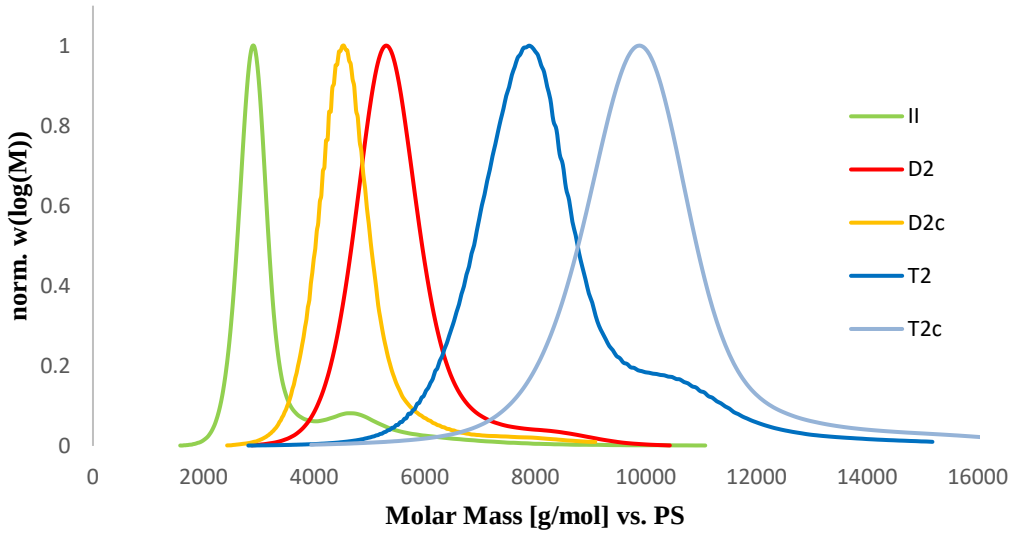

Figure 36: Molar mass distribution of the GPC-analysis of monomer **II** (bright green), dimer $\mathbf{D_2}$ (red) and trimer $\mathbf{T_2}$ (blue), as well as the respective pyramidal structures $\mathbf{D_{2c}}$ (orange) and $\mathbf{T_{2c}}$ (bright blue) (all calibrated against a polystyrene standard).

Using the synthetic methods established for **I**, also H-shaped monomer **III** was oligomerised yielding $\mathbf{D_3}$ in 23% and $\mathbf{T_3}$ in 22% yield after separation via recGPC. Deprotection with TBAF and subsequent cyclization yielded the bowl-shaped dimer $\mathbf{D_{3c}}$ and trimer $\mathbf{T_{3c}}$ in 76% and 44%, respectively.

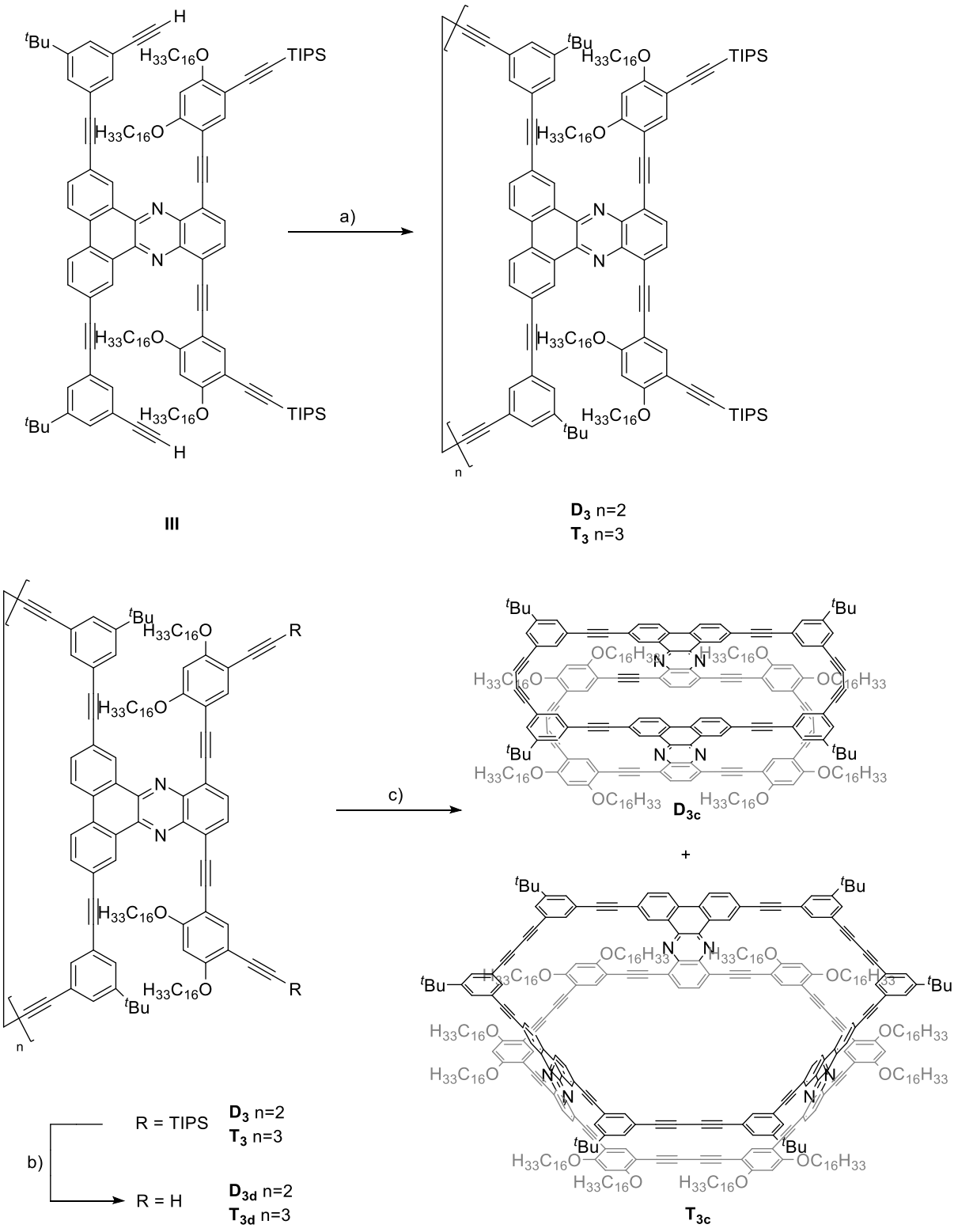

Scheme 20: Palladium-catalysed oligomerisation of the H-shaped monomer **III** and subsequent closure to the pyramidal target structures: a) $PdCl_2(PPh_3)_2$ (cat.), CuI (cat.), I_2, THF:DIPA (1:1), 50 °C, injection over 24 h, 23% **D**$_3$ and 22% **T**$_3$; b) TBAF (1 M in THF), THF, 35 °C, 3 h, 91% **D**$_{3d}$ and 76% **T**$_{3d}$; c) $PdCl_2(PPh_3)_2$ (cat.), CuI (cat.), I_2, THF:DIPA (1:1), 50 °C, injection over 48 h, 76% **D**$_{3c}$ and 44% **T**$_{3c}$.

Interestingly, the oligomers were easier to separate than that of **I** and **II**. Moreover, the deprotected oligomers could be obtained in pure form and were fully characterised, which might explain why the following cyclization then gave much higher yields.

To evaluate the influence of the second ring of the PNTs upon adsorption to a surface (i.e. HOPG), compared to the macrocycles synthesized in the *Höger* group before,[53] a monomer with only one type of oligomerisable angled rigid-rods was synthesized. The structures gained from this molecule should then serve as model system for the bottom-macrocycle of the PNTs to enable a comparative STM-study of the self-assembly on HOPG. Hence, **31** was coupled with commercially available *o*-phenylene diamine **42** in a condensation under acidic conditions, to give **43** in quantitative yields.

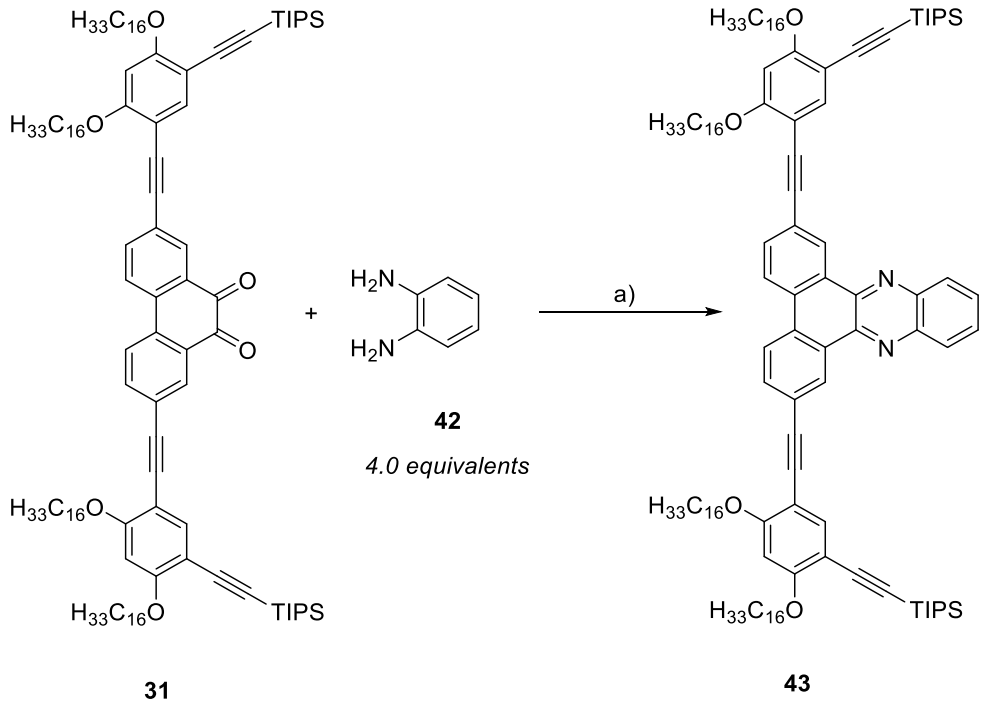

Scheme 21: Synthesis of the U-shaped phenazine **43**: a) AcOH, $CHCl_3$, reflux, 24 h, >99%.

Quantitative deprotection of the terminal acetylenes using TBAF and oligomerisation under the same conditions as for the other H-shaped monomers unexpectedly did not give the dimer and trimer (as for the other monomers), but instead the trimer **T4** and tetramer **Tet4** were obtained in 13% and 7%, respectively. In contrast to the other H-shaped monomers here also the tetramer was obtained in its closed form. This behaviour might be connected to the higher flexibility of the monomer, due to the missing second angled rigid-rod. Furthermore, a test

reaction using a different catalyst system ($Pd(OAc)_2$ and *XPhos*) gave the desired dimer and trimer, but the reaction seemed to proceed slower in general and 22% of the monomer were regained. However, in the MALDI(+) mass spectrum $[M+2H]^+$ signals were observed as main peaks indicating that the open-chain forms of the respective oligomers were obtained. Additionally, even though the products were purified via recGPC and pure according to analytical GPC, the ^{1}H-NMR spectra showed more signals than expected and the characteristic terminal-acetylene signal showed only half of the expected intensity. These inconclusive analytical results can be explained by the size difference of open-chain and closed forms of the oligomers formed from **IV** being smaller than that of the other H-shaped monomers, due to its increased flexibility. Hence, separation of both forms via recGPC might not be possible.

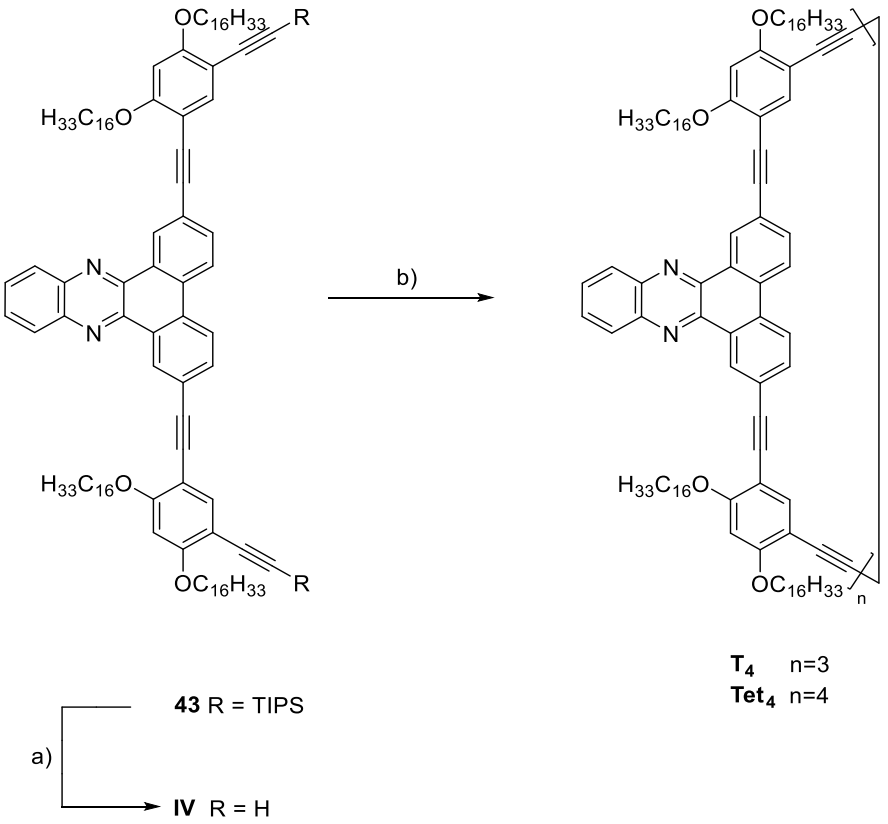

Scheme 22: Deprotection and subsequent palladium-catalysed oligomerisation of the H-shaped monomer **IV**: a) TBAF (1 M in THF), THF, r.t., 23 h, >99%; b) $PdCl_2(PPh_3)_2$ (cat.), CuI (cat.), I_2, THF:DIPA (1:1), 50 °C, injection over 24 h, 13% **T_4** and 7% **Tet_4**.

To verify this assumption STM images of the oligomers shall be obtained to clarify if indeed a mixture of open-chain and closed structures was obtained. Additionally, DOSY-NMR

spectra did not show multiple distinct species being present, but the difference in diffusion between open-chain and closed variant of the respective target molecules might be too small to be observed this way (cp. Figure 37).

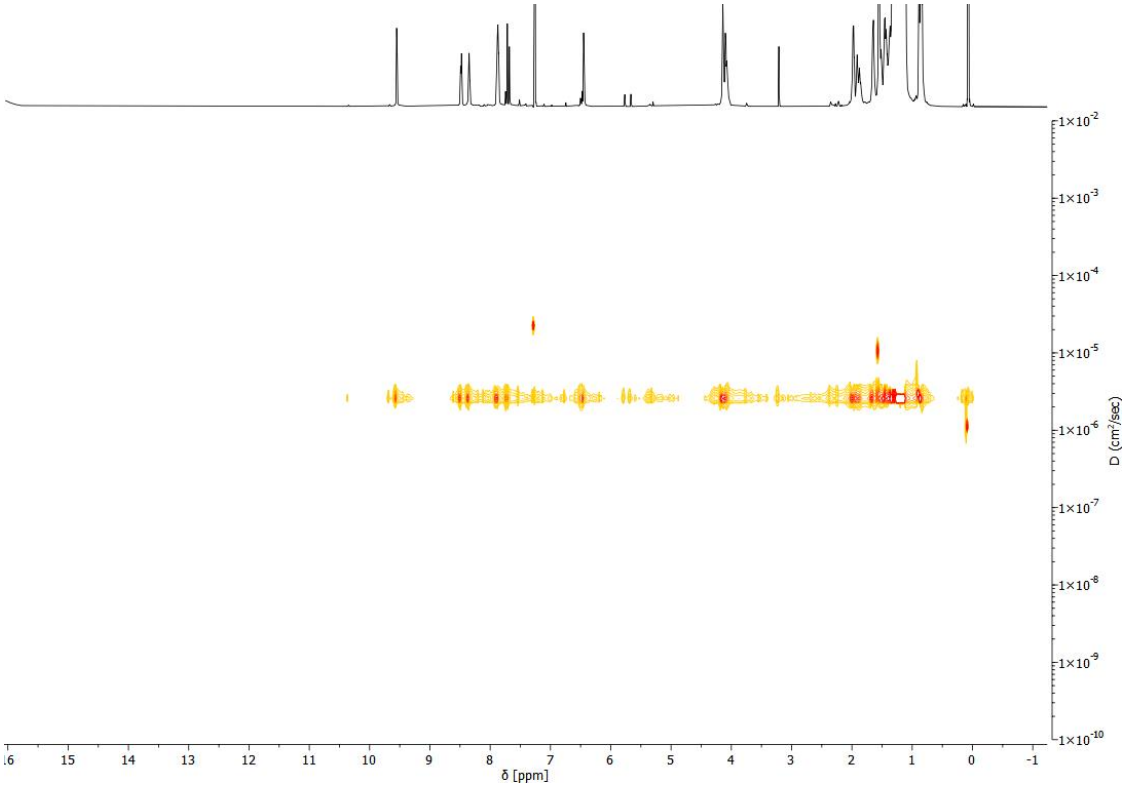

Figure 37: DOSY-NMR spectrum of the dimeric product species obtained from oligomerization of **IV** (700 MHz, $CDCl_3$, 298 K).

In general, this test reaction with a different catalyst-system showed that the desired oligomers could be obtained in principle. Further modification regarding the used catalyst, base, the injection-time, and oxidant might optimize the desired product formation. However, due to the extensive screening and material consumption needed for this and the fact that the desired molecules were only to serve as model systems, this was not attempted. After successful synthesis of the desired PNTs for this work in the following, the analytical results shall be presented, showing their behaviour upon adsorption on surfaces and their potential in the field of organic electronic applications.

7. Analytical Results

7.1 Photophysical Measurements

As discussed before, already the H-shaped monomers showed interesting optical properties. Compounds **I** to **III** all fluoresced in solid-state and in solution. As can be seen below, the maximum of absorbance in the *UV/Vis* spectra are all comparable in the region of 315 nm.

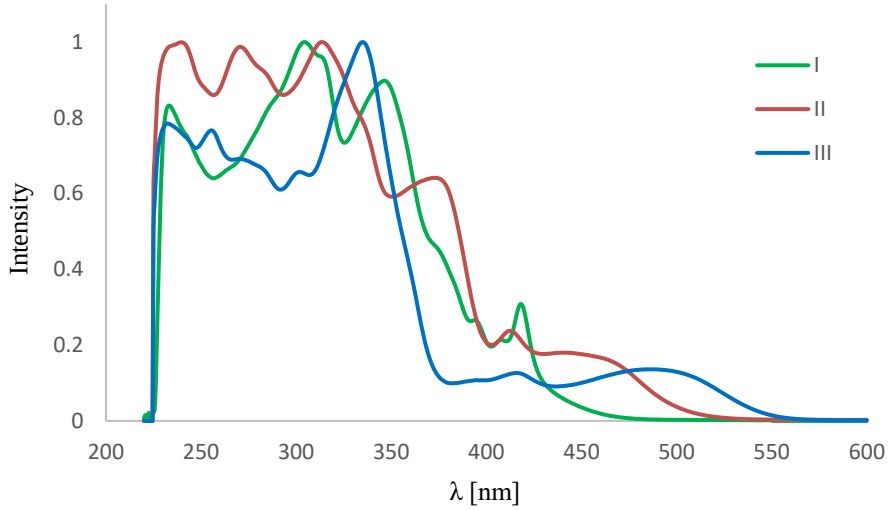

Figure 38: *UV/Vis*-absorption spectra of monomers **I**, (green, λ_{max} = 304.5 nm), **II** (brown, λ_{max} = 313.5 nm) and **III** (blue, λ_{max} = 335.0 nm) (all measured in dichloromethane).

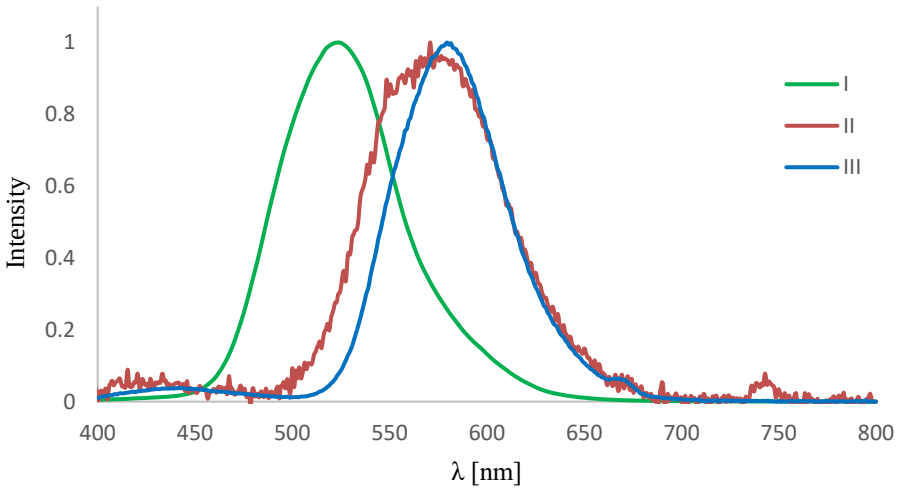

Figure 39: Fluorescence emission spectra of monomers **I** (green, λ_{em} = 523.5 nm), **II** (brown, λ_{em} = 571.0 nm) and **III** (blue, λ_{em} = 579.5 nm) (all measured in dichloromethane); the maximum of intensity found in the *UV/Vis*-absorption spectra were used as excitation wavelengths, respectively.

When looking at the respective fluorescence spectra gained by excitation of **I** to **III** with the maximal absorbance λ_{max} of the *UV/Vis* spectra, an unexpected outcome is observed. Even though the total conjugated π-systems of **II** and **III** are smaller than that of **I**, their maximum of emission is red-shifted which is usually associated with larger π-systems.[104] To understand this inverted behaviour, it is necessary to investigate effects that can be leading to a blue-shift for **I** and a red-shift for **II** and **III** and hence combined give a rationale for the observed emission.

It could be surmised that **II** forms dimers or multimers, and hence upon excitation excimer complexes. These complexes could be formed via π-π-stacking interactions and are lower in energy than their monomeric excited states. This lower energy then leads to the observed longer wavelength of excitation (cp. Figure 40).[105] On the one hand, this is possible due to the missing *^{t}Bu*-groups which were omitted to enable stacking behaviour of the nanotubes gained from **II**, so no steric bulk hinders the π-π-stacking of the molecules. On the other hand, this explains the low quantum yield of emission compared to **I** and **III**, which is a characteristic of excimers (cp. Figure 39; low-quality of the curve for **II** after normalization).[106]

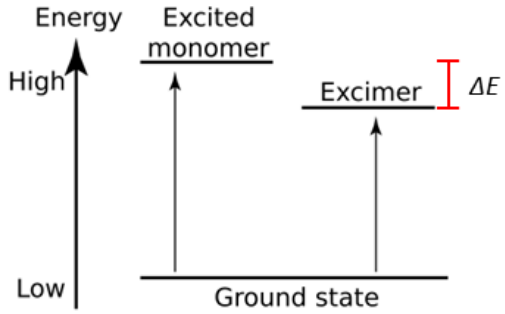

Figure 40: Schematic energy diagram, showing the relative energy difference *ΔE* of an excited monomer and its respective excimer.

However, that the emission maximum of **III** is red-shifted compared to that of **I**, but does not show the same low emission as **II**, shows that excimer formation is not the main contributing factor to the red-shift. Another possible explanation for this behaviour might be the difference in HOMO and LUMO localization for **I**, compared to **II** and **III.** There, the unsymmetric spacer of **II** and **III** could lead to an intramolecular charge-transfer. Quantum chemical calculations of the molecular orbital localizations (cp. Figure 41) for the symmetric phenanthracene-spacer of **I** compared to the unsymmetric phenanthracene-spacer of **II** and **III**

give more insight into this assumption. While the HOMO and LUMO localization is distributed symmetrically over the aromatic system for the symmetric spacer of **I**, the HOMO is localized more on the side of the larger aromatic phenanthrene-side and the LUMO on the benzene-side for the unsymmetric spacer of **II** and **III.** This gives a first indication, that intramolecular charge-transfer might indeed be a relevant contributing factor to the red-shift of **II** and **III**. Additionally, the LUMO+1, which shows the opposite behaviour for the unsymmetric spacer lies significantly higher in energy and thus would presumably not partake in the charge-transfer. However, to further clarify this effect more experimental studies need to be performed, which are subject of current research.

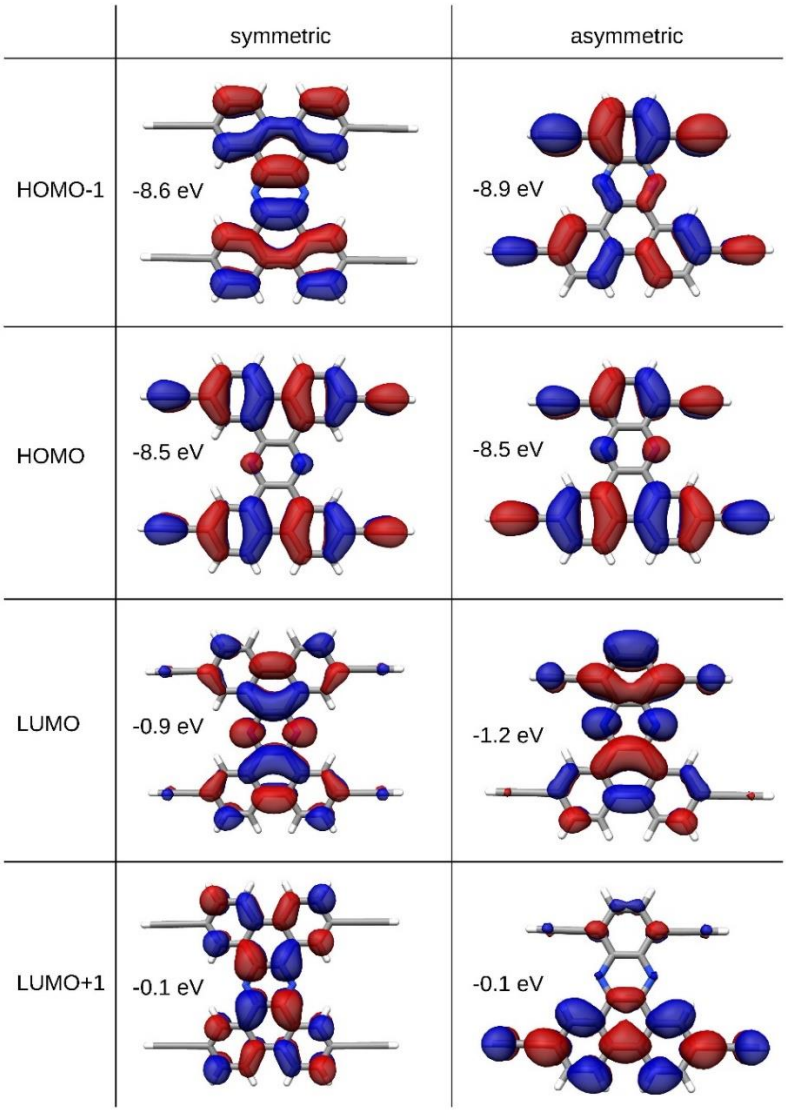

Figure 41: HOMO and LUMO localization, as well as the molecular orbital energies for the symmetric (**I**) and the unsymmetric (**II** and **III**) phenanthracene core of the PNTs at the wB979X-3c hybrid DFT level of theory.

Regarding the blue-shift in emission for **I**, an interesting phenomenon can explain this behaviour, namely the formation of an intramolecular aggregate between both rigid-rods when they have the same length (due to their parallel orientation). The formed H-aggregate is then blue-shifted explaining the lower maximum in emission λ_{em}, even though **I** has a larger overall conjugated π-system than **II** and **III**. To prove this assumption, a model system with only one rigid-rod connected to the phenazine-spacer was designed. For this, phenanthrene-9,10-diamine was synthesized by forming the twofold imine with hydroxylammonium chloride under basic conditions in 86% yield and subsequent reduction using hydrazine and Pd/C to give **45** in 25% yield after recrystallization.

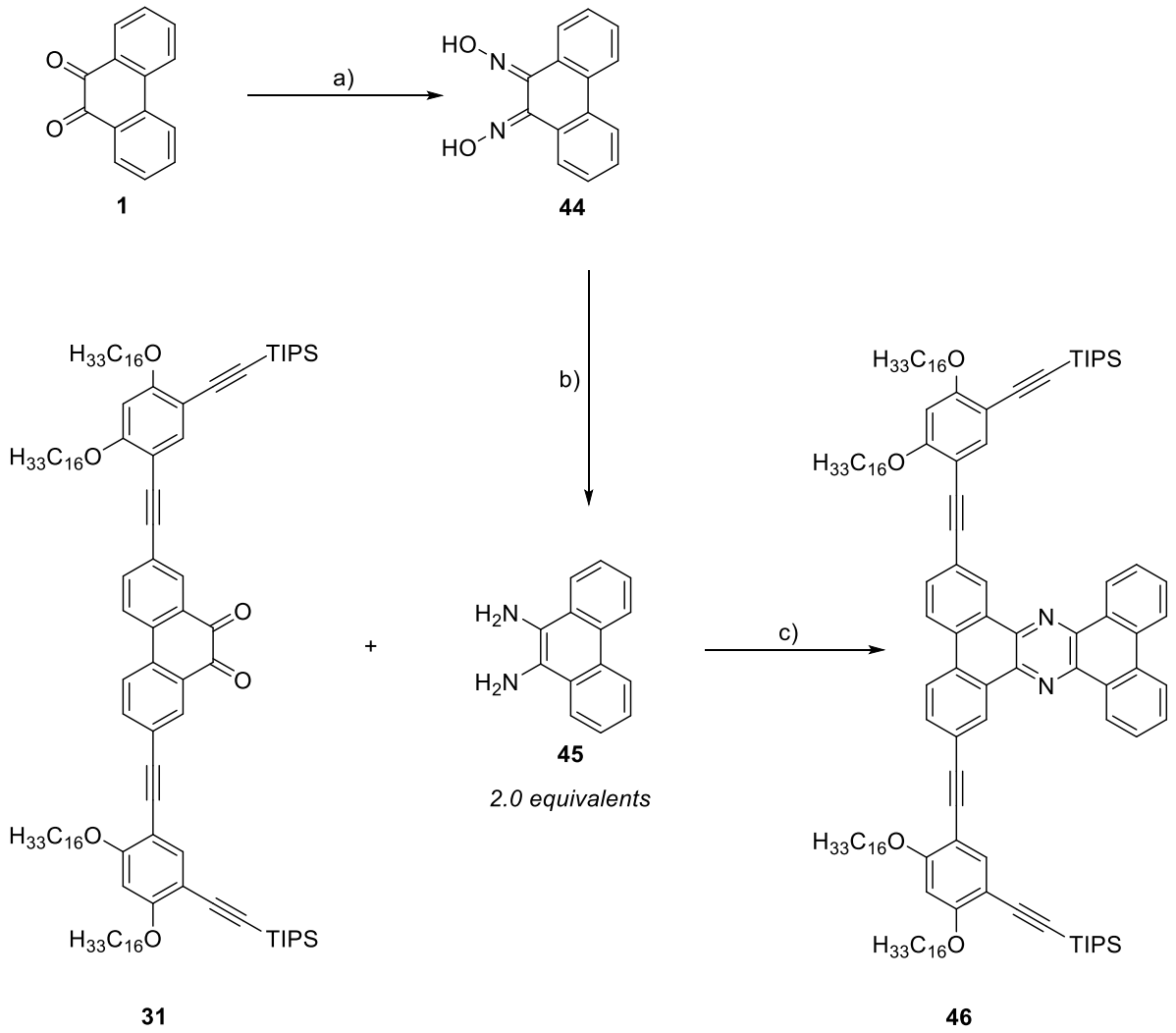

Scheme 23: Synthesis of the T-shaped model system **45**: a) Hydroxylammonium chloride, $BaCO_3$, EtOH, reflux, 66 h, 86%; b) Pd/C (10%), hydrazine monohydrate, EtOH, reflux, 19 h, 25%; c) $CHCl_3$, AcOH, reflux, 24 h, >99%.

Compared to the brominated phenanthrene-9,10-diamine **8**, **45** is not stable under ambient conditions and decomposes within minutes, as was already known in the *Höger*-group from previous works.[84] Hence, phenanthrene-9,10-diamine **45** was directly coupled with angled rigid-rod **31** in an acid-catalysed condensation to give the desired T-shaped model system **46** in quantitative yields. To test the aforementioned assumption concerning the formation of H-aggregates, single-molecule fluorescence spectroscopy experiments by the group of *Prof. John Lupton* at the University of Regensburg were performed. The method of single-molecule fluorescence spectroscopy enables the investigation of the properties of one single molecule in a bulk, rather than the averaged results over all molecules (like in "standard" fluorescence spectroscopy). A single molecule can be probed by pumping an excitation using a laser pulse and only accessing the molecule that is resonant with the used optical wavelength. Repeating this many times allows to obtain a frequency histogram of the actual distribution of values, rather than the average. This can then be used to extract interesting properties of the respective molecules, like the fluorescence lifetime.[107]

These experiments revealed indeed the formation of intramolecular H-aggregates for H-shaped monomer **I** and not for the T-shaped model system **46**, leading to a nearly doubled fluorescence lifetime of 9.1 ns for **I** compared to 5.5 ns for **46**.

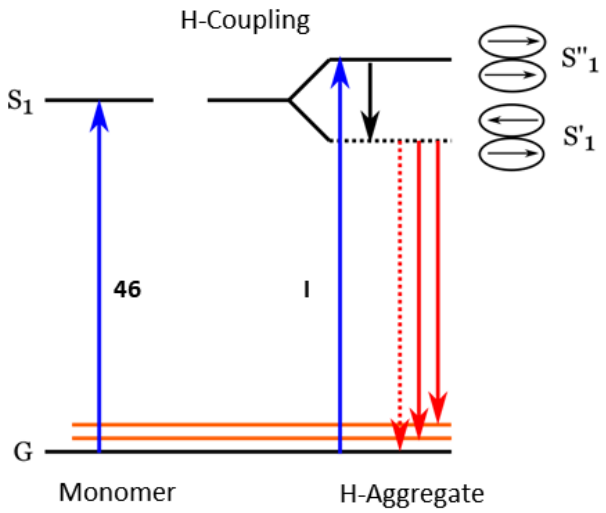

Figure 42: Illustration of the effect of an H-aggregate on the excitation and relaxation of an electron.

The observed longer lifetime of the H-aggregate excited state of **I** is based on the excitation from the ground state to the lowest excited state being dipole-forbidden (after splitting of the monomer excited state upon formation of the H-aggregate). But, since fluorescence occurs by

relaxation from the lowest excited state to the ground state according to *Kasha's rule*, first relaxation in the excited state has to occur. Hence, elongating the lifetime of this state of **I** compared to the non-aggregated excited state of **46** (cp. Figure 42). Moreover, shorter fluorescence lifetimes for both systems were observed under ambient conditions compared to under nitrogen atmosphere. Here inter-system crossing and subsequent relaxation to the ground state leads to the formation of reactive singlet oxygen, that in turn leads to quenching of the excited state (cp. Figure 43).

Generally, the blue-shift in emission of **I** combined with a red-shift in emission of **II** and **III** can give an explanation for the inverted order of the maximum emission wavelength with respect to the π-system size. However, further investigations on the photophysical behaviour of the in this work synthesized molecules, including why **III** is red-shifted in the fluorescence spectrum, but does not show the lowered quantum yield like **II** that is associated with excimer formation are subject of current research.

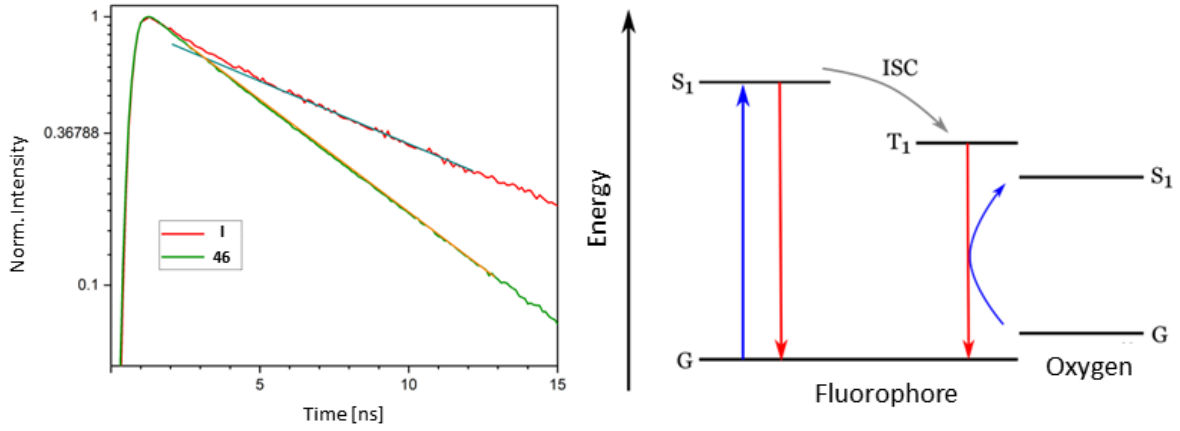

Figure 43: (Multi-) Exponential decay of the fluorescence of **I** and **46** (left) and illustration of the generation of singlet oxygen during single-molecule fluorescence spectroscopy under ambient conditions (right).

Additionally, the studies on the monomers also reveal the photophysical behaviour of the respective PNTs. This is due to the length of the π-system and the chromophore not changing from the monomers to the respective final compounds.

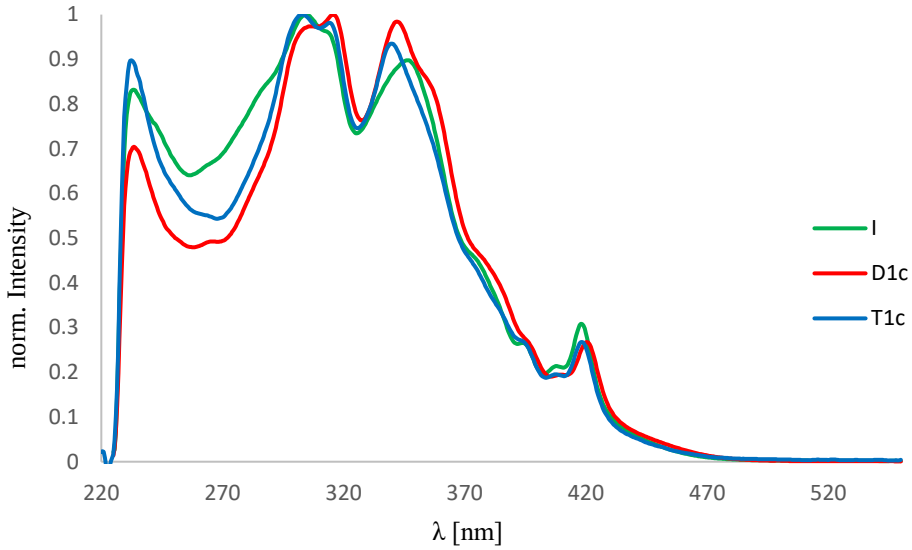

Figure 44: *UV/Vis*-absorption spectra of monomer **I** (green, λ_{max} = 304.5 nm), as well as the PNTs **D$_{1c}$** (red, λ_{max} = 315.5 nm) and **T$_{1c}$** (blue, λ_{max} = 303.0 nm) (all measured in dichloromethane).[102]

Since the angled rigid-rods are *meta*-connected at their outermost benzenes and thus discontinue the conjugation, nearly identical *UV/Vis* and fluorescence spectra of a monomer and its respective phenanthracene nanotubes are obtained, as is shown exemplary for H-shaped monomer **I** and its respective PNTs (cp. Figure 44 and Figure 45).

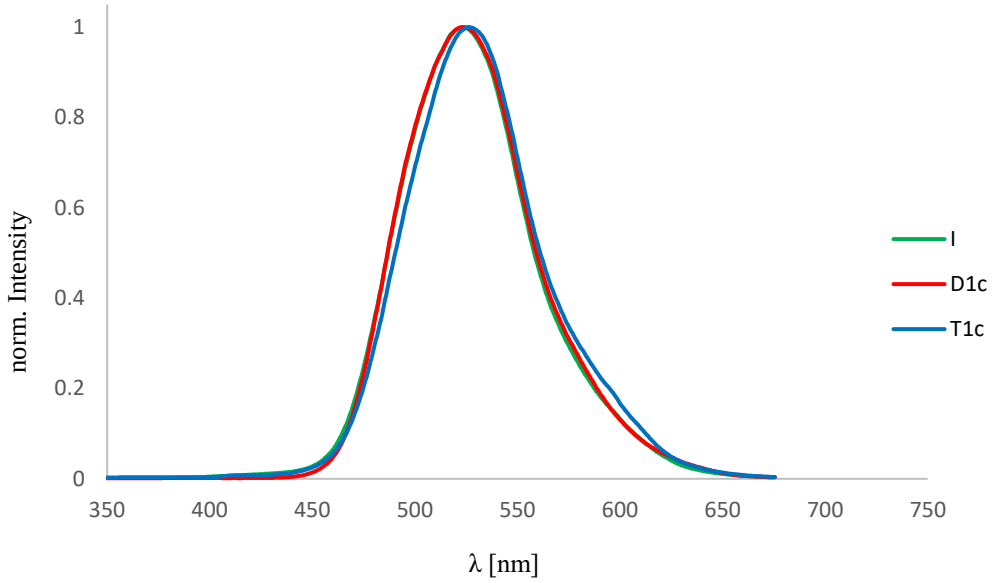

Figure 45: Fluorescence emission spectra of monomer **I** (green, λ_{em} = 523.5 nm), as well as the PNTs **D$_{1c}$** (red, λ_{em} = 523.5 nm) and **T$_{1c}$** (blue, λ_{em} = 525.5 nm) (all measured in dichloromethane); the maximum of intensity found in the *UV/Vis*-absorption spectra were used as excitation wavelengths, respectively.[102]

7.2 Scanning Tunneling Microscopy

The STM images presented in this chapter were obtained by measurements of *J. Bahr* in the group of *Dr. S.-S. Jester*. As explained before (cp. 3.4 Scanning Tunnelling Microscopy as a Tool to Investigate Surface Morphologies), STM is a powerful tool to investigate the behaviour of molecules on templating surfaces in particular with respect to the formation of self-assembled monolayers. Hence, STM images of the first synthesized PNTs, i.e. cylindrical **D$_{1c}$** and **T$_{1c}$** were measured at the solid/liquid interface (HOPG/1,2,4-trichlorobenzene).

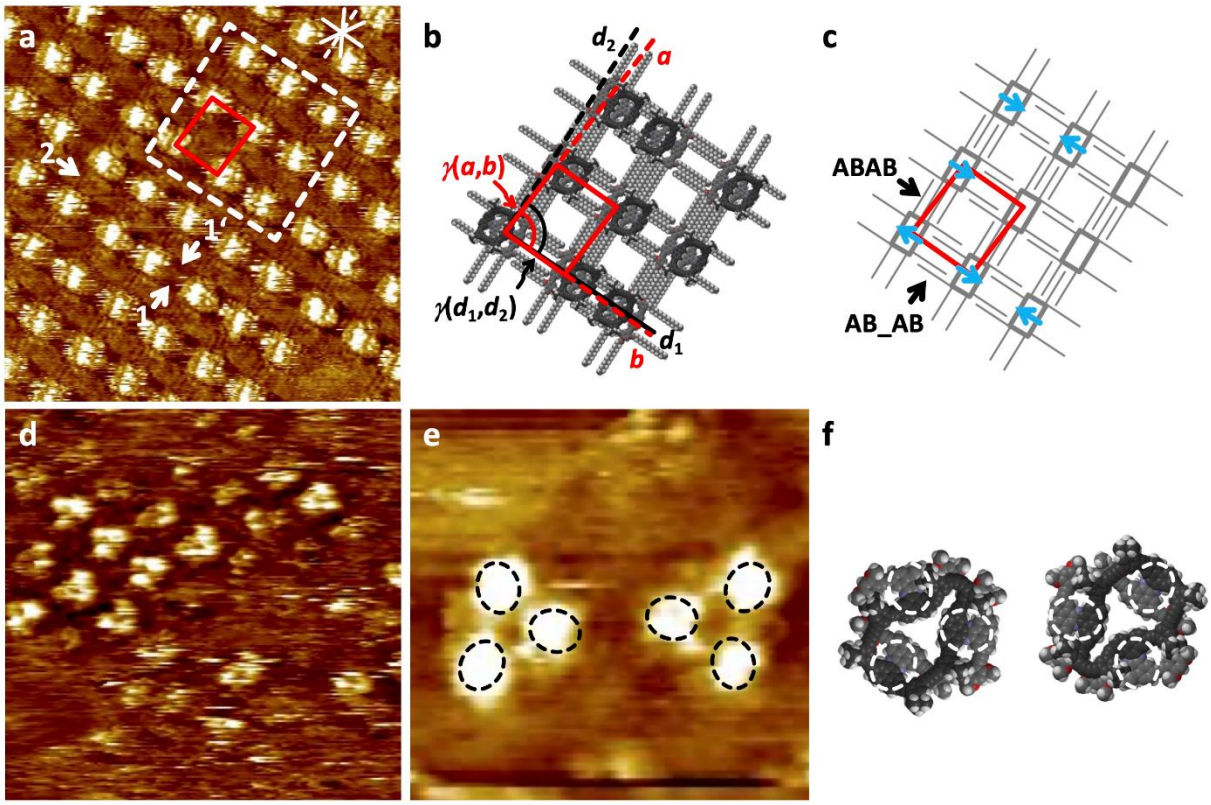

Figure 46: (a), (d), (e) Scanning tunneling microscopy images, (b) proposed supramolecular model, (c) schematic model of the bottom rim, and (f) molecular models (neglecting the side chains) of (a) – (c) a self-assembled monolayer of **D$_{1c}$** and (d) – (f) **T$_{1c}$** at the solution/solid interface of the respective compound in 1,2,4-trichlorobenzene and highly oriented pyrolytic graphite. Image and unit cell parameters: (a) 1_2: $c = 5 \times 10^{-6}$ M, 30 × 30 nm², $V_S = -1.3$ V, $I_t = 23$ pA; $a = (4.3 \pm 0.2)$ nm, $b = (3.7 \pm 0.2)$ nm, $\gamma(a,b) = (87 \pm 2)°$, $\gamma(b,d_1) = (1 \pm 2)°$, $\gamma(d_1,d_2) = (90 \pm 4)°$; (d) 1_3: $c = 3 \times 10^{-5}$ M, 40 × 40 nm² (internal scanner calibration), $V_S = -0.7$ V, $I_t = 18$ pA; (e) 1_3: $c = 3 \times 10^{-5}$ M, 9.4 × 9.4 nm² (internal scanner calibration), $V_S = -0.7$ V, $I_t = 20$ pA; all samples thermally annealed for 20 s at 80 °C. Red lines in (a) – (c) indicate the unit cell; white and black solid (and dashed) lines in (a) and (b) indicate the HOPG main axis (and armchair) directions; grey boxes and lines in (c) indicate the bottom rims and interdigitation pattern of the hexadecyloxy side chains; blue arrows in (c) indicate the tilting directions of 6 out of 9 top rims in the marked surface region in (a); black and white dashed ovals in (e) and (f) highlight the phenanthracene units.[102]

For **D$_{1c}$** a chequerboard-like pattern is observed (cp. Figure 46 (a)), where the bright spots can be attributed to the aromatic phenanthracene backbone and the dark contrast areas to the

alkoxy-chain periphery. The ordered pattern indicates, that as expected the alkoxy-chain bearing SPM adsorbs to the HOPG surface, serving as a two-dimensional anchor for the whole molecule. Four of the eight alkoxy-chains align along one of the HOPG main-axes in a "widened" interdigitation pattern AB_AB (cp. Figure 46 (b) (c)). The other four chains align orthogonal to them and not along a HOPG main-axis. While this behaviour is unexpected and rare it has been observed for comparable molecules before.[54,108] While the resolution does not allow to investigate specific details of the upper and lower SPM of **D$_{1c}$** it is clear that only one bright spot is visible instead of the expected two for the phenanthracene backbones. Together with quantum chemical models (cp. Figure 50) this behaviour can be explained in terms of the PNTs general flexibility. Hence, when they are not seen as rigid channel-like structures, the phenanthracene backbones can act as "hinges" that randomly flip to either side and stay in that position to maximize the π-π-interactions between them. Thus, this leads to the observed STM image where a distinction in position of the bright spots can be made when comparing to neighbouring molecules (cp. Figure 46 (b) (c) and Figure 47; blue arrows).[102]

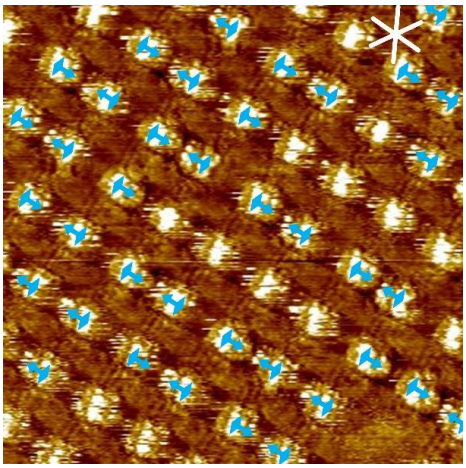

Figure 47: STM image of **D$_{1c}$** at the solid/liquid interface between HOPG and a solution of the respective compound in TCB. Thermally annealed for 20 s at 80 °C, c = 5 × 10^{-6} M, 30 × 30 nm², V_S = –1.3 V, I_t = 23 pA; reprint of Figure **46**a with additional markers indicating the assumed flip direction of the upper backbone rim (blue arrow tips). White lines indicate the HOPG main axis directions.[102]

For **T$_{1c}$** the tendency to form regular 2D patterns is far less pronounced and only small regions with ordered patterns could be observed. There, rows of triangles that point in opposite directions alternate (cp. Figure 48). However, here the expected three bright spots for the aromatic phenanthracene backbones are visible (cp. Figure 46 (e) (f)). The dark contrast areas again can be attributed to the alkyl-chain periphery, indicating the respective SPM of **T$_{1c}$**

being adsorbed to the surface. On the other hand, the resolution is not high enough to determine the exact position and pattern of the alkyl chains.

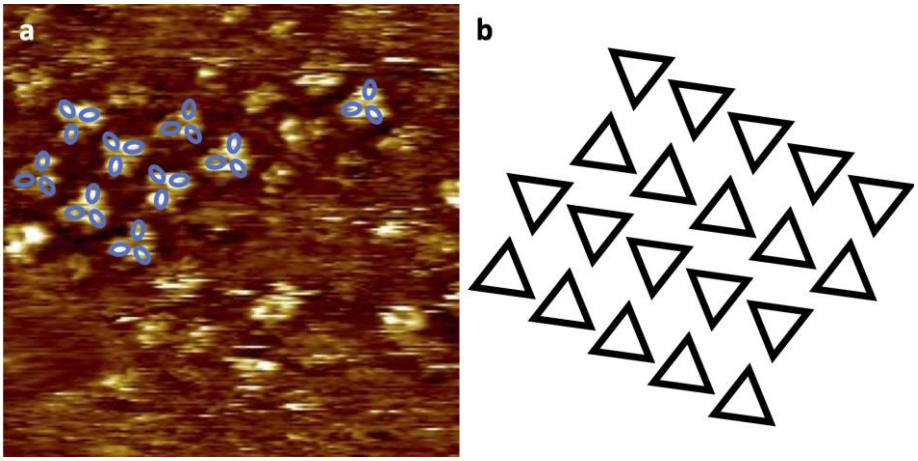

Figure 48: (a) STM image of $\mathbf{T_{1c}}$ at the solid/liquid interface between HOPG and a solution of the respective compound in TCB. Thermally annealed for 20 s at 80 °C, $c = 3 \times 10^{-5}$ M, 40 × 40 nm² (internal scanner calibration), V_S = -0.7 V, I_t = 18 pA. (b) Schematic representation of the assumed antiparallel orientations and periodic pattern of $\mathbf{T_{1c}}$ on HOPG.[102]

The STM investigation of the other PNTs synthesized in this work, as well as the SPM-model system for the alkoxy-chain bearing SPM are subject of current research. This shall then be followed up by experiments with co-adsorption for the bowl-shaped PNTs ($\mathbf{D_{3c}}$ and $\mathbf{T_{3c}}$), as well as investigation of the stacking behaviour for the pyramidal PNTs ($\mathbf{D_{2c}}$ and $\mathbf{T_{2c}}$) with the special focus on fully elucidating the structure of $\mathbf{T_{2c}}$. Furthermore, also the investigation of the angled H-shaped monomers **I**, **II** and **III** are of interest with respect to the formed patterns in comparison with previously investigated linear H-shaped monomers.[76,78]

7.3 Computational Models

The computations for the models presented in this chapter were in part performed by *J. Kohn* and in part during a *lab rotation* under her mentorship in the group of *Prof. S. Grimme*. After obtaining the unexpected STM images for $\mathbf{D_{1c}}$ and $\mathbf{T_{1c}}$ it was of large interest to see if quantum chemical models could support the rationalization for these results surmised above. Simple idealized models for these PNTs (cp. Figure 49) yield rigid structures, that cannot explain why in the STM images for $\mathbf{D_{1c}}$ only one bright spot can be seen instead of two.

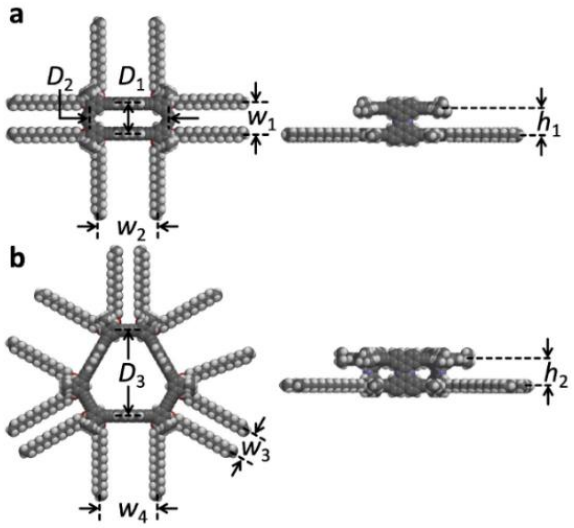

Figure 49: Top and side views of idealized molecular models of (a) **D$_{1c}$** and (b) **T$_{1c}$**; D_1 = 2.4 nm; D_2 = 0.8 nm; h_1 = 0.7 nm; w_1 = 0.9 nm; w_2 = 1.6 nm; D_3 = 2.4 nm^2; h_2 = 0.7 nm; w_3 = 0.8 nm; w_4 = 1.6 nm.[102]

However, when optimizing the geometry of the PNTs on a graphene sheet -as model system for the HOPG- at the GFN2-xtb level, much more flexible structures are observed, leading to a compressed conformation being lowest in energy (cp. Figure 50). There, the aromatic phenanthracene backbones of **D$_{1c}$** overlap, as assumed before. Moreover, as expected, the shape-persistent macrocycle bearing the alkoxy-side chains adsorbs onto the surface leading to a cavity accessible from above for host-guest chemistry. When comparing these results to the other PNTs synthesized in this work, it can be seen, that the bowl-shaped PNTs have a similar conformation, but with a larger cavity opening which should enable the reception of fullerenes in future STM experiments. The pyramidal PNTs on the other hand, show a more rigid and upright structure (especially **T$_{2c}$**). This characteristic, combined with the absent ^{t}*Bu*-groups at the upper shape-persistent macrocycle should enable interesting stacking behaviour, which could then be investigated via STM with respect to the indirect templating effect of the HOPG to PNTs that are farther away from the template, i.e. in multilayers of stacked molecules.

These results clearly show that quantum chemical models are not only a relevant addition to explain the experimental results and support theoretical assumptions to rationalize them. But they can also -within certain restrictions- be utilized to predict potential properties and applications of molecules, and hence are useful to plan the necessary experiments accordingly.

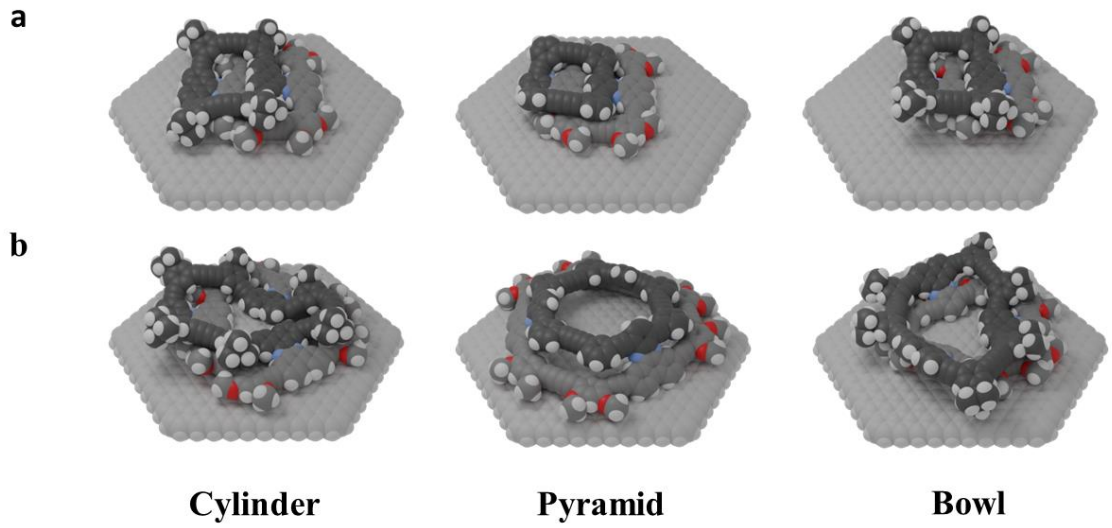

Figure 50: Perspective views of (a) dimeric and (b) trimeric forms of the synthesized PNTs **D$_{1c}$/T$_{1c}$** (cylinder), **D$_{2c}$/T$_{2c}$** (pyramid), and **D$_{3c}$/T$_{3c}$** (bowl) on a graphene cutout optimized at the GFN2-xTB level of theory (with hexadecyloxy side chains omitted and graphene cut to $C_{600}H_{60}$ for clarity.[102]

In addition, to show not only the most stable conformation, but also, if the molecules for example can flip the before mentioned "hinges" to change their conformation, molecular dynamic simulations on the same level of theory were performed for **D$_{1c}$** and **T$_{1c}$**. The results not only demonstrated, that indeed the idealized sturdy structures (cp. Figure 49) are neither stable in solution, nor when adsorbed on a graphene surface. But they show also that once the structure reaches its compressed form via π-π-stacking interactions of the phenanthracene backbones, no more flipping of the "hinges" to another conformations is observed in solution, as well as adsorbed on graphene.[102] However, these simulations also open up the possibility to compare the general rigidity of the PNTs to that of their SPM analogues (cp. Figure 51). Hence, molecular dynamic simulations for the four molecules were performed on the GFN-FF level of theory in solution and adsorbed on graphene and then analysed with respect to their rigidity by the means of distance distribution analysis of opposing phenanthracene backbones of the alkyl-chain bearing rim.

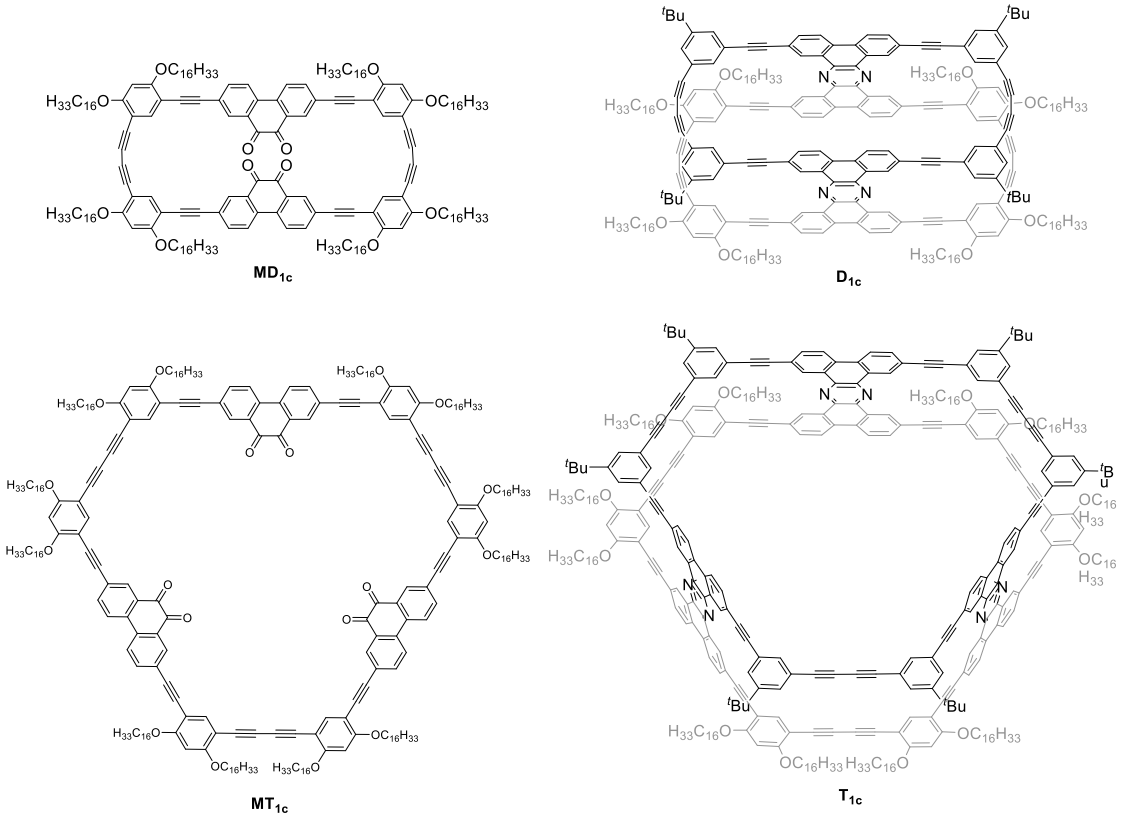

Figure 51: Chemical structures of the PNTs **D$_{1c}$** and **T$_{1c}$** (right), as well as the respective macrocyclic model compounds **MD$_{1c}$** and **MT$_{1c}$** (left) used in the molecular dynamic simulations.[102]

The results are depicted below. From this data it can be concluded that the tubular systems exhibit a narrower distance distribution than the cyclic analogues which indicates a larger rigidity.[102]

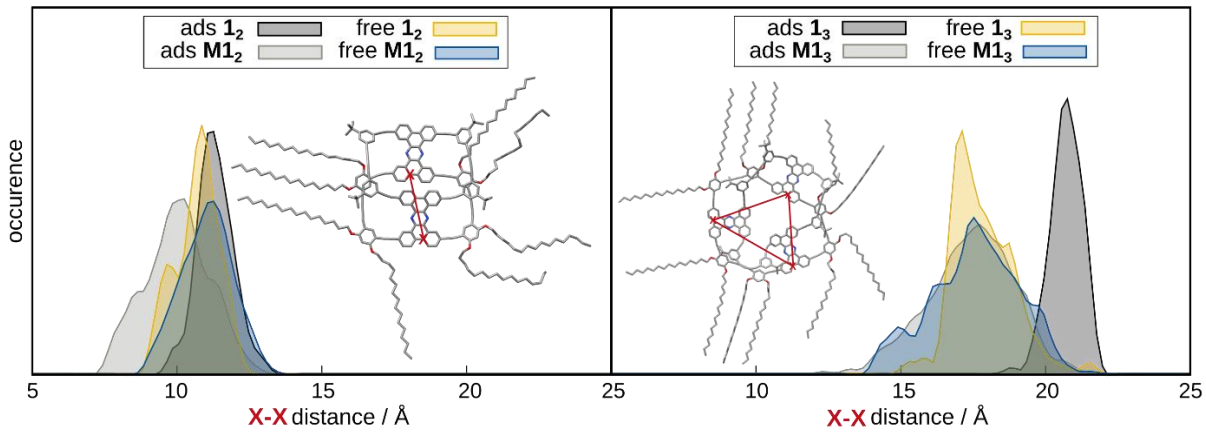

Figure 52: Alkyl-chain bearing rim (X-X) distance distributions in solution and adsorbed on graphene obtained from GFN-FF level molecular dynamic simulations for the PNTs **D$_{1c}$** and **T$_{1c}$** as well as the respective macrocyclic model compounds **MD$_{1c}$** and **MT$_{1c}$.**[102]

7.4 Chemiresistive Sensors

The measurements presented in this chapter were all performed under mentorship of *L. S.-X. Luo* during a three-month research stay in the group of *Prof. T. M. Swager* at the Massachusetts Institute of Technology.

As explained before, one possible application of the in this work synthesized PNTs is the use as selectors in chemiresistive sensors (cp. 3.3 Chemiresistive Sensors). Due to its compressed cylindrical structure with both aromatic backbones close to each other (cp. Figure 46 and Figure 50) it was envisioned, that especially the cylindrical dimer **D$_{1c}$** would be suitable to act as a selector via π-π-stacking interactions with aromatic guest-molecules.

To test if adsorption and desorption of analytes was generally possible using **D$_{1c}$**, quartz crystal microbalance measurements were performed. For this, a solution of **D$_{1c}$** in *o*-DCB was drop-casted onto a quartz resonator with gold-electrodes and after drying under vacuum different analytes were added in 10 ppm concentration for five minutes under constant flow conditions. Dry air was used as carrier gas and the analytes were transferred to the gas phase by heating in a gas generator. Subsequently, they were mixed with the dry air in the desired concentration by means of a mass-flow controller. Based on its piezoelectric properties, mechanical deformation of the quartz crystal, due to the increased mass on the electrode via adsorption of the analytes by **D$_{1c}$**, leads to the formation of a voltage. This way, adsorption and desorption of analytes could be observed as change in the resonant frequency of the quartz crystal microbalance. As the results show, using electron-rich (anisole), electron neutral (toluene, benzene) and electron-deficient (nitrobenzene) aromatic analytes, a reversible process of adsorption followed by desorption, after ending exposure to the analyte, was observed. This was the first prerequisite to be able to use the PNTs in a sensor, allowing for repeated detection of analytes.[102]

Furthermore, a clear preference for the electron-deficient nitrobenzene was observed, reinforcing the idea that **D$_{1c}$** might be a suitable selector for aromatic molecules with different electronic properties. Based on these results and the observed structured and self-assembled monolayers of **D$_{1c}$** on HOPG, it was reasonable to test if utilizing **D$_{1c}$** in a graphene-based chemiresistor would make it possible to detect nitroaromatics. It was envisioned, that due to the similarity of graphene and HOPG, **D$_{1c}$** would form self-assembled monolayers on the graphene surface as well, when drop-casted and upon exposure to nitrobenzene a signal would be observed. A shift of the current-voltage (*I*-*V*) curve (depicting the current between

source- and drain-electrode as function of the gate voltage) to more positive voltages after analyte exposure was expected, due to the *p*-doping nature of the electron-deficient nitrobenzene.

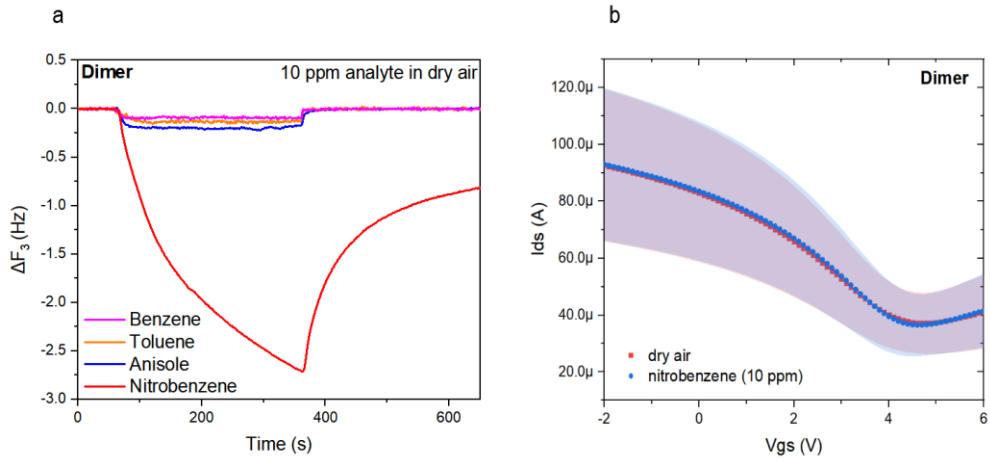

Figure 53: a) Quartz crystal microbalance measurements with dimer **D1c** for different analytes (10 ppm in dry air); depicted is the change in the third harmonic of the resonant frequency with time upon analyte exposure; b) current-voltage (*I-V*) characteristics of a graphene-based FET with **D1c**.[102]

However, no signal response to the analyte could be detected. Since the quartz microbalance results showed that adsorption of the analyte by **D1c** was possible, the issue was determined to be the mechanism of function of the graphene-based chemiresistor. The device is composed of a graphene sheet between two electrodes, comparable to the SWCNT-based chemiresistors described before (cp. 3.3 Chemiresistive Sensors) and a signal response to an analyte is observed as increase or decrease in conductivity of the semiconducting graphene depending on the analyte being *p*-doping or *n*-doping respectively. This means, that when drop-casting the PNTs onto the graphene surface, the analyte adsorbed could only interact with the graphene by a charge-transfer via **D1c** which did not seem possible.

When changing the substrate of the chemiresistor to SWCNTs and simply drop-casting the PNTs onto the pre-deposited SWCNT-network also no signal response toward nitroaromatics was detected, strengthening the presumption that a mechanism involving charge-transfer via **D1c** was not feasible. But SWCNTs, in contrast to graphene, allow for a different sensing-mechanism via swelling. Using SWCNTs, not a single SWCNT -like a single sheet for graphene- connects the two electrodes, but a network, where the charge is transported through several SWCNTs. This means, that a signal can not only be observed due to charge-transfer from the analyte to a single SWCNT (intra-SWCNT mechanism). In this case

an increase in conductivity would be observed due to the *p*-doping effect of the electron-deficient nitroaromatic analytes and the hole-conducting nature of the SWCNTs. But also when interactions between two SWCNTs are inhibited (inter-SWCNT mechanism) a signal can be observed.[102]

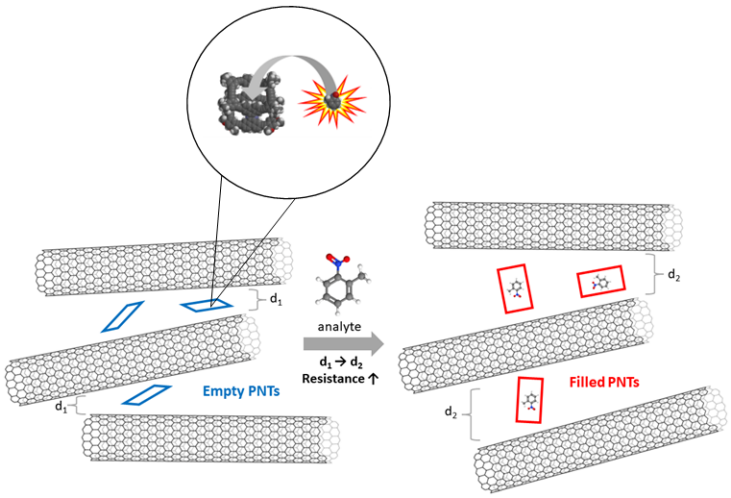

Figure 54: Illustration of a swelling-based sensing mechanism, showing the expansion of the SWCNT-network ($d_2 > d_1$) upon binding of nitrotoluene to the PNTs.[102]

Thereby, it was envisioned when incorporating **D$_{1c}$** into the SWCNT-network rather than simply drop-casting it onto the network, analytes might be detected by a swelling-mechanism, i.e. swelling of the PNTs upon incorporation of an analyte into their cavity leading to inhibition of charge-transport between multiple SWCNTs (cp. Figure 54). Contrasting the intra-SWCNT mechanism, here a lowering of the conductivity would be expected.[102]

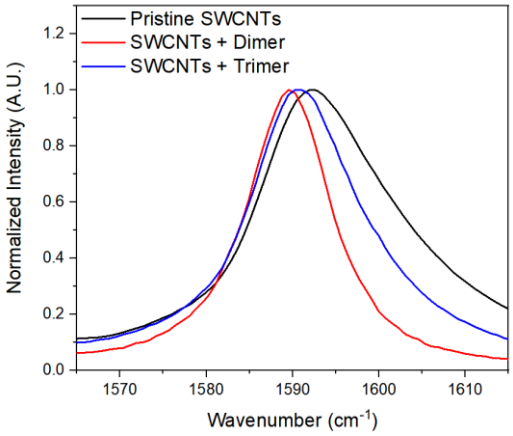

Sample	*Raman* G band [cm^{-1}]
Pristine SWCNTs	1592.52 ± 0.37
SWCNTs + Dimer **D$_{1C}$**	1589.67 ± 0.16
SWCNTs + Trimer **T$_{1C}$**	1590.26 ± 0.24

Figure 55: *Raman*-spectrum showing the SWCNT C(sp^2)-C(sp^2) stretching mode of pristine SWCNTs, as well as SWCNTs with dimer **D$_{1c}$** and trimer **T$_{1c}$** on glass substrates at 633 nm excitation wavelength (left) and corresponding average and standard deviations of the peak positions from 4 different locations (right).[102]

For the swelling of PNTs to be able to break the interconnections between SWCNTs they need to have a strong interaction with them. This interaction could be shown by *Raman*-spectroscopy. Here, a shift to lower wavenumbers of the SWCNT C(sp^2)-C(sp^2) stretching mode (G band) was observed upon interaction of the SWCNTs with the dimer **D$_{1c}$** and trimer **T$_{1c}$**, compared to pristine SWCNTs (cp. Figure 55). Thus, indicating a strong interaction via an *n*-type doping influence from the PNTs to the intrinsically *p*-type SWCNTs.[109]

For the preparation of the sensor chip, a dispersion of **D$_{1c}$** with SWCNTs was made by ultrasonication in *o*-dichlorobenzene, which was subsequently drop-casted between the electrodes and dried under vacuum. The 10:1 ratio of PNTs to SWCNTs was chosen on the one hand, to suppress background signal responses obtained by interaction of the pristine-SWCNTs with the analytes by an intra-SWCNT mechanism, which would lower the selectivity of the sensor. On the other hand, it should ensure a large amount of **D$_{1c}$** molecules in the vicinity of junctions between the SWCNTs, to give a good signal response when breaking them up via the swelling-mechanism.

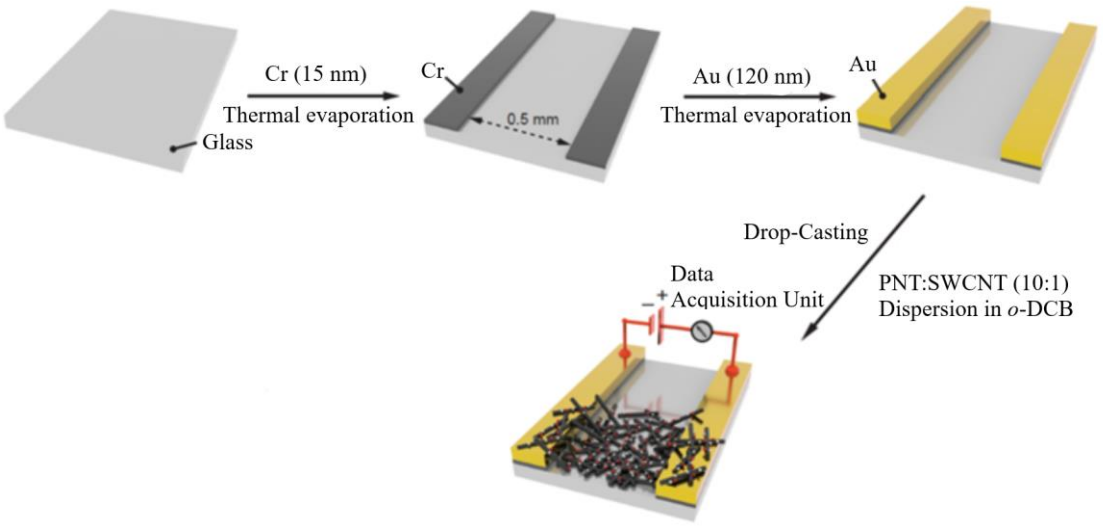

Figure 56: Illustration of the chemiresistor fabrication using SWCNTs and dimer **D$_{1c}$**.[102]

Moreover, each fabricated chemiresistor chip consists of four channels (i.e. measuring electrodes) and one counter electrode, effectively allowing to measure four devices at once, to observe deviations in the signal response and obtain the internal measurement errors of the device without disturbance from deviations that naturally occur between different individually manufactured chips. Indeed, using these devices, signals towards different analytes could be

obtained and are presented in the following. For this, the analytes were transferred to the gas phase by heating in a gas generator and subsequently were mixed with the dry air carrier gas in the desired concentration by means of a mass-flow controller. The chemiresistor chips were then exposed to the analytes under constant flow conditions for five minutes.

Figure 57: a chemiresistor chip with a network of **D$_{1c}$** and SWCNTs in the gap between the measuring electrodes (left) and a 10:1 dispersion of **D$_{1c}$** and SWCNTs in *o*-dichlorobenzene (right).

Analysing the results, it is visible, that the devices showed a clear selectivity for nitroaromatic compounds (cp. Figure 58). The initially proposed sensing via π-π-stacking interactions with aromatic analytes correlating to their electronic structure, cannot fully explain these results, as signals for electron-deficient aromatic compounds like the trifluorobenzene or benzonitrile were noticeably lower than the signals for nitrobenzene or nitrotoluene. In fact, they were comparable to the signal of the electron-rich anisole.

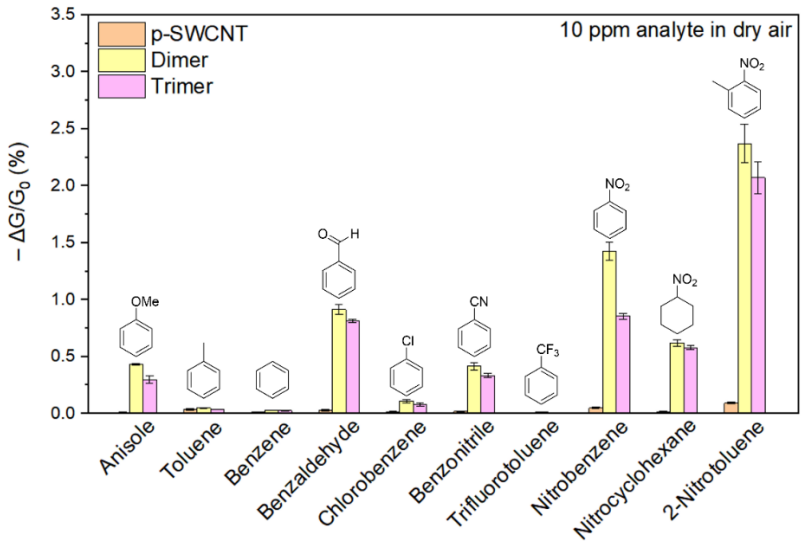

Figure 58: Signal response as relative lowering in conductivity *G* upon exposure to 10 ppm of various analytes in dry air for different devices with pristine-SWCNTs (orange), 10:1 **D$_{1c}$** : SWCNTs (yellow) and 10:1 **T$_{1c}$** : SWCNTs (pink).[102]

Moreover, the nitro-group is not the primary selectivity factor either, as the closest related non-aromatic compound to nitrobenzene, i.e. nitrocyclohexane gave a significantly lower

signal response. Additionally, analytes with a higher boiling and melting point adsorb more easily onto surfaces, however also here no significant trend could be observed.

It can be concluded that a multi-component sensing mechanism involving interaction of the aromatic system and the nitro-group with the respective PNTs **D$_{1c}$** or **T$_{1c}$** led to the observed selectivity towards nitroaromatic analytes. This interaction itself, is then proposedly based on a differently efficient induced-fit of the nanotubular host-molecules towards the respective analyte guest-molecules, i.e. not only the electronic structure but also the shape of the analyte influence the sensing response. Furthermore, it is visible, that the interaction of the analytes with the PNTs is essential, as the chemiresistors with pristine-SWCNTs showed only low signal response in general and no selectivity whatsoever. Hence, the potential of the in this work synthesized PNTs as selectors in chemiresistive sensors was demonstrated. However, to gain further insights into the sensing-mechanism and clarify the swelling of the PNTs -acting as molecular actuators- upon host-guest interaction, extensive quantum chemical simulations at a high level of theory would be necessary, which are currently not available for such large systems like the PNTs. Moreover, it can be observed that the cylindrical trimer **T$_{1c}$** consistently gave lower responses for all analytes than the dimer **D$_{1c}$**, showing that a stronger interaction with the analytes is observed for a smaller cavity size. Being the precursor to these cylindrical molecules and easier to synthesize, it would simplify the manufacturing of the chemiresistive sensors if the planar H-shaped monomer **I** could be utilized as selector.

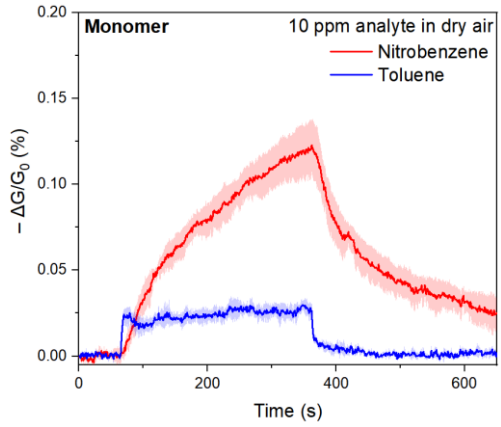

Figure 59: Signal response trace for **I**-SWCNT chemiresistors upon exposure to 10 ppm nitrobenzene and toluene in dry air.[102]

However, since there no cavity for molecule adsorption is present, no swelling would be observed upon analyte interaction. This assumption was based on the lowered signal

responses measured for the larger cavity molecule **T$_{1c}$**, displaying the need for a 3D-structure comprising a cavity, to interact with the analytes via an induced-fit mechanism. The resulting signal-response curve of monomer **I** as selector validates this assumption, showing only a small response towards nitrobenzene comparable to that of pristine SWCNTs (cp. Figure 59). Moreover, the monomer dispersed the SWCNTs poorly, compared to **D$_{1c}$** and **T$_{1c}$**, leading to phase-separated aggregates.

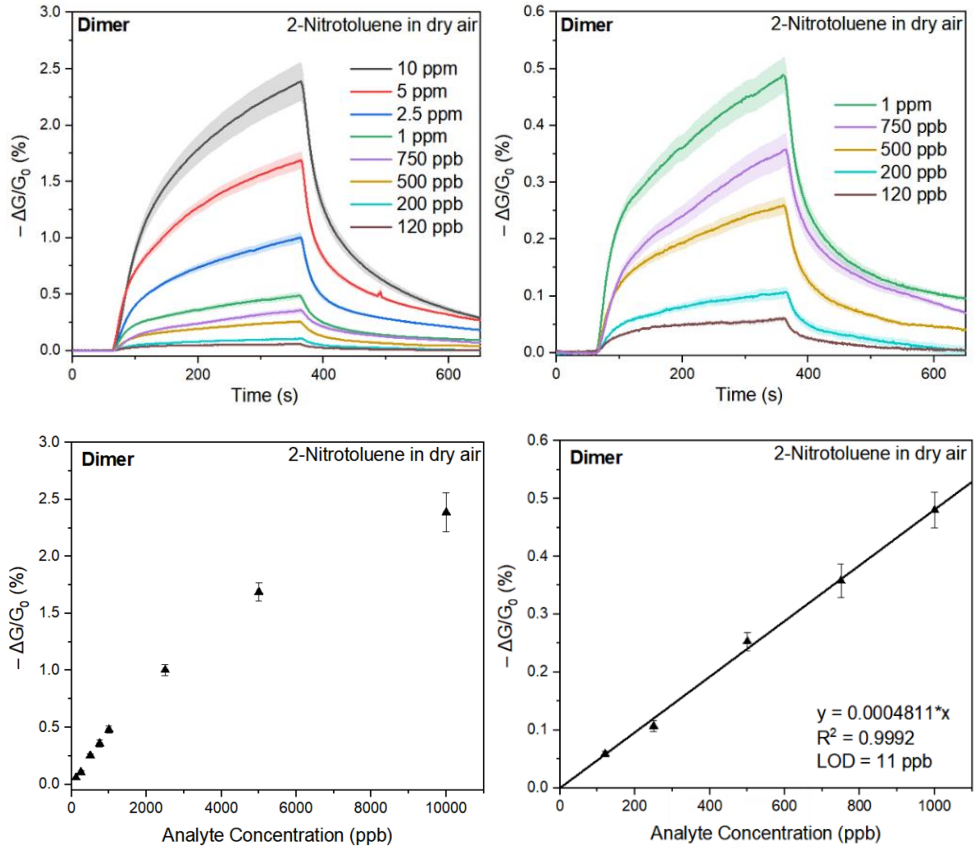

Figure 60: Signal response traces and signal strength to analyte concentration ratio for **D$_{1c}$**-SWCNT chemiresistors upon exposure to different concentrations of 2-nitrotoluene in dry air including analyte concentrations above 1 ppm (left) and only showing analyte concentrations below 1 ppm (right).[102]

Additionally, in the context of good selectivity towards nitroaromatic analytes, it is relevant to be able to sense low concentrations of 2-nitrotoluene as marker for TNT and thus contribute to the development of new lightweight, portable and solution processable explosive sensors. Regarding TNT, the detection of markers like 2-nitrotoluene, that are always present in TNT samples is a more promising approach in gas-phase sensing compared to the direct sensing of TNT. This is because of the low vapour pressure of TNT at room temperature, due to its high melting and boiling point.[110] Hence, the LOD (i.e. the smallest amount of analyte that gives a

mean signal larger than three times the standard deviation of the baseline) for the detection of 2-nitrotoluene was determined. For that, the signal response towards different concentrations of 2-nitrotoluene was measured and then signal strength and analyte concentration were correlated (cp. Figure 60). Only for analyte concentrations below 1 ppm a linear dependency could be observed, which may be due to saturation of the sensor with the analyte at higher concentrations. When only analyte concentrations below 1 ppm are taken into consideration the linear dependency of signal strength to analyte concentration was given with a good coefficient of determination $R^2=0.999$. This linear correlation was then used to determine the calculated LOD, which amounted to 11 ppb.[102]

Comparing the LOD of the in this work manufactured sensors to other chemiresistors shows, that the result obtained here in the range of few ppb is among the best results published to this date (cp. Table 4). Moreover, lower LODs were obtained for solution sensing, however the usability of these devices in explosive sensing is low, since they cannot detect the explosive substance vapours emitted into the air.[111]

Table 4: Comparing limits of detection of significant works on chemiresistive sensors towards nitroaromatic compounds published in recent years.[112]

Sensor Material	Sensing Environment	LOD [ppb]	Analyte	Published in [year]
ZnO-nanowires / SWCNTs	gas phase	60	TNT	2010[113]
single-chain antibody / SWCNTs	in water	0.5	TNT	2010[114]
SWCNTs	gas phase	0.5	2,4-dinitrotoluene	2013[115]
SWCNTs /Si /SiO_2	in water	0.01	TNT	2014[111]
Oligomer-coated SWCNTs	gas phase	40	2-nitrotoluene	2015[116]
Vacuum-filtered SWCNTs	gas phase	2	2,4-dinitrotoluene	2018[117]

Furthermore, other sensing methods which are not based on a chemiresistive response but rather employ chromatography or fluorescence quenching, give two orders of magnitude lower LODs in the range of few ppq.[110,118] However, they require larger devices and are more costly to manufacture, because they do not benefit from e.g. easy solution processability of the compounds like chemiresistive sensors. Additional disadvantages are their higher energy consumption making portable devices, that could e.g. be implemented as badges into

work-clothing for hazardous environments or deployed in arrays to survey large areas, not feasible.

Regarding the measurements using the cylindrical trimer $\mathbf{T_{1c}}$ a slightly higher LOD of 16 ppb was obtained, which is in good correlation with the overall lower signal response observed for this chemiresistive sensor (cp. Figure 61).

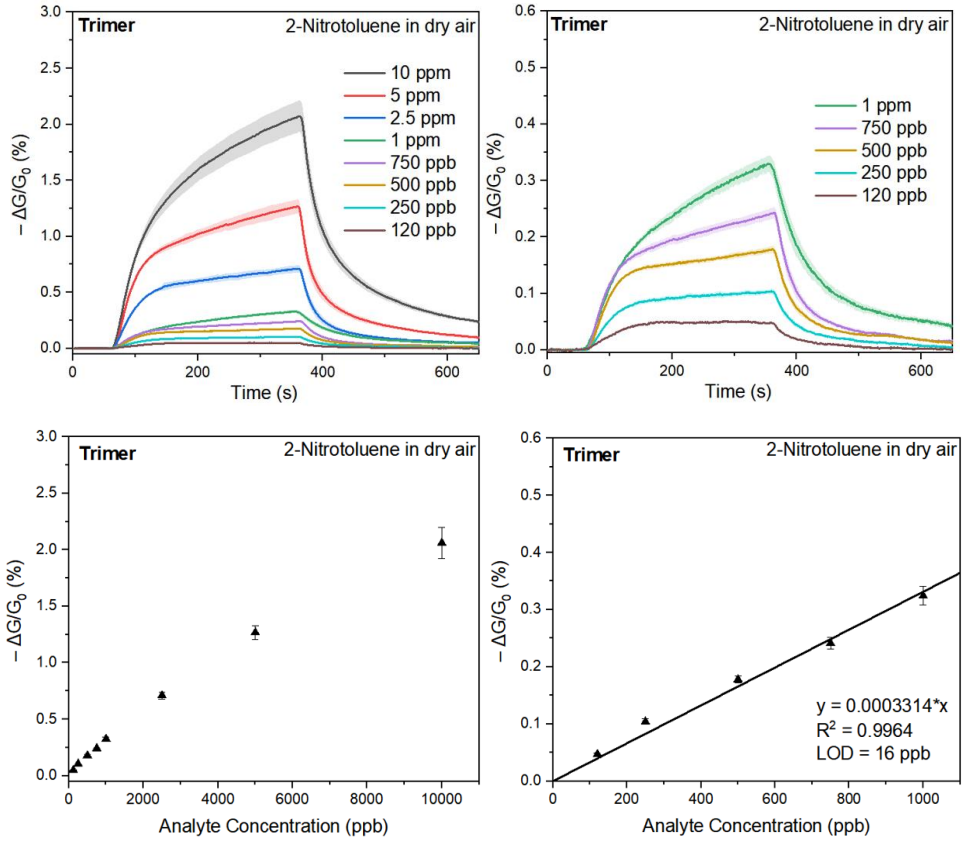

Figure 61: Signal response traces and signal strength to analyte concentration ratio for $\mathbf{T_{1c}}$-SWCNT chemiresistors upon exposure to different concentrations of 2-nitrotoluene in dry air including analyte concentrations above 1 ppm (left) and only showing analyte concentrations below 1 ppm (right).[102]

After investigation of the selectivity of the sensors and determination of the limit of detection, measurements were performed to test for the interference of other common so-called volatile organic compounds (short: VOCs). This is relevant for applications since these VOCs have a high vapour pressure and are abundant in the environment. Hence, they could disturb the selectivity of the sensor, or give false positive signals even though they only interact weakly with the sensor, simply due to their much higher concentration.

As the results show, even though the volatile organic compounds were added in a ten times higher concentration than the 2-nitrotoluene, no significant signal response was measured for

any of the analytes when using sensors comprised of SWCNTs and either **D1c** or **T1c** (cp. Figure 62). For pristine-SWCNTs, however, the signal response for the VOCs was comparable to that towards the 2-nitrotoluene. This way not only the superior selectivity when utilizing PNTs as selectors, but also their tolerance concerning interference was demonstrated.

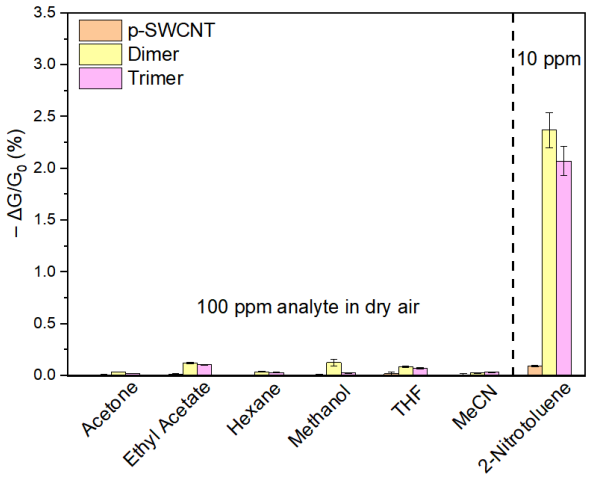

Figure 62: Signal response as relative lowering in conductivity *G* upon exposure to 100 ppm of various volatile organic compounds in dry air for different devices with pristine-SWCNTs (orange), 10:1 **D1c** : SWCNTs (yellow) and 10:1 **T1c** : SWCNTs (pink).[102]

To finalize the sensing experiments, humidity and stability studies were performed, to ensure that reliable sensing responses to the desired nitroaromatic analytes would be obtained under real-world conditions over a longer period of time.

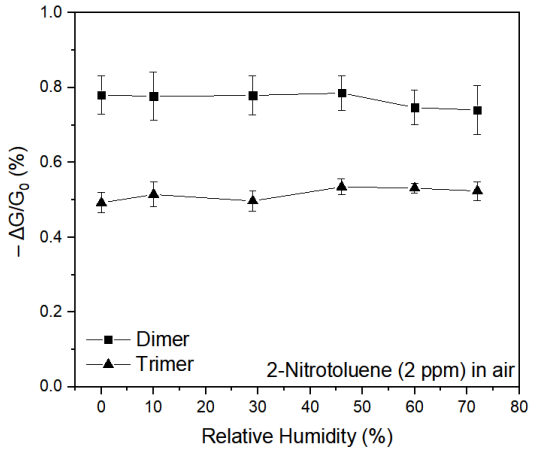

Figure 63: Signal response as relative lowering in conductivity *G* upon exposure to 2 ppm of 2-nitrotoluene in dry air enriched with moisture for sensors containing 10:1 **D1c** : SWCNTs (squares) and 10:1 **T1c** : SWCNTs (triangles).[102]

Thus, under the same conditions as before, the chemiresistive sensors were used to measure the signal response towards 2 ppm of 2-nitrotoluene. However, the dry air was gradually enriched with moisture. As can be seen from the results, increasing the relative humidity did not lead to a significantly decreased signal response (cp. Figure 63), showing that the chemiresistors can be used reliably under the always changing ambient conditions.

Furthermore, measurements were performed at distinct time intervals after sensor device fabrication. It was observed that even after one month storing the sensors under ambient conditions at room temperature, the signal response towards 2-nitotoluene retained 70% of the original strength for dimer $\mathbf{D_{1c}}$ and trimer $\mathbf{T_{1c}}$ alike (cp. Figure 64). This way the stability of the sensors was demonstrated. These last experiments concluded the sensing experiments, having not only manufactured solution processable, low-energy consumption devices, but also sensors with high selectivity, sensitivity, and stability under ambient conditions.

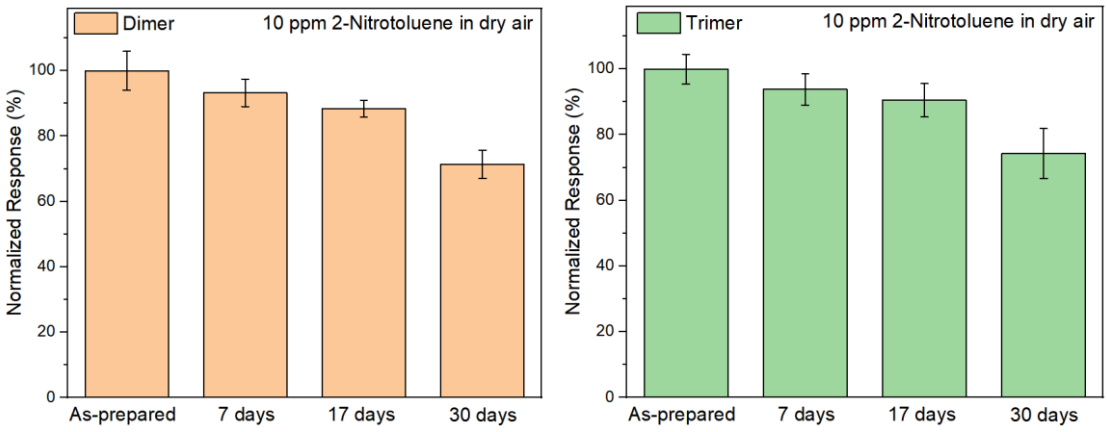

Figure 64: Normalized signal response [%] of sensors containing 10:1 $\mathbf{D_{1c}}$: SWCNTs (left) and 10:1 $\mathbf{T_{1c}}$: SWCNTs (right) upon exposure to 10 ppm of 2-nitrotoluene in dry air at distinct time intervals after sensor fabrication.[102]

8. Summary & Outlook

8.1 Summary

The primary aim of this work was the bottom-up synthesis of phenanthracene nanotubes (PNTs) for organic electronic applications.

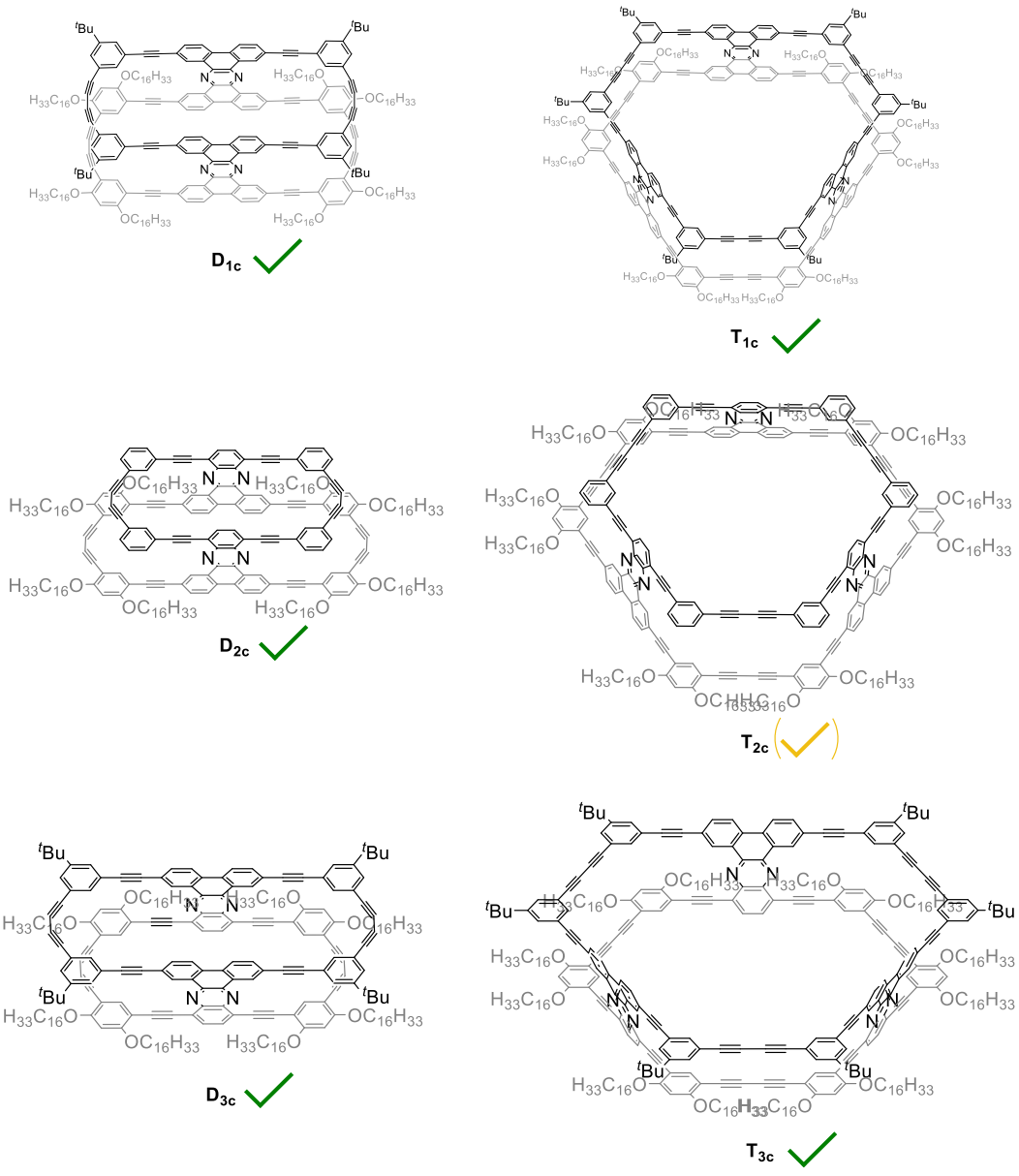

Figure 65: Schematic overview of the chemical structure of the in this work synthesized phenanthracene nanotubes; showing fully characterised molecules (green tick) and molecules whose structures is not yet fully elucidated (yellow tick).

In the first part, cylindrical phenanthracene nanotubes **D$_{1c}$** and **T$_{1c}$** were synthesized, and the synthetic strategy was optimized to give access to larger amounts of material (in total ~28 mg of dimer **D$_{1c}$** and ~7 mg of trimer **T$_{1c}$**). This modular synthetic strategy was then expanded to yield bowl-shaped and pyramidal phenanthracene nanotubes. While the strategy was applied successfully giving comparable yields for the bowl-shaped molecules **D$_{3c}$** and **T$_{3c}$**, the pyramidal structures **D$_{2c}$** and **T$_{2c}$** were obtained in yields <3% in the last step. This might be attributed to the fact that these structures are the only ones that do not possess *^{t}Bu*-groups at the upper rim (cp. Figure 65). Hence, upon closing the second macrocycle the molecules might aggregate, leading to a larger amount of intermolecularly coupled byproduct. In addition, a T-shaped monomer as model system for the investigation of the photophysical behaviour of the PNTs, as well SPMs based on **31** to investigate the adsorption of the alkyl-chain bearing ring of the PNTs on HOPG with STM have been synthesized successfully in the scope of this work.

The synthesized molecules were then investigated via STM on HOPG as a templating surface, showing adsorbed molecules in self-assembled monolayers for **D$_{1c}$** and small assemblies of adsorbed molecules for **T$_{1c}$**. No fullerenes could be deposited in the cavities due to their collapsed conformation, which was not only observed via STM, but also in the quantum chemical calculations. Further STM investigations of the bowl-shaped molecules and attempting to insert fullerenes in their cavities, as well as the pyramidal molecules, including the investigation of potential stacking-behaviour and the conclusive elucidation of the structure of **T$_{2c}$** are subject of current research. The same holds true for the investigation of the macrocyclic model-systems in comparison and the self-assembly of the angled H-shaped monomers themselves.

Based on the results of the STM experiments, **D$_{1c}$** and **T$_{1c}$** were investigated regarding their potential for host-guest chemistry and an affinity towards nitroaromatic molecules was found. Optimization and testing then led to the successful manufacturing of single-walled carbon nanotube chemiresistors for explosive detection, an organic electronic device employing a template-design by the directed adsorption of **D$_{1c}$** and **T$_{1c}$** on a carbon-based substrate. With **D$_{1c}$** and **T$_{1c}$** as selectors the performance of the devices was enhanced in terms of durability, selectivity and sensitivity (LOD = 11 ppb), a result that is among the best published to this date.[102]

Additionally, first steps towards the investigation of the photophysical properties of the in this work synthesized molecules were made. Here, it could be shown that the easier synthesizable H-shaped monomers **I**, **II** and **III** can serve as model systems exerting the same photophysical behaviour as their corresponding PNTs. However, a complete elucidation of the observed phenomena, as well as verification of the made assumptions are still subject of current research.

Summarising, based on the combined approaches of the modular synthesis towards H-shaped molecules and known methods for the generation of shape-persistent macrocycles, a new class of 3D-molecules (phenanthracene nanotubes) were synthesized, and a reliable modular synthetic strategy was established. Already now, these molecules could be used in an organic electronic sensing device and further investigations are still subject of current research and may yield even more interesting properties that lead to applications in organic electronics.

8.2 Research Directions

Based on the synthetic successes of this work, i.e. a reliable modular approach towards angled H-shaped molecules and PNTs thereof, several interesting expansions to this synthetic route are conceivable.

One such derivatization would be to enhance the rigidity of the PNTs and thus stabilize their nanoporous structure by reacting them with sulfur. In this way, the bis-alkynes connecting the H-shaped molecules in the PNTs would be transformed into thiophenes via a trisulfur radical anion, as has been shown in the literature for variously substituted 1,3-diynes.[119] A similar rigidifying effect can be achieved, when the angled rigid-rods are bearing bromines instead of alkynes and the SPMs are formed in the Pt-mediated cyclization of aryl-bromides by *Yamago et al.* that has been used in the synthesis of SPMs before.[120] In this way, the H-shaped monomers would be connected directly with single-bonds to each other without the relatively flexible bis-alkynes. However, to achieve this a completely new synthetic strategy would need to be devised.

Another possibility to expand the PNTs application, would be to use a pyridine-core instead of a benzene-core for the non-alkyl chain bearing angled rigid-rods. Hence these could be functionalized in the end, for example with polyethylene-glycol chains, to give a three-dimensional polar cavity for host-guest chemistry, an expansion to the work of

Höger et al. with respect to their amphiphilic SPM.[56] If such chains would be attached to both rims of a PNT, it could be incorporated into a lipid-bilayer membrane and be investigated in terms of the potential as large trans-membrane channel with possible bactericidal effect by making their membrane porous and permeable.

In addition, it would be thinkable to exchange the phenanthrene core-units with their *N*- or *S*-heterocyclic counterparts, like phenanthroline. This would enable complex-formation with a suitable square-planar coordinating metal-centre (e.g. Pt or Au) to connect the PNTs to large nanotubes (cp. Figure 66; left). This could also be taken a step further using an A-B functionalized central-spacer to covalently connect a multitude of SPMs to larger PNTs in a step-growth polymerisation (polycondensation). For this purpose, instead of phenanthrene, a pyrene-core could be chosen and on one side be functionalized with 1,2-diketones and on the other side with 1,2-diamines (cp. Figure 66; right). A similar approach to synthesize long pyrene-based nanoribbons was already successfully applied by *Mateo-Alonso et al.*[121]

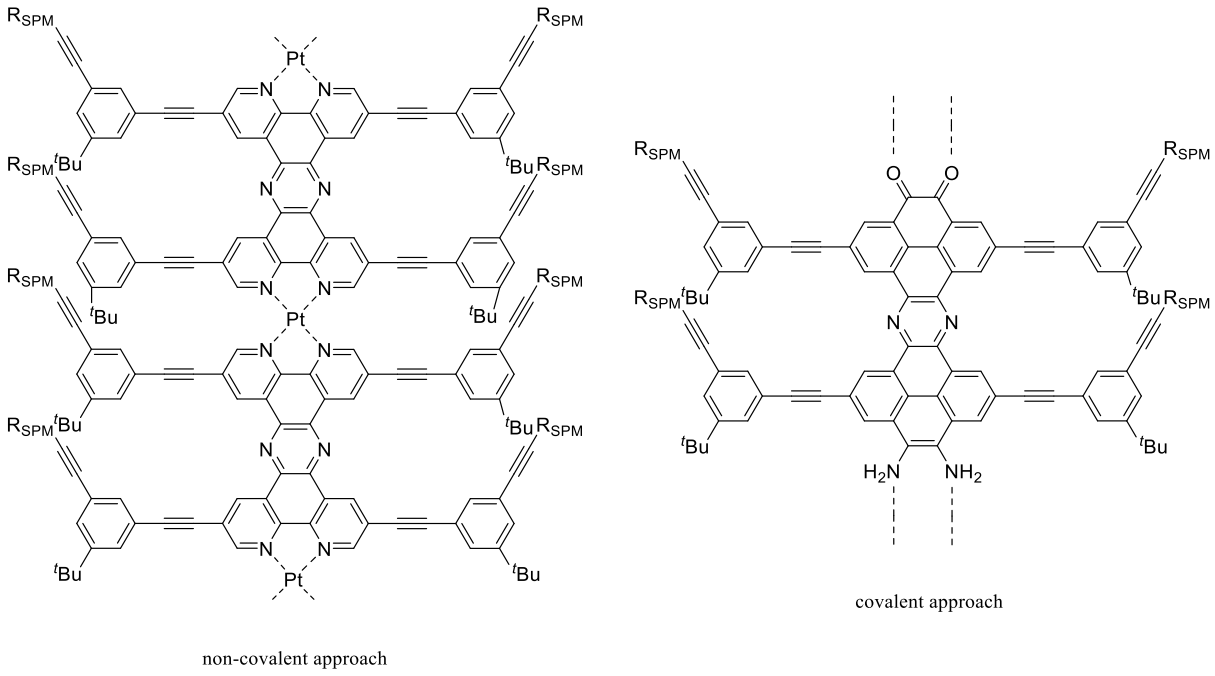

Figure 66: Schematic side-view illustration of the non-covalent approach (left) and covalent approach (right) towards larger nanotubes based on PNTs (R_{SPM} denominating the other side of the PNTs; here omitted for better visibility).

Concerning further use of the in this work synthesized molecules in organic electronics, the angled H-shaped molecules might prove to be interesting materials for OSCs or OLEDs. On the one hand, this is due to their small molecule nature making a templating-approach to obtain ordered structures in thin films possible and allowing for easy solution processability, compared to polymer-based optoelectronically active materials. On the other hand, their modular structure allows to fine tune their donor and acceptor properties and give donor-acceptor-donor (A-D-A) or acceptor-donor-acceptor (D-A-D) structures, depending on how the angled rigid-rods are substituted making them more, or less electron-rich than the phenanthracene-spacer. Such A-D-A and D-A-D type molecules are to this date the best-performing class of active materials regarding OSC efficiency.[122] Furthermore, being able to synthesize donors and acceptors just via modification of the same molecule attenuates problems during device manufacturing, such as miscibility issues between donor and acceptor molecules.

Hence, while the analysis of the synthesized PNTs regarding their photophysical behaviour and their potential to form self-assembled monolayers on HOPG is still subject of current research. The results gained in this work already show new pathways to applications in the field of organic electronics and from a synthetic perspective allow for expansion of the developed concepts to gain large nanotubes via a bottom-up approach.

9. Experimental Discussion

9.1 Materials and Methods

Substances and Solvents:

Commercially available reagents were used without further purification, unless stated otherwise. [(3-cyanopropyl)dimethylsilyl]acetylene (CPDMS-acetylene) was synthesized according to literature procedures.[123] Preliminary studies on the synthesis of molecules **2**, **5**, **6**, **7**, **22**, **24**, **25** and **28** were perfomed as part of a Master's Thesis.[31] SWCNTs (Signis SG65i with a diameter of 0.7-0.9 nm, (6,5) chirality, ≥93% carbon as SWCNTs, lot no.: MKBZ1159V) were purchased from Sigma-Aldrich and used as received. For the sensing experiments laboratory-grade compressed air was used as carrier gas. All oxygen- and moisture-sensitive reactions were carried out using standard *Schlenk* techniques under argon. Dry solvents (THF, toluene, methanol, ethanol) were obtained from an M. Braun SPS 800 Solvent Drying System under argon atmosphere. Piperidine was distilled under argon over CaH_2. Pyridine (99.5+%, anhydrous) and diisopropylamine (99.95% purified by redistillation in Sure/Seal™) were obtained from commercial suppliers. Solvents used for workup and purification were either distilled (dichloromethane, cyclohexane), or obtained from commercial suppliers of analytical reagent grade quality (toluene, acetonitrile, ethanol, acetone, methanol, chloroform) or HPLC-grade (THF). Deviations in the R_f values for the same compound obtained by different synthetic routes are ascribed to residual solvents and temperature differences upon performing the TLC. In addition, if several synthetic routes to a compound are presented the route with the highest yield is preferred.

Mass Spectrometry:

EI	MAT 95 XL sector field instrument, Manufacturer: ThermoQuest Finnigan
ESI (POS/NEG)	LTQ Orbitrap XL, Manufacturer: Thermo Fisher Scientific
APCI	LTQ Orbitrap XL, Manufacturer: Thermo Fisher Scientific
MALDI (POS)	ultrafleXtreme MALDI-TOF/TOF Manufacturer: Bruker Daltonics

Nuclear Magnetic Resonance Spectroscopy (NMR):

^{1}H- and ^{13}C-NMR	Bruker Avance I 400 (400 MHz or 101 MHz respectively), Bruker Avance I 500 (500 MHz or 126 MHz respectively), Bruker Avance III HD 500 (500 MHz or 126 MHz respectively), Bruker Avance III HD 700 (700 MHz or 176 MHz respectively),
Deuterated Solvents:	DEUTERO GmbH
References	$CDCl_3$ (^{1}H: 7.26 ppm, ^{13}C: 77.2 ppm) DMSO-d_6 (^{1}H: 2.50 ppm, ^{13}C: 39.5 ppm)[124]

For the analysis of the experimental spectra the software MestReNova[125] was used.

Column Chromatography:

Columns	Glass columns with implemented glass frit (Ø 10 – 50 mm)
Stationary Phase	Silica gel (60 M, 40-63 µm)
Mobile Phase	As mixtures or pure solvents CH, DCM, Tol

Flash Chromatography:

Pump	puriFlash® Minibox (max. pressure 7 bar), Supplier: Interchim
Columns	puriFlash® PF-30SI-JP/25G; readily packed with Silica gel (30 µm), Supplier: Interchim
Mobile Phase	As mixtures or pure solvents CH, DCM

Thin Layer Chromatography:

TLC Plates	TLC Silica gel 60 F_{254} (175 – 225 µm silica gel with fluorescence indicator), Supplier: Merck
Detection	Quenching of the fluorescent indicator (λ = 254 nm) Intrinsic fluorescence of the applied substance (λ = 366 nm)

Further Spectroscopy:

Fluorescence emission	Perkin Elmer LS-50B (10 mm quartz cuvettes)

UV/vis absorption	Perkin Elmer Lambda 18 (10 mm quartz cuvettes) Perkin Elmer Lambda 365+ (10 mm quartz cuvettes)
Raman spectra	Horiba Jobin-Yvon LabRAM (Model HR800) Raman confocal microscope with a 633 nm laser.

9.2 GPC Experiment

Analytical gel permeation chromatography (GPC) was performed in THF at 35 °C on an Agilent Technologies system at a flow rate of 1 mL/min using an IsoPump G1310A, ALS G1329A autosampler, PSS columns (set of 4 columns 8 mm x 300 mm, polystyrene, porosity of 10^2, 10^3, 10^5 and 10^6 Å, with precolumn, Polymer Standards Service GmbH), and a VWD G1314B and a RID G1362A detector. Calibration was carried out with polystyrene standards from Polymer Standards Service GmbH.

Recycling GPC (recGPC) was performed in THF at 35 °C on a Shimadzu system at a flow rate of 5 mL/min using a LC-20 AD pump, DGU-20 A3 degasser, SIL-20 A HAT autosampler, CTO-20 A oven, FRC-10 A fraction collector, FCV-20 AH2 switching valve, PSS columns (set of 3 columns 20 mm x 300 mm, polystyrene, preparative PSS SDV linear S with precolumn 20 mm x 50 mm, preparative PSS SDV) and a SPD-20A UV-detector (λ_1 = 254 nm and λ_2 = 366 nm).

9.3 STM Experiment

Scanning tunneling microscopy (STM) was performed under ambient conditions (r.t.) at the solution/solid interface, using 1,2,4-trichlorobenzene (TCB) as solvent and highly oriented pyrolytic graphite (HOPG) as substrate. In a typical experiment, 2 µl of a 3×10^{-5} M to 5×10^{-6} M solution of the compound(s) of interest was dropped onto a freshly cleaved HOPG substrate at elevated temperature (80 °C), kept at this temperature for 20 s, and allowed to cool to room temperature before the STM measurements were performed with the tip immersed into the solution. Bias voltages between -1.3 V and -0.7 V and tunneling current set points in the range of 18 pA to 23 pA were applied to image the supramolecular adlayers shown here. The experimental setup consists of an Agilent 5500 scanning probe microscope that is placed on a Halcyonics actively isolated microscopy workstation. It is acoustically

shielded with a home-built box. Scissors cut Pt/Ir (80/20) tips were used and further modified after approach by applying short voltage pulses until the desired resolution was achieved. HOPG was obtained from TipsNano (via Anfatec) in ZYB-SS quality. All STM images (unless otherwise noted) were calibrated by subsequent immediate acquisition of an additional image at reduced bias voltage, therefore the atomic lattice of the HOPG surface is observed which is used as a calibration grid. Data processing, also for image calibration, was performed using the SPIP 5 (Image Metrology) software package. (Supra-) molecular modelling was performed using Wavefunction Spartan '16 and '18. Equilibrium geometries of the backbone structures were obtained from GFN2-xTB level of theory. Alkoxy side chains – where applicable – were subsequently attached with the alkoxy-backbone angles as observed by STM.

9.4 Computational Details

All calculations were performed with the freely available xtb 6.5.1 program package.[126] Structures were generated using the built-in 2D to 3D converter of xtb at the GFN-FF[127] level. Further structure builds and modifications were conducted using Avogadro.[128] Geometry optimizations were performed at the GFN2-xTB[129] level of theory using the implicit solvation model ALPB[130] with dichloromethane and employing default convergence criteria $5x10^{-6}$ Eh for energies and 10^{-3} Eh · $Bohr^{-1}$ for gradients. During the optimization the underlaying graphene sheet was fully constrained in space to avoid undulation. All calculations were performed on Intel®Xeon® CPU E3-1270 v5 @ 3.60GHz nodes. Molecular dynamic (MD) simulations were obtained by the same protocol of GFN2-xTB/ALPB(DCM) as already described employing a NVT ensemble at room temperature with a simulation length of 500 ps, from which the first 150 ps were assigned to the equilibration phase. Additional MDs for the adsorbed species of $\mathbf{D_{1c}}$ and $\mathbf{T_{1c}}$ on graphene were performed at the GFN-FF level of theory, again with implicit solvation and the settings mentioned before, to visualize the movement and flexibility of the molecules on a surface. Moreover, MDs for free and adsorbed SPMs $\mathbf{MD_{1c}}$ and $\mathbf{MT_{1c}}$, as well as for free $\mathbf{D_{1c}}$ and $\mathbf{T_{1c}}$, were performed at the GFN-FF level with the settings described above. Stable cutouts of all 8 GFN-FF MDs were used to explore the rigidity of the SPMs and PNTs by the means of distance distribution function analysis.

9.5 Sensing Experiments

Preliminary Studies:

Quartz crystal microbalance (QCMB) measurement. A 5 µl amount of a **D_{1c}** solution (1 mg/ml in *o*-dichlorobenzene) was drop-casted on the gold coating of QCM electrodes, followed by drying *in vacuo*. The third overtone of frequency (ΔF_3) of a film on a QCM sensor were measured by three cycles of exposure of a film to an analyte vapor for 5 min at 23 °C. Typical procedures include 5 min equilibration time followed by 5 min exposure to analyte in air and then 5 min of recovery.

The QCMB experiments were performed using Q-Sense E1 (Q-Sense, Stockholm, Sweden) with gold-coated AT-cut quartz crystal sensors (QSX 301 Gold, Q-Sense) with a 5 MHz fundamental resonance frequency.

Graphene field effect transistor (GFET) measurement. GFETs were fabricated according to a previous literature.[131] A 1 µl amount of a **D_{1c}** solution (1 mg/mL in *o*-dichlorobenzene) was drop-casted on the GFETs and dried at room temperature under vacuum. All electrical measurements were performed using a custom-built measurement system[132] at room temperature. For *I-V* sweep measurements, the drain-source voltage V_{ds} was held constant and the gate-source voltage V_{gs} was swept from –2 V to 6 V in 50 mV increments. A ten-second hold time was used before the gate-source voltage V_{gs} was swept at a rate of 50 mV / 500 ms.

Sensor Fabrication and Operation:

Preparation of the sensor. Glass substrates deposited with chromium adhesion layers (15 nm) and gold electrodes (50 nm) were prepared according to a modified literature procedure.[133] Briefly, glass slides (VWR Microscope Slides) were cleaned by sonication in acetone and isopropyl alcohol for 5 min each. After drying with an N_2 stream, the glass substrates were immersed in piranha solution (H_2SO_4:$H_2O_{2(aq)}$ (30%), 3:1, v/v; (Caution! Highly corrosive, must be prepared fresh before each use and never stored.) for 30 min, rinsed thoroughly with distilled water and then dried in an oven (180 °C) for 18 hours. After cooling to room temperature, a 10 nm layer of chromium (99.99%, R.D. Mathis) and a subsequent 50 nm layer of gold (99.99%, R.D. Mathis) were deposited on the glass slides through a custom stainless-steel mask using a thermal evaporator (Angstrom Engineering). This resulted

in five sets of electrode patterns on a single glass slide, which was cut into five individual devices (Figure 67). Each device contains a gold pattern of four isolated working electrodes with one shared reference-counter electrode on the glass substrate. The gap between one pair of gold electrodes is 0.5 mm. Prior to the deposition of the chemiresistor platform, the glass substrates were cleaned again by sonication in acetone and isopropyl alcohol for 5 min each to remove dust. After drying completely, the glass substrates were immersed in piranha solution (H_2SO_4:$H_2O_{2(aq)}$ (30%), 3:1, v/v) for 30 min, rinsed thoroughly with distilled water and then dried under N_2.

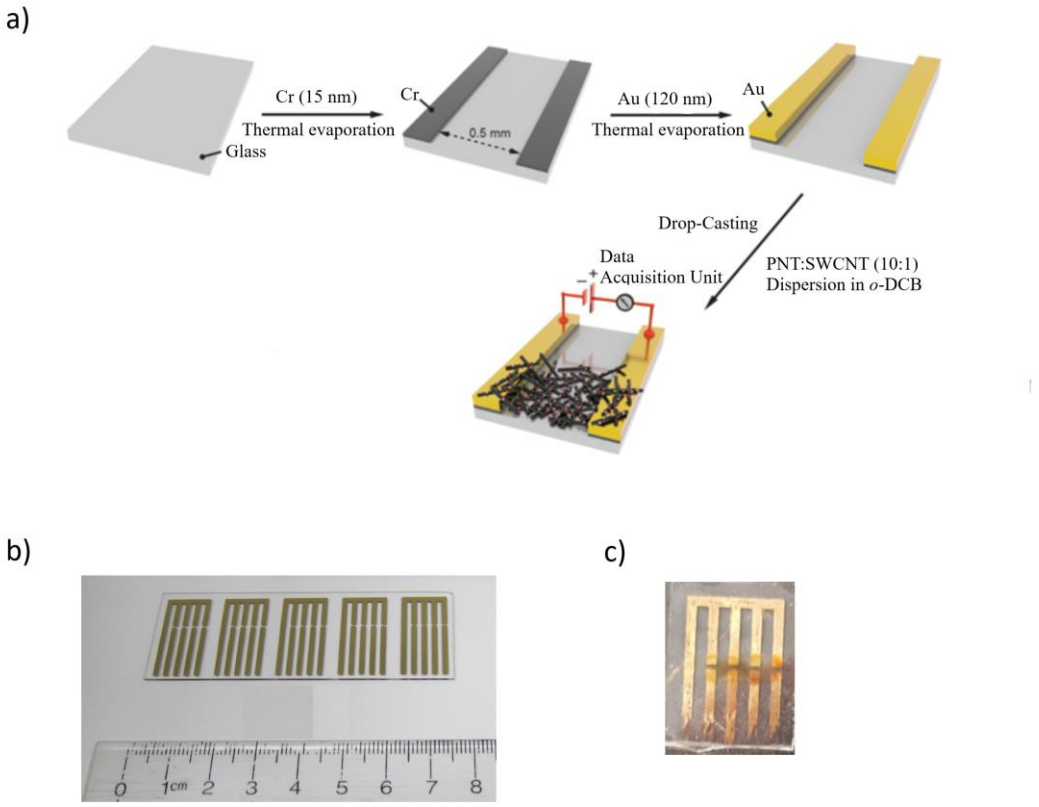

Figure 67: a) Illustration of the sensor fabrication and selector incorporation; b) microscope glass slide with five electrode patterns after thermal deposition of Cr (10 nm) and Au (100 nm) layers; c) enlargement of an individual device with drop-casted **SWCNT-PNT** selector system after drying under vacuum.

Fabrication of the SWCNT-PNT chemiresistor platform. For pristine SWCNTs, a stock solution of 2 mg of SG65i SWCNTs in 2 ml of *o*-dichlorobenzene was prepared by bath sonication at room temperature for 30 min (Branson 3510). For SWCNT-PNT dispersions 2 mg of the respective phenanthracene nanotube (PNT) $\mathbf{D_{1c}}$ or $\mathbf{T_{1c}}$ were dissolved in 2 ml of

o-dichlorobenzene and sonicated in a water bath for 10 min (Branson 3510). Then, 0.2 mg of SG65i SWCNTs were added, and the resulting mixture was chilled with ice and sonicated for 20 min using a tip-sonicator (Qsonica Q125) at 63 W with a pulse sequence (10 seconds ON and 5 seconds OFF). The supernatant was directly used for the device fabrication via drop-casting (1 µl drop per working electrode gap). Then, the solvent was evaporated under vacuum for 30 min and subsequently transferred into a sensing chamber.

Analyte detection measurements. The fabricated device containing the **SWCNT-PNT** chemiresistor was inserted into a 2 x 30 pin edge connector (TE Connectivity AMP Connectors) mounted on a solderless breadboard (Figure 68A), and then enclosed with a custom-built PTFE chamber containing a small gas inlet and outlet (Figure 68B). The gold electrodes of the device were connected to an Agilent Keysight 34970A datalogger equipped with a 34901A 20-channel multiplexer (2/4-wire) module (Figure 68C). The datalogger was connected to the sensing laptop using an Agilent 82357B GPIB-USB Interface High-Speed USB 2.0 serial cable and controlled using BenchLink Data Logger 3 (available free of charge online). The scan rate was set to 1 scan/second.

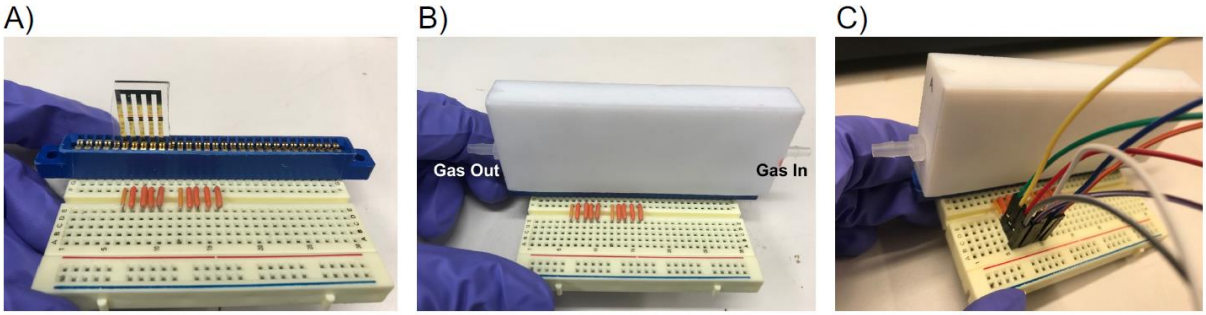

Figure 68: (*A*) Single chemiresistor device (4 channels) inserted into edge connector-breadbord platform. (*B*) Gas-tight enclosure fitted on connector-breadboard platform. (*C*) Electrical leads connecting the breadboard to a potentiostat for the collection of sensing data. In this configuration, four channels are monitored in parallel.[102]

A gas generator (FlexStream, Kin-Tek) was used to produce the analyte vapours from liquids (Figure 69). The change in device resistance resulting from analyte exposure was converted to the normalized change in conductance [$\Delta R/R_0$ (%) = $(R–R_0)/R_0 \times 100\%$; R_0 = baseline resistance], which was taken as the device's response. Typical parameters of the measurements were 30 min equilibration time (for the baseline resistance to stabilize) followed by 5 min exposure to analytes in dry air and then 30 min of recovery (air only). All

presented data are given as the numeral average (N≥ 4) accompanied by the standard deviation. Minor baseline correction was applied to account for the linear drift of the baseline resistance. Humidity effect study was conducted according to a previous literature.[134]

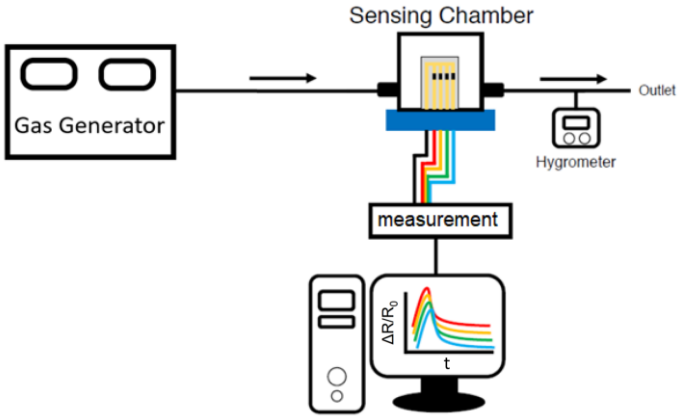

Figure 69: Schematic representation of the sensing setup.[102]

Theoretical limit of detection (LOD) calculation. The limit of detection was calculated following literature procedures.[134] We first calculated the root-mean-square noise (rms) deviation in conductance of the baseline prior to analyte exposure. We took 120 consecutive data points prior to exposure to analyte, plotted the data, and fitted to a fifth-order polynomial. We then calculated V_{x^2} using Eq. S1. In this equation, y_i is the measured conductance value and y is the corresponding value from the fifth-order polynomial fit. We then used Eq. S2 to calculate rms_{noise} of the sensors, where N is the number of data points used for curve fitting (N = 120). In Eq. S3, the slope of the linear regression fit for the sensor response *vs.* concentration plot is used to yield the theoretical LOD of the sensors.

$$V_{x^2} = \sum (y_i - y)^2 \qquad \text{Eq. S1}$$

$$rms_{noise} = \sqrt{\frac{V_{x^2}}{N}} \qquad \text{Eq. S2}$$

$$LOD = \frac{3(rms_{noise})}{slope} \qquad \text{Eq. S3}$$

9.6 Syntheses

2 (SR-1)

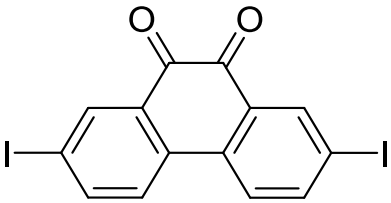

For the synthesis of compound **2**, a modified reaction procedure by *D. S. Kopchuk et al.* was applied.[135]

N-Iodosuccinimide (8.63 g, 38.4 mmol, 4.0 eq.) was added to cold (0 °C) conc. H_2SO_4 (95%, 120 ml) and the resulting mixture was stirred at 0 °C for 25 min. Then, phenanthrene-9,10-dione **1** (2.00 g, 9.60 mmol, 1.0 eq.) was added and the reaction mixture was slowly warmed to room temperature and stirred for 24 h. Afterwards, the reaction mixture was poured added dropwise into ice-cold water (200 ml) under stirring. The thus formed precipitate was filtered off, washed with water, and dried under vacuum overnight. **2** (4.19 g, 9.10 mmol, 95%) was received as a red crystalline solid.

Analytics:

Sum formula:	$C_{14}H_6I_2O_2$
Molar mass:	460.01 g/mol

^{1}H-NMR (700 MHz, $CDCl_3$, 298 K):

δ [ppm] = 8.50 (d, J = 2.0 Hz, 2H), 8.04 (dd, J = 8.4 Hz, 2.0 Hz, 2H), 7.71 (d, J = 8.4 Hz, 2H).

^{13}C-NMR (176 MHz, $CDCl_3$, 298 K):

δ [ppm] = 178.4, 144.9, 139.6, 134.6, 132.1, 125.6, 95.9.

MS (EI, 70 eV) *m/z* (%): 459.8 (70) $[M]^{+\bullet}$, 431.8 (100) $[M\text{-}CO]^{+}$, 304.9 (20) $[M\text{-}COI]^{+}$, 276.9 (36) $[M\text{-}2CO\text{-}I]^{+}$, 150.0 (54) $[C_{12}H_6]^{+}$; calculated: 459.85 Da.

3 (SR-117/-120)

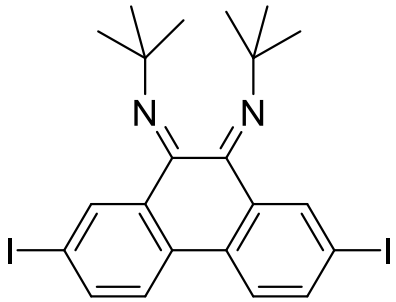

For the synthesis of compound **3**, a modified reaction procedure by *V. Cherkasovet al.* was applied.[136]

2,7-Diiodophenanthrenequinone **2** (2.00 g, 4.35 mmol, 1.0 eq.) and *tert*-butylamine (2.70 ml, 26.1 mmol, 6.0 eq.) were suspended in toluene (30 ml). Then, $TiCl_4$ (0.48 ml, 4.35 mmol, 1.0 eq.) was added dropwise and the reaction mixture was stirred at room temperature for 23 h. Water was added slowly to quench the reaction and the phases were separated. The aqueous phase was extracted with DCM (3 x 20 ml) and the combined organic phases were washed once with water and dried over $MgSO_4$. The solvent was removed under reduced pressure and the crude product was purified via recrystallization from acetonitrile giving **3** (1.73 g, 3.03 mmol, 70%) as a yellow-orange crystalline solid. A mixture of three different isomers (*EE*, *EZ*, *ZZ*) was obtained.

Analytics:

Sum formula:	$C_{22}H_{24}I_2N_2$
Molar mass:	570.26 g/mol

^{1}H-NMR (500 MHz, $CDCl_3$, 298 K):

δ [ppm] = 8.35 (d, J = 2.0 Hz, 2H), 8.21 (d, J = 2.0 Hz, 2H), 8.15 (d, J = 1.9 Hz, 2H), 7.95 (dd, J = 8.4 Hz, 2.0 Hz, 2H), 7.80 (dd, J = 8.4 Hz, 2.0 Hz, 2H), 7.77-7.72 (m, 2H), 7.60 (d, J = 8.4 Hz, 2H), 7.51 (d, J = 8.4 Hz, 2H), 7.36 (d, J = 8.2 Hz, 2H), 1.46 (s, 9H), 1.45 (s, 9H), 1.25 (s, 9H).

^{13}C-NMR (126 MHz, $CDCl_3$, 298 K):

δ [ppm] = 187.4, 161.6, 159.8, 153.5, 143.4, 139.7, 139.2, 139.0, 138.5, 137.2, 136.8, 136.7, 136.5, 136.1, 135.6, 135.3, 135.0, 134.6, 133.1, 130.9, 126.3, 125.0, 124.8, 124.6, 95.7, 95.0, 94.2, 92.0, 59.3, 58.8, 58.7, 31.8, 30.5.

MS (ESI+) *m/z* (%): 571.0 (100) $[M+H]^+$, 458.9 (24) $[C_{15}H_{11}I_2N]^+$, 111.0 (49) $[C_9H_3]^+$; calculated: 570.00 Da.

4 (SR-113)

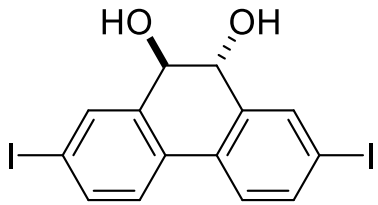

For the synthesis of compound **4**, a reaction procedure by *K. Platt et al.* was applied.[137] $NaBH_4$ (0.38 g, 10.1 mmol, 10 eq.) was suspended in EtOH (26 ml) and H_2O (4 ml), ensuring the availability of airflow. Then, 2,7-diiodophenanthrenequinone **2** (0.50 g, 1.09 mmol, 1.0 eq.) was slowly added in portions, leading to the formation of a yellow suspension. The reaction suspension was then stirred at room temperature for 23 h. Afterwards, ice-cold H_2O (100 ml) were added, and it was acidified with aq. HCl (10%). The beige coloured precipitate was filtered off, washed with H_2O, and dried under vacuum giving **4**(*rac.*) (0.46 g, 0.99 mmol, 91%).

Analytics:

Sum formula:	$C_{14}H_{10}I_2O_2$
Molar mass:	464.04 g/mol

^{1}H-NMR (500 MHz, DMSO-d_6, 298 K):

δ [ppm] = 7.89 (d, J = 1.9 Hz, 2H), 7.71 (dd, J = 8.1 Hz, 1.9 Hz, 2H), 7.59 (d, J = 8.2 Hz, 2H), 5.83 (dd, J = 3.3 Hz, 1.9 Hz, 2H), 4.43 (bs, 2H, OH).

^{13}C-NMR (126 MHz, DMSO-d_6, 298 K):

δ [ppm] = 140.6, 136.5, 134.9, 131.1, 125.6, 94.5, 71.3.

MS (EI, 70 eV) *m/z* (%): 463.9 (74) $[M]^{+\bullet}$, 445.9 (100) $[M\text{-}H_2O]^+$, 432.9 (64) $[C_{13}H_7I_2O]^+$, 338.0 (18) $[M+H\text{-}I]^+$, 320.0 (38) $[M\text{-}I\text{-}OH]^+$, 307.0 (21) $[C_{13}H_8IO_3]^+$, 291.0 (33) $[C_{13}H_8I]^+$; calculated: 463.88 Da.

5 (SR-4)

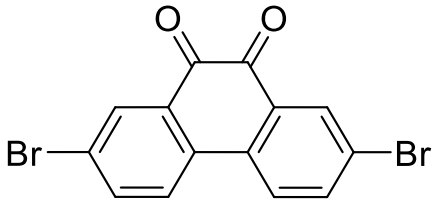

For the synthesis of compound **5**, a reaction procedure by *W. Liu et al.* was applied.[138] Phenanthrene-9,10-dione **1** (2.00 g, 9.60 mmol, 1.0 eq.) was added to conc. H_2SO_4 (95%, 60 ml). Then, *N*-bromosuccinimide (3.76 g, 21.1 mmol, 2.2 eq.) was added slowly and the reaction mixture was stirred overnight. Afterwards, the reaction mixture was poured into ice-cold water (400 ml). The thus formed precipitate was filtered off, washed thoroughly with water, and dried under vacuum. The crude product was purified via recrystallization from toluene. **5** (2.07 g, 5.66 mmol, 59%) was received as an orange crystalline solid.

Analytics:

Sum formula:	$C_{14}H_6Br_2O_2$
Molar mass:	366.01 g/mol

^{1}H-NMR (500 MHz, DMSO-d_6, 298 K):

δ [ppm] = 8.25 (d, J = 8.6 Hz, 2H), 8.08 (d, J = 2.3 Hz, 2H), 7.96 (dd, J = 8.5 Hz, 2.3 Hz, 2H).

^{13}C-NMR (126 MHz, DMSO-d_6, 298 K):

δ [ppm] = 176.8, 137.4, 133.6, 133.1, 131.0, 126.9, 122.8.

MS (APCI) *m/z* (%): 364.9 (100) $[M+H]^+$, 287.0 (54) $[M+H-Br]^+$, 259.0 (26) $[M+H-CO-Br]^+$, 179.0 (54) $[C_8H_5Br]^+$, 131.0 (77) $[C_8H_3O_2]^+$; calculated: 363.87 Da.

6 (SR-6/-10)

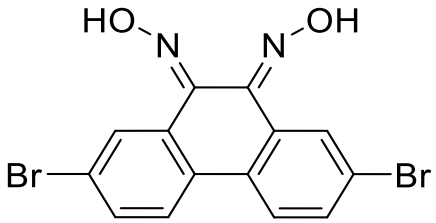

Route a):

For the synthesis of compound **6**, a reaction procedure by *P. Murer et al.* was applied.[139]

2,7-Dibromophenanthrene-9,10-dione **5** (1.83 g, 4.99 mmol, 1.0 eq.) was suspended in EtOH (15 ml). Subsequently, hydroxylammonium chloride (1.39 g, 20.0 mmol, 4.0 eq.) and sodium acetate (1.03 g, 12.5 mmol, 2.5 eq.) were added and the reaction mixture was refluxed overnight. After cooling to room temperature, the yellow precipitate was filtered off. Then, the solid residue was suspended in water (10 ml) and filtered off again. It was washed with water and cyclohexane. The crude product was recrystallized successively from methanol, acetonitrile, and acetone and dried under vacuum overnight. **6** (0.40 g, 1.02 mmol, 20%) was received as a yellow solid. However, small amounts of substrate remained unreacted and could not be separated from the product. Therefore, compound **6** was used in the next reaction without further purification.

Route b):

For the synthesis of compound **6**, a modified reaction procedure by *Y. Xie et al.* was applied.[140]

2,7-Dibromophenanthrene-9,10-dione **5** (1.98 g, 5.41 mmol, 1.0 eq.) and hydroxylammonium chloride (3.76 g, 54.1 mmol, 10.0 eq.) were suspended in EtOH (20 ml). Subsequently, pyridine (6 ml) was added, and the reaction mixture was refluxed for 24 h. After cooling to room temperature, the solvent was removed under reduced pressure. Then, the solid residue was suspended in H_2O (20ml) and acidified with conc. HCl (37%). The

yellow precipitate was filtered off, washed with H_2O, and dried under vacuum. The crude product was recrystallized from acetone giving **6** (1.72 g, 4.34 mmol, 80%) as a bright-yellow solid. However, small amounts of substrate remained unreacted and could not be separated from the product. Therefore, compound **6** was used in the next reaction without further purification.

Analytics:

Sum formula:	$C_{14}H_8Br_2N_2O_2$
Molar mass:	396.04 g/mol

^{1}H-NMR (400 MHz, DMSO-d_6, 298 K):

δ [ppm] = 12.59 + 12.54 + 12.46 + 12.29 (4 x s, 2H, OH) 8.61 (d, J = 2.2 Hz, 2H), 8.06 (d, J = 8.7 Hz, 2H), 7.75 (dd, J = 8.6 Hz, 2.2 Hz, 2H).

^{13}C-NMR (126 MHz, DMSO-d_6, 298 K):

δ [ppm] = 143.9, 142.2, 134.5, 133.1, 133.0, 131.0, 121.9, 121.3.

MS (ESI-) *m/z* (%): 392.8 (100) $[M-H]^-$, 379.8 (23) $[M-OH]^-$, 362.8 (12) $[M-2OH+2H]^-$; calculated: 393.90 Da.

7 (SR-11)

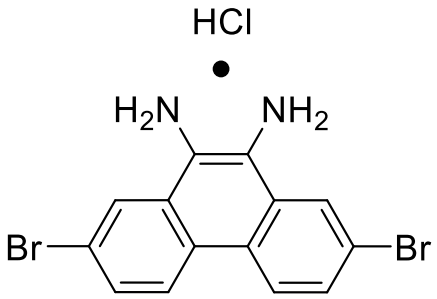

For the synthesis of compound **7**, a reaction procedure by *M. Putala et al.* was applied.[141] 2,7-Dibromophenanthrene-9,10-dione dioxime **6** (0.40 g, 1.02 mmol, 1.0 eq.) was suspended in EtOH (150 ml). Subsequently, tin(II) chloride dihydrate (2.28 g, 10.0 mmol, 10.0 eq.)

dissolved in conc. HCl (37%, 10 ml) was added and the reaction mixture was stirred at 70 °C for 3 h. After cooling to room temperature, the formed beige precipitate was filtered off, washed several times with EtOH, twice with a small amount of Et_2O and dried under vacuum. **7** (0.23 g, 0.57 mmol, 56%) was received as a beige solid.

Analytics:

Sum formula:	$C_{14}H_{10}Br_2N_2$*HCl
Molar mass:	402.51 g/mol

^{1}H-NMR (500 MHz, DMSO-d_6, 298 K):
δ [ppm] = 8.87 (d, J = 9.0 Hz, 2H), 8.66 (s, 2H), 7.88 (d, J = 9.0 Hz, 2H).

Due to the poor solubility of the compound no **^{13}C-NMR** spectrum could be obtained.

MS (ESI+) *m/z* (%): 388.9 (100) $[M\text{-}Cl+H+Na]^+$, 311.0 (21) $[C_{14}H_{13}BrN_2Na]^+$.

MS (ESI-) *m/z* (%): 448.0 (27) $[M\text{-}HCl+NaHNO_3]^-$, 422.9 (62) $[M+Na]^-$, 386.9 (100) $[M\text{-}HCl+Na]^-$; calculated: 399.90 Da.

8 (SR-34/-68/-121)

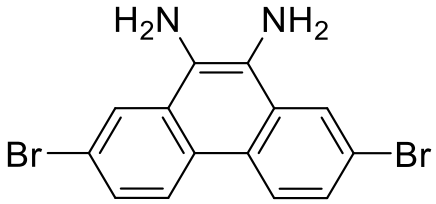

Route a):

For the synthesis of compound **8**, a reaction procedure by *Y. Xie et al.* was applied.[140]
2,7-Dibromophenanthrene-9,10-dione dioxime **6** (1.55 g, 3.91 mmol, 1.0 eq.) was suspended in EtOH (15 ml). Subsequently, anhydrous tin(II) chloride (3.71 g, 19.6 mmol, 5.0 eq.) dissolved in conc. HCl (37%, 5 ml) was added at 0 °C and the reaction mixture was refluxed for 3 h. After cooling to room temperature the formed beige precipitate was filtered off,

washed several times with water and a small amount of cold EtOH and dried under vacuum. Afterwards, the precipitate was suspended in a saturated $NaHCO_3$ solution and subsequently extracted with DCM several times. The combined organic phases were dried over $MgSO_4$ and the solvent was removed under reduced pressure. **8** (0.40 g, 1.09 mmol, 28%) was received as a yellow-green solid.

Route b):

For the synthesis of compound **8**, a modified reaction procedure by *Y. Xie et al.* was applied.[140]

2,7-Dibromophenanthrene-9,10-dione dioxime **6** (1.72 g, 4.34 mmol, 1.0 eq.) was suspended in EtOH (15 ml). Subsequently, anhydrous tin(II) chloride (4.12 g, 21.7 mmol, 5.0 eq.) dissolved in conc. HCl (37%, 5 ml) was added at 0 °C and the reaction mixture was refluxed for 3 h. After cooling to room temperature the beige precipitate was filtered off, washed several times with water, a small amount of EtOH and dried under vacuum. Afterwards, the precipitate was suspended in aqueous NaOH (2 M) and subsequently extracted with DCM several times. The combined organic phases were dried over $MgSO_4$ and the solvent was removed under reduced pressure. **8** (0.72 g, 1.97 mmol, 45%) was received as a green solid.

Analytics:

Sum formula:	$C_{14}H_{10}Br_2N_2$
Molar mass:	366.06 g/mol

^{1}H-NMR (400 MHz, DMSO-d_6, 298 K):

δ [ppm] = 8.58 (d, J = 8.9 Hz, 2H), 8.26 (d, J = 2.1 Hz, 2H), 7.49 (dd, J = 8.8 Hz, 2.0 Hz 2H), 5.20 (s, 4H, NH_2).

^{13}C-NMR (176 MHz, DMSO-d_6, 298 K):

δ [ppm] = 127.3, 125.2, 125.1, 123.2, 123.1, 120.3.

MS (EI) *m/z* (%): 363.8 (100) $[M]^{+\bullet}$, 335.8 (13) $[C_{13}H_8Br_2N]^{+\bullet}$, 284.9 (9) $[M\text{-}Br]^+$; calculated: 363.92 Da.

10 (SR-108)

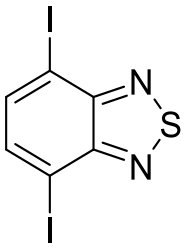

For the synthesis of compound **10**, a reaction procedure by *S. Meißner et al.* was applied.[76] 2,1,3-Benzothiadiazole **9** (2.73 g, 20.0 mmol, 1.0 eq.), iodine (16.0 g, 63.1 mmol, 3.15 eq.) and Ag_2SO_4 (25.0 g, 80.2 mmol, 4.0 eq.) were added to conc. H_2SO_4 (95%, 80 ml) and the resulting mixture was stirred at 70 °C for 18 h. Then, it was added dropwise to ice-cold water (400 ml). The thus formed precipitate was filtered off, copiously washed with water and then suspended in toluene for 1 h. It was filtered off again and washed with toluene several times. The filtrate was concentrated under reduced pressure and cold EtOH was added, leading to the formation of a yellow precipitate, which was filtered off, washed with EtOH and dried under vacuum. **10** (3.43 g, 8.84 mmol, 44%) was received as a yellow crystalline solid.

Analytics:

Sum formula:	$C_6H_2I_2N_2S$
Molar mass:	387.96 g/mol

^{1}H-NMR (500 MHz, $CDCl_3$, 298 K):
δ [ppm] = 7.82 (s, 2H).

^{13}C-NMR (126 MHz, $CDCl_3$, 298 K):
δ [ppm] = 154.1, 140.0, 87.9.

MS (EI, 70 eV) *m/z* (%): 387.9 (100) $[M]^{+\bullet}$, 261.0 (20) $[M\text{-}I]^+$, 134.1 (13) $[M\text{-}I_2]^+$; calculated: 387.80 Da.

11 (SR-123/-151)

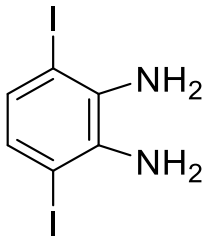

For the synthesis of compound **11**, a reaction procedure by *S. Meißner et al.* was applied.[76] 4,7-Diiodo-2,1,3-benzothiadiazole **10** (1.38 g, 3.56 mmol, 1.0 eq.), $NaBH_4$ (0.54 g, 14.2 mmol, 4.0 eq.) and $CoCl_2 \bullet 6\ H_2O$ (8.00 mg, 36.0 µmol, 0.01 eq.) were dissolved in THF (6 ml) and EtOH (17 ml) under an argon atmosphere and the resulting mixture was refluxed for 3 h. After cooling to room temperature, the solvents were removed under reduced pressure. Then, the residue was dissolved in DCM and H_2O. The phases were separated, and the aqueous phase was extracted with DCM (3 x 20 ml). The combined organic phases were washed once with water and brine, dried over $MgSO_4$ and the solvent was removed under reduced pressure. The crude product was purified via flash chromatography (PF-30SI-JP/25G; CH:DCM = 1:2, R_f = 0.41) yielding **11** (0.42 g, 1.17 mmol, 33%) as a yellow solid.

Analytics:

Sum formula:	$C_6H_6I_2N_2$
Molar mass:	359.94 g/mol

^{1}H-NMR (700 MHz, $CDCl_3$, 298 K):
δ [ppm] = 6.69 (s, 2H), 4.88 (s, 4H, NH_2).

^{13}C-NMR (176 MHz, $CDCl_3$, 298 K):
δ [ppm] = 134.7, 128.1, 83.8.

MS (APCI) *m/z* (%): 360.9 (100) $[M+H]^+$, 333.0 (17) $[C_5H_5I_2N]^+$; calculated: 359.86 Da.

13 (SR-14)

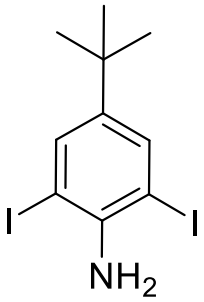

For the synthesis of compound **13**, a reaction procedure by *Y. Miura et al.* was applied.[142] 4-*tert*-Butylaniline **12** (4.00 g, 26.8 mmol, 1.0 eq.) was dissolved in conc. HCl (37%, 4 ml) and water (35 ml). Then, a suspension of iodine monochloride (10.9 g, 67.0 mmol, 2.5 eq.) in conc. HCl (37%, 20 ml) and water (40 ml) was added over the period of 1 h and the resulting reaction mixture was stirred at room temperature for another hour. Afterwards, chloroform (200 ml) was added, and the mixture was neutralized with an aq. NaOH-solution (2 M). The phases were separated, and the aqueous phase was extracted with chloroform (3 x 20 ml). The combined organic phases were washed successively with an aq. $NaHSO_3$-solution (40%) and water, dried over $MgSO_4$ and the solvent was removed under reduced pressure. The crude product was purified via column chromatography (CH:Tol = 1:1, R_f = 0.76) yielding **13** (9.43 g, 23.5 mmol, 88%) as a brown oil.

Analytics:

Sum formula:	$C_{10}H_{13}I_2N$
Molar mass:	401.03 g/mol

^{1}H-NMR (500 MHz, $CDCl_3$, 298 K):

δ [ppm] = 7.62 (s, 2H), 3.68 (bs, 2H, NH_2), 1.24 (s, 9H).

^{13}C-NMR (126 MHz, $CDCl_3$, 298 K):

δ [ppm] = 144.8, 143.9, 136.7, 81.8, 33.9, 31.5.

MS (EI, 70 eV) *m/z* (%): 400.9 (43) $[M]^{+\bullet}$, 385.9 (100) $[M\text{-}CH_3]^+$; calculated: 400.91 Da.

14 (SR-15)

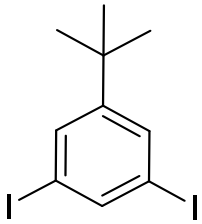

For the synthesis of compound **14**, a reaction procedure by *Y. Miura et al.* was applied.[142] 2,6-Diiodo-4-tert-butylaniline **13** (9.43 g, 23.5 mmol, 1.0 eq.) was dissolved in EtOH (80 ml) and cooled to 0 °C. Then, conc. H_2SO_4 (95%, 3 ml) was added dropwise. After warming to room temperature sodium nitrite (8.10 g, 118 mmol, 5.0 eq.) was added as fast as possible leading to a foaming reaction mixture, which was refluxed for 21 h. Then, the solvent was evaporated, and the residue was neutralized with an aq. NaOH-solution (2 M). Afterwards, chloroform (50 ml) was added, the phases were separated, and the aqueous phase was extracted with chloroform (3 x 50 ml). The combined organic phases were dried over $MgSO_4$, and the solvent was removed under reduced pressure. The crude product was purified via column chromatography (CH, R_f = 0.84) yielding **14** (5.56 g, 14.4 mmol, 61%) as a bright red oil.

Analytics:

Sum formula:	$C_{10}H_{12}I_2$
Molar mass:	386.01 g/mol

^{1}H-NMR (400 MHz, $CDCl_3$, 298 K):

δ [ppm] = 7.86 (t, J = 1.5 Hz, 1H), 7.65 (d, J = 1.5 Hz, 2H), 1.27 (s, 9H).

^{13}C-NMR (101 MHz, $CDCl_3$, 298 K):

δ [ppm] = 155.7, 142.4, 134.3, 95.0, 35.0, 31.2.

MS (EI, 70 eV) *m/z* (%): 385.9 (80) $[M]^{+\bullet}$, 370.9 (100) $[M\text{-}CH_3]^+$, 342.9 (18) $[M\text{-}C_3H_6]^+$, 260.1 (37) $[M+H\text{-}I]^+$, 245.0 (70) $[M\text{-}CH_3\text{-}I]^+$, 117.2 (19) $[C_9H_9]^+$; calculated: 385.90 Da.

15 (SR-17)

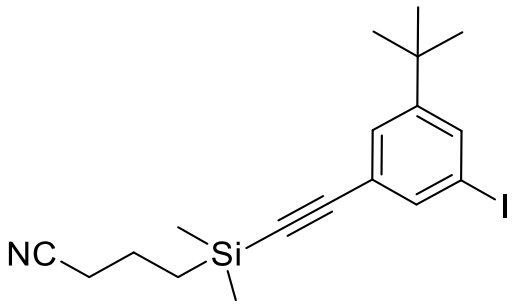

For the synthesis of compound **15**, a reaction procedure by *A. Idelson et al.* was applied.[143] 1-*tert*-Butyl-3,5-diiodobenzene **14** (5.56 g, 14.4 mmol, 1.0 eq.) was dissolved in THF (15 ml) and piperidine (30 ml) and the solution was purged with argon for 45 min. Then, $PdCl_2(PPh_3)_2$ (0.20 g, 0.29 mmol, 0.02 eq.), triphenylphosphane (0.19 g, 0.72 mmol, 0.05 eq.) and copper(I) iodide (0.08 g, 0.43 mmol, 0.03 eq.) were added. Afterwards, CPDMS-acetylene (2.23 g, 14.7 mmol, 1.02 eq.) was added dropwise and the reaction mixture was stirred at room temperature for 19 h. Then, the reaction mixture was diluted with aq. HCl (10%) and DCM. The phases were separated, and the aqueous phase was extracted with DCM (3 x 20 ml). The combined organic phases were washed once with water and brine, dried over $MgSO_4$ and the solvent was removed under reduced pressure. The crude product was purified via column chromatography (CH:DCM = 1:2, R_f = 0.60) yielding **15** (2.88 g, 7.03 mmol, 49%) as a yellow-orange oil.

Analytics:

Sum formula:	$C_{18}H_{24}INSi$
Molar mass:	409.39 g/mol

^{1}H-NMR (500 MHz, $CDCl_3$, 298 K):

δ [ppm] = 7.67 (dd, J = 1.7 Hz, 1.7 Hz, 1H), 7.63 (dd, J = 1.5 Hz, 1.5 Hz, 1H), 7.42 (dd, J = 1.6 Hz, 1.6 Hz, 1H), 2.43 (t, J = 7.0 Hz, 2H), 1.86-1.79 (m, 2H), 1.29 (s, 9H), 0.87-0.83 (m, 2H), 0.25 (s, 6H).

^{13}C-NMR (126 MHz, $CDCl_3$, 298 K):

δ [ppm] = 153.6, 137.8, 135.4, 128.6, 124.4, 119.9, 105.2, 93.9, 93.0, 34.9, 31.2, 20.8, 20.7, 15.8, -1.7.

MS (EI, 70 eV) *m/z* (%): 409.1 (20) $[M]^{+\bullet}$, 394.1 (26) $[M\text{-}CH_3]^+$, 341.1 (100) $[M\text{-}C_4H_6N]^+$; calculated: 409.07 Da.

16 (SR-18)

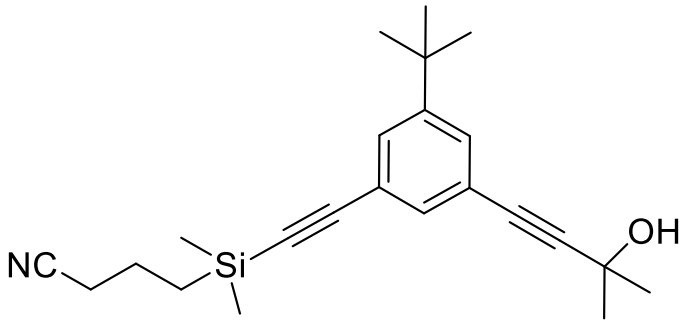

For the synthesis of compound **16**, a reaction procedure by *A. Idelson et al.* was applied.[143] Compound **15** (2.87 g, 7.01 mmol, 1.0 eq.) was dissolved in THF (15 ml) and piperidine (20 ml) and the solution was purged with argon for 45 min. Then, $PdCl_2(PPh_3)_2$ (0.10 g, 0.14 mmol, 0.02 eq.), triphenylphosphane (0.09 g, 0.35 mmol, 0.05 eq.) and copper(I) iodide (0.04 g, 0.21 mmol, 0.03 eq.) were added. Afterwards, 2-methylbut-3-yn-2-ol (0.75 ml, 7.71 mmol, 1.1 eq.) was added dropwise and the reaction mixture was stirred at room temperature for 20 h. Then, the reaction mixture was diluted with aq. HCl (10%) and DCM. The phases were separated, and the aqueous phase was extracted with DCM (3 x 20 ml). The combined organic phases were washed once with water and brine, dried over $MgSO_4$ and the solvent was removed under reduced pressure. The crude product was purified via column chromatography (DCM, R_f = 0.24) yielding **16** (2.41 g, 6.58 mmol, 93%) as a yellow oil.

Analytics:

Sum formula:	$C_{23}H_{31}NOSi$
Molar mass:	365.59 g/mol

^{1}H-NMR (500 MHz, $CDCl_3$, 298 K):

δ [ppm] = 7.41 (dd, J = 1.7 Hz, 1.7 Hz, 1H), 7.40 (dd, J = 1.7 Hz, 1.7 Hz, 1H), 7.36 (dd, J = 1.5 Hz, 1.5 Hz, 1H), 2.44 (t, J = 7.0 Hz, 2H), 1.86-1.79 (m, 2H), 1.61 (s, 6H), 1.30 (s, 9H), 0.87-0.82 (m, 2H), 0.25 (s, 6H).

^{13}C-NMR (126 MHz, $CDCl_3$, 298 K):

δ [ppm] = 151.7, 132.5, 129.4, 129.1, 122.7, 119.9, 106.2, 93.7, 92.1, 81.9, 65.8, 34.8, 31.6, 31.2, 20.8, 20.6, 15.9, -1.7.

MS (APCI) *m/z* (%): 366.2 (4) $[M+H]^+$, 348.2 (75) $[M-OH]^+$, 139.1 (17) $[C_7H_{13}NSi]^+$, 126.1 (100) $[C_6H_{12}NSi]^+$; calculated: 365.22 Da.

17 (SR-50/-48)

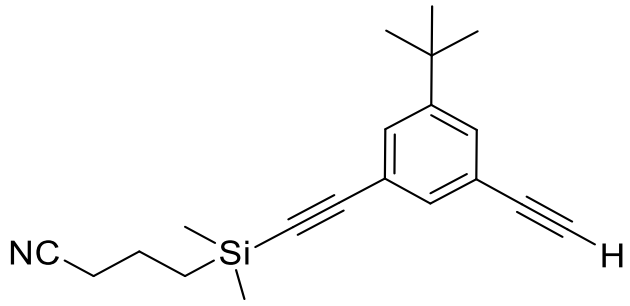

For the synthesis of compound **17**, a modified reaction procedure by *V. Valderrey et al.* was applied.[144]

Compound **16** (1.20 g, 3.28 mmol, 1.0 eq.) was dissolved in dry toluene (40 ml). Then, a microgranulate of NaOH (1.31. g, 32.8 mmol, 10.0 eq.) was molten *in vacuo*. After cooling to room temperature, the substrate (dissolved in toluene) was added under argon atmosphere. Subsequently, the reaction mixture was refluxed for 30 min. After cooling to room temperature, the reaction mixture was filtered, and the solvent was removed under reduced pressure. The crude product was purified via column chromatography (DCM, R_f = 0.81) yielding **17** (0.61 g, 1.99 mmol, 61%) as a light-yellow oil.

Analytics:

Sum formula:	$C_{20}H_{25}NSi$
Molar mass:	307.51 g/mol

^{1}H-NMR (700 MHz, $CDCl_3$, 298 K):

δ [ppm] = 7.48 (dd, J = 1.7 Hz, 1.7 Hz, 1H), 7.45 (dd, J = 1.7 Hz, 1.7 Hz, 1H), 7.42 (dd, J = 1.5 Hz, 1.5 Hz, 1H), 3.05 (s, 1H), 2.44 (t, J = 7.0 Hz, 2H), 1.86-1.81 (m, 2H), 1.30 (s, 9H), 0.87-0.84 (m, 2H), 0.26 (s, 6H).

^{13}C-NMR (176 MHz, $CDCl_3$, 298 K):

δ [ppm] = 151.8, 132.9, 129.9, 129.7, 122.9, 122.2, 119.9, 106.1, 92.3, 83.3, 34.8, 31.2, 20.8, 20.6, 15.9, -1.7.

MS (EI, 70 eV) *m/z* (%): 307.1 (17) $[M]^{+\bullet}$, 292.1 (22) $[M\text{-}CH_3]^+$, 279.1 (16) $[M\text{-}CH\text{-}CH_3]^+$, 264.1 (18) $[C_{17}H_{18}NSi]^+$, 239.1 (100) $[M\text{-}C_4H_6N]^+$, 223.0 (13) $[M\text{-}C_5H_{10}N]^+$, 98.0 (18) $[C_5H_{10}Si]^+$; calculated: 307.18 Da.

19 (SR-100)

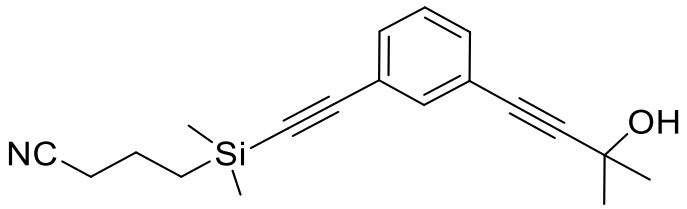

For the synthesis of compound **19**, a modified reaction procedure by *A. Idelson et al.* was applied.[143]

1-Bromo-3-iodobenzene **18** (2.00 g, 7.07 mmol, 1.0 eq.) was dissolved in THF (7,5 ml) and piperidine (15 ml) and the solution was purged with argon for 1 h. Then, $PdCl_2(PPh_3)_2$ (0.10 g, 0.14 mmol, 0.02 eq.), triphenylphosphane (0.09 g, 0.35 mmol, 0.05 eq.) and copper(I) iodide (0.04 g, 0.21 mmol, 0.03 eq.) were added. CPDMS-acetylene (1.09 g, 7.21 mmol, 1.02 eq.) was added dropwise and the solution was stirred at room temperature for 20 h. Afterwards, 2-methylbut-3-yn-2-ol (1.38 ml, 14.1 mmol, 2.0 eq.) was added dropwise

and the reaction mixture was stirred at room temperature for another 22 h. Then, the reaction mixture was diluted with aq. HCl (10%) and DCM. The phases were separated, and the aqueous phase was extracted with DCM (3 x 20 ml). The combined organic phases were washed once with water and brine, dried over $MgSO_4$ and the solvent was removed under reduced pressure. The crude product was purified via column chromatography (DCM, R_f = 0.17) yielding **19** (0.68 g, 2.20 mmol, 31%) as a yellow oil.

Analytics:

Sum formula:	$C_{19}H_{23}NOSi$
Molar mass:	309.48 g/mol

^{1}H-NMR (500 MHz, $CDCl_3$, 298 K):

δ [ppm] = 7.53 (td, J = 1.6 Hz, 0.6 Hz, 1H), 7.37 (ddt, J = 9.4 Hz, 7.9 Hz, 1.3 Hz, 2H), 7.27-7.23 (m, 1H), 2.43 (t, J = 7.0 Hz, 2H), 1.86-1.79 (m, 2H), 1.61 (s, 6H), 0.87-0.82 (m, 2H), 0.25 (s, 6H).

^{13}C-NMR (126 MHz, $CDCl_3$, 298 K):

δ [ppm] = 135.3, 131.9, 131.7, 128.5, 123.2, 123.1, 119.8, 105.6, 94.6, 92.9, 81.3, 65.7, 31.6, 20.8, 20.6, 15.8, -1.7.

MS (EI) *m/z* (%): 309.2 (2) $[M]^+$, 294.1 (43) $[M\text{-}CH_3]^+$, 266.1 (11) $[M\text{-}OH\text{-}CN]^+$, 241.1 (100) $[M\text{-}C_4H_6N]^+$, 223.1 (49) $[C_{14}H_{14}NSi]^+$, 126.1 (61) $[C_{13}H_{11}O]^+$, 98.1 (18) $[C_5H_{10}Si]^+$; calculated: 309.15 Da.

20 (SR-127)

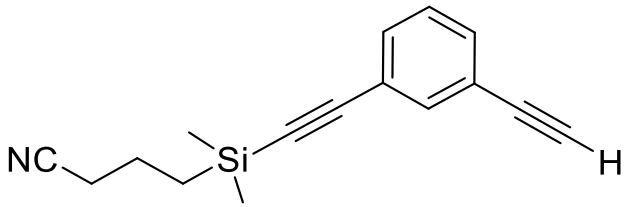

For the synthesis of compound **20**, a modified reaction procedure by *V. Valderrey et al.* was applied.[144]

Compound **19** (0.68 g, 2.20 mmol, 1.0 eq.) was dissolved in dry toluene (15 ml). Then, a NaOH-powder (0.88. g, 22.0 mmol, 10.0 eq.) was molten *in vacuo*. After cooling to room temperature, the substrate (dissolved in toluene) was added under argon atmosphere. Subsequently, the reaction mixture was refluxed for 30 min. After cooling to room temperature, the reaction mixture was filtered, and the solvent was removed under reduced pressure. The crude product was purified via column chromatography (CH:DCM = 1:2, R_f = 0.52) yielding **20** (0.25 g, 0.99 mmol, 45%) as a yellow oil.

Analytics:

Sum formula:	$C_{16}H_{17}NSi$
Molar mass:	251.40 g/mol

^{1}H-NMR (500 MHz, $CDCl_3$, 298 K):

δ [ppm] = 7.59 (td, J = 1.7 Hz, 0.6 Hz, 1H), 7.43 (ddt, J = 8.0 Hz, 6.6 Hz, 1.4 Hz, 2H), 7.2 (td, J = 7.8 Hz, 0.6 Hz, 1H), 3.08 (s, 1H), 2.43 (t, J = 7.0 Hz, 2H), 1.86-1.79 (m, 2H), 0.88-0.82 (m, 2H), 0.25 (s, 6H).

^{13}C-NMR (126 MHz, $CDCl_3$, 298 K):

δ [ppm] = 135.7, 132.4, 132.3, 128.5, 123.3, 122.6, 119.8, 105.4, 94.6, 93.1, 82.7, 78.0, 20.7, 20.6, 15.8, -1.7.

MS (EI, 70 eV) *m/z* (%): 251.1 (8) $[M]^{+\bullet}$, 236.1 (23) $[M\text{-}CH_3]^+$, 223.1 (18) $[C_{14}H_{13}NSi]^+$, 208.1 (22) $[C_{13}H_{10}NSi]^+$, 183.1 (100) $[M\text{-}C_4H_6N]^+$, 153.0 (11) $[C_{10}H_5Si]^+$; calculated: 251.11 Da.

22 (SR-13)

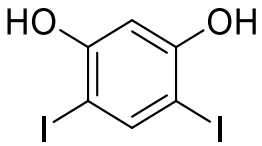

For the synthesis of compound **22**, a reaction procedure by *I. Thomsen et al.* was applied.[145] Resorcinol **21** (2.00 g, 18.2 mmol, 1.0 eq.) was dissolved in dry Et_2O (25 ml). At 0 °C a solution of iodine monochloride (1 M in DCM, 36.7 ml, 36.7 mmol, 2.02 eq.) was added slowly. Afterwards, the reaction solution was warmed to room temperature and further stirred for 1 h. Then, water (40 ml) and sodium sulphite (1.50 g) were added, whereupon a light-yellow solution was obtained. The phases were separated, and the aqueous phase was extracted with Et_2O (3 x 20 ml). The combined organic phases were dried over $MgSO_4$, filtered and the solvent was removed under reduced pressure. The crystalline residue was triturated in water (40 ml) for 30 min. Subsequently, it was filtered off, washed with water once and dried under vacuum overnight. **22** (5.75 g, 15.9 mmol, 87%) was received as a beige crystalline solid.

Analytics:

Sum formula:	$C_6H_4I_2O_2$
Molar mass:	361.90 g/mol

^{1}H-NMR (500 MHz, $CDCl_3$, 298 K):

δ [ppm] = 7.84 (s, 1H), 6.71 (s, 1H), 5.30 (s, 2H, OH).

^{13}C-NMR (126 MHz, $CDCl_3$, 298 K):

δ [ppm] = 156.8, 144.7, 102.0, 75.7.

MS (EI, 70 eV) *m/z* (%): 361.9 (100) $[M]^{+\bullet}$, 234.9 (10) $[M\text{-}I]^{+}$, 108.0 (10) $[M\text{-}I_2]^{+}$; calculated: 361.83 Da.

23 (SR-90/-153)

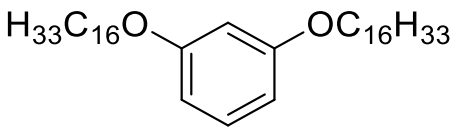

Route a):

For the synthesis of compound **23**, a modified reaction procedure by *L. Assies et al.* was applied.[91]

Resorcinol **21** (2.00 g, 18.2 mmol, 1.0 eq.) was dissolved in acetone (80 ml) under argon atmosphere. Then, anhydrous potassium carbonate (6.29 g, 45.5 mmol, 2.5 eq.), potassium iodide (0.60 g, 3.64 mmol, 0.2 eq.) and 1-bromohexadecane (13.3 g, 43.7 mmol, 2.4 eq.) were added and the reaction mixture was refluxed for 47 h. After cooling to room temperature, H_2O (150 ml) was added and the formed beige precipitate was filtered off. It was washed with H_2O, a small amount of hot acetone and the solvent was removed under reduced pressure. The crude product was purified via column chromatography (CH, R_f = 0.26; changing the eluent gradually to CH:DCM = 1:1 after separation of 1-bromohexadecane) yielding **23** (6.68 g, 11.9 mmol, 66%) as a colourless crystalline solid.

Route b):

For the synthesis of compound **23**, a modified reaction procedure by *L. Assies et al.* was applied.[91]

Resorcinol **21** (2.00 g, 18.2 mmol, 1.0 eq.) was dissolved in acetone (80 ml) under argon atmosphere. Then, caesium carbonate (14.8 g, 45.5 mmol, 2.5 eq.), potassium iodide (0.60 g, 3.64 mmol, 0.2 eq.) and 1-bromohexadecane (13.3 g, 43.7 mmol, 2.4 eq.) were added and the reaction mixture was refluxed for 46 h. After cooling to room temperature, H_2O (150 ml) was added and the formed beige precipitate was filtered off. It was washed with H_2O, a small amount of acetone and the solvent was removed under reduced pressure, yielding **23** (10.0 g, 17.9 mmol, 98%) as a colourless crystalline solid.

Analytics:

Sum formula:	$C_{38}H_{70}O_2$
Molar mass:	558.98 g/mol

^{1}H-NMR (500 MHz, $CDCl_3$, 289 K):

δ [ppm] = 7.15 (t, J = 8.1 Hz, 1H), 6.48 (dd, J = 8.2 Hz, 2.3 Hz, 2H), 6.45 (t, J = 2.3 Hz, 1H), 3.92 (t, J = 6.6 Hz, 4H), 1.80-1.72 (m, 4H), 1.48-1.39 (m, 4H), 1.37-1.20 (m, 48H), 0.88 (t, J = 6.9 Hz, 6H).

^{13}C-NMR (126 MHz, $CDCl_3$, 289 K):

δ [ppm] = 160.5, 129.9, 106.7, 101.4, 68.1, 32.1, 29.9, 29.8, 29.7, 29.6, 29.5, 29.4, 26.2, 22.9, 14.3.

MS (EI, 70 eV) *m/z* (%): 558.5 (100) $[M]^{+\bullet}$, 334.2 (27) $[M\text{-}C_{16}H_{32}]^+$, 110.0 (100) $[C_6H_6O_2]^+$; calculated: 558.54 Da.

24 (SR-8 /-19 /-25/-154)

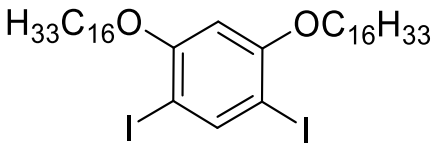

Route a):

For the synthesis of compound **24**, a modified reaction procedure by *A. Segade et al.* was applied.[146]

4,6-Diiodoresorcinol **22** (5.7 g, 15.7 mmol, 1.0 eq.), anhydrous potassium carbonate (8.68 g, 62.8 mmol, 4.0 eq.) and potassium iodide (0.13 g, 0.79 mmol, 0.05 eq.) were dissolved in acetone (65 ml). Then, 1-bromohexadecane (0.13 g, 0.79 mmol, 2.5 eq.) was added and the reaction mixture was refluxed for 43 h. Afterwards, the solvent was removed under reduced pressure and the residue was dissolved in DCM and water. The phases were separated, and the aqueous phase was extracted with DCM several times. The combined organic phases were washed twice with water and once with brine, dried over $MgSO_4$ and the solvent was removed

under reduced pressure. The crude product was purified via column chromatography two times (CH:DCM = 1:1 and CH:DCM = 6:1, R_f = 0.80 (CH:DCM = 6:1)). Then, it was dissolved in chloroform, precipitated from methanol, and filtered. Subsequent recrystallization from toluene yielded **24** (0.98 g, 1.21 mmol, 8%) as a colourless crystalline solid. However, after purification the product still contained small amounts of impurities.

Route b):

For the synthesis of compound **24**, a modified reaction procedure by *A. Segade et al.* was applied.[146]

4,6-Diiodoresorcinol **22** (2.80 g, 7.74 mmol, 1.0 eq.) and caesium carbonate (10.1 g, 31.0 mmol, 4.0 eq.) were dissolved in acetone (80 ml) under argon atmosphere. Then, 1-iodohexadecane (6.81 g, 19.3 mmol, 2.5 eq.) was added and the reaction mixture was refluxed for 44 h. Afterwards, the solvent was removed under reduced pressure and the residue was dissolved in DCM and water. The phases were separated, and the aqueous phase was extracted with DCM (3 x 50 ml). The combined organic phases were washed twice with water and once with brine, dried over $MgSO_4$ and the solvent was removed under reduced pressure. The crude product was purified via column chromatography (CH, R_f = 0.48) yielding **24** (2.33 g, 2.87 mmol, 39%) as a colourless crystalline solid.

Route c):

For the synthesis of compound **24**, a modified reaction procedure by *L. Assies et al.* was applied.[91]

4,6-Diiodoresorcinol **22** (2.89 g, 7.98 mmol, 1.0 eq.) and caesium carbonate (6.50 g, 20.0 mmol, 2.5 eq.) were dissolved in DMF (100 ml) under argon atmosphere. Then, 1-iodohexadecane (6.75 g, 19.2 mmol, 2.4 eq.) was added and the reaction mixture was refluxed for 3 d. After cooling to room temperature H_2O (150 ml) was added. The formed brown precipitate was filtered of and washed with hot acetone. The crude product was purified via column chromatography (CH, R_f = 0.48) and recrystallized from toluene yielding **24** (0.66 g, 0.81 mmol, 10%) as a colourless crystalline solid.

Route d):

For the synthesis of compound **24**, a modified reaction procedure by *L. Assies et al.* was applied.[91]

1,3-Bis(hexadecyloxy)benzene **23** (7.54 g, 13.5 mmol, 1.0 eq.) was dissolved in DCM (30 ml). Then, N-iodosuccinimide (6.07 g, 27.0 mmol, 2.0 eq.) was added slowly and the reaction mixture was stirred vigorously at room temperature for 67 h. The solvent was removed under reduced pressure and the residue was triturated with MeOH for 15 min, yielding product **24** (9.99 g, 12.3 mmol, 91%) as a pale-rose crystalline solid.

Analytics:

Sum formula:	$C_{38}H_{68}I_2O_2$
Molar mass:	810.77 g/mol

^{1}H-NMR (500 MHz, $CDCl_3$, 298 K):

δ [ppm] = 8.02 (s, 1H), 6.32 (s, 1H), 3.98 (t, J = 6.4 Hz, 4H), 1.86-1.79 (m, 4H), 1.54-1.48 (m, 4H), 1.40-1.20 (m, 48H), 0.88 (t, J = 6.9 Hz, 6H).

^{13}C-NMR (126 MHz, $CDCl_3$, 298 K):

δ [ppm] = 159.2, 146.8, 98.1, 76.2, 69.7, 32.1, 29.9, 29.8, 29.7, 29.5, 29.4, 29.2, 26.2, 22.9, 14.3.

MS (EI, 70 eV) *m/z* (%): 810.2 (100) $[M]^{+\bullet}$, 684.3 (24) $[M+H-I]^+$, 586.0 (17) $[M-C_{16}H_{32}]^+$, 361.9 (66) $[M-(C_{16}H_{33})_2]^+$, 261.2 (38) $[C_{17}H_{25}O_2]^+$, 236.0 (22) $[M-I-(C_{16}H_{33})_2+H]^+$, 167.1 (22) $[C_{12}H_{23}]^+$, 149.1 (35) $[C_9H_9O_2]^+$, 112.2 (39) $[C_6H_8O_2]^+$, 97.2 (22) $[C_7H_{13}]^+$, 83.2 (39) $[C_6H_{11}]^+$, 57.2 (59) $[C_4H_9]^+$; calculated: 810.33 Da.

25 (SR-20)

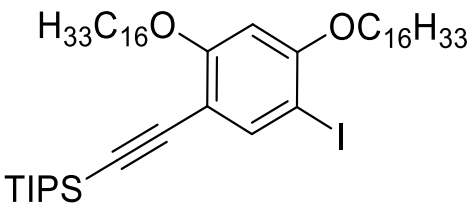

For the synthesis of compound **25**, a reaction procedure by *A. Idelson et al.* was applied.[143] 1,5-Bis(hexadecyloxy)-2,4-diiodobenzene **24** (8.76 g, 10.80 mmol, 1.0 eq.) was dissolved in THF (30 ml) and piperidine (60 ml) and the solution was purged with argon for 1 h. Then, $PdCl_2(PPh_3)_2$ (0.15 g, 0.22 mmol, 0.02 eq.), triphenylphosphane (0.14 g, 0.54 mmol, 0.05 eq.) and copper(I) iodide (0.06 g, 0.32 mmol, 0.03 eq.) were added. Afterwards, TIPS-acetylene (2.47 ml, 11.1 mmol, 1.02 eq.) was added dropwise and the reaction mixture was stirred at 35 °C for 20 h. Then, the reaction mixture was diluted with aq. HCl (10%) and DCM. The phases were separated, and the aqueous phase was extracted with DCM (3 x 20 ml). The combined organic phases were washed once with water and brine, dried over $MgSO_4$ and the solvent was removed under reduced pressure. The crude product was purified via column chromatography (CH:DCM = 40:1, R_f = 0.46 (CH:DCM = 40:1)) yielding product **25** (4.58 g, 5.29 mmol, 49%) and twofold coupled side-product **26** (3.26 g, 3.54 mmol, 33%) as colourless oils.

Analytics:

Sum formula:	$C_{49}H_{89}IO_2Si$
Molar mass:	865.24 g/mol

^{1}H-NMR (500 MHz, $CDCl_3$, 298 K):

δ [ppm] = 7.75 (s, 1H), 6.31 (s, 1H), 4.00-3.95 (m, 4H), 1.87-1.73 (m, 4H), 1.54-1.44 (m, 7H), 1.40-1.22 (m, 48H), 1.12 (d, J = 2.0 Hz, 18H), 0.88 (t, J = 6.9 Hz, 6H).

^{13}C-NMR (126 MHz, $CDCl_3$, 298 K):

δ [ppm] = 162.2, 158.9, 143.0, 107.8, 102.0, 97.4, 94.0, 74.2, 69.6, 69.1, 32.1, 29.9, 29.8, 29.7, 29.5, 29.4, 29.2, 26.3, 26.2, 22.9, 18.9, 14.3, 11.5.

MS (APCI) *m/z* (%): 865.6 (39) $[M+H]^+$, 198.2 (100) $[C_{13}H_{26}O]^+$, 179.0 (22) $[C_{11}H_{19}Si]^+$, 131.0 (28) $[C_8H_{19}O]^+$; calculated: 864.57 Da.

Twofold coupled side product 26:

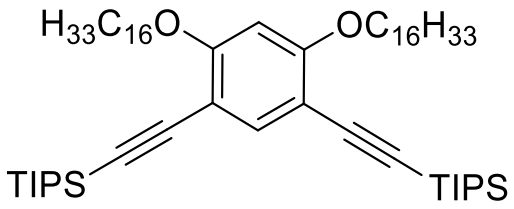

Analytics:

Sum formula:	$C_{60}H_{110}O_2Si_2$
Molar mass:	919.71 g/mol
R_f value (CH:DCM = 40:1)	0.31

^{1}H-NMR (500 MHz, $CDCl_3$, 298 K):

δ [ppm] = 7.46 (s, 1H), 6.30 (s, 1H), 3.97 (t, J = 6.3 Hz, 4H), 1.82-1.75 (m, 4H), 1.56-1.42 (m, 10H), 1.28-1.24 (m, 48H), 1.13 (d, J = 2.4 Hz, 36H), 0.88 (t, J = 6.9 Hz, 6H).

^{13}C-NMR (126 MHz, $CDCl_3$, 298 K):

δ [ppm] = 161.9, 138.5, 105.3, 102.6, 96.8, 93.0, 69.0, 32.1, 29.9, 29.8, 29.7, 29.5, 27.1, 26.3, 22.9, 18.9, 14.3, 11.6.

MS (APCI) *m/z* (%): 919.8 (64) $[M+H]^+$, 198.2 (100) $[C_{13}H_{26}O]^+$, 131.0 (28) $[C_8H_{19}O]^+$; calculated: 918.80 Da.

27 (SR-40/-155)

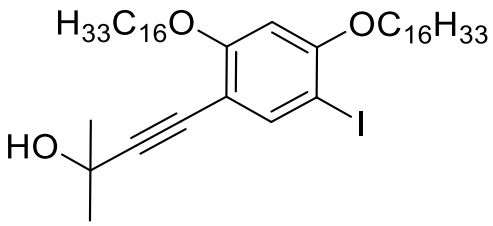

For the synthesis of compound **27**, a reaction procedure by *A. Idelson et al.* was applied.[143] 1,5-Bis(hexadecyloxy)-2,4-diiodobenzene **24** (9.99 g, 12.3 mmol, 1.0 eq.) was dissolved in THF (30 ml) and piperidine (60 ml) and the solution was purged with argon for 1 h. Then, $PdCl_2(PPh_3)_2$ (0.17 g, 0.25 mmol, 0.02 eq.), triphenylphosphane (0.16 g, 0.62 mmol, 0.05 eq.) and copper(I) iodide (0.07 g, 0.37 mmol, 0.03 eq.) were added. Afterwards, 2-methylbut-3-yn-2-ol (1.20 ml, 12.3 mmol, 1.0 eq.) was added dropwise and the reaction mixture was stirred at 40 °C for 23 h. Then, the reaction mixture was diluted with aq. HCl (10%) and DCM. The phases were separated, and the aqueous phase was extracted with DCM (3 x 20 ml). The combined organic phases were washed once with water and brine, dried over $MgSO_4$ and the solvent was removed under reduced pressure. The crude product was purified via column chromatography (CH:DCM = 1:4, R_f = 0.50) yielding **27** (4.66 g, 6.08 mmol, 49%) as a yellow crystalline solid.

Analytics:

Sum formula:	$C_{43}H_{75}IO_3$
Molar mass:	766.97 g/mol

^{1}H-NMR (500 MHz, $CDCl_3$, 298 K):

δ [ppm] = 7.71 (s, 1H), 6.32 (s, 1H), 4.00-3.97 (m, 4H), 1.99 (s, 1H, OH), 1.86-1.76 (m, 4H), 1.60 (s, 6H), 1.53-1.48 (m, 4H), 1.28-1.23 (m, 48H), 0.88 (t, J = 6.9 Hz, 6H).

^{13}C-NMR (126 MHz, $CDCl_3$, 298 K):

δ [ppm] = 161.6, 159.0, 142.6, 106.8, 97.6, 97.3, 74.5, 69.6, 96.1, 65.9, 32.1, 31.7, 29.9, 29.8, 29.7, 29.6, 29.5, 29.4, 29.2, 26.2, 26.1, 22.9, 14.3.

MS (EI, 70 eV) *m/z* (%): 766.4 (18) $[M]^{+\bullet}$, 748.4 (100) $[M\text{-}H_2O]^+$, 299.9 (27) $[C_{11}H_9IO_2]^+$, 183.0 (17) $[C_{13}H_{27}]^+$, 83.1 (28) $[C_5H_7O]^+$, 69.1 (31) $[C_4H_5O]^+$, 57.1 (53) $[C_4H_9]^+$; calculated: 766.48 Da.

28 (SR-21)

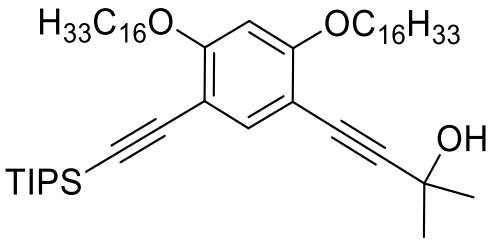

Route a):

For the synthesis of compound **28**, a reaction procedure by *A. Idelson et al.* was applied.[143] Compound **25** (1.51 g, 1.75 mmol, 1.0 eq.) was dissolved in THF (15 ml) and piperidine (20 ml) and the solution was purged with argon for 1 h. Then, $PdCl_2(PPh_3)_2$ (0.025 g, 0.035 mmol, 0.02 eq.), triphenylphosphane (0.023 g, 0.088 mmol, 0.05 eq.) and copper(I) iodide (0.01 g, 0.053 mmol, 0.03 eq.) were added. Afterwards, 2-methylbut-3-yn-2-ol (0.68 ml, 7.00 mmol, 4.0 eq.) was added dropwise and the reaction mixture was stirred at room temperature for 21 h. The reaction mixture was diluted with aq. HCl (10%) and DCM. The phases were separated and the aqueous phase was extracted with DCM (3 x 20 ml). The combined organic phases were washed once with water and brine, dried over $MgSO_4$ and the solvent was removed under reduced pressure. The crude product was purified via column chromatography (CH:DCM = 1:2, R_f = 0.50) yielding **28** (1.11 g, 1.35 mmol, 77%) as a yellow oil.

Route b):

For the synthesis of compound **28**, a reaction procedure by *A. Idelson et al.* was applied.[143] Compound **27** (4.66 g, 6.08 mmol, 1.0 eq.) was dissolved in THF (20 ml) and piperidine (40 ml) and the solution was purged with argon for 1 h. Then, $PdCl_2(PPh_3)_2$ (0.085 g, 0.12 mmol, 0.02 eq.), triphenylphosphane (0.080 g, 0.30 mmol, 0.05 eq.) and copper(I) iodide (0.035 g, 0.18 mmol, 0.03 eq.) were added. Afterwards, TIPS-acetylene (5.46 ml, 24.3 mmol,

4.0 eq.) was added dropwise and the reaction mixture was stirred at 40 °C for 69 h. The reaction mixture was diluted with aq. HCl (10%) and DCM. The phases were separated, and the aqueous phase was extracted with DCM (3 x 20 ml). The combined organic phases were washed once with water and brine, dried over $MgSO_4$ and the solvent was removed under reduced pressure. The crude product was purified via column chromatography (CH:DCM = 1:4, R_f = 0.50) yielding **28** (4.97 g, 6.05 mmol, >99%) as a yellow oil.

Analytics:

Sum formula:	$C_{54}H_{96}O_3Si$
Molar mass:	821.44 g/mol

^{1}H-NMR (500 MHz, $CDCl_3$, 298 K):

δ [ppm] = 7.44 (s, 1H), 6.31 (s, 1H), 4.00-3.96 (m, 4H), 2.00 (s, 1H, OH), 1.85-1.76 (m, 4H), 1.6 (s, 6H), 1.54-1.46 (m, 7H), 1.39-1.22 (m, 48H), 1.12 (d, J = 2.4 Hz, 18H), 0.88 (t, J = 6.9 Hz, 6H).

^{13}C-NMR (126 MHz, $CDCl_3$, 298 K):

δ [ppm] = 161.9, 161.3, 138.2, 105.5, 104.3, 102.5, 97.0, 96.6, 93.2, 78.0, 69.0, 65.9, 32.1, 31.7, 29.9, 29.8, 29.7, 29.6, 29.5, 29.3, 26.3, 26.1, 22.8, 18.9, 14.3, 11.6.

MS (EI, 70 eV) *m/z* (%): 820.7 (8) $[M]^{+\bullet}$, 802.7 (100) $[M\text{-}H_2O]^+$, 759.6 (24) $[M\text{-}H_2O\text{-}C_3H_7]^+$, 535.5 (22) $[M\text{-}C_{19}H_{41}O]^+$, 262.2 (38) $[C_{18}H_{30}O]^+$, 183.2 (24) $[C_{13}H_{27}]^+$, 57.2 (34) $[C_4H_9]^+$; calculated: 820.71 Da.

29 (SR-112)

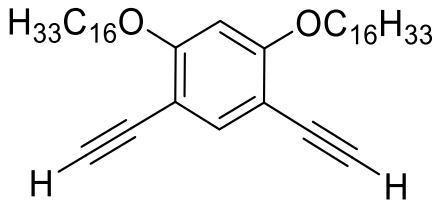

For the synthesis of compound **29**, a modified reaction procedure by *K. Remmersen* was applied.[147]

Compound **26** (4.24 g, 4.61 mmol, 1.0 eq.) was dissolved in dry THF (25 ml) under argon atmosphere and a TBAF-solution (1 M in THF; 18.4 ml, 18.4 mmol, 4.0 eq.) was added. The resulting reaction solution was stirred at 35 °C for 3 h. After cooling to room temperature, the reaction was terminated by addition of H_2O. The phases were separated, and the aqueous phase was extracted with DCM (3 x 20 ml). The combined organic phases were washed once with water and brine, dried over $MgSO_4$ and the solvent was removed under reduced pressure. The crude product was purified via column chromatography (CH:DCM = 4:1, R_f = 0.42), yielding **29** (2.34 g, 3.85 mmol, 84%).

Analytics:

Sum formula:	$C_{42}H_{70}O_2$
Molar mass:	607.02 g/mol

^{1}H-NMR (400 MHz, $CDCl_3$, 298 K):

δ [ppm] = 7.52 (s, 1H), 6.36 (s, 1H), 4.02 (t, J = 6.6 Hz, 4H), 3.16 (s, 2H), 1.84 (p, J = 6.7 Hz, 4H), 1.48 (p, J = 7.3 Hz, 7.0 Hz, 4H), 1.30-1.22 (m, 48H), 0.88 (t, J = 7.2 Hz, 6H).

^{13}C-NMR (126 MHz, $CDCl_3$, 298 K):

δ [ppm] = 162.1, 139.2, 104.1, 97.1, 80.0, 79.9, 79.3, 69.2, 32.1, 29.9, 29.7, 29.5, 29.1, 26.0, 22.9, 14.2.

MS (EI, 70 eV) *m/z* (%): 606.6 (100) $[M]^{+\bullet}$, 158.2 (65) $[C_{10}H_6O_2]^+$, 57.2 (64) $[C_{10}H_9]^+$; calculated: 606.54 Da.

30 (SR-22/-115/-118/-157/-161)

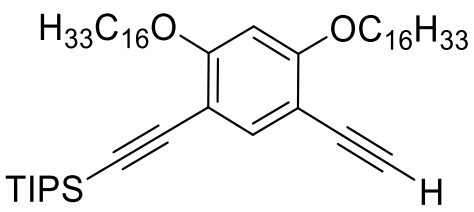

Route a):

For the synthesis of compound **30**, a modified reaction procedure by *V. Valderrey et al.* was applied.[144]

Compound **28** (0.68 g, 0.83 mmol, 1.0 eq.) was dissolved in toluene (15 ml). Then, a microgranulate of NaOH (0.33 g, 8.30 mmol, 10.0 eq.) was added and the reaction mixture was refluxed for 1 h. After cooling to room temperature, the reaction mixture was filtered, and the solvent was removed under reduced pressure. The crude product was purified via column chromatography (CH:DCM = 1:1, R_f = 0.77) yielding **30** (0.61 g, 0.80 mmol, 96%) as a yellow oil.

Route b):

For the synthesis of compound **30**, a modified reaction procedure by *J. Jiao et al.* was applied.[148]

Compound **29** (1.73 g, 2.84 mmol, 1.0 eq.) was dissolved in dry THF (35 ml) and an EtMgBr-solution (1 M in THF; 5.70 ml, 5.70 mmol, 2.0 eq.) was added slowly. Then, TIPS-Cl (0.61 ml, 2.84 mmol, 1.0 eq.) was added dropwise and the reaction solution was stirred at 40 °C for 66 h. After cooling to room temperature, the reaction mixture was diluted with aq. HCl (10%) and DCM. The phases were separated, and the aqueous phase was extracted with DCM (3 x 20 ml). The combined organic phases were washed once with water and brine, dried over $MgSO_4$ and the solvent was removed under reduced pressure. The crude product was purified via column chromatography (CH:DCM = 10:1, R_f = 0.37) yielding **30** (0.66 g, 0.86 mmol, 30%) as a colourless oil.

Route c):

For the synthesis of compound **30**, a modified reaction procedure by *T. He et al.* was applied.[149]

Compound **29** (0.46 g, 0.76 mmol, 1.0 eq.) was dissolved in dry THF (30 ml) and cooled to -78 °C. Then, an *n*-BuLi-solution (2 M in cyclohexane; 0.84 ml, 1.67 mmol, 2.2 eq.) was added dropwise and the reaction mixture was stirred for 30 min at -78 °C. Afterwards, TIPS-Cl (0.16 ml, 0.76 mmol, 1.0 eq.) was added dropwise and the reaction solution was stirred further for 30 min at -78 °C. Then, it was warmed up to room temperature and stirred for 18 h. The reaction was quenched by addition of a saturated NH_4Cl solution. Then, the phases were separated, and the aqueous phase was extracted with DCM (3 x 20 ml). The combined organic phases were washed once with water and brine, dried over $MgSO_4$ and the solvent was removed under reduced pressure. The crude product was purified via column chromatography (CH:DCM = 10:1, R_f = 0.37) yielding **30** (0.05 g, 0.06 mmol, 8%) as a colourless oil.

Analytics:

Sum formula:	$C_{51}H_{90}O_2Si$
Molar mass:	763.36 g/mol

^{1}H-NMR (500 MHz, $CDCl_3$, 298 K):

δ [ppm] = 7.51 (s, 1H), 6.33 (s, 1H), 4.00 (dt, J = 15.7 Hz, 6.4 Hz, 4H), 3.15 (s, 1H), 1.86-1.76 (m, 4H), 1.56-1.42 (m, 7H), 1.39-1.19 (m, 48H), 1.12 (d, J = 2.2 Hz, 18H), 0.88 (t, J = 6.9 Hz, 6H).

^{13}C-NMR (126 MHz, $CDCl_3$, 298 K):

δ [ppm] = 162.2, 161.8, 139.0, 105.6, 103.7, 102.3, 97.0, 93.3, 79.8, 79.6, 69.2, 68.9, 32.1, 29.9, 29.8, 29.7, 29.5, 29.1, 26.3, 26.0, 22.9, 18.9, 14.3, 11.5.

MS (EI, 70 eV) *m/z* (%): 762.6 (20) $[M]^{+\bullet}$, 719.6 (20) $[M\text{-}C_3H_7]^+$, 495.3 (9) $[M\text{-}H\text{-}OC_{16}H_{33}]^+$, 262.1 (38) $[C_{18}H_{29}O]^+$, 112.1 (43) $[C_8H_{16}]^+$, 71.1 (73) $[C_5H_{11}]^+$, 57.1 (100) $[C_4H_9]^+$; calculated: 762.67 Da.

31 (SR-23/-46/-78/-122)

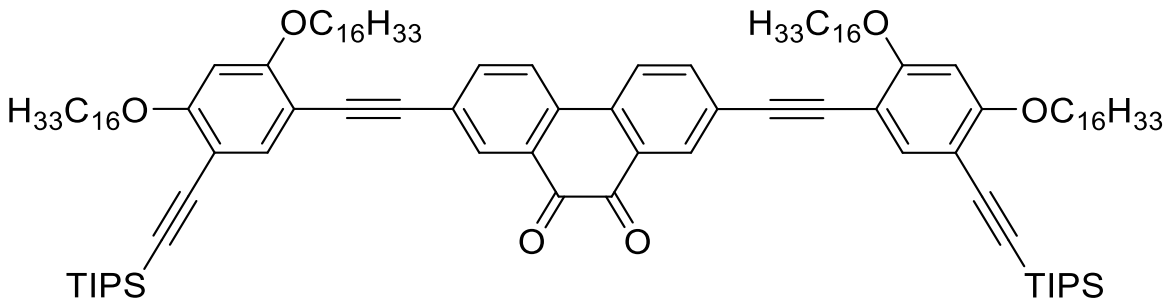

Route a):

For the synthesis of compound **31**, a reaction procedure by *A. Idelson et al.* was applied.[143] Compound **2** (0.16 g, 0.35 mmol, 1.0 eq.) was dissolved in dry THF (7.5 ml) and dry piperidine (10 ml) and the solution was purged with argon for 1 h. Then, $Pd(PPh_3)_4$ (8.00 mg, 7.00 µmol, 0.02 eq.) and copper(I) iodide (2.00 mg, 11.0 µmol, 0.03 eq.) were added. Afterwards, **30** (0.57 g, 0.75 mmol, 2.15 eq.) dissolved in THF (5 ml) was added dropwise and the reaction mixture was stirred at room temperature for 18 h. Then, the reaction mixture was diluted with aq. HCl (10%) and DCM. The phases were separated, and the aqueous phase was extracted with DCM (3 x 20 ml). The combined organic phases were washed once with water and brine, dried over $MgSO_4$ and the solvent was removed under reduced pressure. The crude product was purified via column chromatography (CH:DCM = 1:1, R_f = 0.53) yielding product **SR-23** (0.09 g, 0.05 mmol, 15%) as a violet crystalline solid and onefold-coupled side-product **SR-33** (0.11 g, 0.10 mmol, 29%) as a violet solid.

Route b):

For the synthesis of compound **31**, a reaction procedure by *A. Idelson et al.* was applied.[143] Compound **3** (0.79 g, 1.37 mmol, 1.0 eq.) was dissolved in dry piperidine (20 ml) and **30** (2.32 g, 3.03 mmol, 2.2 eq.) was dissolved in dry THF (10 ml). Both solutions were purged with argon for 1 h separately. Then, $Pd(PPh_3)_2Cl_2$ (19.0 mg, 27.0 µmol, 0.02 eq.), PPh_3 (18.0 mg, 69.0 µmol, 0.05 eq.) and copper(I) iodide (8.00 mg, 41.0 µmol, 0.03 eq.) were added to the solution of **3**. Afterwards, **30** dissolved in THF was added dropwise and the reaction mixture was stirred at 40 °C for 20 h. Then, the reaction mixture was diluted with aq. HCl (10%) and DCM. The phases were separated, and the aqueous phase was extracted with

DCM (3 x 20 ml). The combined organic phases were washed once with water and brine, dried over $MgSO_4$ and the solvent was removed under reduced pressure. The crude product was purified via column chromatography (CH:DCM = 2:1, R_f = 0.22) yielding product **31** (1.48 g, 0.86 mmol, 62%) as a violet crystalline solid and onefold-coupled side-product **33** (0.44 g, 0.40 mmol, 29%) as a violet solid.

Route c):

For the synthesis of compound **31**, a reaction procedure by *A. Idelson et al.* was applied.[143] Compound **33** (0.11 g, 0.10 mmol, 1.0 eq.) was dissolved in dry piperidine (10 ml) and **30** (0.20 g, 0.26 mmol, 2.5 eq.) was dissolved in dry THF (4 ml). Both solutions were purged with argon for 1 h separately. Then, $Pd(PPh_3)_4$ (6.00 mg, 5.00 µmol, 0.05 eq.) and copper(I) iodide (1.00 mg, 3.00 µmol, 0.03 eq.) were added to the solution of **33**. Afterwards, **30** dissolved in THF was added dropwise and the reaction mixture was stirred at 40 °C for 18 h. Then, the reaction mixture was diluted with aq. HCl (10%) and DCM. The phases were separated, and the aqueous phase was extracted with DCM (3 x 20 ml). The combined organic phases were washed once with water and brine, dried over $MgSO_4$ and the solvent was removed under reduced pressure. The crude product was purified via column chromatography (CH:DCM = 1:1, R_f = 0.50) yielding **31** (0.09 g, 0.05 mmol, 50%) as a violet crystalline solid.

Route d):

For the synthesis of compound **32**, a reaction procedure by *A. Idelson et al.* was applied.[143] Compound **4** (0.15 g, 0.31 mmol, 1.0 eq.) was dissolved in dry piperidine (15 ml) and **30** (0.53 g, 0.69 mmol, 2.2 eq.) was dissolved in dry THF (7.5 ml). Both solutions were purged with argon for 1 h separately. Then, $Pd(OAc)_2$ (7.00 mg, 31.0 µmol, 0.10 eq.), *XPhos* (36.0 mg, 78.0 µmol, 0.25 eq.) and copper(I) iodide (9.00 mg, 47.0 µmol, 0.15 eq.) were added to the solution of **4**. Afterwards, **30** dissolved in THF was added dropwise and the reaction mixture was stirred at 40 °C for 20 h. Then, the reaction mixture was diluted with aq. HCl (10%) and DCM. The phases were separated, and the aqueous phase was extracted with DCM (3 x 20 ml). The combined organic phases were washed once with water and brine, dried over $MgSO_4$ and the solvent was removed under reduced pressure. The crude product was purified via column chromatography (CH:DCM = 1:1, R_f = 0.63) yielding product **31** (35.0 mg, 20.2 µmol, 7%) as a violet solid, instead of the expected alcohol **32**.

Analytics:

Sum formula:	$C_{116}H_{184}O_6Si_2$
Molar mass:	1730.91 g/mol

^{1}H-NMR (500 MHz, $CDCl_3$, 298 K):

δ [ppm] = 8.26 (d, J = 1.9 Hz, 2H), 7.92 (d, J = 8.5 Hz, 2H), 7.76 (dd, J = 8.2 Hz, 1.9 Hz, 2H), 7.56 (s, 2H), 6.36 (s, 2H), 4.04 (dt, J = 26.3 Hz, 6.4 Hz, 8H), 1.85 (dt, 38.9 Hz, 8.0 Hz, 8H), 1.59-1.48 (m, 10H), 1.44-1.38 (m, 4H), 1.28-1.21 (m, 96H), 1.14 (d, J = 2.3 Hz, 36H), 0.90-0.84 (m, 12H).

^{13}C-NMR (126 MHz, $CDCl_3$, 298 K):

δ [ppm] = 179.7, 162.5, 161.5, 138.3, 138.1, 134.3, 133.3, 131.0, 126.0, 124.2, 105.9, 104.1, 102.3, 96.9, 93.5, 90.6, 89.5, 69.2, 69.0, 32.1, 29.9, 29.8, 29.7, 29.5, 29.3, 26.3, 26.2, 22.9, 18.9, 14.3, 11.6.

MS (MALDI+) *m/z* (%): 1979.5 (7) $[M+DCTB]^+$, 1729.4 (100) $[M]^+$, 1654.6 (9) $[M+H-C_{16}H_{33}-C_6H_{13}+DCTB]^+$; calculated: 1729.36 Da.

Side Product 33:

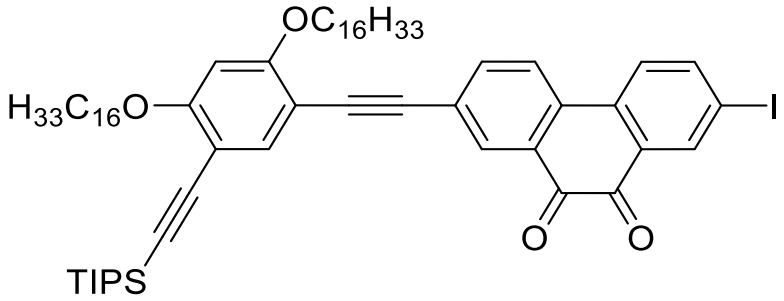

Analytics:

Sum formula:	$C_{65}H_{95}IO_4Si$
Molar mass:	1095.46 g/mol
R_f value (CH:DCM = 1:1)	0.36

^{1}H-NMR (500 MHz, $CDCl_3$, 298 K):

δ [ppm] = 8.47 (d, J = 2.0 Hz, 1H), 8.25 (d, J = 1.9 Hz, 1H), 8.02 (dd, J = 8.4 Hz, 2.0 Hz, 1H), 7.91 (d, J = 8.4 Hz, 1H), 7.75 (dd, J = 8.3 Hz, 1.9 Hz, 1H), 7.69 (d, J = 8.5 Hz, 1H), 7.55 (s, 1H), 6.36 (s, 1H), 4.03 (dt, J = 23.5 Hz, 6.4 Hz, 4H), 1.91-1.79 (m, 4H), 1.59-1.46 (m, 5H), 1.44-1.37 (m, 2H), 1.35-1.18 (m, 48), 1.14 (d, J = 1.2 Hz, 18H), 0.89-0.86 (m, 6H).

^{13}C-NMR (126 MHz, $CDCl_3$, 298 K):

δ [ppm] = 179.1, 179.0, 162.6, 161.5, 144.8, 139.4, 138.3, 138.2, 135.0, 133.7, 133.4, 132.0, 131.1, 126.5, 125.7, 124.1, 105.9, 104.0, 102.3, 96.8, 95.4, 93.6, 90.5, 89.8, 69.2, 69.0, 32.1, 29.9, 29.8, 29.7, 29.5, 29.2, 26.3, 26.2, 22.9, 18.9, 14.3, 11.6.

MS (MALDI+) *m/z* (%): 1344.7 (18) $[M+DCTB]^+$, 1094.6 (100) $[M]^+$, 552.6 (20) $[C_{36}H_{60}O_2Si]^+$; calculated: 1094.60 Da.

34 (SR-106)

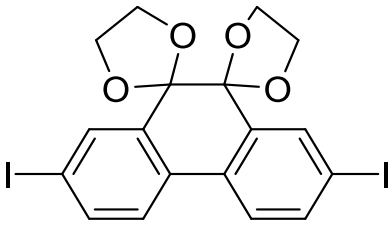

For the synthesis of compound **34**, a modified reaction procedure by *L. Estrada et al.* was applied.[98]

A 1:5-mixture of dry ethylene glycol and dry methanol was purged with argon for 1 h. 2,7-diiodophenanthrenequinone **2** (0.35 g, 0.76 mmol, 1.0 eq.) and (1S)-(+)-camphorsulfonic acid (0.03 g, 0.11 mmol, 0.15 eq.) were transferred to a microwave vial under argon atmosphere. The solvent mixture was added, and the vial was tightly capped. Then, it was heated to 120 °C under stirring in a microwave for 3 h. After cooling to room temperature, the reaction mixture was filtered, washed with H_2O (3x50 ml) and MeOH (2x5 ml) and dried under vacuum. The crude product was purified via column chromatography (CH:DCM = 1:2, R_f = 0.65) yielding **34** (0.04 g, 0.07 mmol, 9%) as a beige crystalline solid.

Analytics:

Sum formula:	$C_{18}H_{14}I_2O_4$
Molar mass:	548.11 g/mol

^{1}H-NMR (500 MHz, $CDCl_3$, 298 K):

δ [ppm] = 8.07 (d, J = 1.9 Hz, 2H), 7.79 (dd, J = 8.4 Hz, 1.9 Hz, 2H), 7.57 (d, J = 8.4 Hz, 2H), 4.21 (bs, 4H), 3.66 (bs, 4H).

^{13}C-NMR (126 MHz, $CDCl_3$, 298 K):

δ [ppm] = 139.2, 135.5, 134.9, 132.0, 125.6, 94.8, 92.0, 66.6.

MS (APCI) *m/z* (%): 548.9 (34) $[M+H]^+$, 423.0 (20) $[C_{18}H_{16}IO_4+H]^+$, 297.1 (100) $[C_{18}H_{16}O_4+H]^+$; calculated: 547.90 Da.

35 (SR-35/-124)

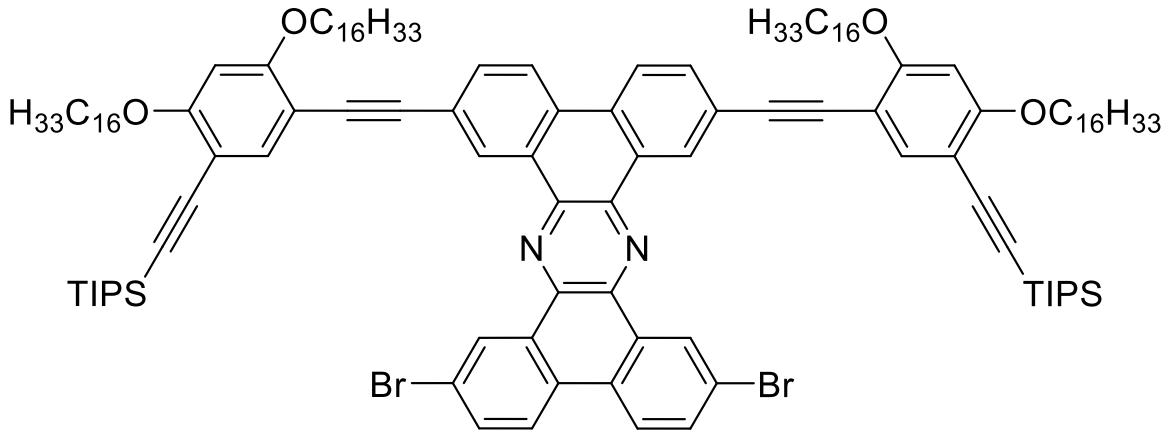

Route a):

For the synthesis of compound **35**, a reaction procedure by *K. P. Loh et al.* was applied.[150] Compound **31** (85.0 mg, 49.0 µmol, 1.0 eq.) and 2,7-dibromophenanthrene-9,10-diamine hydrochloride **7** (22.0 mg, 49.0 µmol, 1.0 eq.) were suspended in EtOH (6 ml) and AcOH (20 ml) under argon atmosphere. Then, the suspension was heated to 100 °C and Et_3N (1 ml) was added. Afterwards, the reaction mixture was refluxed at 130 °C for 20 h. After cooling to

room temperature, the reaction mixture was diluted with AcOH and poured into water (200 ml). The dark violet residue was filtered and dried yielding substrate **31** (74.0 mg, 43.0 µmol, 87%) as dark violet solid.

Route b):

For the synthesis of compound **35**, a modified reaction procedure by *L. Schneider* was applied.[151]

Compound **31** (74.0 mg, 43.0 µmol, 1.0 eq.) and 2,7-dibromophenanthrene-9,10-diamine hydrochloride **7** (19.0 mg, 43.0 µmol, 1.0 eq.) were dissolved in chloroform (5 ml) and AcOH (3 ml). Then, the reaction mixture was refluxed at 130 °C for 24 h. After cooling to room temperature, the reaction mixture was diluted with DCM and water. The phases were separated, and the aqueous phase was extracted with DCM (3 x 20 ml). The combined organic phases were washed once with aq. HCl (10%), water and brine, dried over $MgSO_4$. The solvent was removed under reduced pressure yielding substrate **31** (74.0 mg, 43.0 µmol, 87%) as dark violet solid.

Route c):

For the synthesis of compound **35**, a modified reaction procedure by *S. Claus* was applied.[85]

Compound **31** (76.0 mg, 43.9 µmol, 1.0 eq.) and 2,7-Dibromophenanthrene-9,10-diamine hydrochloride **7** (19.1 mg, 43.9 µmol, 1.0 eq.) were dissolved in dry THF (5 ml). Then, NEt_3 (0.5 ml) was added, and the reaction mixture was refluxed at 130 °C for 24 h. Afterwards, another 0.5 ml of Net_3 were added and the reaction mixture was further refluxed for 23 h. After cooling to room temperature, the reaction mixture was diluted with DCM and water. The phases were separated, and the aqueous phase was extracted with DCM (3 x 20 ml). The combined organic phases were washed once with water and dried over $MgSO_4$. The solvent was removed under reduced pressure and the crude product was purified via column chromatography (CH:DCM = 1:1, R_f = 0.96) yielding **35** (25.0 mg, 12.0 µmol, 28%) as a yellow film.

Route d):

For the synthesis of compound **35**, a modified reaction procedure by *L. Schneider* was applied.[151]

Compound **31** (0.82 g, 0.47 mmol, 1.0 eq.) and 2,7-dibromophenanthrene-9,10-diamine **8** (0.35 g, 0.95 mmol, 2.0 eq.) were dissolved in chloroform (10 ml) and AcOH (6 ml) under argon atmosphere. Then, the reaction mixture was refluxed for 22 h. After cooling to room temperature, the reaction mixture was diluted with DCM and aq. HCl (10%). The phases were separated, and the aqueous phase was extracted with DCM (3 x 20 ml). The combined organic phases were washed once with water and brine, dried over $MgSO_4$ and the solvent was removed under reduced pressure. The crude product was purified via column chromatography (CH:DCM = 1:1, R_f = 0.98) yielding **35** (0.89 g, 0.43 mmol, 92%) as yellow crystalline solid.

Analytics:

Sum formula:	$C_{130}H_{190}Br_2N_2O_4Si_2$
Molar mass:	2060.94 g/mol

^{1}H-NMR (700 MHz, $CDCl_3$, 298 K):

δ [ppm] = 9.47 (d, J = 2.2 Hz, 2H), 9.34 (d, J = 1.7 Hz, 2H), 8.34 (d, J = 8.7 Hz, 2H), 8.21 (d, J = 8.9 Hz, 2H), 7.81 (dd, J = 6.3 Hz, 2.1 Hz, 2H), 7.79 (dd, J = 6.1 Hz, 1.6 Hz, 2H), 7.68 (s, 2H), 6.38 (s, 2H), 4.14 (t, J = 6.4 Hz, 4H), 4.04 (t, J = 6.3 Hz, 4H), 2.02-1.98 (m, 4H), 1.87-1.82 (m, 4H), 1.67-1.61 (m, 4H), 1.59-1.52 (m, 10H), 1.30-1.26 (m, 96H), 1.19 (d, J = 3.8 Hz, 36H), 0.89 (t, J = 7.1 Hz, 6H), 0.84 (t, J = 7.2 Hz, 6H).

^{13}C-NMR (176 MHz, $CDCl_3$, 298 K):

δ [ppm] = 162.1, 161.6, 140.5, 139.3, 138.2, 133.0, 132.9, 131.7, 130.6, 129.9, 129.7, 128.7, 124.5, 123.8, 123.0, 122.9, 105.6, 105.1, 102.8, 97.0, 93.2, 92.6, 87.6, 69.3, 68.9, 32.1, 29.9, 29.8, 29.7, 29.6, 29.5, 26.4, 22.9, 22.8, 19.0, 14.3, 11.6.

MS (MALDI+) *m/z* (%): 2057.3 (100) $[M]^+$; calculated: 2057.26 Da.

36 (SR-51/-126)

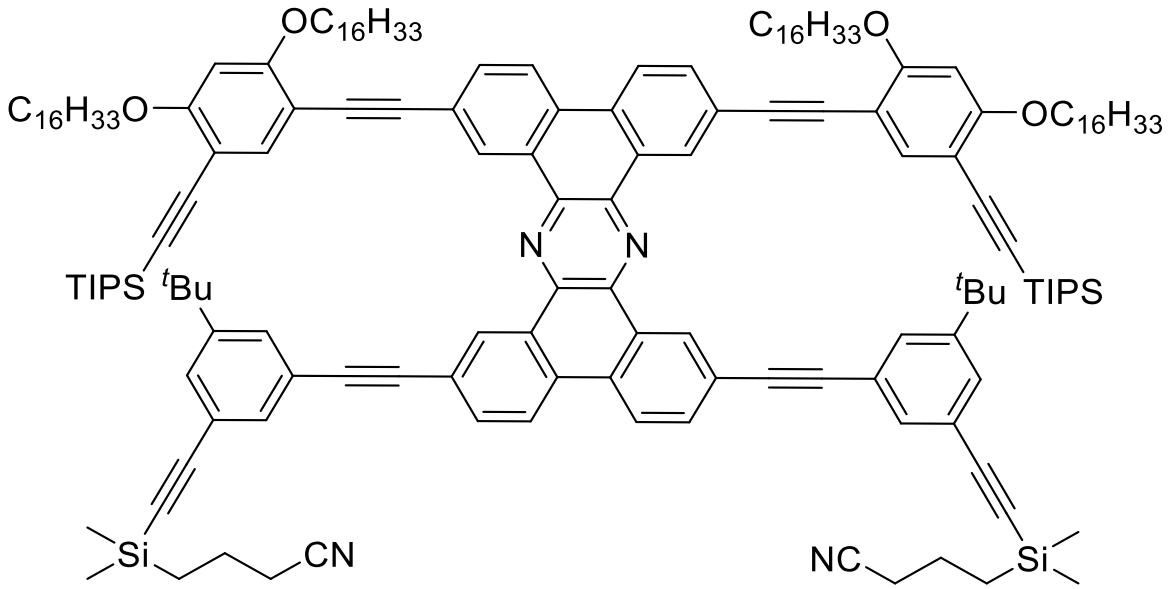

For the synthesis of compound **36**, a modified reaction procedure by *A. Idelson et al.* was applied.[143]

Compound **35** (0.89 g, 0.43 mmol, 1.0 eq.) was dissolved in dry THF (10 ml) and dry piperidine (20 ml). Compound **17** (0.53 g, 1.72 mmol, 4.0 eq.) was dissolved in THF (10 ml) separately and both solutions were purged with argon for 1 h. Then, $Pd(OAc)_2$ (4.00 mg, 17.0 µmol, 0.04 eq.), *XPhos* (20.0 mg, 43.0 µmol, 0.1 eq.) and copper(I) iodide (5.00 mg, 26.0 µmol, 0.06 eq.) were added to the solution of **35**. Afterwards, **17** dissolved in THF was added dropwise and the reaction mixture was stirred at 80 °C for 20 h. After cooling to room temperature, the reaction mixture was diluted with aq. HCl (10%) and DCM. The phases were separated, and the aqueous phase was extracted with DCM (3 x 20 ml). The combined organic phases were washed once with water and brine, dried over $MgSO_4$ and the solvent was removed under reduced pressure. The crude product was purified via column chromatography (CH:DCM = 1:2, R_f = 0.75) yielding **36** (0.72 g, 0.29 mmol, 67%) as a luminous yellow film.

Analytics:

Sum formula:	$C_{170}H_{238}N_4O_4Si_4$
Molar mass:	2514.14 g/mol

^{1}H-NMR (700 MHz, $CDCl_3$, 298 K):

δ [ppm] = 9.75 (d, J = 1.9 Hz, 2H), 9.74 (d, J = 1.9 Hz, 2H), 8.64 (d, J = 8.7 Hz, 2H), 8.60 (d, J = 8.7 Hz, 2H), 7.98 (dd, J = 8.2 Hz, 1.8 Hz, 2H), 7.96 (dd, J = 8.3 Hz, 1.8 Hz, 2H), 7.67 (s, 2H), 7.66 (t, J = 1.7 Hz, 2H), 7.63 (t, J = 1.5 Hz, 2H), 7.48 (t, J = 1.7 Hz, 2H), 6.34 (s, 2H), 4.00 (dt, J = 7.8 Hz, 6.2 Hz, 8H), 2.43 (t, J = 7.0 Hz, 4H), 1.92-1.86 (m, 4H), 1.85-1.80 (m, 8H), 1.59-1.51 (m, 14H), 1.31 (s, 18H), 1.30-1.25 (m, 96H), 1.13 (d, J = 3.4 Hz, 36H), 0.88 (t, J = 7.1 Hz, 6H), 0.86-0.82 (m, 4H), 0.84 (t, J = 7.3 Hz, 6H), 0.26 (s, 12H).

^{13}C-NMR (176 MHz, $CDCl_3$, 298 K):

δ [ppm] = 162.2, 161.7, 151.9, 140.8, 140.4, 138.0, 133.1, 133.0, 132.7, 131.2, 131.0, 130.8, 130.5, 129.5, 129.3, 129.2, 129.1, 123.8, 123.5, 123.4, 123.0, 122.9, 119.9, 106.2, 105.9, 105.0, 102.6, 97.2, 93.3, 92.6, 92.3, 90.9, 89.9, 87.5, 69.5, 68.9, 34.9, 32.1, 31.3, 29.9, 29.8, 29.7, 29.6, 29.5, 26.4, 22.9, 20.8, 20.7, 18.9, 15.6, 14.3, 11.6, -1.7.

MS (MALDI+) *m/z* (%): 2511.8 (100) $[M]^+$, 2473.9 (81) $[M+2H-C_2H_2N]^+$; calculated: 2511.76 Da.

I (SR-52)

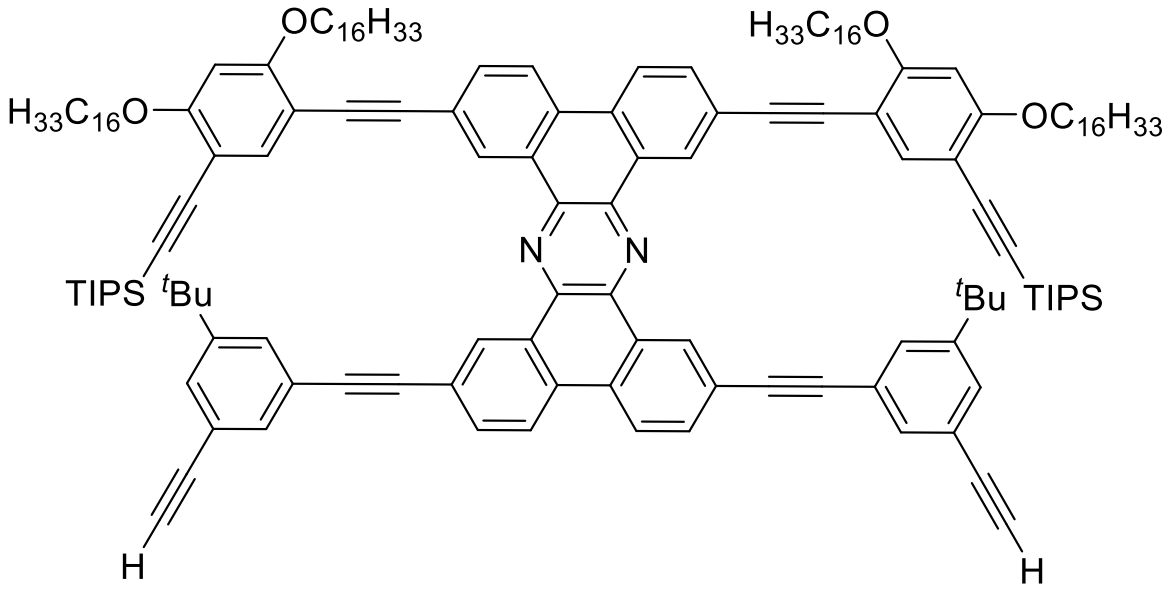

For the synthesis of compound **I**, a modified reaction procedure by *A. Idelson et al.* was applied.[143]

Compound **36** (0.47 g, 0.19 mmol, 1.0 eq.) was dissolved in dry THF (24 ml) and MeOH (12 ml) under argon atmosphere. Then, anhydrous K_2CO_3 (0.26 mg, 1.87 mmol, 10.0 eq.) was added and the reaction solution was stirred at room temperature for 24 h. Afterwards, the reaction mixture was diluted with H_2O and DCM. The phases were separated, and the aqueous phase was extracted with DCM (3 x 20 ml). The combined organic phases were washed once with water and brine, dried over $MgSO_4$ and the solvent was removed under reduced pressure. The crude product was purified via column chromatography (CH:DCM = 1:1, R_f = 0.96) yielding **I** (0.43 g, 0.19 mmol, >99%) as a luminous yellow crystalline solid.

Analytics:

Sum formula:	$C_{158}H_{216}N_2O_4Si_2$
Molar mass:	2263.65 g/mol

^{1}H-NMR (700 MHz, $CDCl_3$, 298 K):

δ [ppm] = 9.75 (d, J = 1.9 Hz, 2H), 9.75 (d, J = 1.9 Hz, 2H), 8.63 (d, J = 8.7 Hz, 2H), 8.59 (d, J = 8.7 Hz, 2H), 7.98 (dd, J = 8.2 Hz, 1.8 Hz, 2H), 7.95 (dd, J = 8.2 Hz, 1.8 Hz, 2H), 7.68 (s, 2H), 7.67 (t, J = 1.7 Hz, 2H), 7.64 (t, J = 1.5 Hz, 2H), 7.52 (t, J = 1.7 Hz, 2H), 6.37 (s, 2H), 4.00 (dt, J = 9.7 Hz, 6.3 Hz, 8H), 3.05 (s, 2H), 1.94-1.88 (m, 4H), 1.86-1.79 (m, 4H), 1.60-1.50 (m, 14H), 1.32 (s, 18H), 1.31-1.20 (m, 96H), 1.14 (d, J = 3.2 Hz, 36H), 0.86 (dt, J = 33.8 Hz, 7.2 Hz, 12H).

^{13}C-NMR (176 MHz, $CDCl_3$, 298 K):

δ [ppm] = 162.2, 161.7, 151.9, 140.8, 140.4, 137.9, 132.7, 131.2, 131.0, 130.5, 129.6, 123.8, 123.4, 123.0, 122.3, 105.8, 105.0, 102.6, 97.2, 93.3, 92.6, 90.9, 89.9, 87.5, 83.5, 69.5, 68.9, 34.9, 32.1, 31.3, 29.9, 29.8, 29.7, 29.6, 29.5, 26.4, 22.9, 18.9, 14.3, 11.6.

MS (MALDI+) *m/z* (%): 2511.8 (2) $[M+DCTB]^+$, 2261.6 (100) $[M]^+$; calculated: 2261.63 Da.

37 (SR-125)

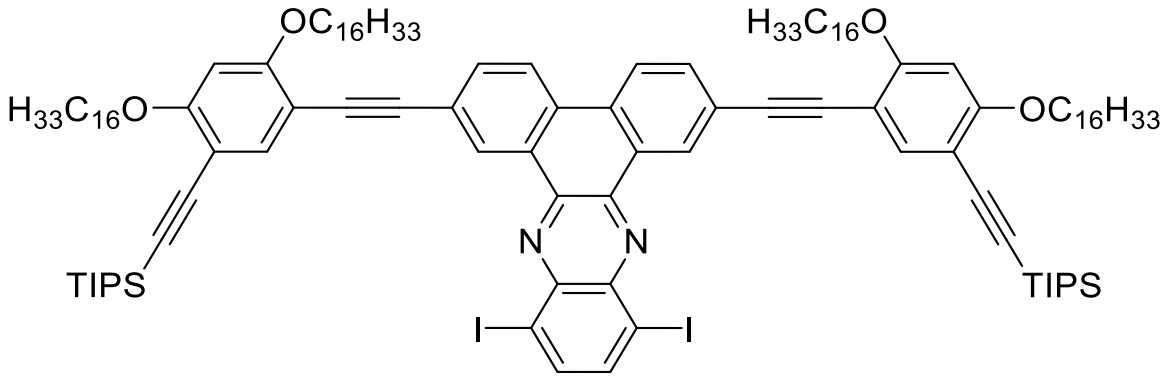

For the synthesis of compound **37**, a modified reaction procedure by *L. Schneider* was applied.[151]

Compound **31** (0.81 g, 0.47 mmol, 1.0 eq.) and 3,6-diiodobenzene-1,2-diamine **11** (0.36 g, 1.00 mmol, 2.1 eq.) were dissolved in chloroform (10 ml) and AcOH (6 ml) under argon atmosphere. Then, the reaction mixture was refluxed for 20 h. After cooling to room

temperature, the reaction mixture was diluted with DCM and aq. HCl (10%). The phases were separated, and the aqueous phase was extracted with DCM (3 x 20 ml). The combined organic phases were washed once with water and brine, dried over $MgSO_4$ and the solvent was removed under reduced pressure. The crude product was purified via column chromatography (CH:DCM = 1:1, R_f = 0.98) yielding **37** (0.91 g, 0.44 mmol, 94%) as bright orange crystalline solid.

Analytics:

Sum formula:	$C_{122}H_{186}I_2N_2O_4Si_2$
Molar mass:	2054.82 g/mol

^{1}H-NMR (500 MHz, $CDCl_3$, 298 K):

δ [ppm] = 9.54 (d, J = 1.9 Hz, 2H), 8.45 (d, J = 8.6 Hz, 2H), 8.16 (s, 2H), 7.90 (dd, J = 8.3 Hz, 1.9 Hz, 2H), 7.67 (s, 2H), 6.41 (s, 2H), 4.07 (dt, J = 34.5 Hz, 6.4 Hz, 8H), 2.00-1.90 (m, 4H), 1.88-1.79 (m, 4H), 1.62-1.49 (m, 10H), 1.44-1.36 (m, 4H), 1.35-1.23 (m, 96H), 1.16 (d, J = 2.2 Hz, 36H), 0.87 (dt, J = 13.9 Hz, 6.9 Hz, 12H).

^{13}C-NMR (126 MHz, $CDCl_3$, 298 K):

δ [ppm] = 162.2, 161.5, 143.7, 141.6, 140.8, 138.3, 134.0, 131.4, 130.1, 129.4, 124.3, 123.3, 105.8, 104.9, 104.2, 102.5, 97.1, 93.4, 92.3, 87.8, 69.3, 69.0, 32.1, 29.9, 29.8, 29.7, 29.5, 29.4, 26.4, 26.3, 22.9, 18.9, 14.3, 11.6.

MS (MALDI+) *m/z* (%): 2241.9 (9) $[M+HCCA]^+$, 2053.2 (100) $[M]^+$; calculated: 2053.20 Da.

38 (SR-128)

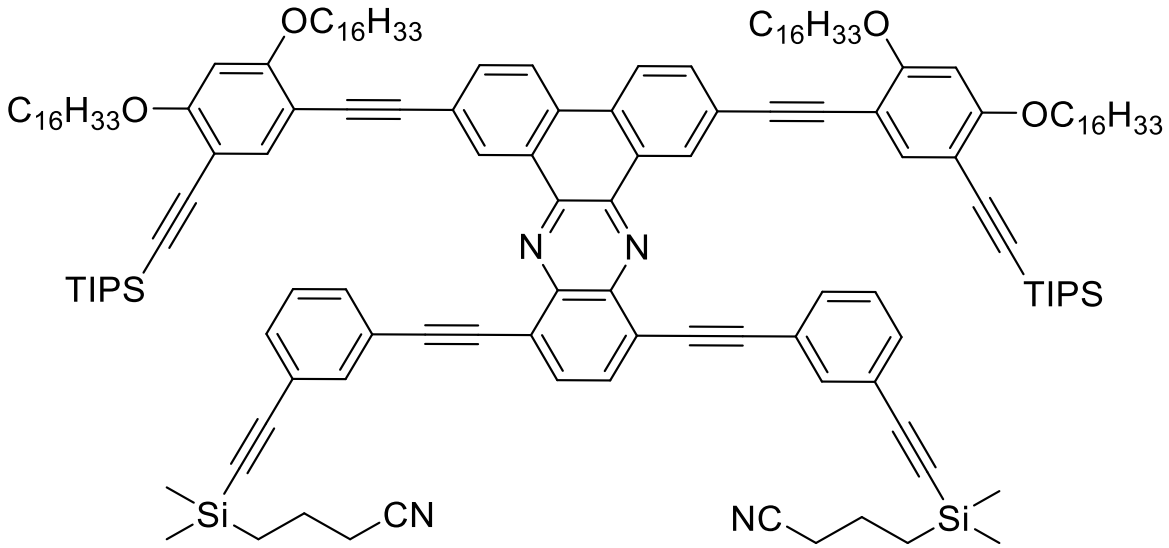

For the synthesis of compound **38**, a modified reaction procedure by *A. Idelson et al.* was applied.[143]

Compound **37** (0.91 g, 0.44 mmol, 1.0 eq.) was dissolved in dry THF (10 ml) and dry piperidine (20 ml). Compound **20** (0.25 g, 0.99 mmol, 2.3 eq.) was dissolved in THF (6 ml) separately and both solutions were purged with argon for 1 h. Then, $Pd(OAc)_2$ (4.00 mg, 18.0 µmol, 0.04 eq.), *XPhos* (21.0 mg, 44.0 µmol, 0.1 eq.) and copper(I) iodide (5.00 mg, 26.0 µmol, 0.06 eq.) were added to the solution of **37**. Afterwards, **20** dissolved in THF was added dropwise and the reaction mixture was stirred at 40 °C for 68 h. After cooling to room temperature, the reaction mixture was diluted with aq. HCl (10%) and DCM. The phases were separated, and the aqueous phase was extracted with DCM (3 x 20 ml). The combined organic phases were washed once with water and brine, dried over $MgSO_4$ and the solvent was removed under reduced pressure. The crude product was purified via column chromatography (CH:DCM = 1:2, R_f = 0.75) yielding **38** (0.57 g, 0.25 mmol, 57%) as an orange-red film.

Analytics:

Sum formula:	$C_{154}H_{218}N_4O_4Si_4$
Molar mass:	2301.80 g/mol

^{1}H-NMR (700 MHz, $CDCl_3$, 298 K):

δ [ppm] = 9.70 (d, *J* = 1.9 Hz, 2H), 8.51 (d, *J* = 8.7 Hz, 2H), 8.04 (s, 2H), 7.96 (dt, *J* = 7.7 Hz, 1.4 Hz, 2H), 7.92 (dd, *J* = 8.2 Hz, 1.9 Hz, 2H), 7.83 (t, *J* = 1.7 Hz, 2H), 7.63 (s, 2H), 7.42 (dt, *J* = 7.7 Hz, 1.4 Hz, 2H), 7.24 (t, *J* = 7.7 Hz, 2H), 6.41 (s, 2H), 4.05 (t, *J* = 6.3 Hz, 4H), 3.97 (t, *J* = 6.4 Hz, 4H), 2.43 (t, *J* = 7.0 Hz, 4H), 1.90-1.79 (m, 8H), 1.79-1.73 (m, 4H), 1.57-1.51 (m, 11H), 1.50-1.44 (m, 3H), 1.35-1.22 (m, 96H), 1.15 (d, *J* = 1.3 Hz, 36H), 0.88 (t, *J* = 7.1 Hz, 6H), 0.84 (t, *J* = 7.2 Hz, 6H), 0.86-0.81 (m, 4H), 0.25 (s, 12H).

^{13}C-NMR (176 MHz, $CDCl_3$, 298 K):

δ [ppm] = 162.3, 161.7, 142.4, 142.3, 137.9, 135.2, 133.4, 132.8, 132.7, 132.3, 131.4, 130.3, 130.0, 129.0, 124.2, 124.0, 123.8, 123.4, 123.3, 119.9, 105.8, 105.7, 104.9, 102.5, 97.7, 97.0, 93.5, 92.9, 92.3, 87.7, 87.4, 69.2, 69.1, 32.1, 29.9, 29.8, 29.7, 29.6, 29.5, 29.3, 27.1, 26.4, 26.3, 22.9, 22.8, 20.8, 20.7, 18.9, 15.8, 14.3, 11.6, -1.7.

MS (MALDI+) *m/z* (%): 2549.7 (3) $[M+DCTB]^+$, 2299.6 (100) $[M]^+$, 2261.8 (34) $[M+2H-C_2H_2N]^+$; calculated: 2299.61 Da.

II (SR-141)

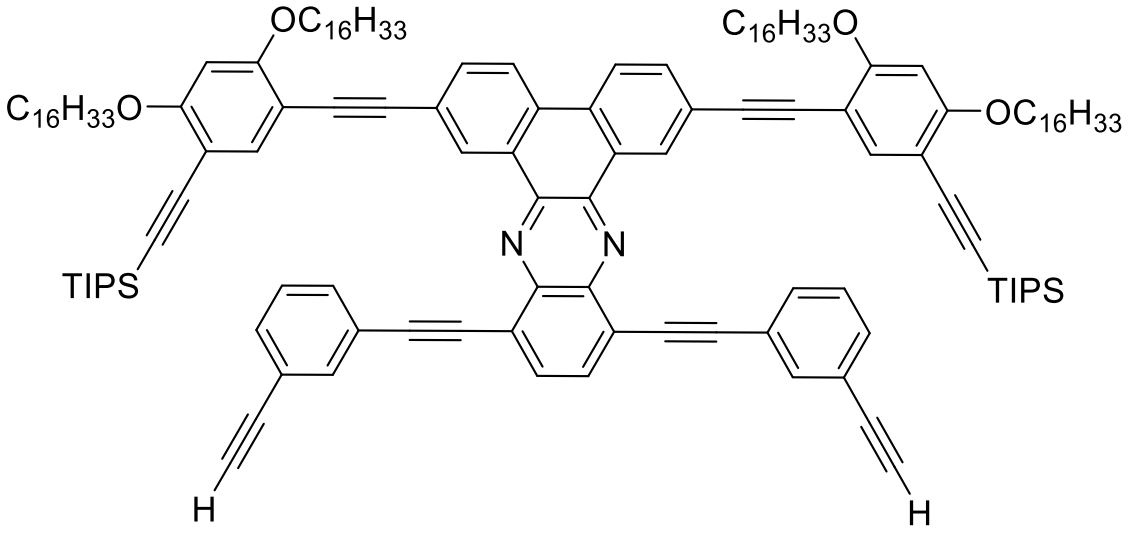

For the synthesis of compound **II**, a modified reaction procedure by *A. Idelson et al.* was applied.[143]

Compound **38** (54.0 mg, 23.0 µmol, 1.0 eq.) was dissolved in dry THF (10 ml) and MeOH (5 ml) under argon atmosphere. Then, anhydrous K_2CO_3 (32.0 mg, 0.21 mmol, 10.0 eq.) was added and the reaction solution was stirred at room temperature for 24 h. Afterwards, the reaction mixture was diluted with H_2O and DCM. The phases were separated, and the aqueous phase was extracted with DCM (3 x 20 ml). The combined organic phases were washed once with water and brine, dried over $MgSO_4$ and the solvent was removed under reduced pressure. The crude product was purified via column chromatography (CH:DCM = 1:1, R_f = 0.80) yielding **II** (47.0 mg, 23.0 µmol, >99%) as an orange solid.

Analytics:

Sum formula:	$C_{142}H_{196}N_2O_4Si_2$
Molar mass:	2051.31 g/mol

^{1}H-NMR (700 MHz, $CDCl_3$, 298 K):

δ [ppm] = 9.68 (d, *J* = 1.9 Hz, 2H), 8.50 (d, *J* = 8.6 Hz, 2H), 8.04 (s, 2H), 7.92 (dt, *J* = 7.8 Hz, 1.5 Hz, 4H), 7.87 (t, *J* = 1.7 Hz, 2H), 7.64 (s, 2H), 7.44 (dt, *J* = 7.7 Hz, 1.4 Hz, 2H), 7.24 (t, *J* = 7.7 Hz, 2H), 6.40 (s, 2H), 4.05 (t, *J* = 6.3 Hz, 4H), 3.95 (t, *J* = 6.4 Hz, 4H), 3.00 (s, 2H), 1.89-1.82 (m, 4H), 1.77-1.71 (m, 4H), 1.57-1.51 (m, 8H), 1.48-1.42 (m, 6H), 1.32-1.22 (m, 96H), 1.16 (s, 36H), 0.88 (t, *J* = 7.0 Hz, 6H), 0.84 (t, *J* = 7.2 Hz, 6H).

^{13}C-NMR (176 MHz, $CDCl_3$, 298 K):

δ [ppm] = 162.3, 161.7, 142.3, 137.9, 135.3, 133.5, 132.8, 132.4, 131.4, 130.3, 130.0, 129.0, 124.2, 124.0, 123.9, 123.3, 122.8, 105.7, 105.0, 102.5, 97.5, 97.0, 93.5, 92.3, 87.7, 87.4, 82.9, 78.1, 69.2, 69.1, 32.1, 29.9, 29.8, 29.7, 29.5, 29.3, 27.1, 26.4, 26.3, 22.9, 18.9, 14.3, 11.6.

MS (MALDI+) *m/z* (%): 2299.6 (14) $[M+DCTB]^+$, 2173.5 (5) $[M+C_6H_{10}NSi]^+$, 2049.5 (100) $[M]^+$; calculated: 2049.47 Da.

39 (SR-150)

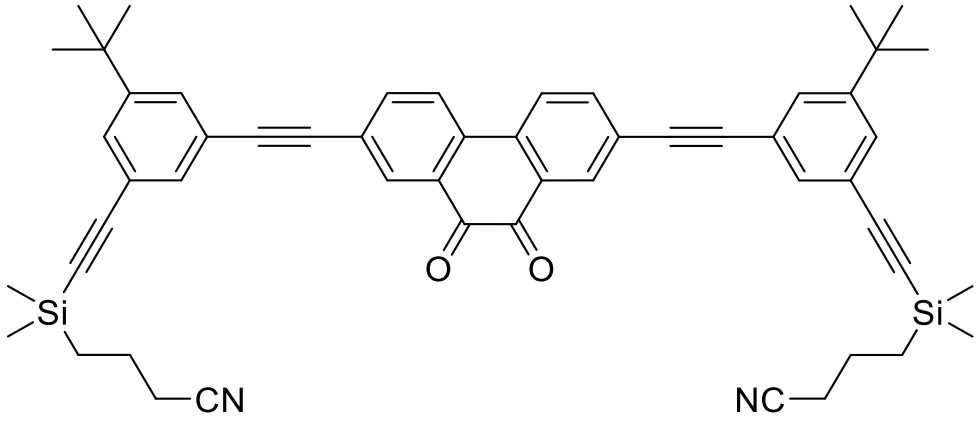

For the synthesis of compound **39**, a reaction procedure by *A. Idelson et al.* was applied.[143] Compound **3** (0.40 g, 0.69 mmol, 1.0 eq.) was dissolved in dry piperidine (20 ml) and **17** (0.47 g, 1.52 mmol, 2.2 eq.) was dissolved in dry THF (10 ml). Both solutions were purged with argon for 1 h separately. Then, $Pd(PPh_3)_2Cl_2$ (10.0 mg, 13.8 µmol, 0.04 eq.), PPh_3 (9.00 mg, 34.5 µmol, 0.10 eq.) and copper(I) iodide (4.00 mg, 20.7 µmol, 0.03 eq.) were added to the solution of **3**. Afterwards, **17** dissolved int THF was added dropwise and the reaction mixture was stirred at 40 °C for 21 h. Then, the reaction mixture was diluted with aq. HCl (10%) and DCM. The phases were separated, and the aqueous phase was extracted with DCM (3 x 20 ml). The combined organic phases were washed once with water and brine, dried over $MgSO_4$ and the solvent was removed under reduced pressure. The crude product was purified via column chromatography (DCM, R_f = 0.48) yielding **39** (0.29 g, 0.35 mmol, 51%) as a red solid.

Analytics:

Sum formula:	$C_{54}H_{54}N_2O_2Si_2$
Molar mass:	819.21 g/mol

^{1}H-NMR (500 MHz, $CDCl_3$, 298 K):

δ [ppm] = 8.33 (d, J = 1.9 Hz, 2H), 8.01 (d, J = 8.4 Hz, 2H), 7.83 (dd, J = 8.2 Hz, 1.9 Hz, 2H), 7.55 (t, J = 1.7 Hz, 2H), 7.49 (dt, J = Hz, 1.6 Hz, 4H), 4.32 (t, J = 7.0 Hz, 4H), 1.89-1.82 (m, 4H), 1.35 (s, 18H), 0.91-0.85 (m, 4H), 0.28 (s, 12H).

^{13}C-NMR (126 MHz, $CDCl_3$, 298 K):

δ [ppm] = 179.5, 152.0, 138.4, 134.8, 133.8, 132.6, 131.1, 129.8, 129.5, 125.3, 124.5, 123.0, 122.5, 119.9, 106.0, 92.7, 92.5, 87.7, 34.9, 31.2, 20.8, 20.7, 15.9, -1.7.

MS (MALDI+) *m/z* (%): 1385.6 (8) $[M+Cu+4H+2DCTB]^+$, 1318.7 (4) $[M+2DCTB]^+$, 1068.5 (27) $[M+DCTB]^+$, 841.4 (17) $[M+Na]^+$, 818.4 (100) $[M]^+$; calculated: 818.37 Da.

40 (SR-152)

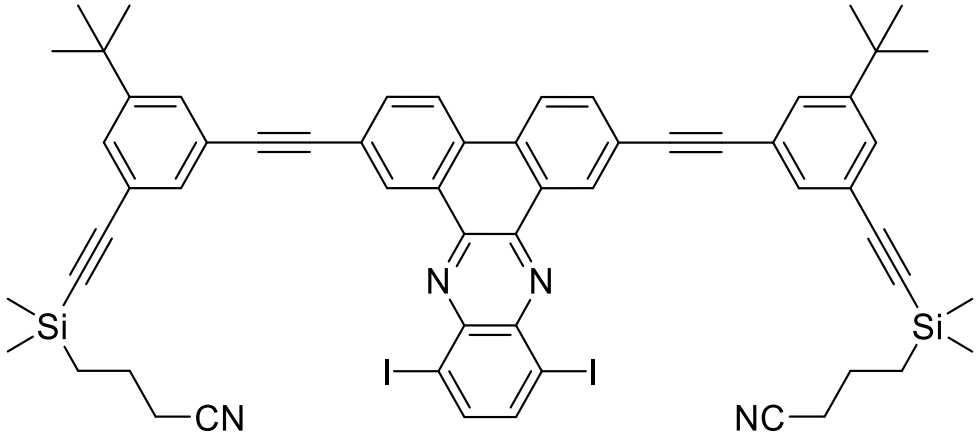

For the synthesis of compound **40**, a modified reaction procedure by *L. Schneider* was applied.[151]

Compound **39** (0.14 g, 0.17 mmol, 1.0 eq.) and 3,6-diiodobenzene-1,2-diamine **11** (0.25 g, 0.69 mmol, 4.0 eq.) were dissolved in chloroform (10 ml) and AcOH (6 ml) under argon atmosphere. Then, the reaction mixture was refluxed for 23 h. After cooling to room temperature, the reaction mixture was diluted with DCM and aq. HCl (10%). The phases were separated, and the aqueous phase was extracted with DCM (3 x 20 ml). The combined organic phases were washed once with water and brine, dried over $MgSO_4$ and the solvent was removed under reduced pressure. The crude product was purified via column chromatography (CH:DCM = 1:2, R_f = 0.29) yielding **40** (0.19 g, 0.17 mmol, >99%) as yellow-brown crystalline solid.

Analytics:

Sum formula:	$C_{60}H_{56}I_2N_4Si_2$
Molar mass:	1143.11 g/mol

^{1}H-NMR (700 MHz, $CDCl_3$, 298 K):

δ [ppm] = 9.45 (d, J = 2.0 Hz, 2H), 8.43 (d, J = 8.6 Hz, 2H), 8.14 (s, 2H), 7.89 (dd, J = 8.4 Hz, 3.1 Hz, 2H), 7.66 (dd, J = 1.7 Hz, 1.7 Hz, 2H), 7.61 (dd, J = 1.5 Hz, 1.5 Hz, 2H), 7.52 (dd, J = 1.7 Hz, 1.7 Hz, 2H), 2.47 (t, J = 7.0 Hz, 4H), 1.90-1.85 (m, 4H), 1.39 (s, 18H), 0.92-0.88 (m, 4H), 0.30 (s, 12H).

^{13}C-NMR (176 MHz, $CDCl_3$, 298 K):

δ [ppm] = 151.9, 134.3, 141.5, 141.1, 134.0, 132.6, 131.6, 130.6, 130.4, 129.6, 129.5, 123.5, 123.4, 123.2, 123.0, 119.9, 106.3, 104.2, 92.4, 91.2, 89.5, 35.0, 31.3, 20.8, 20.7, 15.9, -1.62.

MS (MALDI+) *m/z* (%): 1266.4 (6) $[M+H-I+DCTB]^+$, 1142.2 (100) $[M]^+$, 1016.3 (11) $[M+H-I]^+$; calculated: 1142.21 Da.

41 (SR-158)

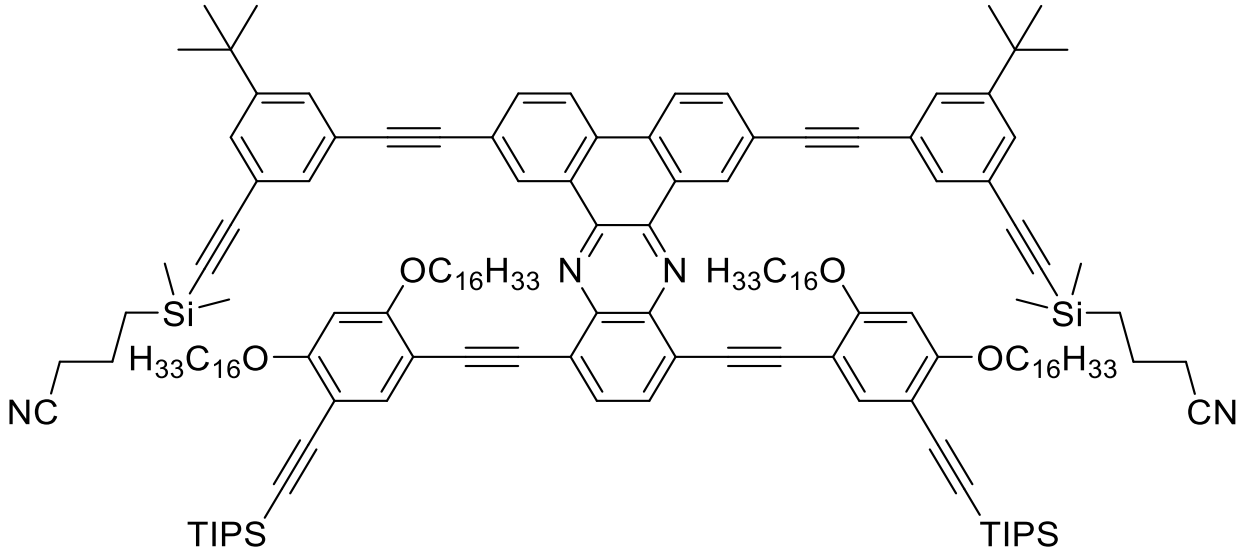

For the synthesis of compound **41**, a modified reaction procedure by *A. Idelson et al.* was applied.[143]

Compound **40** (0.19 g, 0.17 mmol, 1.0 eq.) was dissolved in dry piperidine (20 ml). Compound **30** (0.95 g, 1.24 mmol, 7.3 eq.) was dissolved in THF (10 ml) separately and both solutions were purged with argon for 1 h. Then, $Pd(OAc)_2$ (4.00 mg, 18.0 µmol, 0.1 eq.), *XPhos* (20.0 mg, 43.0 µmol, 0.25 eq.) and copper(I) iodide (5.00 mg, 26.0 µmol, 0.15 eq.) were added to the solution of **40**. Afterwards, **30** dissolved in THF was added dropwise and the reaction mixture was stirred at 40 °C for 45 h. After cooling to room temperature, the reaction mixture was diluted with aq. HCl (10%) and DCM. The phases were separated, and the aqueous phase was extracted with DCM (3 x 20 ml). The combined organic phases were washed once with water and brine, dried over $MgSO_4$ and the solvent was removed under reduced pressure. The crude product was purified via column chromatography (CH:DCM = 1:1, R_f = 0.44) yielding **41** (0.27 g, 0.11 mmol, 66%) as an orange crystalline solid.

Analytics:

Sum formula:	$C_{162}H_{234}N_4O_4Si_4$
Molar mass:	2414.02 g/mol

^{1}H-NMR (700 MHz, $CDCl_3$, 298 K):

δ [ppm] = 9.70 (d, J = 1.8 Hz, 2H), 8.54 (d, J = 8.7 Hz, 2H), 8.04 (s, 2H), 7.92 (dd, J = 8.2 Hz, 1.7 Hz, 2H), 7.73 (s, 2H), 7.52 (dt, J = 5.2 Hz, 1.6 Hz, 4H), 7.47 (t, J = 1.7 Hz, 2H), 6.29 (s, 2H), 4.23 (t, J = 6.6 Hz, 4H), 3.82 (t, J = 6.3 Hz, 4H), 2.44 (t, J = 6.9 Hz, 4H), 1.87-1.74 (m, 12H), 1.52-1.46 (m, 6H), 1.44-1.40 (m, 8H), 1.32 (s, 18H), 1.31-1.23 (m, 96H), 1.13 (d, J = 4.7 Hz, 36H), 0.88 (t, J = 7.1 Hz, 6H), 0.85 (t, J = 7.1 Hz, 6H), 0.86-0.82 (m, 4H), 0.28 (s, 12H).

^{13}C-NMR (176 MHz, $CDCl_3$, 298 K):

δ [ppm] = 162.3, 162.0, 151.9, 142.4, 141.9, 138.4, 133.4, 133.3, 132.4, 131.7, 130.8, 129.4, 129.2, 124.3, 123.4, 123.2, 123.0, 119.8, 106.2, 106.0, 105.6, 102.6, 97.8, 94.5, 93.2, 92.4, 90.9, 90.0, 70.1, 68.8, 34.9, 32.1, 31.3, 29.9, 29.8, 29.7, 29.6, 29.5, 29.4, 29.3, 27.1, 26.4, 26.0, 22.9, 20.8, 20.7, 18.9, 15.9, 14.3, 11.6, -1.7.

MS (MALDI+) *m/z* (%): 2663.9 (5) $[M+DCTB]^+$, 2411.7 (100) $[M]^+$, 2373.9 (10) $[M+2H-C_2H_2N]^+$; calculated: 2411.73 Da.

III (SR-169)

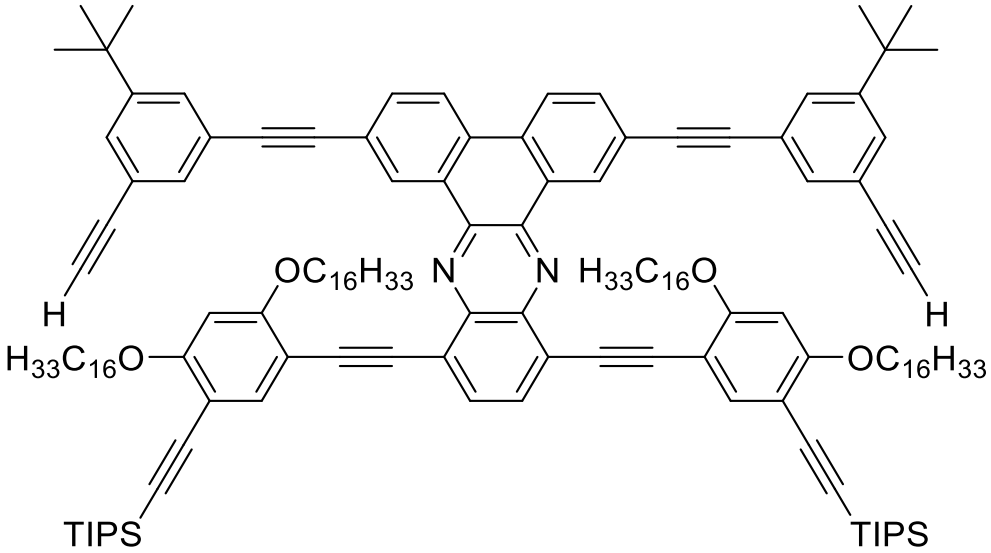

For the synthesis of compound **III**, a modified reaction procedure by *A. Idelson et al.* was applied.[143]

Compound **41** (50.0 mg, 21.0 µmol, 1.0 eq.) was dissolved in dry THF (10 ml) and MeOH (5 ml) under argon atmosphere. Then, anhydrous K_2CO_3 (29.0 mg, 0.21 mmol, 10.0 eq.) was added and the reaction solution was stirred at room temperature for 23 h. Afterwards, the reaction mixture was diluted with H_2O and DCM. The phases were separated, and the aqueous phase was extracted with DCM (3 x 20 ml). The combined organic phases were washed once with water and brine, dried over $MgSO_4$ and the solvent was removed under reduced pressure. The crude product was purified via column chromatography (CH:DCM = 1:1, R_f = 0.99) yielding **III** (47.0 mg, 21.0 µmol, >99%) as an luminous orange solid.

Analytics:

Sum formula:	$C_{150}H_{212}N_2O_4Si_2$
Molar mass:	2163.53 g/mol

^{1}H-NMR (700 MHz, $CDCl_3$, 298 K):

δ [ppm] = 9.76 (d, J = 1.8 Hz, 2H), 8.54 (d, J = 8.6 Hz, 2H), 8.04 (s, 2H), 7.94 (dd, J = 8.2 Hz, 1.9 Hz, 2H), 7.74 (s, 2H), 7.56 (t, J = 1.7 Hz, 2H), 7.50 (dt, J = 12.8 Hz, 1.6 Hz,

4H), 6.35 (s, 2H), 4.23 (t, *J* = 6.6 Hz, 4H), 3.87 (t, *J* = 6.3 Hz, 4H), 3.08 (s, 2H), 1.79 (dt, *J* = 15.8 Hz, 6.5 Hz, 8H), 1.53-1.47 (m, 6H), 1.44-1.42 (m, 8H), 1.33 (s, 18H), 1.32-1.23 (m, 96H), 1.14 (d, *J* = 4.4 Hz, 36H), 0.87 (dt, *J* = 19.3 Hz, 7.1 Hz, 12H).

^{13}C-NMR (176 MHz, $CDCl_3$, 298 K):

δ [ppm] = 162.4, 162.1, 151.9, 142.4, 141.8, 138.4, 133.3, 133.2, 132.5, 131.7, 131.0, 130.8, 129.5, 129.4, 124.3, 123.4, 123.1, 122.3, 106.0, 105.5, 102.7, 97.7, 94.5, 93.1, 90.9, 90.0, 89.9, 83.4, 77.5, 70.1, 68.7, 34.9, 32.1, 31.3, 29.9, 29.8, 29.7, 29.6, 29.5, 29.4, 29.3, 27.1, 26.4, 26.0, 22.9, 18.9, 14.3, 11.6.

MS (MALDI+) *m/z* (%): 2411.8 (3) $[M+DCTB]^+$, 2161.6 (100) $[M]^+$; calculated: 2161.60 Da.

D_1/T_1 (SR-53)

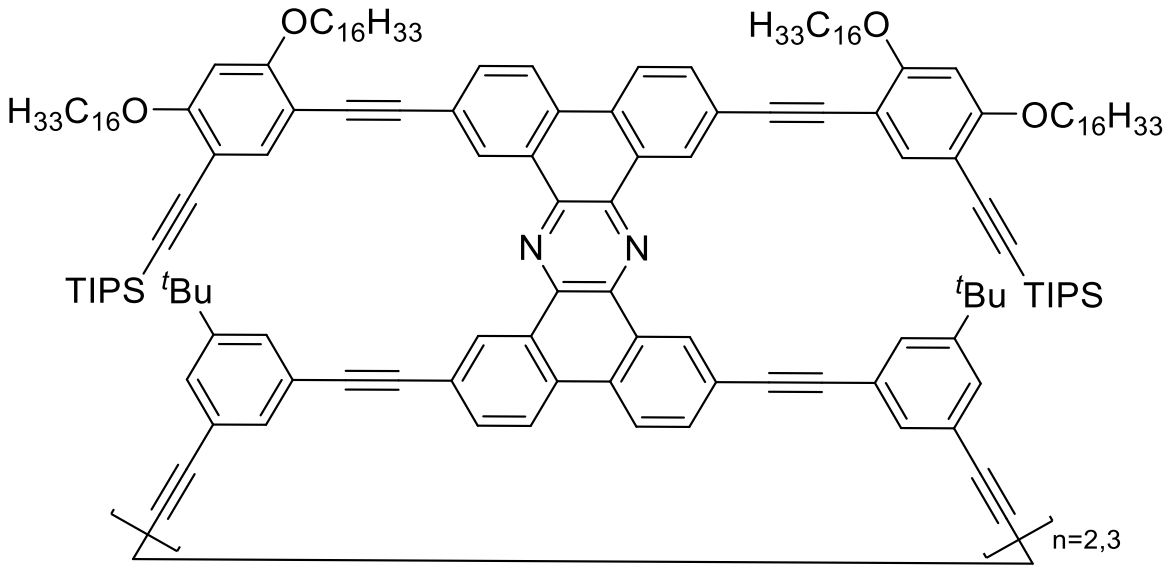

For the synthesis of compound **D_1/T_1**, a modified reaction procedure by *G.Poluektov et al.* was applied.[74,75]

Route a):

Compound **I** (44.0 mg, 19.0 µmol, 1.0 eq.) was dissolved in THF (30 ml) and a solution of DIPA (50 ml) and THF (50 ml) was made. Both solutions were purged with argon for 1 h. Then, $PdCl_2(PPh_3)_2$ (13.0 mg, 19.0 µmol, 1.0 eq.), CuI (7.00 mg, 38.0 µmol, 2.0 eq.) and I_2 (26.0 mg, 102 µmol, 5.4 eq.) were added to the DIPA/THF solution. Subsequently, the solution of **I** in THF was added over a period of 48 h via an automated injection-system to the DIPA/THF solution while stirring vigorously at 50 °C. The resulting reaction solution was further stirred at 50 °C for 68 h. After cooling to room temperature, the reaction mixture was diluted with aq. HCl (10%) and DCM. The phases were separated, and the aqueous phase was extracted with DCM (3 x 20 ml). The combined organic phases were washed once with water and brine, dried over $MgSO_4$ and the solvent was removed under reduced pressure. The crude product was purified via column chromatography (DCM, R_f = 0.97). The formed oligomers were then separated via recGPC yielding dimer **D_1** (9.00 mg, 1.98 µmol, 21%) and trimer **T_1** (5.00 mg, 0.74 µmol, 12%), as well as the substrate **I** (23.0 mg, 10.0 µmol, 53%) as luminous yellow solids.

Route b):

Compound **I** (23.0 mg, 19.0 µmol, 1.0 eq.) was dissolved in THF (30 ml) and a solution of DIPA (45 ml) and THF (45 ml) was made. Both solutions were purged with argon for 1 h. Then, $PdCl_2(PPh_3)_2$ (14.0 mg, 20.0 µmol, 2.0 eq.), CuI (8.00 mg, 40.0 µmol, 4.0 eq.) and I_2 (36.0 mg, 120 µmol, 12.0 eq.) were added to the DIPA/THF solution. Subsequently, the solution of **I** in THF was added over a period of 24 h via an automated injection-system to the DIPA/THF solution while stirring vigorously at 50 °C. The resulting reaction solution was further stirred at 50 °C for 68 h. After cooling to room temperature, the reaction mixture was diluted with aq. HCl (10%) and DCM. The phases were separated, and the aqueous phase was extracted with DCM (3 x 20 ml). The combined organic phases were washed once with water and brine, dried over $MgSO_4$ and the solvent was removed under reduced pressure. The crude product was purified via column chromatography (DCM, R_f = 0.97). The formed oligomers were then separated via recGPC yielding dimer **D_1** (7.00 mg, 1.55 µmol, 31%) and trimer **T_1** (2.00 mg, 0.29 µmol, 9%) as luminous yellow solids.

Analytics Cyclic Dimer (n=2):

Sum formula:	$C_{316}H_{428}N_4O_8Si_4$
Molar mass:	4523.26 g/mol

^{1}H-NMR (700 MHz, $CDCl_3$, 298 K):

δ [ppm] = 9.74 (s, 4H), 9.70 (s, 4H), 8.53 (s, 4H), 8.52 (s, 4H), 7.95 (dd, *J* = 7.9 Hz, 1.8 Hz, 4H), 7.93 (d, *J* = 7.4 Hz, 4H), 7.81 (s, 4H), 7.68 (s, 4H), 7.61 (s, 4H), 7.42 (s, 4H), 6.34 (s, 4H), 4.03 (dt, *J* = 32.8 Hz, 6.3 Hz, 16H), 2.00-1.89 (m, 8H), 1.88-1.80 (m, 8H), 1.62-1.57 (m, 8H), 1.57-1.50 (m, 20H), 1.35 (s, 36H), 1.33-1.24 (m, 192H), 1.15 (d, *J* = 4.0 Hz, 72H), 0.89 (t, *J* = 7.1 Hz, 12H), 0.80 (t, *J* = 7.3 Hz, 12H).

^{13}C-NMR (176 MHz, $CDCl_3$, 298 K):

δ [ppm] = 162.2, 161.7, 152.0, 140.7, 140.4, 138.0, 137.1, 133.8, 133.0, 131.2, 130.9, 130.8, 130.5, 129.1, 128.4, 127.4, 123.9, 123.8, 123.5, 123.3, 123.1, 122.2, 105.8, 105.0, 102.6, 97.1, 93.2, 92.7, 91.0, 87.6, 83.1, 75.1, 69.4, 68.9, 35.0, 32.1, 31.4, 29.9, 29.8, 29.7, 29.6, 29.5, 26.5, 22.9, 22.8, 18.9, 14.3, 11.6.

MS (MALDI+) *m/z* (%): 4519.2 (100) $[M]^+$; calculated: 4519.23 Da.

Analytics Cyclic Trimer (n=3):

Sum formula:	$C_{474}H_{642}N_6O_{12}Si_6$
Molar mass:	6784.89 g/mol

^{1}H-NMR (700 MHz, $CDCl_3$, 298 K):

δ [ppm] = 9.78 (s, 6H), 9.76 (s, 6H), 8.66 (d, *J* = 6.2 Hz, 6H), 8.61 (d, *J* = 9.0 Hz, 6H), 8.01 (d, *J* = 8.1 Hz, 6H), 7.96 (d, *J* = 7.6 Hz, 6H), 7.71 (s, 6H), 7.70-7.65 (m, 12H), 7.58-7.54 (m, 6H), 6.38 (s, 6H), 4.04 (dt, *J* = 36.7 Hz, 6.1 Hz, 24H), 1.97-1.87 (m, 12H), 1.87-1.77 (m, 12H), 1.71-1.56 (m, 12H), 1.56-1.45 (m, 30H), 1.35 (s, 54H), 1.29-1.19 (m, 288H), 1.13 (d, *J* = 3.3 Hz, 108H), 0.90-0.86 (m, 18H), 0.86-0.80 (m, 18H).

^{13}C-NMR (176 MHz, $CDCl_3$, 298 K):

δ [ppm] = 162.2, 161.6, 152.1, 140.4, 138.3, 135.8, 130.4, 125.7, 123.6, 108.5, 105.0, 97.2, 93.3, 69.4, 68.9, 34.9, 32.1, 31.2, 30.5, 29.9, 29.8, 29.7, 29.6, 29.5, 26.5, 22.8, 18.9, 14.3, 11.6.

MS (MALDI+) *m/z* (%): 6778.8 (100) $[M+H]^+$; calculated: 6778.84 Da.

D_{1d}/T_{1d} (SR-56)

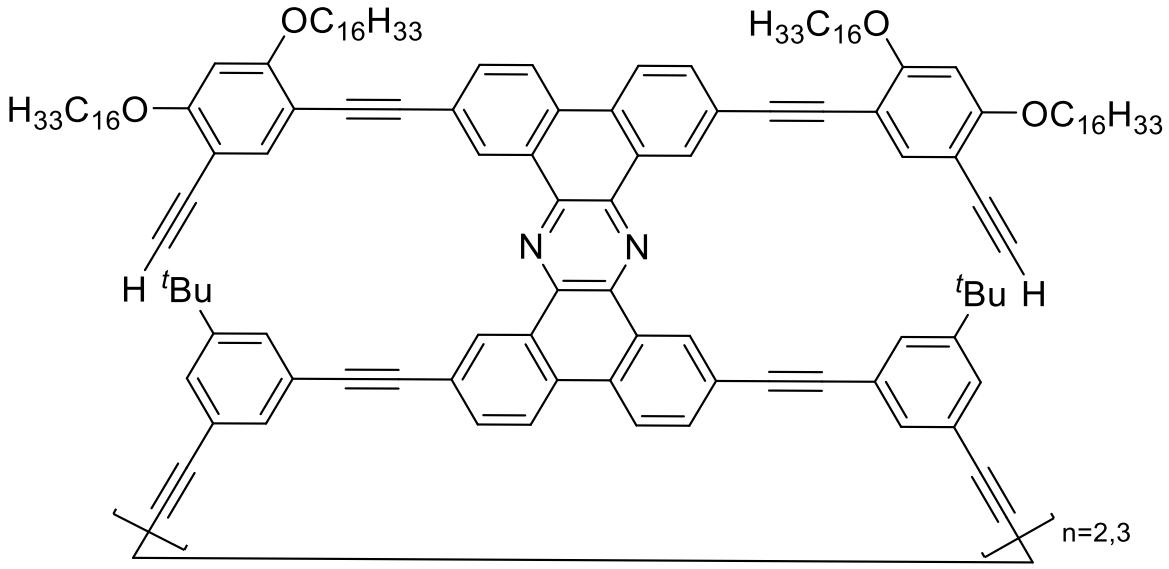

For the synthesis of compound **D_{1d}**, a modified reaction procedure by *K. Remmersen* was applied.[147,152]

Compound **D_1** (13.0 mg, 2.87 µmol, 1.0 eq.) was dissolved in THF (7 ml) and 1 ml of a TBAF-solution (1 M in THF) was added. The resulting reaction solution was stirred at 35 °C for 3 h. After cooling to room temperature, the reaction was terminated by addition of H_2O. The phases were separated, and the aqueous phase was extracted with DCM (3 x 20 ml). The combined organic phases were washed once with water and brine, dried over $MgSO_4$ and the solvent was removed under reduced pressure. The crude product was purified via column chromatography (DCM, R_f = 0.99), yielding the deprotected dimer **D_{1d}** (11.0 mg, 2.85 µmol, 99%) as luminous yellow solid. Due to the reactive nature of the free acetylenes, no further purification via recGPC was performed and the product was used with impurities for the next

reaction with the aim to separate those via recGPC after closing the second ring using a *Glaser* coupling.

For the synthesis of compound **T_{1d}**, a modified reaction procedure by *K. Remmersen* was applied.[147,152]

Compound **T_1** (79.0 mg, 11.6 µmol, 1.0 eq.) was dissolved in THF (10 ml) and 1 ml of a TBAF-solution (1 M in THF) was added. The resulting reaction solution was stirred at 35 °C for 3 h. After cooling to room temperature, the reaction was terminated by addition of H_2O. The phases were separated, and the aqueous phase was extracted with DCM (3 x 20 ml). The combined organic phases were washed once with water and brine, dried over $MgSO_4$ and the solvent was removed under reduced pressure. The crude product was purified via column chromatography (DCM, R_f = 0.99), yielding the deprotected trimer **T_{1d}** (49.0 mg, 8.4 µmol, 72%) as luminous yellow solid. Due to the reactive nature of the free acetylenes, no further purification via recGPC was performed, likewise to the cyclic dimer, and the product was used with impurities for the next reaction with the aim to separate those via recGPC after closing the second ring using a *Glaser* coupling.

Even though the products could not be purified completely, the ^{1}H- and ^{13}C-NMR spectra clearly showed that the TIPS-protecting group was cleaved entirely. Moreover, in the MALDI(+) mass spectra the respective mass of dimer and trimer were observed as main peaks.

Analytics Deprotected Cyclic Dimer (n=2):

Sum formula:	$C_{280}H_{348}N_4O_8$
Molar mass:	3897.88 g/mol

MS (MALDI+) *m/z* (%): 3894.7 (100) $[M]^+$; calculated: 3894.69 Da.

Analytics Deprotected Cyclic Trimer (n=3):

Sum formula:	$C_{420}H_{522}N_6O_{12}$
Molar mass:	5846.83 g/mol

MS (MALDI+) *m/z* (%): 6592.5 (10) [M+3DCTB]$^+$, 6342.3 (28) [M+2DCTB]$^+$, 6092.2 (76) [M+DCTB]$^+$, 5842.0 (100) [M]$^+$; calculated: 5842.04 Da.

D_{1c}/T_{1c} (SR-57)

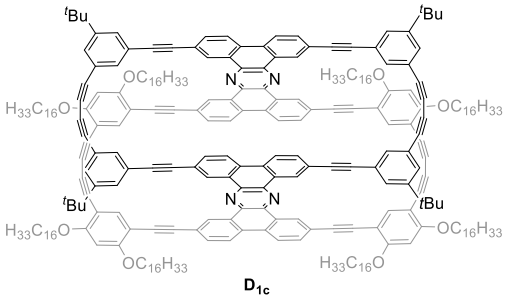

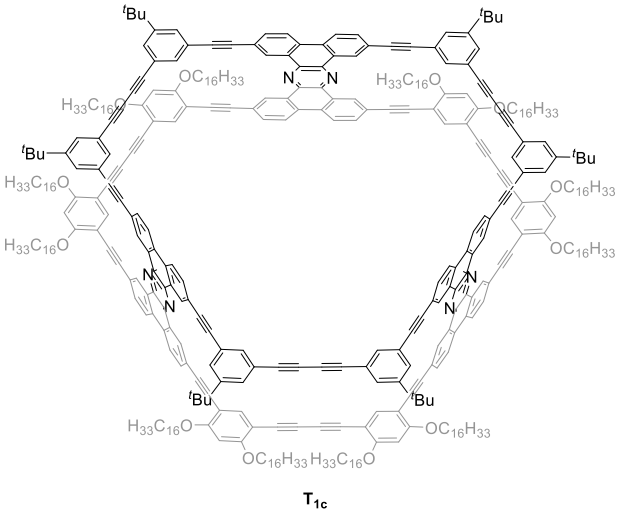

For the synthesis of compound **D_{1c}**, a modified reaction procedure by *G.Poluektov et al.* was applied.[74,75]

Compound **D_{1d}** (11.00 mg, 2.85 µmol, 1.0 eq.) was dissolved in THF (35 ml) and a solution of DIPA (50 ml) and THF (50 ml) was made. Both solutions were purged with argon for 1 h. Then, $PdCl_2(PPh_3)_2$ (8.00 mg, 11.4 µmol, 4.00 eq.), CuI (4.00 mg, 22.8 µmol, 8.00 eq.) and I_2 (12.0 mg, 45.6 µmol, 24.0 eq.) were added to the DIPA/THF solution. Subsequently, the solution of **D_{1d}** in THF was added over a period of 48 h via an automated injection-system to the DIPA/THF solution while stirring vigorously at 50 °C. The resulting reaction solution was further stirred at 50 °C for 20 h. After cooling to room temperature, the reaction mixture was diluted with aq. HCl (10%) and DCM. The phases were separated, and the aqueous phase was extracted with DCM (3 x 20 ml). The combined organic phases were washed once with water and brine, dried over $MgSO_4$ and the solvent was removed under reduced pressure. The crude product was purified via column chromatography (DCM, R_f = 0.98). The product was then further purified via recGPC yielding cylindrical dimer **D_{1c}** (4.50 mg, 1.16 µmol, 41% over 2 steps) as luminous yellow solid.

For the synthesis of compound **T_{1c}**, a modified reaction procedure by *G.Poluektov et al.* was applied.[74,75]

Compound **T_{1d}** (49.0 mg, 8.40 µmol, 1.0 eq.) was dissolved in THF (30 ml) and a solution of DIPA (50 ml) and THF (50 ml) was made. Both solutions were purged with argon for 1 h. Then, $PdCl_2(PPh_3)_2$ (12.0 mg, 16.8 µmol, 2.0 eq.), CuI (6.00 mg, 34.0 µmol, 4.0 eq.) and I_2 (25.0 mg, 98.0 µmol, 12.0 eq.) were added to the DIPA/THF solution. Subsequently, the solution of **T_{1d}** in THF was added over a period of 48 h via an automated injection-system to the DIPA/THF solution while stirring vigorously at 50 °C. The resulting reaction solution was further stirred at 50 °C for 24 h. After cooling to room temperature, the reaction mixture was diluted with aq. HCl (10%) and DCM. The phases were separated, and the aqueous phase was extracted with DCM (3 x 20 ml). The combined organic phases were washed once with water and brine, dried over $MgSO_4$ and the solvent was removed under reduced pressure. The crude product was purified via column chromatography (DCM, R_f = 0.97). The product was then further purified via recGPC yielding cylindrical trimer **T_{1c}** (8.6 mg, 1.47 µmol, 13% over 2 steps) as luminous yellow solid.

For both compounds the ^{1}H-NMR spectra showed a broadening in the aromatic region, making meaningful integration impossible. Hence, also in the ^{13}C-NMR spectra the aromatic signals could not be clearly distinguished from the baseline. This phenomenon could not be resolved by low or high temperature NMR, as well as change of solvent and increasing the concentrations of the respective product.

However, the absence of any terminal-acetylene signal at 3.1 ppm in the ^{1}H-NMR spectra indicates the complete closure of the butadiynes, also shown by the absence of $[M+2H]^+$-signals in the high-resolution MALDI-TOF mass spectra. Moreover, the DOSY-NMR of **D_{1c}**, also shows only one distinct species being present in the solution.

The unobtainability of meaningful NMR spectra was also observed for the other PNTs synthesized in this work.

Analytics Closed Cyclic Dimer:

Sum formula:	$C_{280}H_{344}N_4O_8$
Molar mass:	3893.85 g/mol

MS (MALDI+) *m/z* (%): 3890.7 (100) $[M]^+$; calculated: 3890.66 Da.

Analytics Closed Cyclic Trimer:

Sum formula:	$C_{420}H_{516}N_6O_{12}$
Molar mass:	5840.78 g/mol

MS (MALDI+; Ag^+-salts) *m/z* (%): 6193.1 (25) $[M+Ag+DCTB]^+$, 5977.9 (30) $[M+Ag+Cl]^+$, 5942.9 (100) $[M+Ag]^+$; calculated: 5836.00 Da.

D_2/T_2 (SR-142/-163)

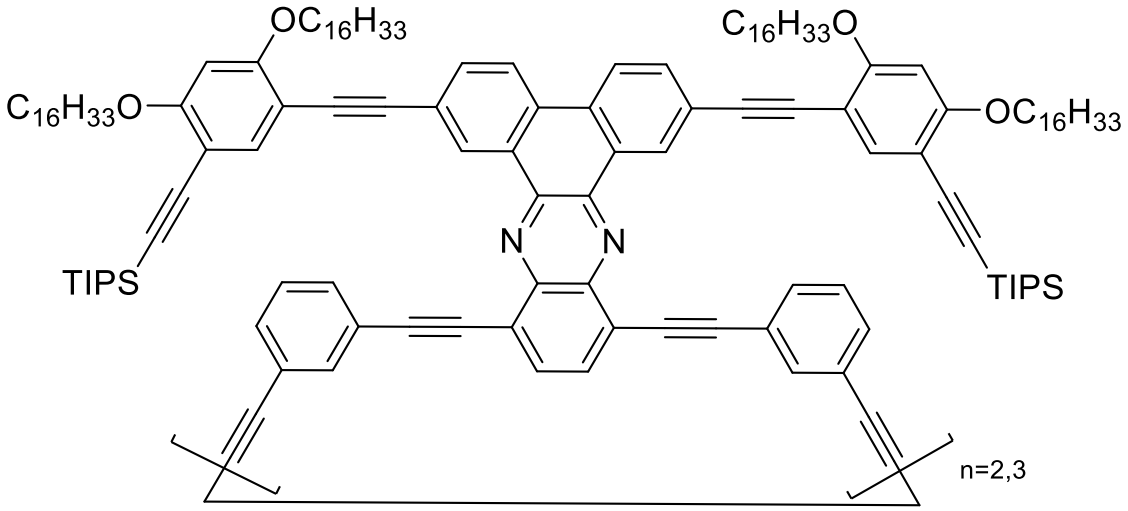

For the synthesis of compound **D_2/T_2**, a modified reaction procedure by *G.Poluektov et al.* was applied.[74,75]

The following procedure was performed in seven batches using a total amount of 350 mg of **II**. Compound **II** (50.0 mg, 24.0 µmol, 1.0 eq.) was dissolved in THF (35 ml) and a solution of DIPA (50 ml) and THF (50 ml) was made. Both solutions were purged with argon for 1 h. Then, $PdCl_2(PPh_3)_2$ (17.0 mg, 24.0 µmol, 1.0 eq.), CuI (9.00 mg, 49.0 µmol, 2.0 eq.) and I_2 (37.0 mg, 146 µmol, 6.0 eq.) were added to the DIPA/THF solution. Subsequently, the solution of **II** in THF was added over a period of 24 h via an automated injection-system to the DIPA/THF solution while stirring vigorously at 50 °C. The resulting reaction solution was further stirred at 50 °C for 24 h. After cooling to room temperature, the reaction mixture was diluted with aq. HCl (10%) and DCM. The phases were separated, and the aqueous phase was

extracted with DCM (3 x 20 ml). The combined organic phases were washed once with water and brine, dried over $MgSO_4$ and the solvent was removed under reduced pressure. The crude product of all batches was then purified together via column chromatography (DCM, R_f = 0.98). The formed oligomers were then separated via recGPC yielding dimer **D2** (76.0 mg, 18.5 µmol, 22%) and trimer **T2** (44.0 mg, 7.20 µmol, 13%) as luminous orange crystalline solids.

Analytics Cyclic Dimer (n=2):

Sum formula:	$C_{284}H_{388}N_4O_8Si_4$
Molar mass:	4098.59 g/mol

^{1}H-NMR (700 MHz, $CDCl_3$, 298 K):

δ [ppm] = 9.27 (s, 4H), 8.04 (s, 4H), 8.01-7.94 (m, 4H), 7.93-7.83 (m, 4H), 7.75-7.68 (m, 8H), 7.51 (s, 4H), 7.25-7.18 (m, 8H), 6.20 (s, 4H), 4.10-3.93 (m, 16H), 1.90-1.81 (m, 8H), 1.81-1.75 (m, 8H), 1.61-1.44 (m, 28H), 1.42-1.23 (m, 192H), 1.22 (d, J = 4.2 Hz, 72H), 0.90 (t, J = 7.1 Hz, 12H), 0.82 (t, J = 7.2 Hz, 12H).

^{13}C-NMR (176 MHz, $CDCl_3$, 298 K):

δ [ppm] = 161.9, 161.6, 141.6, 141.0, 140.1, 137.2, 133.9, 133.6, 131.2, 130.6, 129.7, 128.8, 124.4, 124.2, 124.0, 122.5, 108.1, 105.3, 104.7, 103.4, 97.4, 96.5, 92.7, 89.1, 87.6, 83.0, 75.8, 69.1, 68.6, 68.1, 67.9, 32.1, 29.9, 29.8, 29.7, 29.6, 29.5, 26.5, 26.4, 22.9, 22.8, 19.0, 14.3, 11.7.

MS (MALDI+; Ag^+-salts) *m/z* (%): 4452.2 (6) $[M+Ag+DCTB]^+$, 4326.1 (31) $[M+Ag-C_{10}H_6+DCTB]^+$, 4302.1 (29) $[M+Ag-C_{12}H_6+DCTB]^+$, 4202.0 (100) $[M+Ag]^+$; calculated: 4094.92 Da.

Analytics Cyclic Trimer (n=3):

Sum formula:	$C_{426}H_{582}N_6O_{12}Si_6$
Molar mass:	6147.88 g/mol

^{1}H-NMR (700 MHz, $CDCl_3$, 298 K):

δ [ppm] = 9.16 (s, 6H), 8.00 (d, J = 10.2 Hz, 6H), 7.89 (d, J = 6.3 Hz, 6H), 7.85 (s, 6H), 7.81 (s, 6H), 7.74 (d, J = 7.1 Hz, 6H), 7.49 (s, 6H), 7.36 (t, J = 6.5 Hz, 6H), 7.31 (t, J = 8.9 Hz, 6H), 6.24 (s, 6H), 4.14-3.85 (m, 24H), 1.93-1.79 (m, 24H), 1.63-1.49 (m, 42H), 1.42-1.21 (m, 288H), 1.16 (d, J = 16.6 Hz, 108H), 0.90 (t, J = 7.0 Hz, 18H), 0.83 (t, J = 7.2 Hz, 18H).

^{13}C-NMR (176 MHz, $CDCl_3$, 298 K):

δ [ppm] = 161.8, 161.6, 141.5, 141.3, 136.8, 135.9, 133.5, 132.3, 131.5, 130.3, 129.7, 129.2, 128.9, 124.4, 124.2, 123.7, 122.4, 105.3, 104.5, 103.6, 98.0, 96.5, 93.1, 92.6, 88.2, 87.6, 81.2, 75.3, 69.2, 69.1, 68.6, 32.1, 30.0, 29.9, 29.8, 29.6, 29.5, 26.5, 26.4, 22.9, 22.8, 19.2, 18.9, 14.3, 11.8.

MS (MALDI+; Ag^+-salts) *m/z* (%): 6505.5 (14) $[M+Ag+DCTB]^+$, 6249.3 (100) $[M+Ag]^+$; calculated: 6142.37 Da.

D_{2d}/T_{2d} (SR-164/-166)

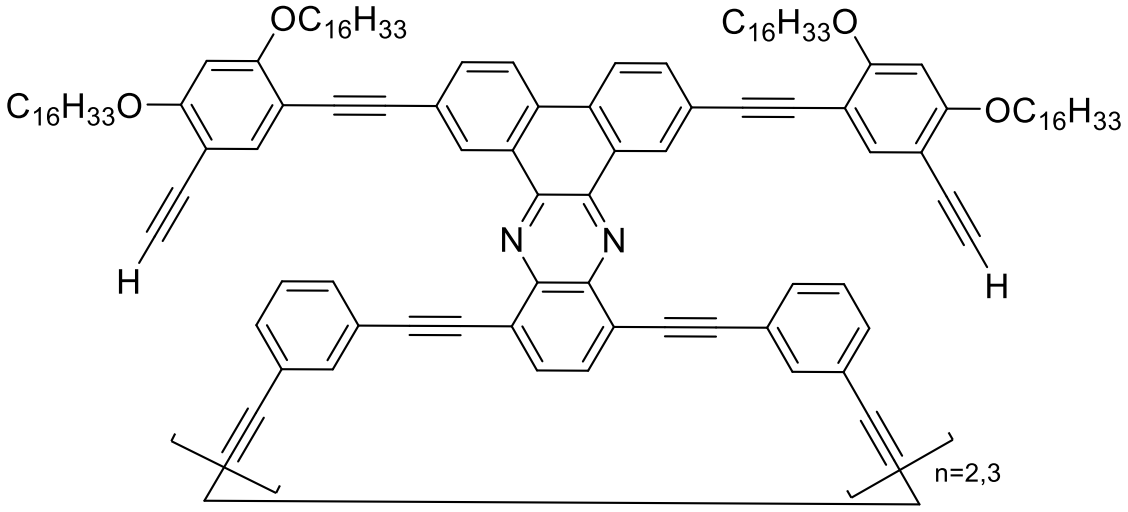

For the synthesis of compound **D_{2d}**, a modified reaction procedure by *K. Remmersen* was applied.[147,152]

Compound **D_2** (85.0 mg, 20.7 µmol, 1.0 eq.) was dissolved in THF (11 ml) and 2 ml of a TBAF-solution (1 M in THF) was added. The resulting reaction solution was stirred at 35 °C

for 3 h. After cooling to room temperature, the reaction was terminated by addition of H_2O. The phases were separated, and the aqueous phase was extracted with DCM (3 x 20 ml). The combined organic phases were washed once with water and brine, dried over $MgSO_4$ and the solvent was removed under reduced pressure. The crude product was purified via column chromatography (DCM, R_f = 0.99), yielding the deprotected dimer **D$_{2d}$** (28.0 mg, 8.10 µmol, 39%) as orange-brown solid. Due to the reactive nature of the free acetylenes, no further purification via recGPC was performed and the product was used with impurities for the next reaction with the aim to separate those via recGPC after closing the second ring using a *Glaser* coupling.

For the synthesis of compound **T$_{2d}$**, a modified reaction procedure by *K. Remmersen* was applied.[147,152]

Compound **T$_2$** (44.0 mg, 7.2 µmol, 1.0 eq.), was dissolved in THF (10 ml) and 1 ml of a TBAF-solution (1 M in THF) was added. The resulting reaction solution was stirred at 35 °C for 3 h. After cooling to room temperature, the reaction was terminated by addition of H_2O. The phases were separated, and the aqueous phase was extracted with DCM (3 x 20 ml). The combined organic phases were washed once with water and brine, dried over $MgSO_4$ and the solvent was removed under reduced pressure. The crude product was purified via column chromatography (DCM, R_f = 0.99), yielding the deprotected trimer **T$_{2d}$** (31.0 mg, 6.0 µmol, 83%) as orange solid. Due to the reactive nature of the free acetylenes, no further purification via recGPC was performed, likewise to the cyclic dimer, and the product was used with impurities for the next reaction with the aim to separate those via recGPC after closing the second ring using a *Glaser* coupling.

Even though the products could not be purified completely, the ^{1}H- and ^{13}C-NMR spectra clearly showed that the TIPS-protecting group was cleaved entirely. Moreover, in the MALDI(+) mass spectra the respective mass of dimer and trimer were observed as main peaks.

Analytics Deprotected Cyclic Dimer (n=2):

Sum formula:	$C_{248}H_{308}N_4O_8$
Molar mass:	3473.21 g/mol

MS (MALDI+) *m/z* (%): 3470.4 (100) $[M]^+$; calculated: 3470.38 Da.

Analytics Deprotected Cyclic Trimer (n=3):

Sum formula:	$C_{372}H_{462}N_6O_{12}$
Molar mass:	5209.82 g/mol

MS (MALDI+) *m/z* (%): 5205.6 (100) $[M]^+$; calculated: 5205.57 Da.

D_{2c}/T_{2c} (SR-165/-167)

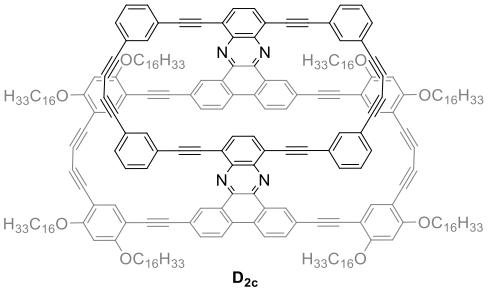

D_{2c}

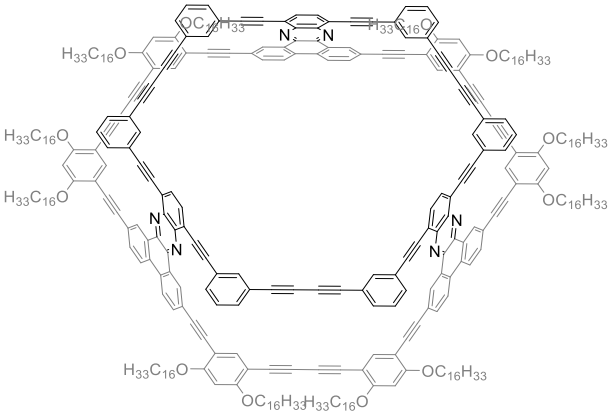

T_{2c}

For the synthesis of compound **D_{2c}**, a modified reaction procedure by *G.Poluektov et al.* was applied.[74,75]

Compound **D_{2d}** (28.0 mg, 8.1 µmol, 1.0 eq.) was dissolved in THF (30 ml) and a solution of DIPA (50 ml) and THF (50 ml) was made. Both solutions were purged with argon for 1 h. Then, $PdCl_2(PPh_3)_2$ (11.0 mg, 16.2 µmol, 2.0 eq.), CuI (6.00 mg, 32.0 µmol, 4.0 eq.) and I_2 (25.0 mg, 97.0 µmol, 12.0 eq.) were added to the DIPA/THF solution. Subsequently, the solution of **D_{2d}** in THF was added over a period of 48 h via an automated injection-system to the DIPA/THF solution while stirring vigorously at 50 °C. The resulting reaction solution was further stirred at 50 °C for 25 h. After cooling to room temperature, the reaction mixture was diluted with aq. HCl (10%) and DCM. The phases were separated, and the aqueous phase was extracted with DCM (3 x 20 ml). The combined organic phases were washed once with water and brine, dried over $MgSO_4$ and the solvent was removed under reduced pressure. The crude

product was purified via column chromatography (DCM, R_f = 0.99). The product was then further purified via recGPC yielding pyramidal dimer **D$_{2c}$** (1.10 mg, 0.32 µmol, 2% over 2 steps) as luminous orange solid.

For the synthesis of compound **T$_{2c}$**, a modified reaction procedure by *G.Poluektov et al.* was applied.[74,75]

Compound **T$_{2d}$** (31.0 mg, 6.00 µmol, 1.0 eq.) was dissolved in THF (30 ml) and a solution of DIPA (50 ml) and THF (50 ml) was made. Both solutions were purged with argon for 1 h. Then, $PdCl_2(PPh_3)_2$ (8.00 mg, 12.0 µmol, 2.0 eq.), CuI (5.00 mg, 24.0 µmol, 4.0 eq.) and I_2 (18.0 mg, 72.0 µmol, 12.0 eq.) were added to the DIPA/THF solution. Subsequently, the solution of **T$_{2d}$** in THF was added over a period of 48 h via an automated injection-system to the DIPA/THF solution while stirring vigorously at 50 °C. The resulting reaction solution was further stirred at 50 °C for 24 h. After cooling to room temperature, the reaction mixture was diluted with aq. HCl (10%) and DCM. The phases were separated, and the aqueous phase was extracted with DCM (3 x 20 ml). The combined organic phases were washed once with water and brine, dried over $MgSO_4$ and the solvent was removed under reduced pressure. The crude product was purified via column chromatography (DCM, R_f = 0.99). The product was then further purified via recGPC yielding pyramidal trimer **T$_{2c}$** (1.0 mg, 0.19 µmol, 3% over 2 steps) as luminous orange solid.

The unobtainability of meaningful NMR spectra here was also observed for the other PNTs synthesized in this work (see synthesis of **D$_{1c}$**/**T$_{1c}$**).

Moreover, for **T$_{2c}$** the largest observable peaks in the MALDI(+) mass spectra were that of a $[2M+H]^+$ peak and its matrix adducts. However, a small $[M]^+$ peak of **T$_{2c}$** was visible as well, hinting at the formation of aggregates (cp. Figure 127, Figure 128).

Analytics Closed Cyclic Dimer:

Sum formula:	$C_{248}H_{304}N_4O_8$
Molar mass:	3469.18 g/mol

MS (MALDI+) *m/z* (%): 3567.4 (23) $[M+K+Cu]^+$, 3466.4 (100) $[M]^+$; calculated: 3466.35 Da.

Analytics Closed Cyclic Trimer:

Sum formula:	$C_{372}H_{456}N_6O_{12}$
Molar mass:	5203.77 g/mol

MS (MALDI+) *m/z* (%): 11150.1 (25) $[2M+H+3DCTB]^+$, 10900.1 (55) $[2M+H+2DCTB]^+$, 10650.1 (100) $[2M+H+DCTB]^+$, 10400.1 (85) $[2M+H]^+$, 5200.1 (38) $[M]^+$; calculated: 5199.53 Da.

D_3/T_3 (SR-171)

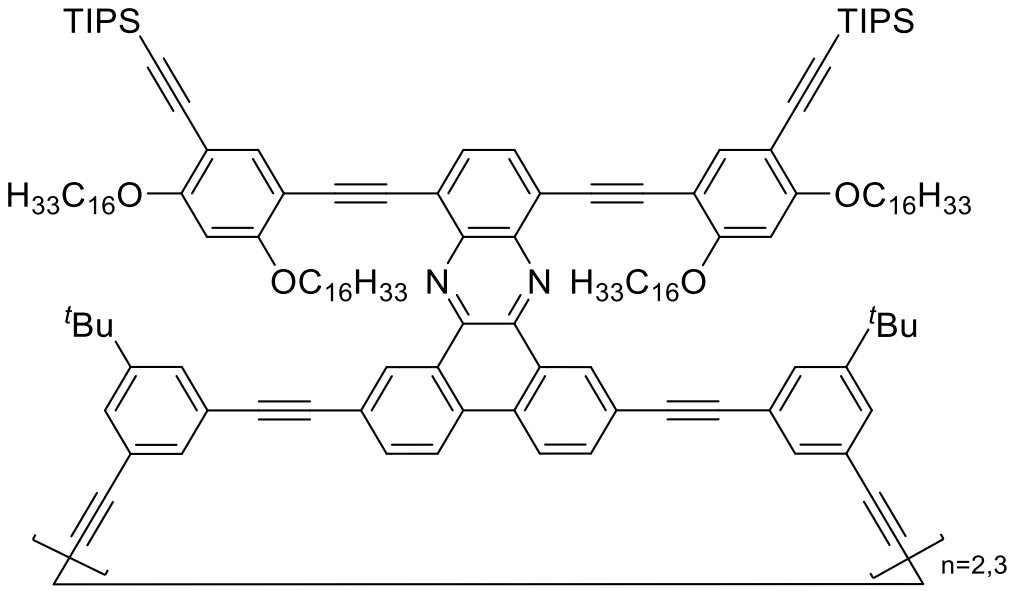

For the synthesis of compound **D_3/T_3**, a modified reaction procedure by *G.Poluektov et al.* was applied.[74,75]

The following procedure was performed in three batches using a total amount of 150 mg of **III**. Compound **III** (46.0 mg, 21.0 µmol, 1.0 eq.) was dissolved in THF (35 ml) and a solution of DIPA (50 ml) and THF (50 ml) was made. Both solutions were purged with argon for 1 h. Then, $PdCl_2(PPh_3)_2$ (15.0 mg, 21.0 µmol, 1.0 eq.), CuI (8.00 mg, 42.0 µmol, 2.0 eq.) and I_2 (32.0 mg, 126 µmol, 6.0 eq.) were added to the DIPA/THF solution. Subsequently, the solution of **III** in THF was added over a period of 24 h via an automated injection-system to the DIPA/THF solution while stirring vigorously at 50 °C. The resulting reaction solution was further stirred at 50 °C for 24 h. After cooling to room temperature, the reaction mixture was

diluted with aq. HCl (10%) and DCM. The phases were separated, and the aqueous phase was extracted with DCM (3 x 20 ml). The combined organic phases were washed once with water and brine, dried over $MgSO_4$ and the solvent was removed under reduced pressure. The crude product of all batches was then purified together via column chromatography (DCM, R_f = 0.96). The formed oligomers were then separated via recGPC yielding Dimer **D3** (10.3 mg, 2.38 µmol, 23%) as orange solid and trimer **T3** (9.80 mg, 1.51 µmol, 22%) as orange-red crystalline solid.

Analytics Cyclic Dimer (n=2):

Sum formula:	$C_{300}H_{420}N_4O_8Si_4$
Molar mass:	4323.02 g/mol

^{1}H-NMR (700 MHz, $CDCl_3$, 298 K):

δ [ppm] = 9.69 (d, J = 1.9 Hz, 4H), 8.48 (d, J = 8.8 Hz, 4H), 7.95 (s, 4H), 7.93 (dd, J = 8.1 Hz, 1.8 Hz, 4H), 7.75 (s, 4H), 7.63 (t, J = 1.5 Hz, 4H), 7.52 (t, J = 1.6 Hz, 4H), 7.41 (t, J = 1.6 Hz, 4H), 6.42 (s, 4H), 4.23 (t, J = 6.4 Hz, 8H), 3.96 (t, J = 6.3 Hz, 8H), 1.83-1.76 (m, 16H), 1.56-1.49 (m, 28H), 1.37 (s, 36H), 1.34-1.22 (m, 192H), 1.08 (d, J = 6.4 Hz, 72H), 0.89 (t, J = 7.0 Hz, 12H), 0.81 (t, J = 7.3 Hz, 12H).

^{13}C-NMR (176 MHz, $CDCl_3$, 298 K):

δ [ppm] = 162.4, 161.8, 151.9, 142.4, 141.9, 138.4, 137.0, 133.5, 133.2, 131.6, 130.8, 130.6, 128.1, 127.0, 125.7, 124.4, 124.0, 123.4, 123.2, 122.0, 106.1, 105.5, 102.6, 97.7, 94.4, 93.0, 91.2, 91.0, 89.8, 83.5, 75.1, 69.9, 68.8, 35.0, 32.1, 31.3, 30.0, 29.9, 29.8, 29.6, 29.5, 29.4, 26.5, 26.2, 22.9, 22.8, 18.9, 14.3, 11.6.

MS (MALDI+; Ag^+-salts) *m/z* (%): 4426.1 (100) $[M+Ag]^+$; calculated: 4319.17 Da.

Analytics Cyclic Trimer (n=3):

Sum formula:	$C_{450}H_{630}N_6O_{12}Si_6$
Molar mass:	6484.53 g/mol

^{1}H-NMR (700 MHz, $CDCl_3$, 298 K):

δ [ppm] = 9.74 (d, J = 1.9 Hz, 6H), 8.55 (d, J = 8.9 Hz, 6H), 8.04 (s, 6H), 7.95 (dd, J = 8.0 Hz, 1.8 Hz, 6H), 7.76 (s, 6H), 7.61 (t, J = 1.5 Hz, 6H), 7.54 (dt, J = 3.4 Hz, 1.6 Hz, 12H), 6.38 (s, 6H), 4.28 (t, J = 6.7 Hz, 12H), 3.89 (t, J = 6.3 Hz, 12H), 1.88-1.76 (m, 24H), 1.59-1.54 (m, 24H), 1.54-1-47 (m, 18H), 1.33 (s, 54H), 1.31-1.20 (m, 288H), 1.11 (d, J = 4.6 Hz, 108H), 0.88 (t, J = 7.3 Hz, 18H), 0.84 (t, J = 7.2 Hz, 18H).

^{13}C-NMR (176 MHz, $CDCl_3$, 298 K):

δ [ppm] = 177.8, 162.3, 161.9, 152.1, 142.4, 141.9, 140.6, 138.6, 133.6, 133.3, 133.2, 131.7, 130.8, 130.6, 129.8, 129.4, 125.7, 124.3, 123.8, 123.4, 123.1, 121.9, 106.1, 105.5, 102.6, 98.6, 97.7, 94.5, 93.2, 90.7, 90.2, 90.0, 81.5, 74.1, 70.0, 68.8, 67.9, 34.9, 32.1, 31.3, 29.9, 29.8, 29.7, 29.6, 29.5, 29.4, 29.3, 26.5, 26.1, 22.9, 18.9, 14.3, 11.6.

MS (MALDI+) *m/z* (%): 6729.9 (8) $[M+H+DCTB]^+$, 6520.7 (26) $[M+H+HCl]^+$, 6479.8 (100) $[M+H]^+$, 6253.5 (12) $[M-C_{16}H_{33}]^+$; calculated: 6478.75 Da.

D_{3d}/T_{3d} (SR-180/-182)

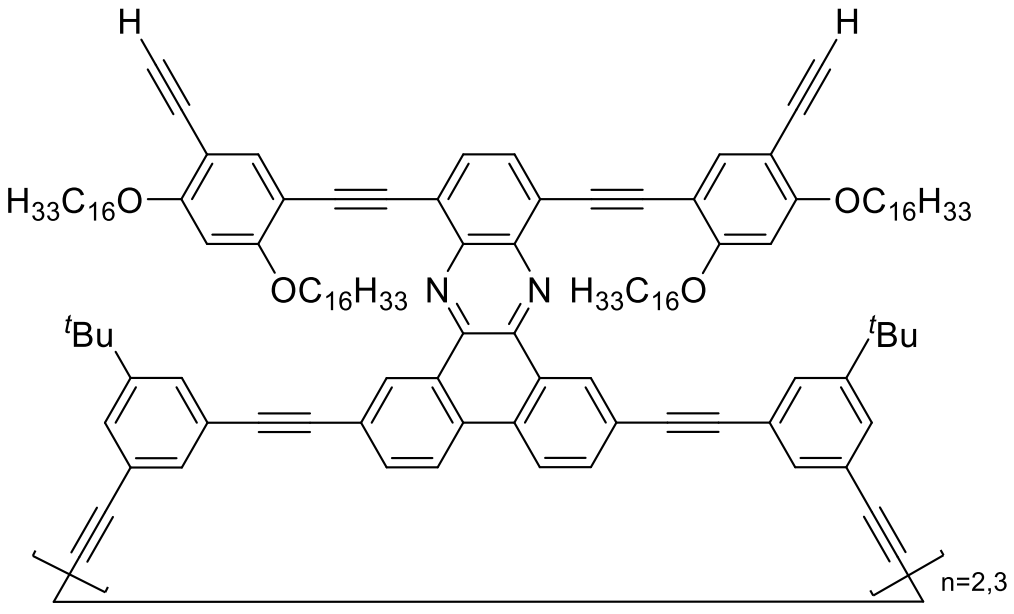

For the synthesis of compound **D_{3d}**, a modified reaction procedure by *K. Remmersen* was applied.[147,152]

Compound **D3** (28.9 mg, 6.69 µmol, 1.0 eq.) was dissolved in THF (10 ml) and 1 ml of a TBAF-solution (1 M in THF) was added. The resulting reaction solution was stirred at 35 °C for 3 h. After cooling to room temperature, the reaction was terminated by addition of H_2O. The phases were separated, and the aqueous phase was extracted with DCM (3 x 20 ml). The combined organic phases were washed once with water and brine, dried over $MgSO_4$ and the solvent was removed under reduced pressure. The crude product was purified via column chromatography (DCM, R_f = 0.98), yielding the deprotected dimer **D3d** (22.4 mg, 6.06 µmol, 91%) as luminous orange solid.

For the synthesis of compound **T3d** a modified reaction procedure by *K. Remmersen* was applied.[147,152]

Compound **T3** (25.9 mg, 3.99 µmol, 1.0 eq.) was dissolved in THF (10 ml) and 1 ml of a TBAF-solution (1 M in THF) was added. The resulting reaction solution was stirred at 35 °C for 3 h. After cooling to room temperature, the reaction was terminated by addition of H_2O. The phases were separated, and the aqueous phase was extracted with DCM (3 x 20 ml). The combined organic phases were washed once with water and brine, dried over $MgSO_4$ and the solvent was removed under reduced pressure. The crude product was purified via column chromatography (DCM, R_f = 0.98), yielding the deprotected trimer **T3d** (16.9 mg, 3.05 µmol, 76%) as bright-red solid.

Unlike the other deprotected cyclic structures in this work **D3d** and **T3d** were obtained in pure form after column chromatography.

Analytics Cyclic Dimer (n=2):

Sum formula:	$C_{264}H_{340}N_4O_8$
Molar mass:	3697.64 g/mol

^{1}H-NMR (700 MHz, $CDCl_3$, 298 K):

δ [ppm] = 9.72 (d, *J* = 1.8 Hz, 4H), 8.48 (d, *J* = 8.8 Hz, 4H), 7.94 (dd, *J* = 8.1 Hz, 1.9 Hz, 4H), 7.90 (s, 4H), 7.81 (s, 4H), 7.61 (d, *J* = 1.5 Hz, 4H), 7.58 (t, *J* = 1.7 Hz, 4H), 7.42 (t, *J* = 1.7 Hz, 4H), 6.43 (s, 4H), 4.14 (t, *J* = 6.4 Hz 8H), 4.00 (t, *J* = 6.6 Hz, 8H), 2.80 (s, 4H), 1.90-1.83 (m, 8H), 1.83-1.76 (m, 8H), 1.54-1.48 (m, 8H), 1.44-1.39 (m, 8H), 1.39 (s, 36H), 1.35-1.24 (m, 192H), 0.89 (t, *J* = 7.1 Hz, 12H), 0.82 (t, *J* = 7.1 Hz, 12H).

^{13}C-NMR (176 MHz, $CDCl_3$, 298 K):

δ [ppm] = 162.3, 162.0, 151.9, 142.3, 141.9, 138.6, 137.2, 133.2, 133.1, 131.6, 130.8, 128.2, 127.0, 124.3, 123.9, 123.4, 123.3, 122.0, 105.6, 104.6, 97.4, 94.2, 91.3, 90.8, 89.9, 83.5, 79.7, 79.3, 75.1, 69.6, 68.9, 35.9, 32.1, 31.4, 30.0, 29.9, 29.7, 29.5, 29.3, 26.2, 22.9, 14.3.

MS (MALDI+) *m/z* (%): 4245.8 (4) $[M+H+DCTB]^+$, 3730.7 (43) $[M-2H+K]^+$, 3694.7 (100) $[M]^+$, 3471.4 (7) $[M-C_{16}H_{33}]^+$; calculated: 3694.63 Da.

Analytics Cyclic Trimer (n=3):

Sum formula:	$C_{396}H_{510}N_6O_{12}$
Molar mass:	5546.47 g/mol

^{1}H-NMR (700 MHz, $CDCl_3$, 298 K):

δ [ppm] = 9.75 (d, J = 1.9 Hz, 6H), 8.57 (d, J = 8.8 Hz, 6H), 8.02 (s, 6H), 7.98 (dd, J = 8.2 Hz, 1.9 Hz, 6H), 7.83 (s, 6H), 7.66 (d, J = 1.4 Hz, 6H), 7.60 (t, J = 1.7 Hz, 6H), 7.55 (t, J = 1.7 Hz, 6H), 6.42 (s, 6H), 4.22 (t, J = 6.4 Hz 12H), 3.98 (t, J = 6.6 Hz, 12H), 2.96 (s, 6H), 1.91-1.85 (m, 12H), 1.85-1.79 (m, 12H), 1.53-1.46 (m, 12H), 1.46-1.40 (m, 12H), 1.36 (s, 54H), 1.31-1.20 (m, 288H), 0.87 (t, J = 6.2 Hz, 18H), 0.83 (t, J = 6.4 Hz, 18H).

^{13}C-NMR (176 MHz, $CDCl_3$, 298 K):

δ [ppm] = 162.3, 162.1, 152.0, 142.3, 141.9, 138.8, 133.7, 133.4, 133.2, 131.7, 130.8, 130.5, 129.9, 129.8, 124.3, 123.7, 123.5, 123.2, 121.9, 105.7, 104.6, 97.6, 94.3, 90.8, 90.2, 81.5, 80.1, 79.4, 69.8, 69.1, 35.0, 32.1, 31.3, 29.9, 29.8, 29.7, 29.6, 29.5, 29.4, 29.3, 26.1, 22.9, 14.3.

MS (MALDI+) *m/z* (%): 6792.1 (14) $[M+DCTB]^+$, 5542.0 (100) $[M+H]^+$, 5316.7 (21) $[M-C_{16}H_{33}]^+$; calculated: 5541.95 Da.

D3c/T3c (SR-181/183)

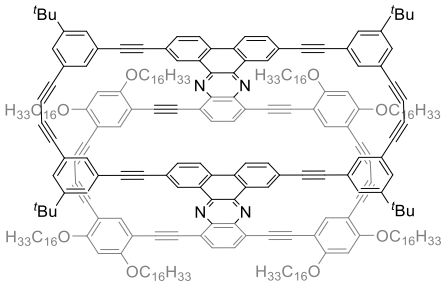

D3c

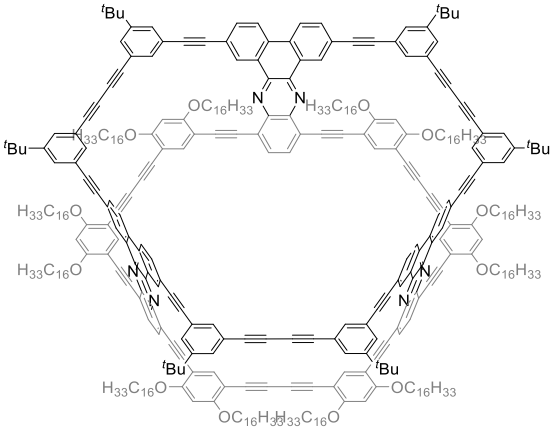

T3c

For the synthesis of compound **D3c**, a modified reaction procedure by *G.Poluektov et al.* was applied.[74,75]

Compound **D3d** (22.0 mg, 5.95 µmol, 1.0 eq.) was dissolved in THF (35 ml) and a solution of DIPA (50 ml) and THF (50 ml) was made. Both solutions were purged with argon for 1 h. Then, $PdCl_2(PPh_3)_2$ (8.00 mg, 11.9 µmol, 2.0 eq.), CuI (9.00 mg, 47.6 µmol, 4.0 eq.) and I_2 (18.0 mg, 71.4 µmol, 12.0 eq.) were added to the DIPA/THF solution. Subsequently, the solution of **D3d** in THF was added over a period of 48 h via an automated injection-system to the DIPA/THF solution while stirring vigorously at 50 °C. The resulting reaction solution was further stirred at 50 °C for 68 h. After cooling to room temperature, the reaction mixture was diluted with aq. HCl (10%) and DCM. The phases were separated, and the aqueous phase was extracted with DCM (3 x 20 ml). The combined organic phases were washed once with water and brine, dried over $MgSO_4$ and the solvent was removed under reduced pressure. The crude product was purified via column chromatography (DCM, R_f = 0.96). The product was then further purified via recGPC yielding bowl-shaped dimer **D3c** (16.7 mg, 4.52 µmol, 76%) as luminous orange solid.

For the synthesis of compound **T3c**, a modified reaction procedure by *G.Poluektov et al.* was applied.[74,75]

Compound **T3d** (17.0 mg, 3.07 µmol, 1.0 eq.) was dissolved in THF (35 ml) and a solution of DIPA (50 ml) and THF (50 ml) was made. Both solutions were purged with argon for 1 h. Then, $PdCl_2(PPh_3)_2$ (4.00 mg, 6.14 µmol, 2.0 eq.), CuI (2.00 mg, 12.3 µmol, 4.0 eq.) and I_2

(9.00 mg, 36.8 µmol, 12.0 eq.) were added to the DIPA/THF solution. Subsequently, the solution of **T_{3d}** in THF was added over a period of 48 h via an automated injection-system to the DIPA/THF solution while stirring vigorously at 50 °C. The resulting reaction solution was further stirred at 50 °C for 68 h. After cooling to room temperature, the reaction mixture was diluted with aq. HCl (10%) and DCM. The phases were separated, and the aqueous phase was extracted with DCM (3 x 20 ml). The combined organic phases were washed once with water and brine, dried over $MgSO_4$ and the solvent was removed under reduced pressure. The crude product was purified via column chromatography (DCM, R_f = 0.96). The product was then further purified via recGPC yielding bowl-shaped trimer **T_{3c}** (7.4 mg, 1.34 µmol, 44%) as luminous red solid.

The unobtainability of meaningful NMR spectra here was also observed for the other PNTs synthesized in this work (see synthesis of **D_{1c}/T_{1c}**).

Analytics Cyclic Dimer (n=1):

Sum formula:	$C_{264}H_{336}N_4O_8$
Molar mass:	3693.61 g/mol

MS (MALDI+) *m/z* (%): 3690.6 (100) $[M]^+$; calculated: 3690.60 Da.

Analytics Cyclic Trimer (n=2):

Sum formula:	$C_{396}H_{504}N_6O_{12}$
Molar mass:	5540.42 g/mol

MS (MALDI+; Ag^+-salts) *m/z* (%): 5899.0 (7) $[M+Ag+DCTB]^+$, 5642.8 (100) $[M+Ag]^+$, 5539.9 (7) $[M+Ag-C_9H_{20}]^+$; calculated: 5535.90 Da.

43 (SR-176)

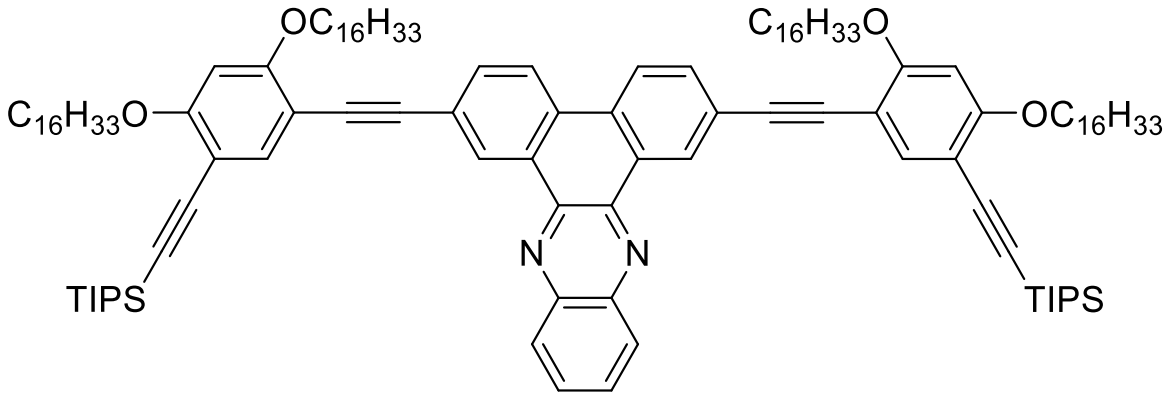

For the synthesis of compound **43**, a modified reaction procedure by *L. Schneider* was applied.[151]

Compound **31** (0.60 g, 0.35 mmol, 1.0 eq.) and *o*-phenylene diamine **42** (0.15 g, 1.39 mmol, 4.0 eq.) were dissolved in chloroform (10 ml) and AcOH (6 ml) under argon atmosphere. Then, the reaction mixture was refluxed for 24 h. After cooling to room temperature, the reaction mixture was diluted with DCM and aq. HCl (10%). The phases were separated, and the aqueous phase was extracted with DCM (3 x 20 ml). The combined organic phases were washed once with water and brine, dried over $MgSO_4$ and the solvent was removed under reduced pressure. The crude product was purified via column chromatography (CH:DCM = 1:1, R_f = 0.65) yielding **43** (0.62 g, 0.35 mmol, >99%) as luminous yellow crystalline solid.

Analytics:

Sum formula:	$C_{122}H_{188}N_2O_4Si_2$
Molar mass:	1803.03 g/mol

^{1}H-NMR (700 MHz, $CDCl_3$, 298 K):

δ [ppm] = 9.55 (d, J = 1.8 Hz, 2H), 8.47 (d, J = 8.7 Hz, 2H), 8.34 (dd, J = 6.4 Hz, 3.4 Hz, 2H), 7.89-7.85 (m, 4H), 7.68 (s, 2H), 6.42 (s, 2H), 4.12 (t, J = 6.4 Hz 4H), 4.04 (t, J = 6.3 Hz, 4H), 1.99-1.93 (m, 4H), 1.86-1.81 (m, 4H), 1.67-1.61 (m, 4H), 1.56-1.50 (m, 10H), 1.47-1.42 (m, 4H), 1.38-1.31 (m, 4H), 1.30-1.23 (m, 88H), 1.16 (d, J = 3.2 Hz, 36H), 0.87 (dt, J = 19.6 Hz, 7.1 Hz, 12H).

^{13}C-NMR (176 MHz, $CDCl_3$, 298 K):

δ [ppm] = 162.2, 161.5, 142.5, 142.1, 138.3, 133.0, 131.0, 130.6, 130.1, 129.7, 129.4, 123.9, 123.2, 105.8, 105.0, 102.6, 97.2, 93.3, 92.5, 87.4, 69.3, 69.0, 32.1, 29.9, 29.8, 29.7, 29.6, 29.5, 29.4, 26.4, 26.3, 22.9, 18.9, 14.3, 11.6.

MS (MALDI+) *m/z* (%): 1801.4 (100) $[M]^+$; calculated: 1801.41 Da.

IV (SR-177)

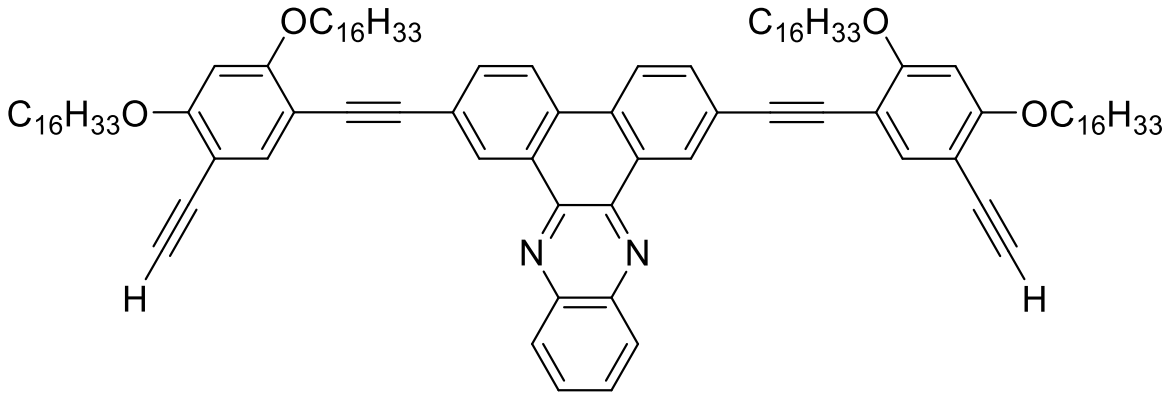

For the synthesis of compound **IV**, a modified reaction procedure by *K. Remmersen* was applied.[147,152]

Compound **43** (0.20 g, 0.11 mmol, 1.0 eq.) was dissolved in THF (10 ml) and 2 ml of a TBAF-solution (1 M in THF) were added. The resulting reaction solution was stirred at room temperature for 23 h. Then, the reaction was terminated by addition of H_2O. The phases were separated, and the aqueous phase was extracted with DCM (3 x 20 ml). The combined organic phases were washed once with water and brine, dried over $MgSO_4$ and the solvent was removed under reduced pressure. The crude product was purified via column chromatography (CH:DCM = 1:1, R_f = 0.53), yielding **IV** (0.16 g, 0.11 mmol, >99%) as luminous yellow solid.

Analytics:

Sum formula:	$C_{104}H_{148}N_2O_4$
Molar mass:	1490.34 g/mol

^{1}H-NMR (700 MHz, $CDCl_3$, 298 K):

δ [ppm] = 9.54 (d, J = 1.8 Hz, 2H), 8.48 (d, J = 8.6 Hz, 2H), 8.34 (dd, J = 6.4 Hz, 3.4 Hz, 2H), 7.89-7.86 (m, 4H), 7.68 (s, 2H), 6.45 (s, 2H), 4.13 (t, J = 6.4 Hz 4H), 4.08 (t, J = 6.6 Hz, 4H), 3.21 (s, 2H), 1.99-1.94 (m, 4H), 1.90-1.85 (m, 4H), 1.67-1.61 (m, 4H), 1.53-1.49 (m, 4H), 1.47-1.43 (m, 4H), 1.41-1.36 (m, 4H), 1.36-1.23 (m, 88H), 0.87 (dt, J = 20.2 Hz, 7.1 Hz, 12H).

^{13}C-NMR (176 MHz, $CDCl_3$, 298 K):

δ [ppm] = 162.1, 161.8, 142.5, 142.1, 138.5, 133.0, 131.0, 130.6, 130.1, 129.7, 129.4, 123.9, 123.3, 105.3, 104.3, 97.3, 92.6, 87.1, 80.0, 79.5, 69.3, 32.1, 29.9, 29.8, 29.7, 29.6, 29.5, 29.4, 29.2, 26.3, 26.1, 22.9, 22.8, 14.3.

MS (MALDI+) *m/z* (%): 1739.2 (34) $[M+DCTB]^+$, 1489.1 (100) $[M]^+$; calculated: 1489.14 Da.

T_4/Tet_4 (SR-178/-179)

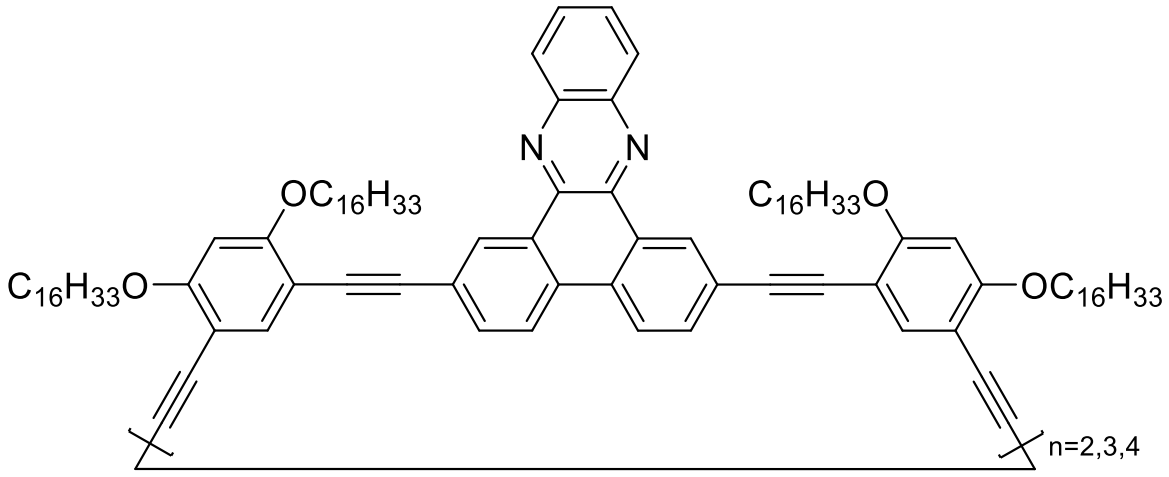

For the synthesis of compound **T_4/Tet_4**, a modified reaction procedure by *G.Poluektov et al.* was applied.[74,75]

Route a):

Compound **IV** (50.0 mg, 34.0 µmol, 1.0 eq.) was dissolved in THF (35 ml) and a solution of DIPA (50 ml) and THF (50 ml) was made. Both solutions were purged with argon for 1 h. Then, $PdCl_2(PPh_3)_2$ (24.0 mg, 34.0 µmol, 1.0 eq.), CuI (13.0 mg, 68.0 µmol, 2.0 eq.) and I_2 (51.0 mg, 200 µmol, 6.0 eq.) were added to the DIPA/THF solution. Subsequently, the solution of **IV** in THF was added over a period of 24 h via an automated injection-system to the DIPA/THF solution while stirring vigorously at 50 °C. The resulting reaction solution was further stirred at 50 °C for 24 h. After cooling to room temperature, the reaction mixture was diluted with aq. HCl (10%) and DCM. The phases were separated, and the aqueous phase was extracted with DCM (3 x 20 ml). The combined organic phases were washed once with water and brine, dried over $MgSO_4$ and the solvent was removed under reduced pressure. The crude product was then purified via column chromatography (DCM, R_f = 0.99). The formed oligomers were separated via recGPC yielding trimer **T_4** (6.6 mg, 1.48 µmol, 13%) and tetramer **Tet_4** (3.5 mg, 0.59 µmol, 7%) as yellow solids.

Route b):

Compound **IV** (50.0 mg, 24.0 µmol, 1.0 eq.) was dissolved in THF (35 ml) and a solution of DIPA (50 ml) and THF (50 ml) was made. Both solutions were purged with argon for 1 h. Then, $Pd(OAc)_2$ (8.00 mg, 34.0 µmol, 1.0 eq.), *XPhos* (40.0 mg, 85.0 µmol, 1.0 eq.), CuI (13.0 mg, 68.0 µmol, 2.0 eq.) and I_2 (51.0 mg, 200 µmol, 6.0 eq.) were added to the DIPA/THF solution. Subsequently, the solution of **IV** in THF was added over a period of 24 h via an automated injection-system to the DIPA/THF solution while stirring vigorously at 50 °C. The resulting reaction solution was further stirred at 50 °C for 24 h. After cooling to room temperature, the reaction mixture was diluted with aq. HCl (10%) and DCM. The phases were separated, and the aqueous phase was extracted with DCM (3 x 20 ml). The combined organic phases were washed once with water and brine, dried over $MgSO_4$ and the solvent was removed under reduced pressure. The crude product was then purified via column chromatography (DCM, R_f = 0.99). The formed oligomers were separated via recGPC yielding dimeric species **D_{4OC}** (7.5 mg, 2.51 mmol, 15%) and trimeric **T_{4OC}** (3.7 mg, 0.83 µmol, 7%) as luminous yellow crystalline solids.

However, even though analytical GPC and MALDI(+)-TOF spectra suggest that the open-chain forms are obtained, signal doubling in the NMR-spectra and only half of the

expected intensity of the free-acetylene signal in the respective ^{1}H-NMR spectra indicate that a mixture of cyclic and open-chain species was obtained. Meaningful integration of the ^{1}H-NMR spectra was not possible.

Analytics Cyclic Trimer (n=3):

Sum formula:	$C_{312}H_{438}N_6O_{12}$
Molar mass:	4464.97 g/mol

^{1}H-NMR (700 MHz, $CDCl_3$, 298 K):

δ [ppm] = 9.57 (d, *J* = 1.8 Hz, 6H), 8.50 (d, *J* = 8.6 Hz, 6H), 8.37 (dd, *J* = 7.2 Hz, 3.6 Hz, 6H), 7.90 (dd, *J* = 8.1 Hz, 1.8 Hz, 6H), 7.88 (dd, *J* = 6.5 Hz, 3.3 Hz, 6H), 7.76 (s, 6H), 6.45 (s, 6H), 4.15 (t, *J* = 5.8 Hz 12H), 4.10 (t, *J* = 6.7 Hz, 12H), 2.01-1.95 (m, 12H), 1.94-1.87 (m, 12H), 1.70-1.62 (m, 12H), 1.50-1.44 (m, 12H), 1.44-1.39 (m, 12H), 1.39-1.31 (m, 12H), 1.32-1.22 (m, 264H), 0.86 (dt, *J* = 9.5 Hz, 7.2 Hz, 36H).

^{13}C-NMR (176 MHz, $CDCl_3$, 298 K):

δ [ppm] = 162.6, 161.8, 142.5, 142.1, 139.4, 135.9, 133.0, 131.1, 130.6, 130.2, 129.8, 129.5, 125.7, 123.6, 123.3, 105.7, 104.6, 97.4, 92.7, 87.1, 69.4, 69.3, 34.4, 32.1, 30.5, 29.9, 29.8, 29.7, 29.6, 29.5, 29.4, 29.2, 26.9, 26.1, 22.9, 22.8, 14.3.

MS (MALDI+; Ag^+-salts) *m/z* (%): 4711.5 (20) $[M+H+Ag+Na-C_9H_{19}+DCTB]^+$, 4640.4 (40) $[M-C_5H_{11}+DCTB]^+$, 4568.3 (100) $[M+Ag]^+$; calculated: 4461.38 Da.

Analytics Cyclic Tetramer (n=4):

Sum formula:	$C_{416}H_{584}N_8O_{16}$
Molar mass:	5953.29 g/mol

^{1}H-NMR (700 MHz, $CDCl_3$, 298 K):

δ [ppm] = 9.56 (d, *J* = 1.8 Hz, 8H), 8.49 (d, *J* = 8.8 Hz, 8H), 8.35 (dd, *J* = 6.4 Hz, 3.4 Hz, 8H), 7.89 (dd, *J* = 8.1 Hz, 1.9 Hz, 8H), 7.84 (dd, *J* = 6.5 Hz, 3.5 Hz, 8H), 7.73 (s, 8H), 6.45 (s, 8H), 4.14 (t, *J* = 6.1 Hz 16H), 4.09 (t, *J* = 6.7 Hz, 16H), 2.00-1.94 (m, 16H), 1.94-1.87 (m,

16H), 1.68-1.61 (m, 16H), 1.49-1.44 (m, 16H), 1.42-1.38 (m, 16H), 1.38-1.30 (m, 16H), 1.30-1.18 (m, 352H), 0.88 (t, *J* = 7.3 Hz, 24H), 0.85 (t, *J* = 7.3 Hz, 24H).

^{13}C-NMR (176 MHz, $CDCl_3$, 298 K):
δ [ppm] = 162.8, 161.9, 142.5, 142.0, 139.0, 133.0, 131.1, 130.6, 130.1, 129.5, 125.7, 123.9, 123.3, 105.7, 104.6, 97.4, 87.1, 69.4, 69.3, 32.1, 30.5, 29.9, 29.8, 29.6, 29.5, 29.4, 29.2, 26.3, 26.1, 22.8, 14.3.

MS (MALDI+; Ag^+-salts) *m/z* (%): 6306.5 (7) $[M+H+Ag+DCTB]^+$, 6056.4 (100) $[M+H+Ag]^+$, 5949.5 (7) $[M+H]^+$; calculated: 5948.51 Da.

Analytics Open-Chain Dimer (n=2):

Sum formula:	$C_{208}H_{294}N_4O_8$
Molar mass:	2978.66 g/mol

.

MS (MALDI+) *m/z* (%): 3226.4 (8) $[M+DCTB]^+$, 2976.3 (100) $[M]^+$; calculated: 2976.27 Da.

Analytics Open-Chain Trimer (n=3):

Sum formula:	$C_{312}H_{440}N_6O_{12}$
Molar mass:	4466.98 g/mol

MS (MALDI+) *m/z* (%): 4963.6 (11) $[M+2DCTB]^+$, 4713.5 (44) $[M+DCTB]^+$, 4463.4 (100) $[M]^+$; calculated: 4463.40 Da.

45 (SR-82) via **44**

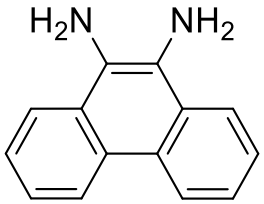

For the synthesis of compound **45**, a reaction procedure by *S. Bodige et al.* was applied.[153] Phenanthrenequinone (1.00 g, 4.80 mmol, 1.0 eq.) was suspended in EtOH (80 ml). Subsequently, hydroxylammonium chloride (1.17 g, 16.8 mmol, 3.5 eq.) and barium carbonate (1.42 g, 7.20 mmol, 1.5 eq.) were added and the reaction mixture was refluxed for 66 h. After cooling to room temperature, the solvent was removed under reduced pressure. Then, the solid residue was suspended in aq. HCl (10%, 75 ml) and filtered off. It was washed with water and a small amount of EtOH. The crude product **44** (0.98 g, 4.11 mmol, 86%) was received as a yellow-green solid, dried under vacuum, and used in the next reaction step without further purification.

Phenanthrene-9,10-dione dioxime **44** (0.98 g, 4.11 mmol, 1.0 eq.) was suspended in EtOH (30 ml) and Pd/C (10%, 0.64 g) was added. Then, the reaction suspension was heated to 80 °C and a solution of hydrazine monohydrate (8.1 ml) in EtOH (15 ml) was added slowly in portions over 1 h, leading to foam formation. Subsequently, the reaction mixture was refluxed for 19 h and then filtered hot through a bed of Celite. The filter cake was washed with boiling EtOH several times and the filtrate was dried under vacuum. The solid residue was then suspended in H_2O (100 ml) and stored at 2 °C overnight. The yellow precipitate was filtered off, washed with water, and recrystallized from EtOH giving **45** (0.25 g, 1.20 mmol, 25%) as a yellow crystalline solid.

Analytics:

Sum formula:	$C_{14}H_{12}N_2$
Molar mass:	208.26 g/mol

^{1}H-NMR (500 MHz, DMSO-d_6, 298 K):

δ [ppm] = 8.66 (d, J = 8.2 Hz, 2H), 8.02 (dd, J = 8.3 Hz, 1.0 Hz, 2H), 7.52 (ddd, J = 8.2 Hz, 6.8 Hz, 1.2 Hz, 2H), 7.38 (ddd, J = 8.2 Hz, 6.8 Hz, 1.2 Hz, 2H) 4.95 (s, 4H, NH_2).

^{13}C-NMR (126 MHz, DMSO-d_6, 298 K):

δ [ppm] = 126.1, 126.0, 124.9, 122.7, 122.3, 120.8.

MS (EI, 70 eV) *m/z* (%): 208.0 (91) $[M]^{+\bullet}$, 193.0 (100) $[M\text{-}NH]^{+}$, 180.0 (38) $[C_{13}H_{10}N]^{+}$, 165.0 (38) $[C_{13}H_9]^{+}$; calculated: 208.10 Da.

46 (SR-84)

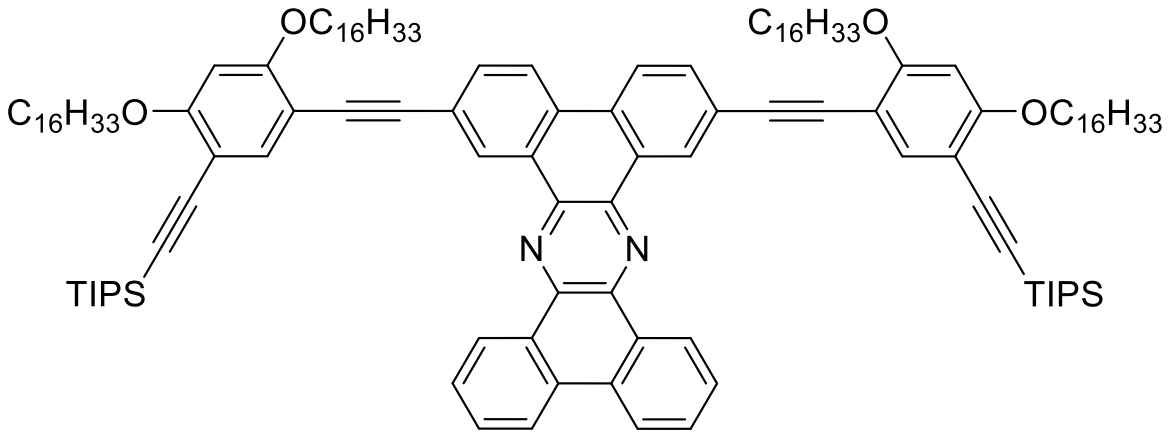

For the synthesis of compound **46**, a modified reaction procedure by *L. Schneider* was applied.[151]

Compound **31** (33.0 mg, 19.0 µmol, 1.0 eq.) and phenanthrene-9,10-diamine **45** (8.00 mg, 38.0 µmol, 2.0 eq.) were dissolved in chloroform (5 ml) and AcOH (3 ml) under argon atmosphere. Then, the reaction mixture was refluxed for 24 h. After cooling to room temperature, the reaction mixture was diluted with DCM and water. The phases were separated, and the aqueous phase was extracted with DCM (3 x 20 ml). The combined organic phases were washed once with aq. HCl (10%), water and brine, dried over $MgSO_4$ and the solvent was removed under reduced pressure. The crude product was purified via column chromatography (CH:DCM = 1:1, R_f = 0.96) yielding **46** (36.6 mg, 19.0 µmol, >99%) as a luminous yellow crystalline solid.

Analytics:

Sum formula:	$C_{130}H_{192}N_2O_4Si_2$
Molar mass:	1903.15 g/mol

^{1}H-NMR (700 MHz, $CDCl_3$, 298 K):

δ [ppm] = 9.65 (d, J = 1.8 Hz, 2H), 9.64-9.61 (m, 2H), 8.66-8.62 (m, 2H), 8.53 (d, J = 8.7 Hz, 2H), 7.90 (dd, J = 8.3 Hz, 1.8 Hz, 2H), 7.85-7.81 (m, 4H), 7.72 (s, 2H), 6.44 (s, 2H), 4.15 (t, J = 6.4 Hz, 4H), 4.06 (t, J = 6.3 Hz 4H), 2.03-1.96 (m, 4H), 1.87-1.82 (m, 4H), 1.68-1.62 (m, 4H), 1.58-1.50 (m, 10H), 1.35-1.20 (m, 96H), 1.18 (d, J = 3.0 Hz, 36H), 0.88 (t, J = 7.1 Hz, 6H), 0.84 (t, J = 7.2 Hz, 6H).

^{13}C-NMR (176 MHz, $CDCl_3$, 298 K):

δ [ppm] = 162.2, 161.5, 140.9, 140.1, 138.2, 132.5, 132.0, 130.7, 130.5, 129.9, 128.9, 127.9, 126.4, 123.7, 123.2, 123.0, 105.8, 105.1, 102.6, 97.2, 93.4, 92.8, 87.2, 69.3, 69.0, 32.1, 29.9, 29.8, 29.7, 29.6, 29.5, 29.4, 26.4, 26.3, 22.9, 18.9, 14.3, 11.6.

MS (MALDI+) *m/z* (%): 1901.4 (100) $[M]^+$; calculated: 1901.44 Da.

10. Literature

[1] Z. Liu in *Global energy interconnection* (Ed.: Z. Liu), Elsevier, Amsterdam, Boston, Heidelberg, London, New York, Oxford, Paris, San Diego, San Francisco, Singapore, Sydney, Tokyo, **2015**, pp. 1–64.

[2] a) H. Shirakawa, T. Ito, S. Ikeda, *Polym. J.* **1973**, *4*, 460; b) H. Shirakawa, E. J. Louis, A. G. MacDiarmid, C. K. Chiang, A. J. Heeger, *J. Chem. Soc., Chem. Commun.* **1977**, 578; c) C. K. Chiang, C. R. Fincher, Y. W. Park, A. J. Heeger, H. Shirakawa, E. J. Louis, S. C. Gau, A. G. MacDiarmid, *Phys. Rev. Lett.* **1977**, *39*, 1098.

[3] Grand View Research Inc., "China printed Electronics by Device 2014-2025", can be found under https://sites.google.com/site/electronicindustryhighlights/printed-electronics-market-to-cross-19-15-billion-by-2025-key-industry-players-enfucell-oy-gsi-technologies.

[4] L. Basiricò, G. Mattana, M. Mas-Torrent, *Front. Phys.* **2022**, *10*.

[5] M. Riede, D. Spoltore, K. Leo, *Adv. Energy Mater.* **2021**, *11*, 2002653.

[6] C. E. Fritts, *Am. J. Sci.* **1883**, *26*, 465.

[7] Chapin D. M., Fuller C. S., G. L. Pearso in *Semiconductor Devices: Pioneering Papers* (Ed.: S. M. Sze), world scientific, **1991**, pp. 969–970.

[8] J. F. Geisz, R. M. France, K. L. Schulte, M. A. Steiner, A. G. Norman, H. L. Guthrey, M. R. Young, T. Song, T. Moriarty, *Nat. Energy* **2020**, *5*, 326.

[9] A. Fernandez, "How a Solar Cell Works", can be found under https://www.acs.org/content/acs/en/education/resources/highschool/chemmatters/past-issues/archive-2013-2014/how-a-solar-cell-works.html#:~:text=A%20solar%20cell%20is%20made,energy%20level%20than%20does%20silicon.

[10] N. Rathore, N. L. Panwar, F. Yettou, A. Gama, *Int. J. Ambient Energy* **2021**, *42*, 1200.

[11] O. A. Abdulrazzaq, V. Saini, S. Bourdo, E. Dervishi, A. S. Biris, *Part. Sci. Technol.* **2013**, *31*, 427.

[12] K. Forberich, G. Dennler, M. C. Scharber, K. Hingerl, T. Fromherz, C. J. Brabec, *Thin Solid Films* **2008**, *516*, 7167.

[13] T. Trupke, M. A. Green, P. Würfel, *J. Appl. Phys.* **2002**, *92*, 4117.

[14] Y. Jestin, S. Chandra, B. Cass, H. Ahmed, S. J. McCormack in *Comprehensive Renewable Energy*, Elsevier, **2022**, pp. 534–560.

[15] P. K. Nayak, S. Mahesh, H. J. Snaith, D. Cahen, *Nat. Rev. Mater.* **2019**, *4*, 269.

[16] G. Li, R. Zhu, Y. Yang, *Nat. Photon.* **2012**, *6*, 153.

[17] M. Karakawa, K. Suzuki, T. Kuwabara, T. Taima, K. Nagai, M. Nakano, T. Yamaguchi, K. Takahashi, *Org. Electron.* **2020**, *76*, 105448.

[18] P. Kumaresan, S. Vegiraju, Y. Ezhumalai, S. Yau, C. Kim, W.-H. Lee, M.-C. Chen, *Polymers* **2014**, *6*, 2645.

[19] H. Hoppe, N. S. Sariciftci, *J. Mater. Res.* **2004**, *19*, 1924.

[20] Y. Kim, S. Cook, S. M. Tuladhar, M. Sachetan, S. A. Choulis, J. Nelson, J. R. Durrant, D. D. C. Bradley, M. Giles, I. McCulloch, C.-S. Ha, M. Ree in *Materials for Sustainable Energy* (Ed.: V. Dusastre), Co-Published with Macmillan Publishers Ltd, London, **2010**, pp. 63–69.

[21] M. Zhang, L. Zhu, G. Zhou, T. Hao, C. Qiu, Z. Zhao, Q. Hu, B. W. Larson, H. Zhu, Z. Ma, Z. Tang, W. Feng, Y. Zhang, T. P. Russell, F. Liu, *Nat. Commun.* **2021**, *12*, 309.

[22] a) D. Venkataraman, S. Yurt, B. H. Venkatraman, N. Gavvalapalli, *J. Phys. Chem. Lett.* **2010**, *1*, 947; b) L. F. Dössel, V. Kamm, I. A. Howard, F. Laquai, W. Pisula, X. Feng, C. Li, M. Takase, T. Kudernac, S. de Feyter, K. Müllen, *J. Am. Chem. Soc.* **2012**, *134*, 5876.

[23] a) Y. Liu, C. Zhang, D. Hao, Z. Zhang, L. Wu, M. Li, S. Feng, X. Xu, F. Liu, X. Chen, Z. Bo, *Chem. Mater.* **2018**, *30*, 4307; b) J. D. Zimmerman, B. E. Lassiter, X. Xiao, K. Sun, A. Dolocan, R. Gearba, D. A. Vanden Bout, K. J. Stevenson, P. Wickramasinghe, M. E. Thompson, S. R. Forrest, *ACS Nano* **2013**, *7*, 9268.

[24] D. M. Wilson, S. Hoyt, J. Janata, K. Booksh, L. Obando, *IEEE Sens. J.* **2001**, *1*, 256.

[25] V. Schroeder, S. Savagatrup, M. He, S. Lin, T. M. Swager, *Chem. Rev.* **2019**, *119*, 599.

[26] B. Yoon, S.-J. Choi, T. M. Swager, G. F. Walsh, *ACS Sens.* **2021**, *6*, 3056.

[27] R. Zhu, J. M. Azzarelli, T. M. Swager, *Angew. Chem. Int. Ed.* **2016**, *128*, 9662.

[28] a) V. Schroeder, T. M. Swager, *J. Am. Chem. Soc.* **2018**, *140*, 10721; b) E. Bekyarova, I. Kalinina, X. Sun, T. Shastry, K. Worsley, X. Chi, M. E. Itkis, R. C. Haddon, *Adv. Mater.* **2010**, *22*, 848.

[29] Y. Zhang, M. Xu, B. R. Bunes, N. Wu, D. E. Gross, J. S. Moore, L. Zang, *ACS Appl. Mater. Interfaces* **2015**, *7*, 7471.

[30] G. Binning, H. Rohrer, CH643397A5, **1979**.

[31] S. C. Rickert, *Master Thesis*, Rheinische Friedrich-Wilhelms-Universität Bonn, Bonn, **2020**.

[32] a) M. Schmid, "The Scanning Tunneling Microscope", can be found under http://www.iap.tuwien.ac.at/www/surface/stm_gallery/stm_schematic#copyright_notice, **2011**; b) M. Pickel, U. Starke, "The Scanning Tunneling Microscope", can be found under https://www2.fkf.mpg.de/ga/research/stmtutor/stmtheo.html, **2000**.

[33] C. J. Chen, *Introduction to scanning tunneling microscopy*, Oxford Univ. Press, New York, NY, **1993**.

[34] Y. Kuk, P. J. Silverman, *Rev. Sci. Instrum.* **1989**, *60*, 165.

[35] M. Baykul, *Mater. Sci. Eng. B* **2000**, *74*, 229.

[36] B. Ilan, G. M. Florio, M. S. Hybertsen, B. J. Berne, G. W. Flynn, *Nano Lett.* **2008**, *8*, 3160.

[37] A. J. Groszek, *Proc. R. Soc. Lond. A* **1970**, *314*, 473.

[38] J. P. Rabe, S. Buchholz, *Science* **1991**, *253*, 424.

[39] J. P. Rabe, S. Buchholz, L. Askadskaya, *Phys. Scr.* **1993**, *T49A*, 260.

[40] G. C. McGonigal, R. H. Bernhardt, D. J. Thomson, *Appl. Phys. Lett.* **1990**, *57*, 28.

[41] T. Yang, S. Berber, J.-F. Liu, G. P. Miller, D. Tománek, *J. Chem. Phys.* **2008**, *128*, 124709.

[42] M. P. Yothers, A. E. Browder, L. A. Bumm, *Rev. Sci. Instrum.* **2017**, *88*, 013708.

[43] a) G. Meyer, K.-H. Rieder, *Surf. Sci.* **1997**, *377-379*, 1087; b) G. Meyer, *Rev. Sci. Instrum.* **1996**, *67*, 2960.

[44] S. Maruno, K. Inanaga, T. Isu, *Appl. Phys. Lett.* **1993**, *63*, 1339.

[45] H. Ulbricht, G. Moos, T. Hertel, *Phys. Rev. Lett.* **2003**, *90*, 095501.

[46] A. Jenkins, P. Kratochvil, R. Stepto, U. Suter, *Pure Appl. Chem.* **1996**, *68*, 2287.

[47] W. Zhang, J. S. Moore, *Angew. Chem. Int. Ed.* **2006**, *45*, 4416.

[48] S. Höger, *Pure Appl. Chem.* **2010**, *82*, 821.

[49] H. Staab, K. Neunhoeffer, *Synthesis* **1974**, *6*, 424.

[50] C. Krieger, F. Diederich, D. Schweitzer, H. Staab, *Angew. Chem. Int. Ed.* **1979**, *18*, 699.

[51] S. Bhattacharyya, Y. Mastai, R. Narayan Panda, S.-H. Yeon, M. Z. Hu, *J. Nanomater.* **2014**, *2014*, 1.

[52] R. May, S.-S. Jester, S. Höger, *J. Am. Chem. Soc.* **2014**, *136*, 16732.

[53] S.-S. Jester, E. Sigmund, S. Höger, *J. Am. Chem. Soc.* **2011**, *133*, 11062.

[54] A. Wawkuschewski, H.-J. Cantow, S. N. Magonov, M. Möller, W. Liang, M.-H. Whangbo, *Adv. Mater.* **1993**, *5*, 821.

[55] M. K. Smith, O. Š. Miljanić, *Org. Biomol. Chem.* **2015**, *13*, 7841.

[56] D. L. Morrison, S. Höger, *Chem. Commun.* **1996**, *20*, 2313.

[57] S. Chandrasekhar, B. K. Sadashiva, K. A. Suresh, *Pramana* **1977**, *9*, 471.

[58] Z. Aliakbar Tehrani, K. S. Kim, *Int. J. Quantum Chem.* **2016**, *116*, 622.

[59] C. A. Hunter, J. K. M. Sanders, *J. Am. Chem. Soc.* **1990**, *112*, 5525.

[60] J. Zhang, J. S. Moore, *J. Am. Chem. Soc.* **1992**, *114*, 9701.

[61] A. S. Shetty, J. Zhang, J. S. Moore, *J. Am. Chem. Soc.* **1996**, *118*, 1019.

[62] K. Becker, P. G. Lagoudakis, G. Gaefke, S. Höger, J. M. Lupton, *Angew. Chem. Int. Ed.* **2007**, *46*, 3450.

[63] a) F. Diederich, P. Stang (Eds.) *Modern Acetylene Chemistry*, Wiley-VCH, Hoboken, NJ (U.S.), **2008**; b) G. Pattenden, B. M. Trost, I. Fleming (Eds.) *Comprehensive organic synthesis. Selectivity, strategy & efficiency in modern organic chemistry*, Pergamon Press, Oxford, **1993**.

[64] J. S. Moore, J. Zhang, *Angew. Chem. Int. Ed.* **1992**, *31*, 922.

[65] S. Höger, *Chem. Eur. J.* **2004**, *10*, 1320.

[66] S. Höger, A.-D. Meckenstock, H. Pellen, *J. Org. Chem.* **1997**, *62*, 4556.

[67] S. Höger, V. Enkelmann, K. Bonrad, C. Tschierske, *Angew. Chem. Int. Ed.* **2000**, *39*, 2267.

[68] S. Höger, *J. Polym. Sci. A Polym. Chem.* **1999**, *37*, 2685.

[69] D. W. J. McCallien, J. K. M. Sanders, *J. Am. Chem. Soc.* **1995**, *117*, 6611.

[70] J. Porath, Flodin P., *Nature* **1959**, *183*, 1657.

[71] J. C. Moore, *J. Polym. Sci., Part A: Gen. Pap.* **1964**, *2*, 835.

[72] D. Mössinger, S.-S. Jester, E. Sigmund, U. Müller, S. Höger, *Macromolecules* **2009**, *42*, 7974.

[73] G.-B. Pan, X.-H. Cheng, S. Höger, W. Freyland, *J. Am. Chem. Soc.* **2006**, *128*, 4218.

[74] G. Poluektov, T. J. Keller, A. Jochemich, A. Krönert, U. Müller, S. Spicher, S. Grimme, S.-S. Jester, S. Höger, *Angew. Chem. Int. Ed.* **2021**, *60*, 27264.

[75] Georgiy Poluektov, *Dissertation*, Rheinische Friedrich-Wilhelms-Universität Bonn, Bonn, **2018**.

[76] S. A. Meißner, T. Eder, T. J. Keller, D. A. Hofmeister, S. Spicher, S.-S. Jester, J. Vogelsang, S. Grimme, J. M. Lupton, S. Höger, *Nat. Commun.* **2021**, *12*, 6614.

[77] U. Kador, P. Mehnert, *Makromol. Chem.* **1971**, *144*, 37.

[78] M. Hündgen, K. A. Maier, S. Höger, S.-S. Jester, *Chem. Commun.* **2018**, *54*, 10558.

[79] a) W. Li, Q. Liu, K. Jin, M. Cheng, F. Hao, W.-Q. Wu, S. Liu, Z. Xiao, S. Yang, S. Shi, L. Ding, *Mater. Chem. Front.* **2020**, *4*, 1454; b) H. J. Song, M. Goh, K. H. Choi, S. Lee, D. K. Moon, G. J. Shin, *J. Ind. Eng. Chem.* **2015**, *23*, 338.

[80] K. Y. Cheung, K. Watanabe, Y. Segawa, K. Itami, *Nat. Chem.* **2021**, *13*, 255.

[81] a) S. Hitosugi, W. Nakanishi, T. Yamasaki, H. Isobe, *Nat. Commun.* **2011**, *2*, 492; b) Z. Xia, S. H. Pun, H. Chen, Q. Miao, *Angew. Chem. Int. Ed. Engl.* **2021**, *60*, 10311.

[82] S. Zhe, K. Ikemoto, T. M. Fukunaga, T. Koretsune, A. Ryotaro, S. Sato, H. Isobe, Z. Sun, R. Arita, *Science* **2019**, *363*, 151.

[83] a) D. Gärtner, *Master Thesis*, Rheinische Friedrich-Wilhelms-Universität Bonn, Bonn, **2016**; b) N. Noujeim, K. Zhu, V. N. Vukotic, S. J. Loeb, *Org. Lett.* **2012**, *14*, 2484.

[84] Daniel Gärtner, *Master Thesis*, Rheinische Friedrich-Wilhelms-Universität Bonn, Bonn, **2016**.

[85] Simon Claus, *Dissertation*, Rheinische Friedrich-Wilhelms-Universität Bonn, Bonn, **2015**.

[86] a) B. d. Darwent, *Nat. Stand. Ref. Data Ser., Nat. Bur. Stand. (U.S.)* **1970**, *31*, 17; b) M. Schilz, H. Plenio, *J. Org. Chem.* **2012**, *77*, 2798.

[87] Stefanie Meißner, *Dissertation*, Rheinische Friedrich-Wilhelms-Universität Bonn, Bonn, **2020**.

[88] B. A. D. Neto, A. S. Lopes, M. Wüst, V. E. Costa, G. Ebeling, J. Dupont, *Tetrahedron Lett.* **2005**, *46*, 6843.

[89] A. Ernst, L. Gobbi, A. Vasella, *Tetrahedron Lett.* **1996**, *37*, 7959.

[90] L. Emmanuvel, R. K. Shukla, A. Sudalai, S. Gurunath, S. Sivaram, *Tetrahedron Lett.* **2006**, *47*, 4793.

[91] L. Assies, C. Fu, P. Kovaříček, Z. Bastl, K. A. Drogowska, J. Lang, V. L. P. Guerra, P. Samorì, E. Orgiu, D. F. Perepichka, M. Kalbáč, *J. Mater. Chem. C* **2019**, *7*, 12240.

[92] M. R. an der Heiden, H. Plenio, S. Immel, E. Burello, G. Rothenberg, H. C. J. Hoefsloot, *Chem. Eur. J.* **2008**, *14*, 2857.

[93] H. Clavier, S. P. Nolan, *Chem. Commun.* **2010**, *46*, 841.

[94] B. P. Fors, P. Krattiger, E. Strieter, S. L. Buchwald, *Org. Lett.* **2008**, *10*, 3505.

[95] S. Wagschal, L. A. Perego, A. Simon, A. Franco-Espejo, C. Tocqueville, J. Albaneze-Walker, A. Jutand, L. Grimaud, *Chem. Eur. J.* **2019**, *25*, 6980.

[96] J. W. Ciszek, J. M. Tour, *Tetrahedron Lett.* **2004**, *45*, 2801.

[97] L. A. Estrada, D. C. Neckers, *J. Org. Chem.* **2009**, *74*, 8484.

[98] L. A. Estrada, D. C. Neckers, *Org. Lett.* **2011**, *13*, 3304.

[99] G. Eglinton, A. R. Galbraith, *J. Chem. Soc.* **1959**, 889.

[100] A. S. Hay, *J. Org. Chem.* **1962**, *27*, 3320.

[101] J.-H. Li, Y. Liang, X.-D. Zhang, *Tetrahedron* **2005**, *61*, 1903.

[102] S. C. Rickert, S.-X. L. Luo, J. Bahr, J. Kohn, M. Xue, A. Hansen, S. Grimme, S.-S. Jester, T. M. Swager, S. Höger, *J. Am. Chem. Soc.* **2024**, *146*, 2986.

[103] S. Höger, J. Spickermann, D. L. Morrison, P. Dziezok, H. J. Räder, *Macromolecules* **1997**, *30*, 3110.

[104] B. Matarranz, G. Ghosh, R. Kandanelli, A. Sampedro, K. K. Kartha, G. Fernández, *Chem. Commun.* **2021**, *57*, 4890.

[105] Q. Luo, L. Li, H. Ma, C. Lv, X. Jiang, X. Gu, Z. An, B. Zou, C. Zhang, Y. Zhang, *Chem. Sci.* **2020**, *11*, 6020.

[106] a) S. A. Jenekhe, J. A. Osaheni, *Science* **1994**, *265*, 765; b) A. J. Musser, S. K. Rajendran, K. Georgiou, L. Gai, R. T. Grant, Z. Shen, M. Cavazzini, A. Ruseckas, G. A. Turnbull, I. D. W. Samuel, J. Clark, D. G. Lidzey, *J. Mater. Chem. C* **2017**, *5*, 8380.

[107] W. E. Moerner, D. P. Fromm, *Rev. Sci. Instrum.* **2003**, *74*, 3597.

[108] T. J. Keller, C. Sterzenbach, J. Bahr, T. L. Schneiders, M. Bursch, J. Kohn, T. Eder, J. M. Lupton, S. Grimme, S. Höger, S.-S. Jester, *Chem. Sci.* **2021**, *12*, 9352.

[109] A. M. Rao, P. C. Eklund, S. Bandow, A. Thess, R. E. Smalley, *Nature* **1997**, *388*, 257.

[110] D. S. Moore, *Rev. Sci. Instrum.* **2004**, *75*, 2499.

[111] L. Wei, D. Lu, J. Wang, H. Wei, J. Zhao, H. Geng, Y. Zhang, *Sens. Actuators B Chem.* **2014**, *190*, 529.

[112] T. Han, A. Nag, S. Chandra Mukhopadhyay, Y. Xu, *Sens. Actuator A Phys.* **2019**, *291*, 107.

[113] P.-C. Chen, S. Sukcharoenchoke, K. Ryu, L. Gomez de Arco, A. Badmaev, C. Wang, C. Zhou, *Adv. Mater.* **2010**, *22*, 1900.

[114] M. Park, L. N. Cella, W. Chen, N. V. Myung, A. Mulchandani, *Biosens. Bioelectron.* **2010**, *26*, 1297.

[115] V. Kayastha, C. Jones, W. S. Shih, C. Landorf in *Technical proceedings of the 2013 NSTI Nanotechnology Conference and Expo, NSTI-Nanotech 2013* (Eds.: M. Laudon, B. Romanowicz), CRC Press; NSTI Nano Science and Technology Inst, Danville, CA (U.S.), **2013**, pp. 268–271.

[116] Y. Zhang, M. Xu, B. R. Bunes, N. Wu, D. E. Gross, J. S. Moore, L. Zang, *ACS Appl. Mater. Interfaces* **2015**, *7*, 7471.

[117] D. Kumar, P. Jha, A. Chouksey, R. P. Tandon, P. K. Chaudhury, J. S. Rawat, *J. Mater. Sci. Mater. Electron.* **2018**, *29*, 6200.

[118] C. J. Cumming, C. Aker, M. Fisher, M. Fok, M. J. La Grone, D. Reust, M. G. Rockley, T. M. Swager, E. Towers, V. Williams, *IEEE Trans. Geosci. Remote Sens.* **2001**, *39*, 1119.

[119] a) L. Feng, T. Hu, S. Zhang, H.-Y. Xiong, G. Zhang, *Org. Lett.* **2019**, *21*, 9487; b) G. Zhang, H. Yi, H. Chen, C. Bian, C. Liu, A. Lei, *Org. Lett.* **2014**, *16*, 6156.

[120] a) S. Yamago, Y. Watanabe, T. Iwamoto, *Angew. Chem. Int. Ed.* **2010**, *49*, 757; b) J. S. Wössner, D. Wassy, A. Weber, M. Bovenkerk, M. Hermann, M. Schmidt, B. Esser, *J. Am. Chem. Soc.* **2021**, *143*, 12244.

[121] F. Hernández-Culebras, M. Melle-Franco, A. Mateo-Alonso, *Angew. Chem. Int. Ed.* **2022**, *61*, e202205018.

[122] a) G. Zhang, F. R. Lin, F. Qi, T. Heumüller, A. Distler, H.-J. Egelhaaf, N. Li, P. C. Y. Chow, C. J. Brabec, A. K.-Y. Jen, H.-L. Yip, *Chem. Rev.* **2022**, *122*, 14180; b) A. Mishra, P. Bäuerle, *Angew. Chem. Int. Ed.* **2012**, *51*, 2020.

[123] S. Höger, K. Bonrad, *J. Org. Chem.* **2000**, *65*, 2243.

[124] G. R. Fulmer, A. J. M. Miller, N. H. Sherden, H. E. Gottlieb, A. Nudelman, B. M. Stoltz, J. E. Bercaw, K. I. Goldberg, *Organometallics* **2010**, *29*, 2176.

[125] Mestrelab Research S. L., MestReNova© **2012**.

[126] a) C. Bannwarth, E. Caldeweyher, S. Ehlert, A. Hansen, P. Pracht, J. Seibert, S. Spicher, S. Grimme, *WIREs Comput. Mol. Sci.* **2021**, *11*; b) "Semiempirical Extended Tight-Binding Program Package", can be found under https://github.com/grimme-lab/xtb.

[127] S. Spicher, S. Grimme, *Angew. Chem. Int. Ed.* **2020**, *59*, 15665.

[128] M. D. Hanwell, D. E. Curtis, D. C. Lonie, T. Vandermeersch, E. Zurek, G. R. Hutchison, *J. Cheminformatics* **2012**, *4*, 17.

[129] C. Bannwarth, S. Ehlert, S. Grimme, *J. Chem. Theory Comput.* **2019**, *15*, 1652.

[130] S. Ehlert, M. Stahn, S. Spicher, S. Grimme, *J. Chem. Theory Comput.* **2021**, *17*, 4250.

[131] S.-X. L. Luo, W. Yuan, M. Xue, H. Feng, M. J. Bezdek, T. Palacios, T. M. Swager, *ACS Nano* **2023**, *17*, 2679.

[132] M. Xue, C. Mackin, W.-H. Weng, J. Zhu, Y. Luo, S.-X. L. Luo, A.-Y. Lu, M. Hempel, E. McVay, J. Kong, T. Palacios, *Nat. Commun.* **2022**, *13*, 5064.

[133] K. M. Frazier, T. M. Swager, *Anal. Chem.* **2013**, *85*, 7154.

[134] S.-X. L. Luo, C.-J. Lin, K. H. Ku, K. Yoshinaga, T. M. Swager, *ACS Nano* **2020**, *14*, 7297.

[135] D. S. Kopchuk, A. F. Khasanov, I. S. Kovalev, G. V. Zyryanov, G. A. Kim, I. L. Nikonov, V.L. Rusinov, O. N. Chupakhin, *Chem. Heterocycl. Comp.* **2014**, *50*, 871.

[136] V. K. Cherkasov, N. O. Druzhkov, T. N. Kocherova, A. S. Shavyrin, G. K. Fukin, *Tetrahedron* **2012**, *68*, 1422.

[137] K. L. Platt, F. Oesch, *Synthesis* **1982**, *1982*, 459.

[138] W. Liu, X. Luo, Y. Bao, Y. P. Liu, G.-H. Ning, I. Abdelwahab, L. Li, C. T. Nai, Z. G. Hu, D. Zhao, B. Liu, S. Y. Quek, K. P. Loh, *Nature Chem.* **2017**, *9*, 563.

[139] Peter Murer, Thomas Gessner, Christian Eickhoff, Jan Birnstock, Falk May, Klaus Kahle, WO2016020516, **2015**.

[140] Y. Xie, T. Fujimoto, S. Dalgleish, Y. Shuku, M. M. Matsushita, K. Awaga, *J. Mater. Chem. C* **2013**, *1*, 3467.

[141] M. Putala, N. Kastner-Pustet, A. Mannschreck, *Tetrahedron: Asymmetry* **2002**, *12*, 3333.

[142] Y. Miura, Y. Ushitani, K. Inui, Y. Teki, T. Takui, K. Itoh, *Macromolecules* **1993**, *26*, 3698.

[143] A. Idelson, C. Sterzenbach, S.-S. Jester, C. Tschierske, U. Baumeister, S. Höger, *J. Am. Chem. Soc.* **2017**, *139*, 4429.

[144] V. Valderrey, E. C. Escudero-Adán, P. Ballester, *J. Am. Chem. Soc.* **2012**, *134*, 10733.

[145] I. Thomsen, K. B. G. Torssell, H. Lund, K. P. J. O'Reilly, A. Ertan, E. Kleinpeter, *Acta Chem. Scand.* **1991**, *45*, 539.

[146] A. Segade, M. Castella, F. López-Calahorra, D. Velasco, *Chem. Mater.* **2005**, *17*, 5366.

[147] Klaas Remmersen, *Dissertation*, Rheinische Friedrich-Wilhelms-Universität Bonn, Bonn, **2018**.

[148] J. Jiao, K. Hyodo, H. Hu, K. Nakajima, Y. Nishihara, *J. Org. Chem.* **2014**, *79*, 285.

[149] T. He, Z.-W. Qu, H. F. T. Klare, S. Grimme, M. Oestreich, *Angew. Chem. Int. Ed.* **2022**, *61*, e202203347.

[150] K. P. Loh, Liu Wei, WO2017180062, **2017**.

[151] Lydia Schneider, *Master Thesis*, Rheinische Friedrich-Wilhelms-Universität Bonn, Bonn, **2019**.

[152] T. Eder, J. Vogelsang, S. Bange, K. Remmerssen, D. Schmitz, S.-S. Jester, T. J. Keller, S. Höger, J. M. Lupton, *Angew. Chem. Int. Ed.* **2019**, *58*, 18898.

[153] S. Bodige, F. M. MacDonnel, *Tetrahedron Lett.* **1997**, *38*, 8159.

11. Appendix

11.1 Analytical GPC Measurements

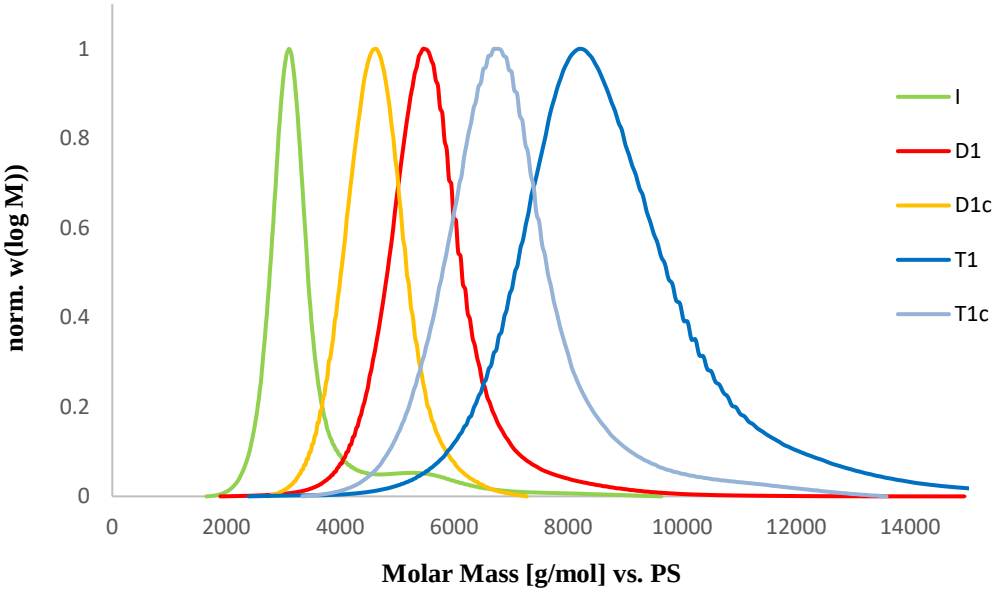

Figure 70: Molar mass distribution of the GPC-analysis of monomer **I** (bright green), dimer $\mathbf{D_1}$ (red) and trimer $\mathbf{T_1}$ (blue), as well as the respective cylindrical structures $\mathbf{D_{1c}}$ (orange) and $\mathbf{T_{1c}}$ (bright blue) (all calibrated against a polystyrene standard).[102]

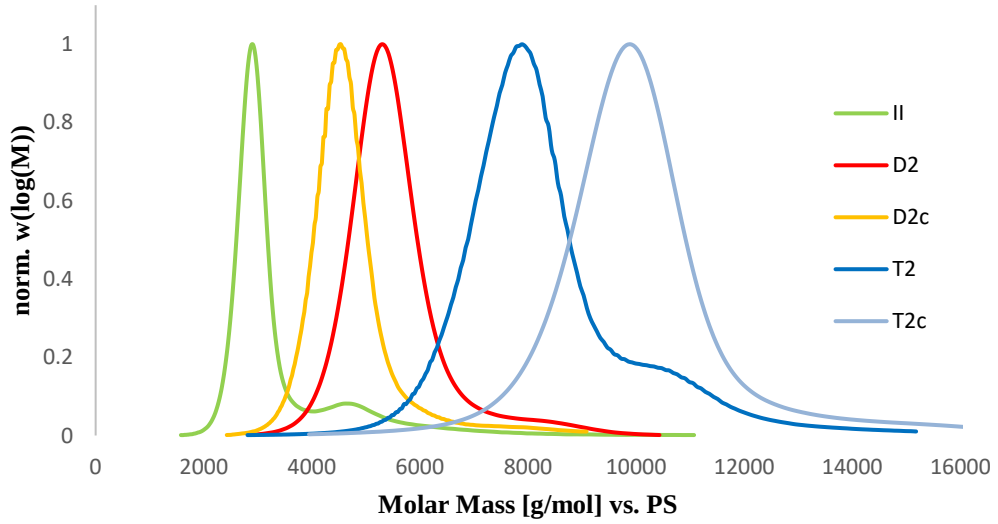

Figure 71: Molar mass distribution of the GPC-analysis of monomer **II** (bright green), dimer $\mathbf{D_2}$ (red) and trimer $\mathbf{T_2}$ (blue), as well as the respective pyramidal structures $\mathbf{D_{2c}}$ (orange) and $\mathbf{T_{2c}}$ (bright blue) (all calibrated against a polystyrene standard).

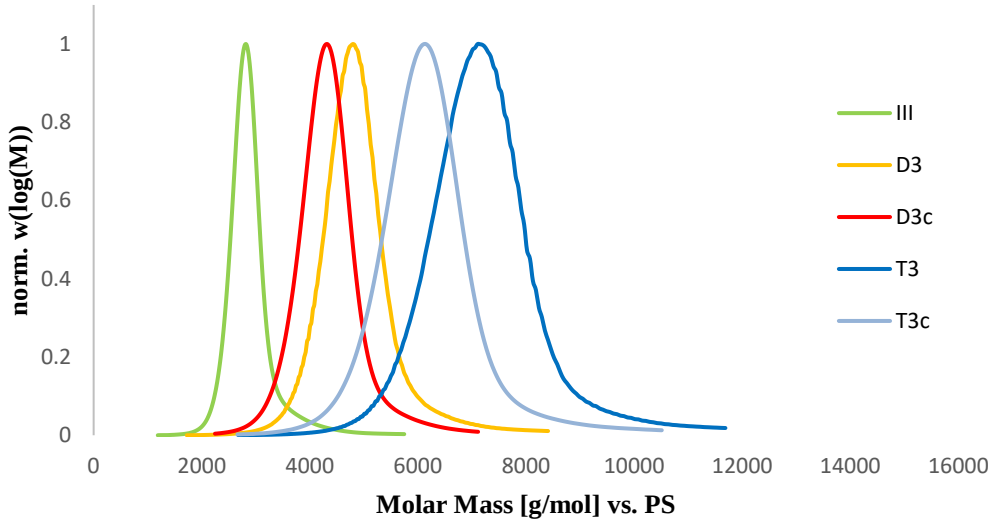

Figure 72: Molar mass distribution of the GPC-analysis of monomer **III** (bright green), dimer **D$_3$** (red) and trimer **T$_3$** (blue), as well as the respective bowl-shaped structures **D$_{3c}$** (orange) and **T$_{3c}$** (bright blue) (all calibrated against a polystyrene standard).

11.2 UV/Vis and Fluorescence Spectra

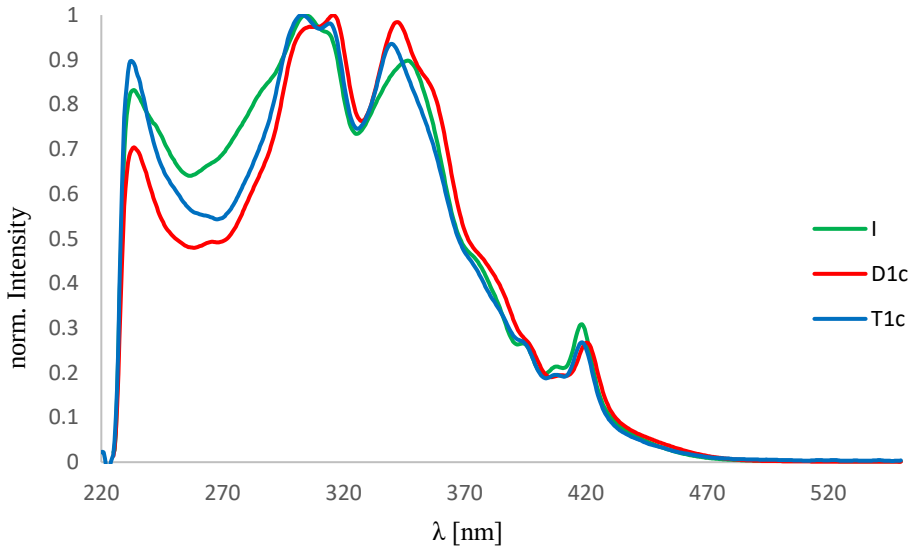

Figure 73: *UV/Vis*-absorption spectra of monomer **I** (green, λ_{max} = 304.5 nm), as well as the PNTs **D$_{1c}$** (red, λ_{max} = 315.5 nm) and **T$_{1c}$** (blue, λ_{max} = 303.0 nm) (all measured in dichloromethane).[102]

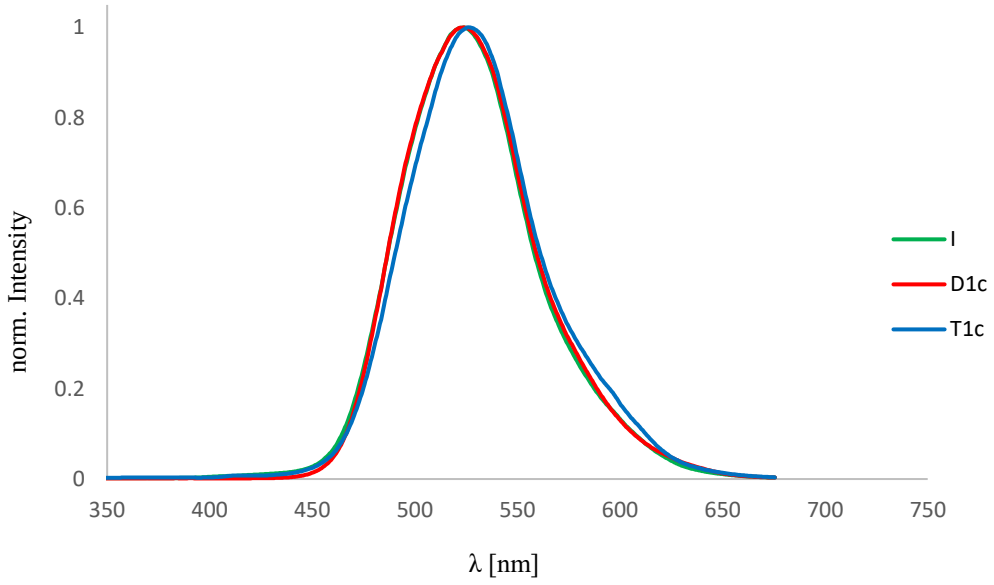

Figure 74: Fluorescence emission spectra of monomer **I** (green, λ_{em} = 523.5 nm), as well as the PNTs $\mathbf{D_{1c}}$ (red, λ_{em} = 523.5 nm) and $\mathbf{T_{1c}}$ (blue, λ_{em} = 525.5 nm) (all measured in dichloromethane); the maximum of intensity found in the *UV/Vis*-absorption spectra were used as excitation wavelengths, respectively.[102]

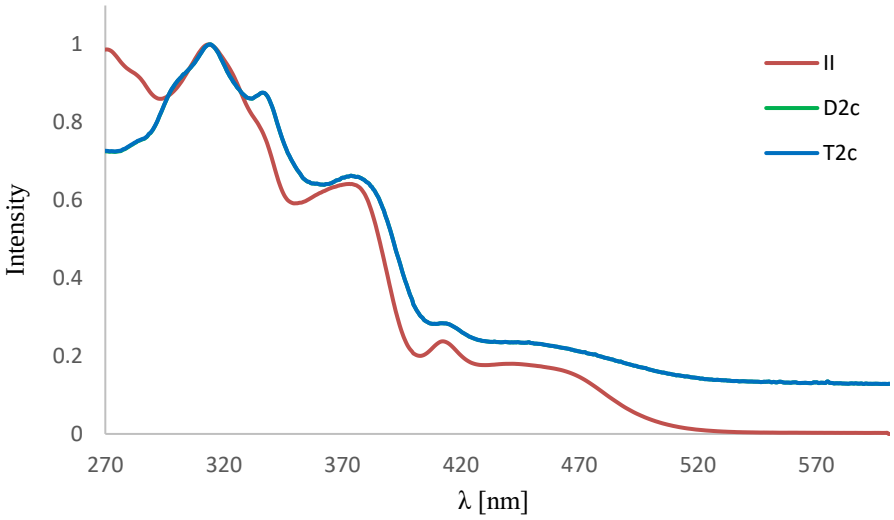

Figure 75: *UV/Vis*-absorption spectra of monomer **II** (brown, λ_{max} = 313.5 nm), as well as the PNTs $\mathbf{D_{2c}}$ (green, λ_{max} = 314.5 nm) and $\mathbf{T_{2c}}$ (blue, λ_{max} = 314.5 nm) (all measured in dichloromethane).

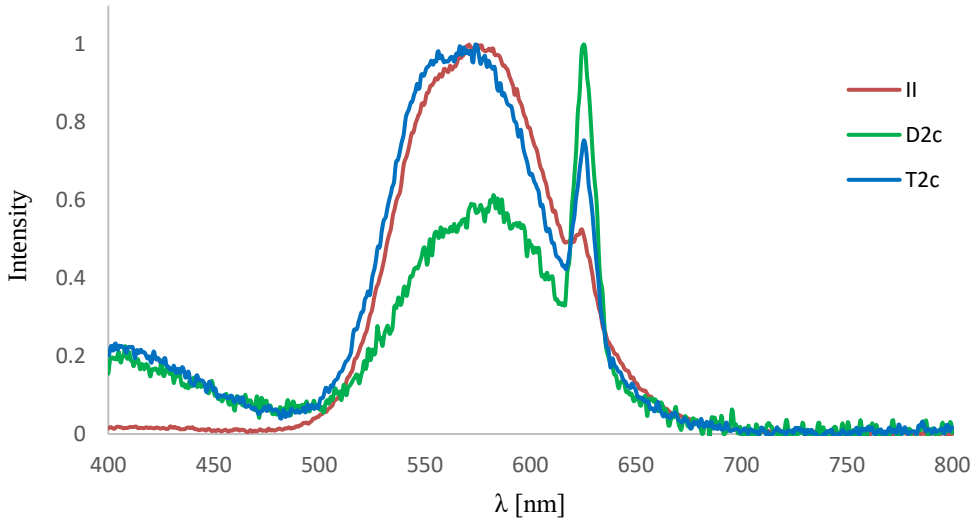

Figure 76: Fluorescence emission spectra of monomer **II** (brown, λ_{em} = 571.0 nm), as well as the PNTs $\mathbf{D_{2c}}$ (green, λ_{em} = 582.5 nm) and $\mathbf{T_{2c}}$ (blue, λ_{em} = 574.0 nm) (all measured in dichloromethane); the maximum of intensity found in the *UV/Vis*-absorption spectra were used as excitation wavelengths, respectively.

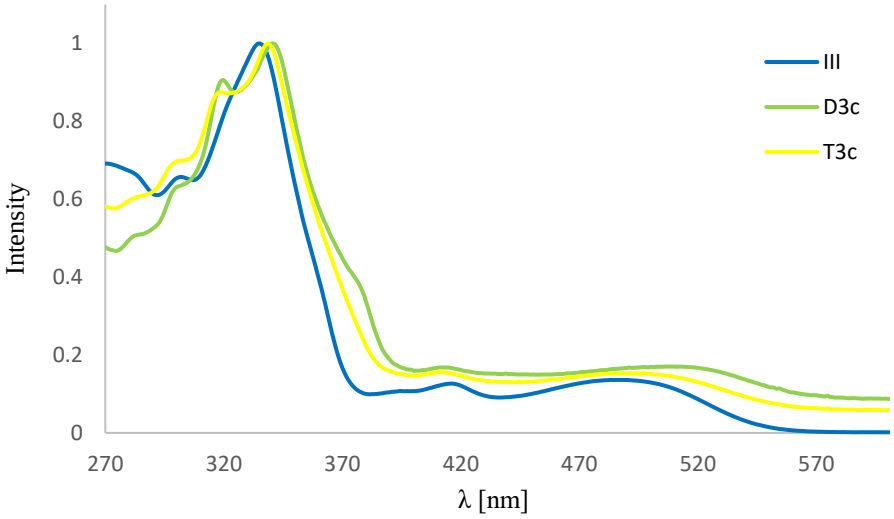

Figure 77: *UV/Vis*-absorption spectra of monomer **III** (blue, λ_{max} = 335.0 nm), as well as the PNTs $\mathbf{D_{3c}}$ (bright green, λ_{max} = 340.5 nm) and $\mathbf{T_{3c}}$ (yellow, λ_{max} = 338.5 nm) (all measured in dichloromethane).

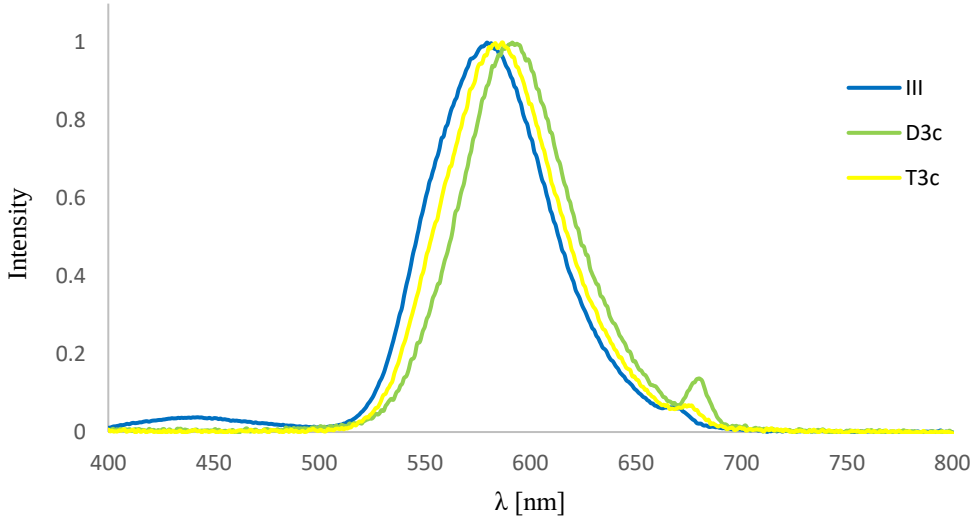

Figure 78: Fluorescence emission spectra of monomer **III** (blue, λ_{em} = 579.5 nm), as well as the PNTs **D$_{3c}$** (bright green, λ_{em} = 591.5 nm) and **T$_{3c}$** (yellow, λ_{em} = 586.5 nm) (all measured in dichloromethane); the maximum of intensity found in the *UV/Vis*-absorption spectra were used as excitation wavelengths, respectively.

11.3 ^{1}H- and ^{13}C-NMR Spectra

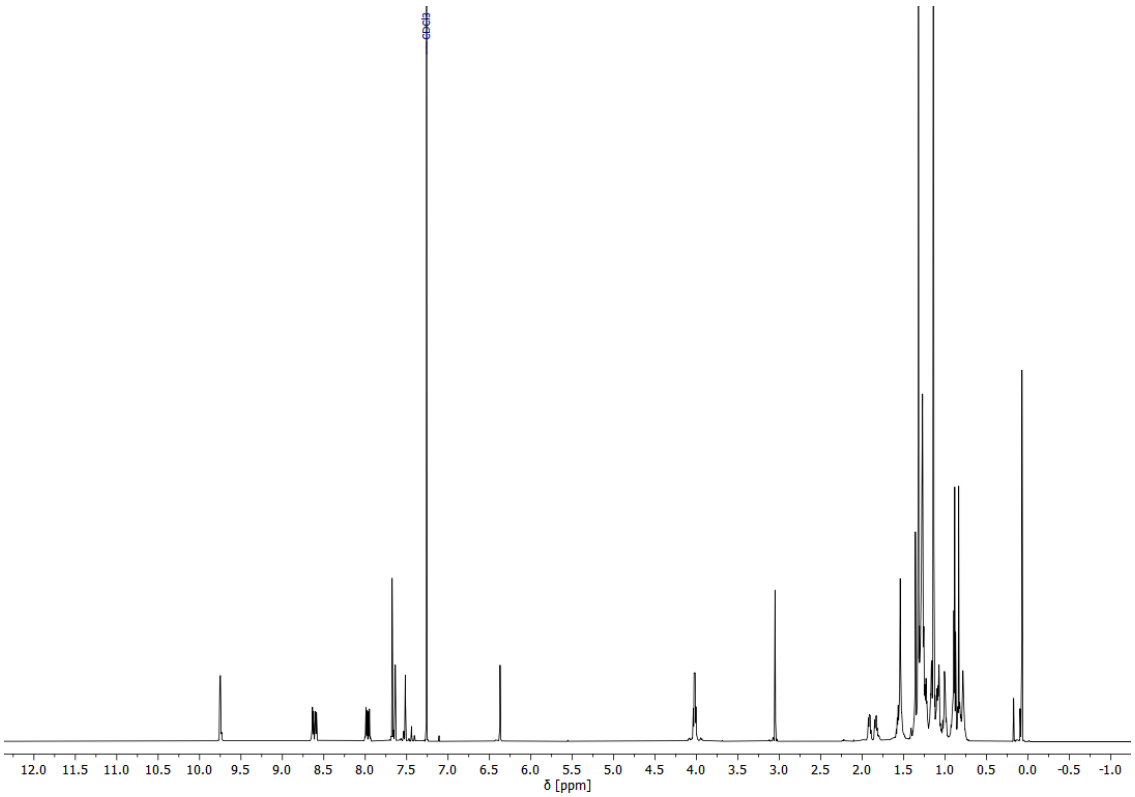

Figure 79: ^{1}H-NMR spectrum of **I** (700 MHz, $CDCl_3$, 298 K).[102]

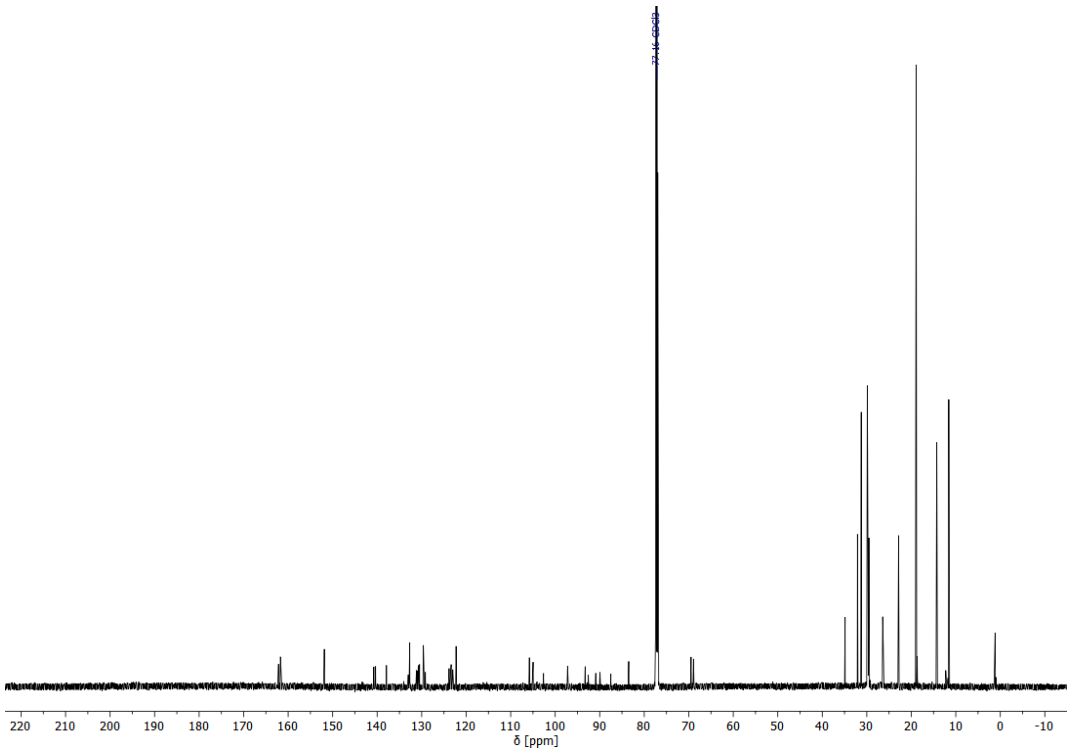

Figure 80: ^{13}C-NMR spectrum of **I** (176 MHz, $CDCl_3$, 298 K).[102]

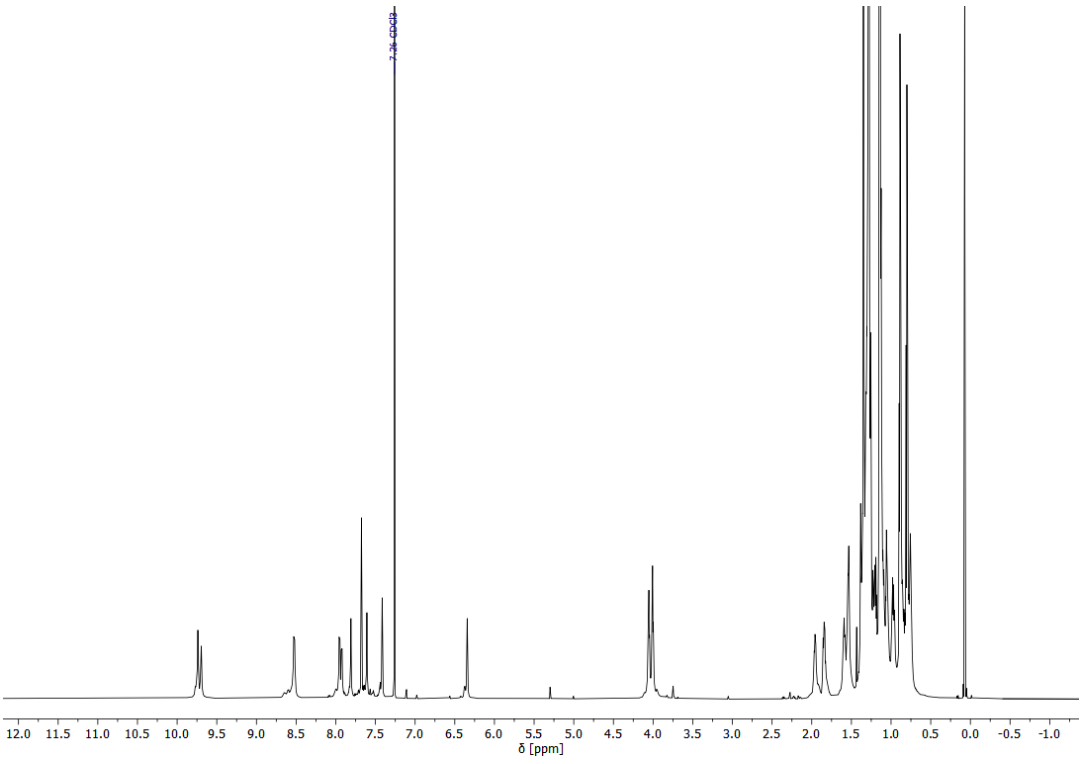

Figure 81: ^{1}H-NMR spectrum of **D$_1$** (700 MHz, $CDCl_3$, 298 K).

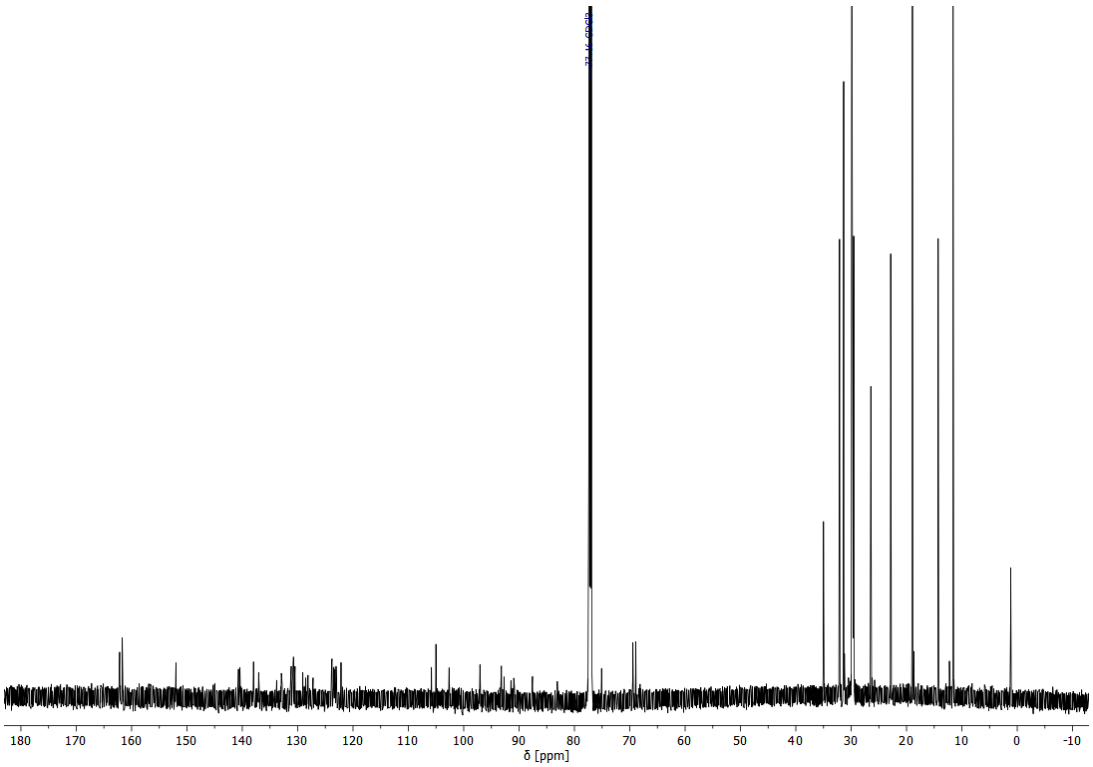

Figure 82: ^{13}C-NMR spectrum of **D₁** (176 MHz, $CDCl_3$, 298 K).

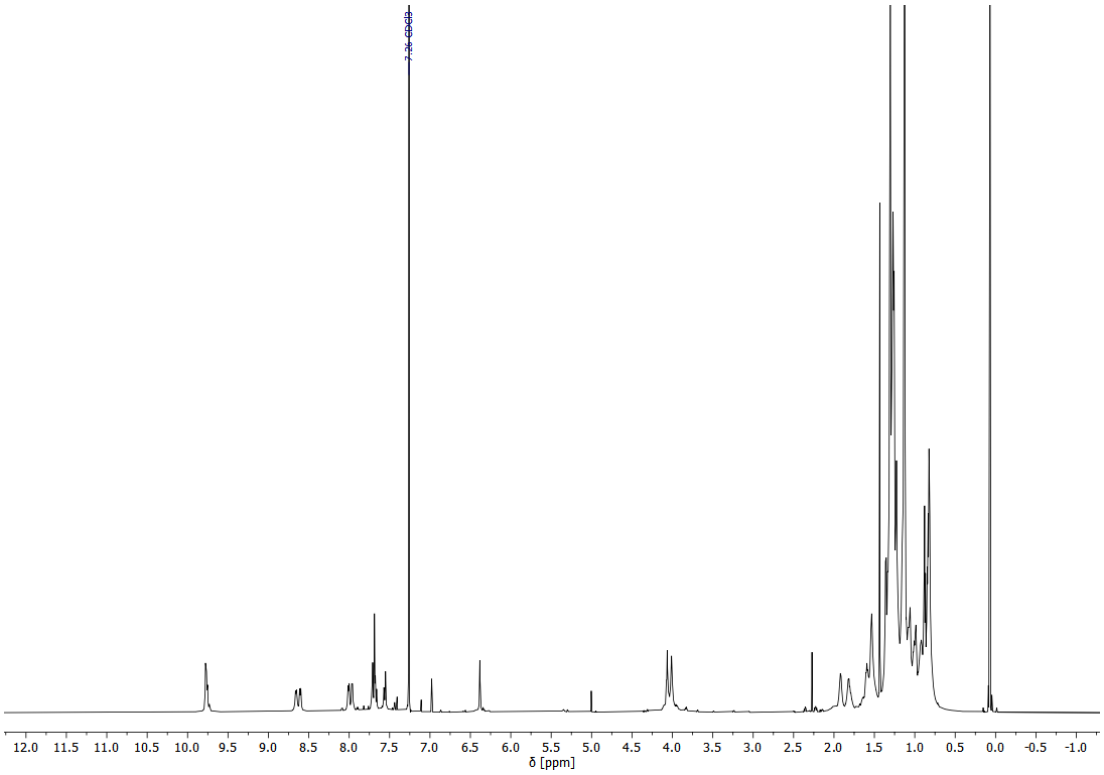

Figure 83: ^{1}H-NMR spectrum of **T₁** (700 MHz, $CDCl_3$, 298 K).

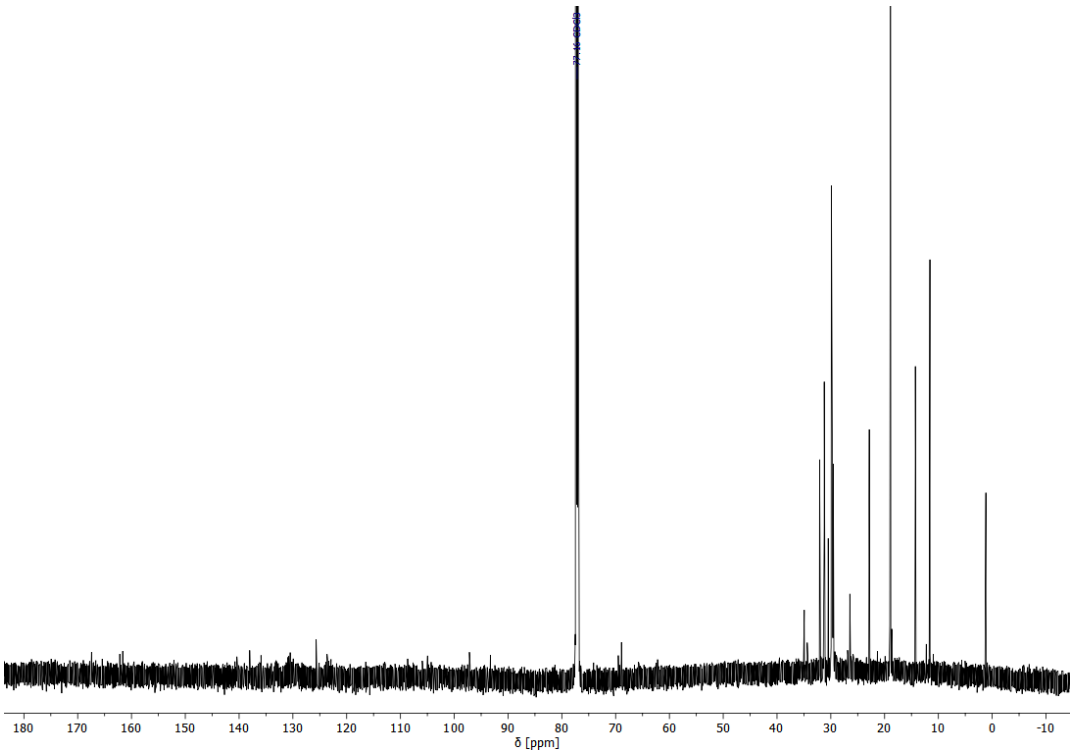

Figure 84: ^{13}C-NMR spectrum of **T₁** (176 MHz, $CDCl_3$, 298 K).

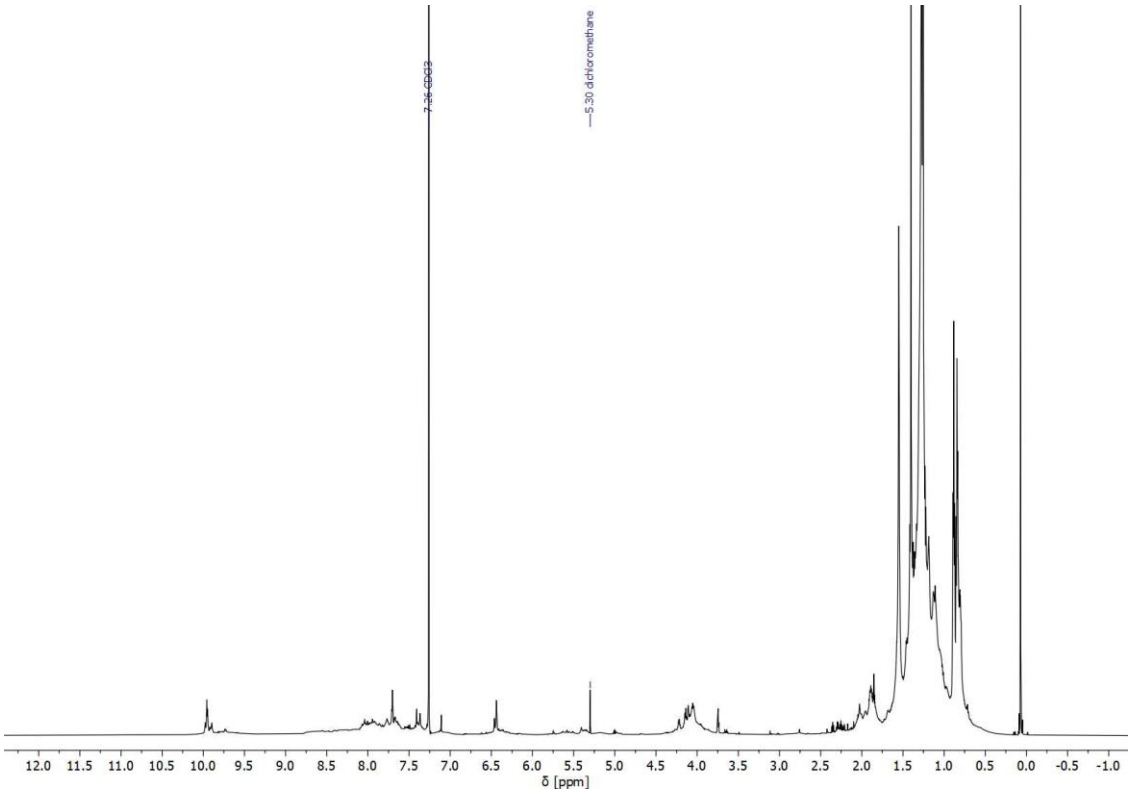

Figure 85: ^{1}H-NMR spectrum of **D₁c** (700 MHz, $CDCl_3$, 298 K).[102]

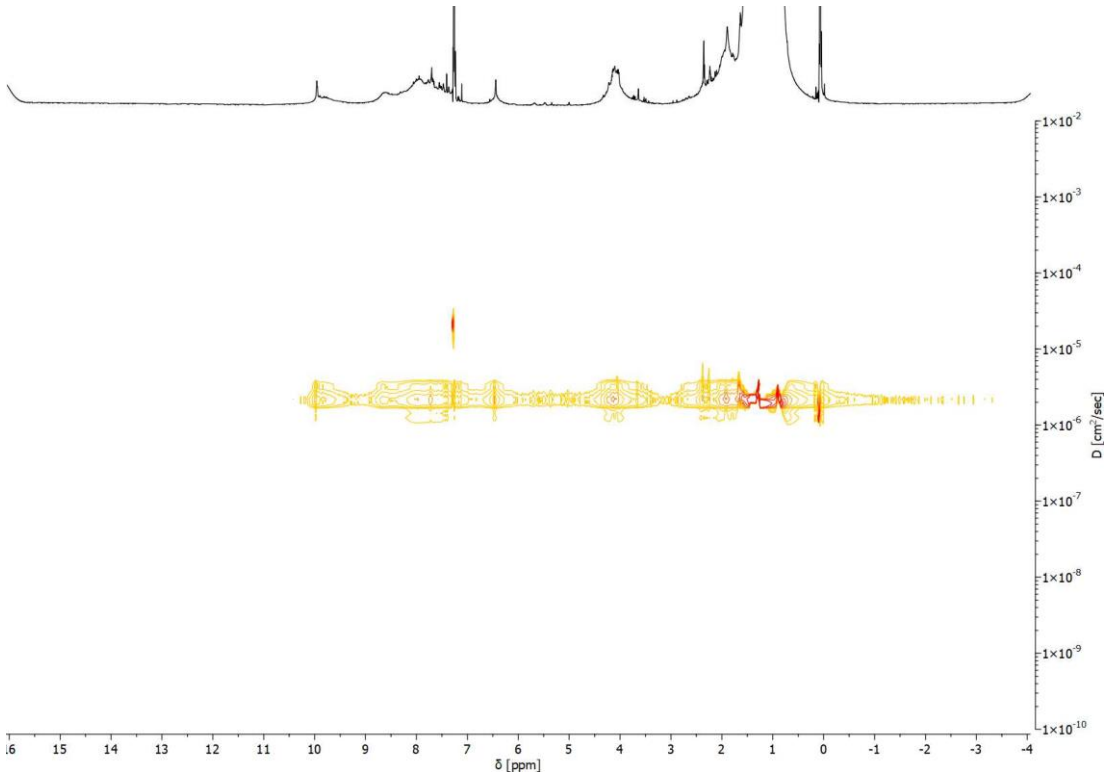

Figure 86: DOSY-NMR spectrum of **D_{1c}** (700 MHz, $CDCl_3$, 298 K).[102]

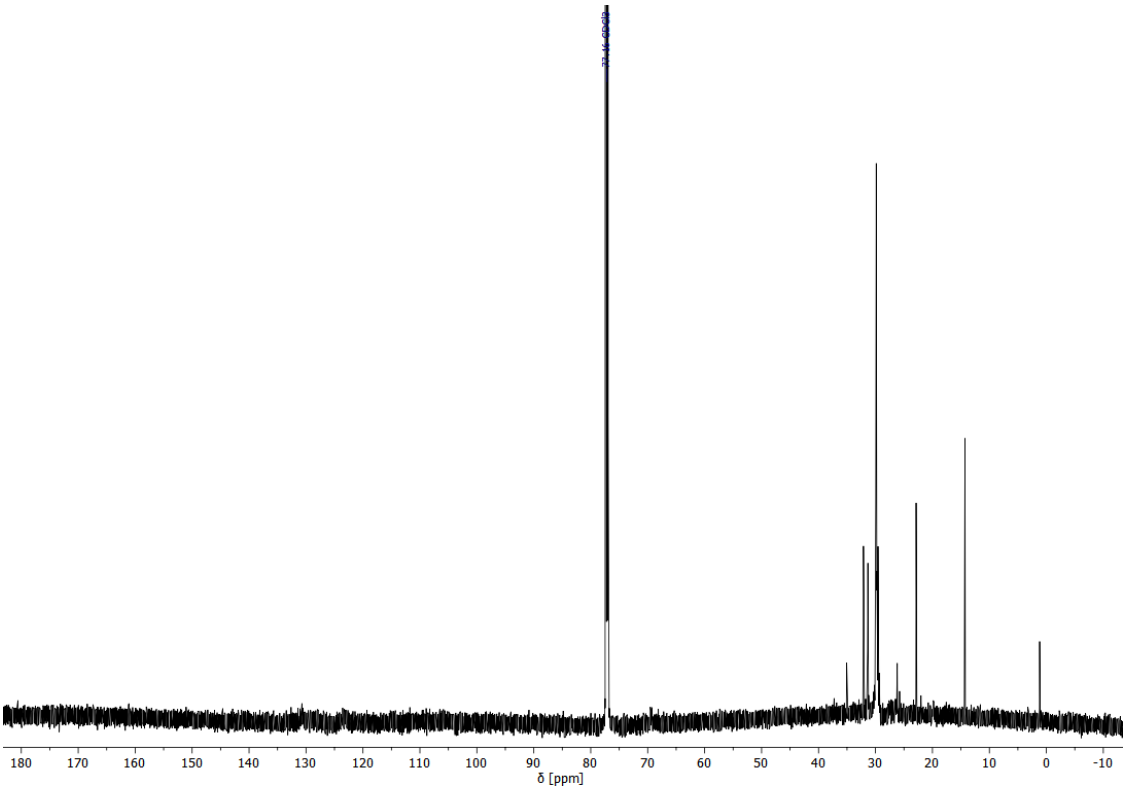

Figure 87: ^{13}C-NMR spectrum of **D_{1c}** (176 MHz, $CDCl_3$, 298 K).

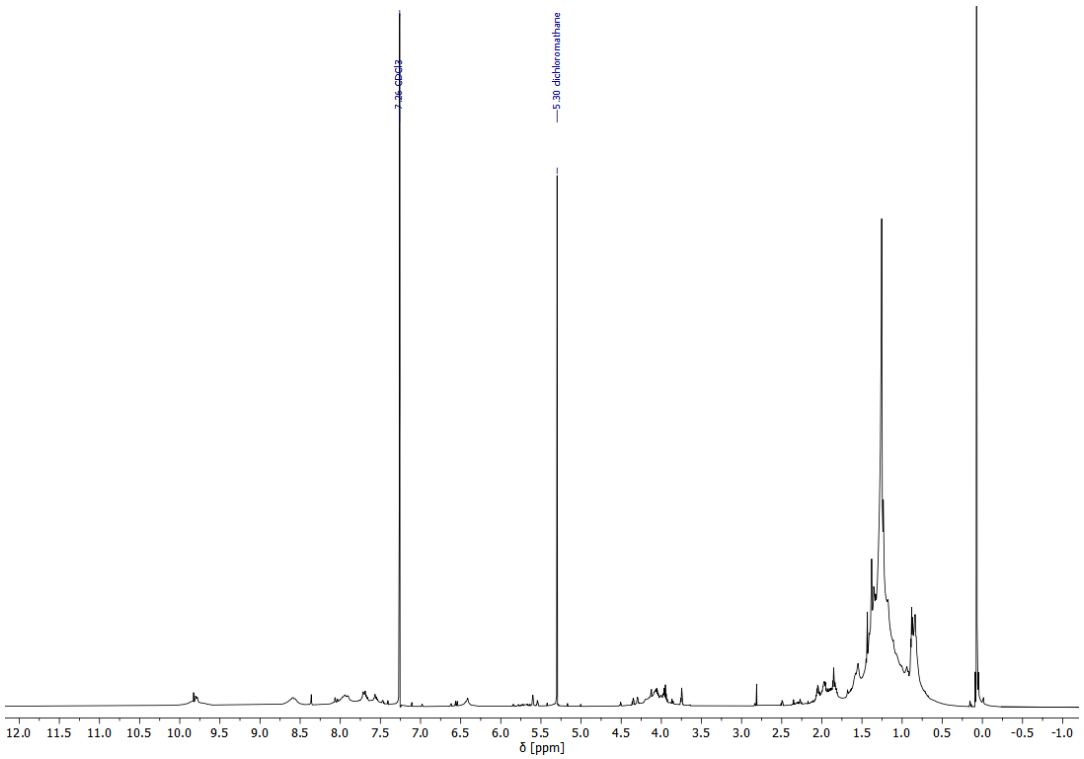

Figure 88: ^{1}H-NMR spectrum of **T$_{1c}$** (700 MHz, $CDCl_3$, 298 K).

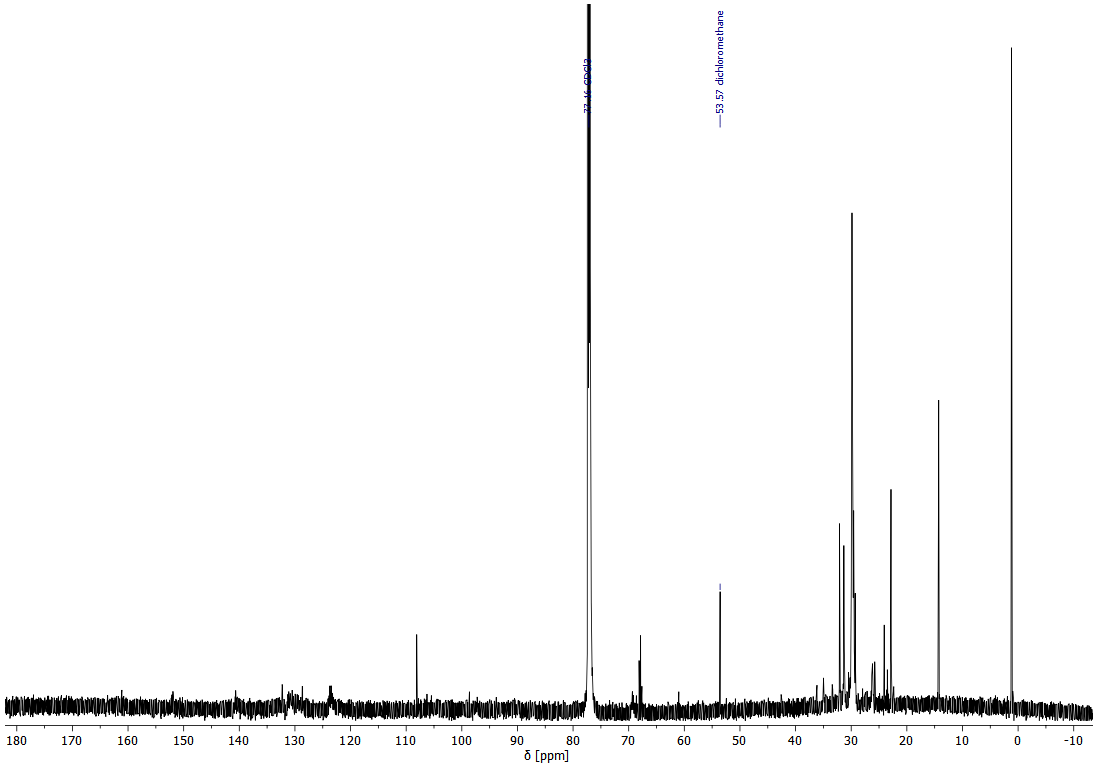

Figure 89: ^{13}C-NMR spectrum of **T$_{1c}$** (176 MHz, $CDCl_3$, 298 K).

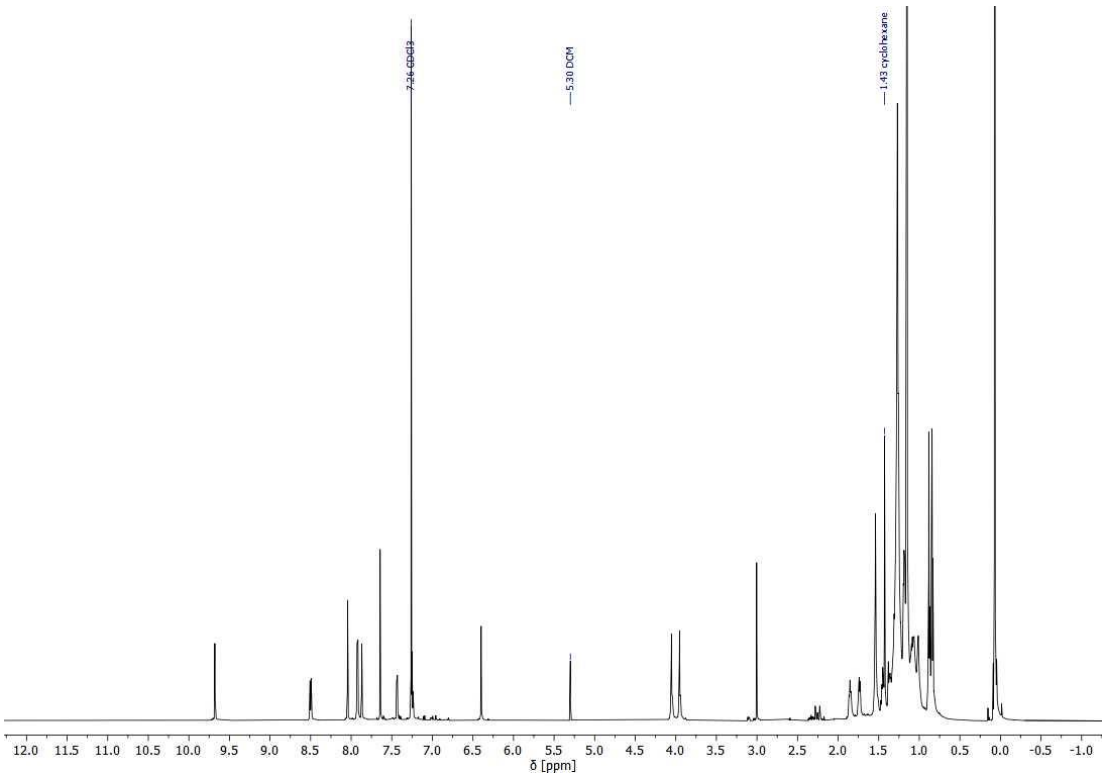

Figure 90: ^{1}H-NMR spectrum of **II** (700 MHz, $CDCl_3$, 298 K).

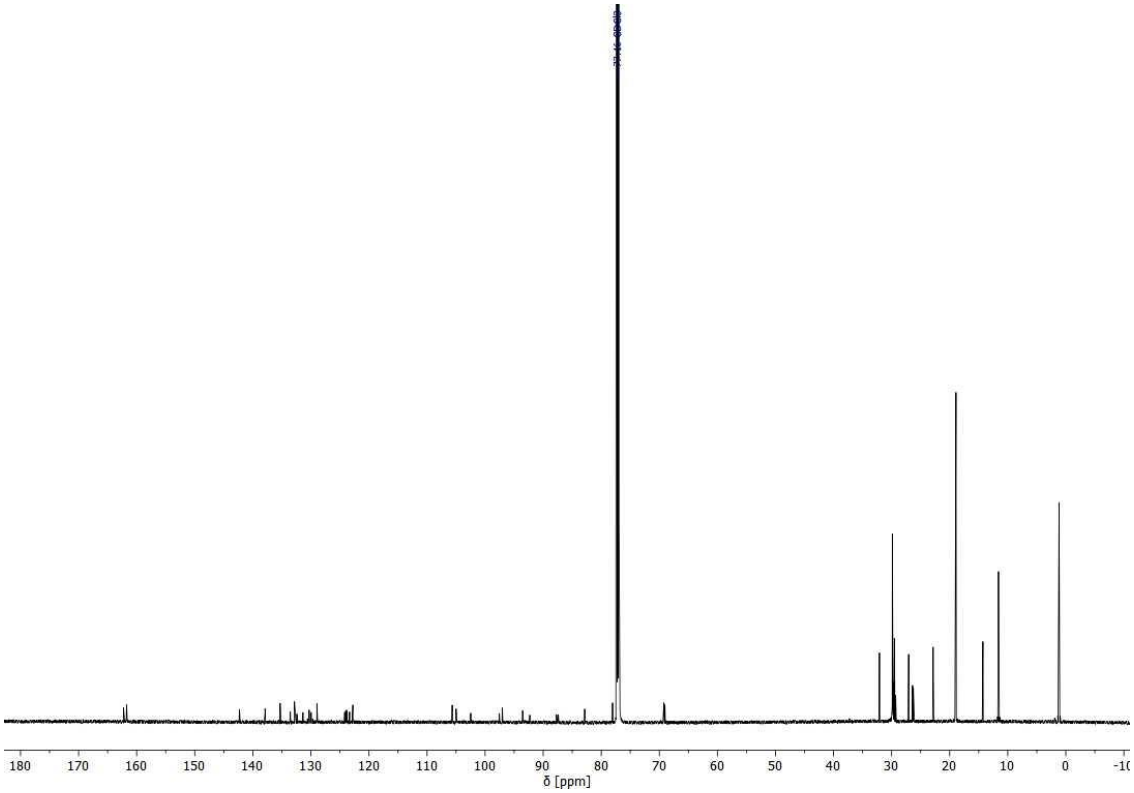

Figure 91: ^{13}C-NMR spectrum of **II** (176 MHz, $CDCl_3$, 298 K).

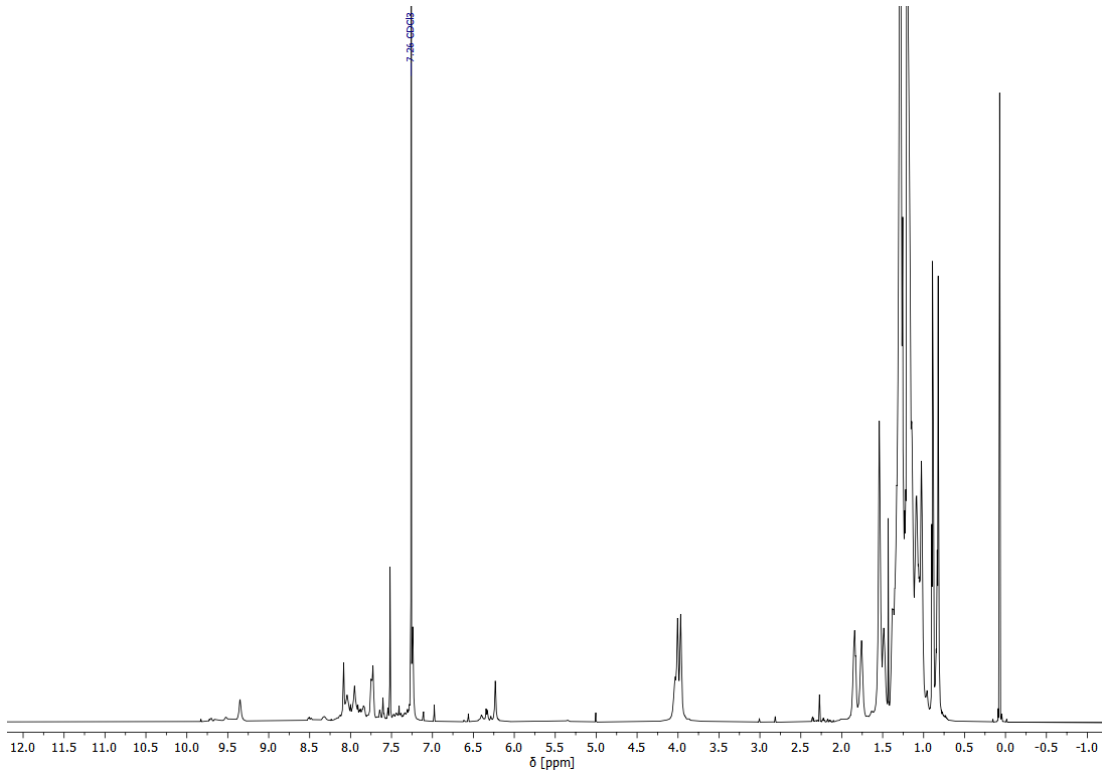

Figure 92: ^{1}H-NMR spectrum of **D2** (700 MHz, $CDCl_3$, 298 K).

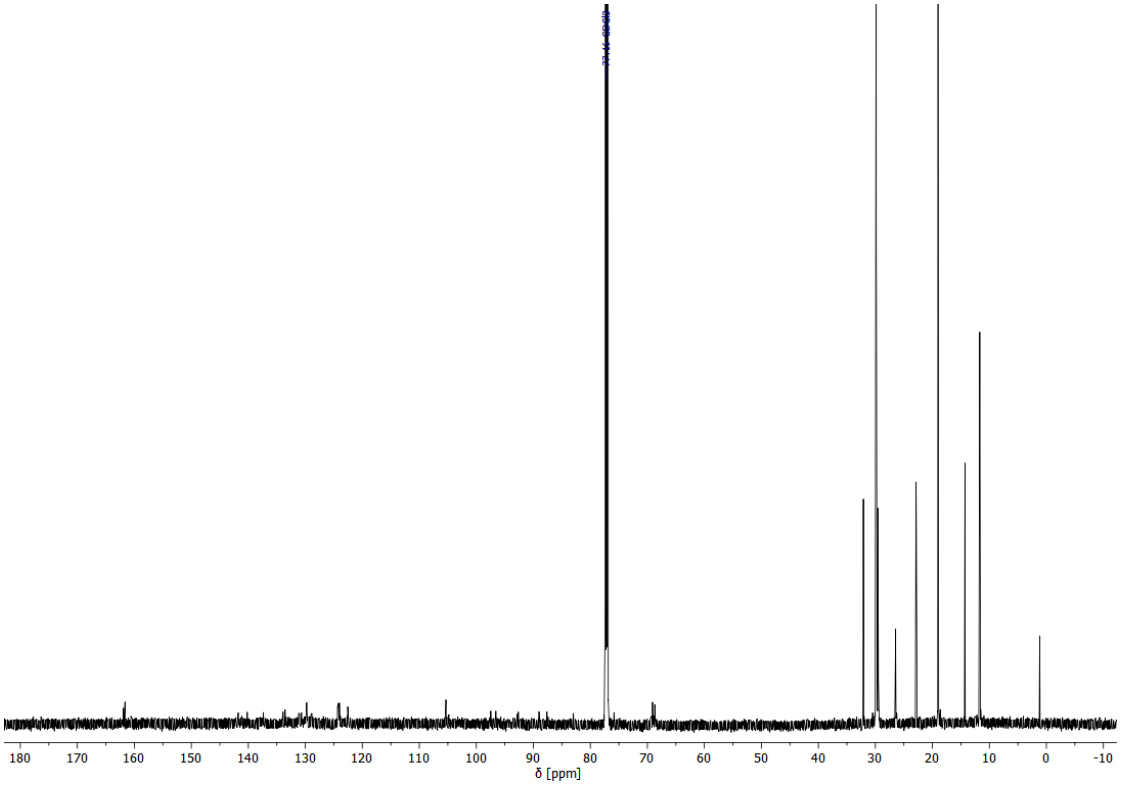

Figure 93: ^{13}C-NMR spectrum of **D2** (176 MHz, $CDCl_3$, 298 K).

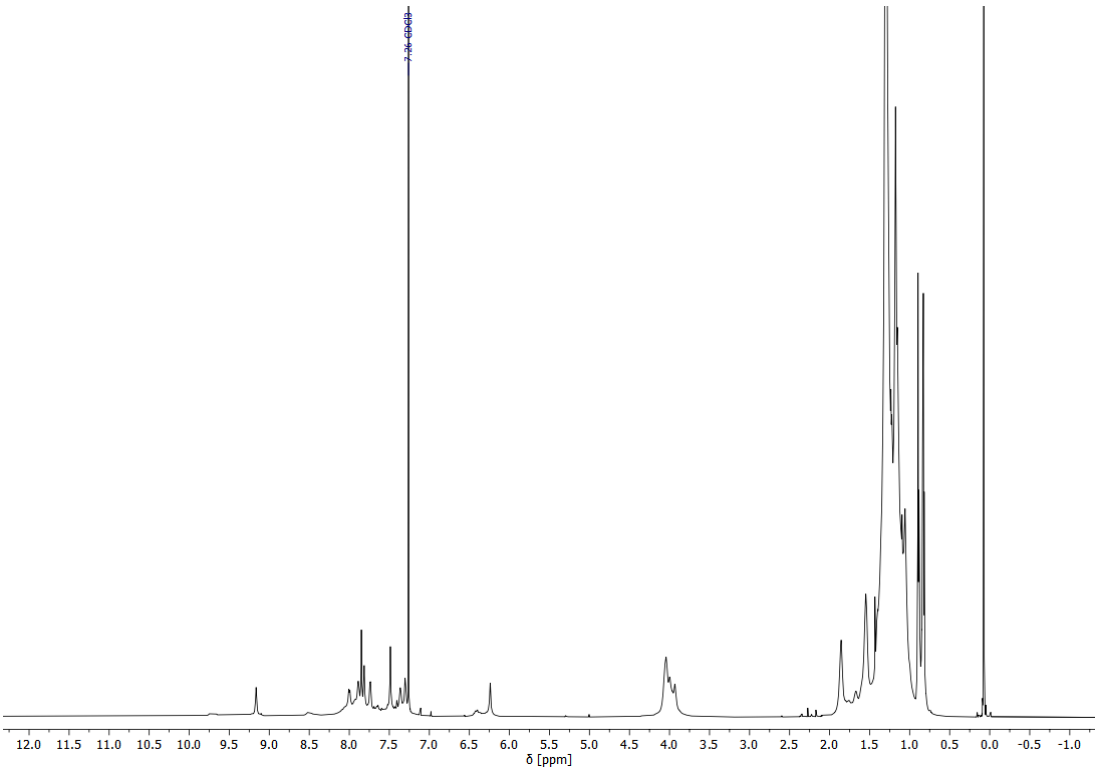

Figure 94: ^{1}H-NMR spectrum of **T₂** (700 MHz, $CDCl_3$, 298 K).

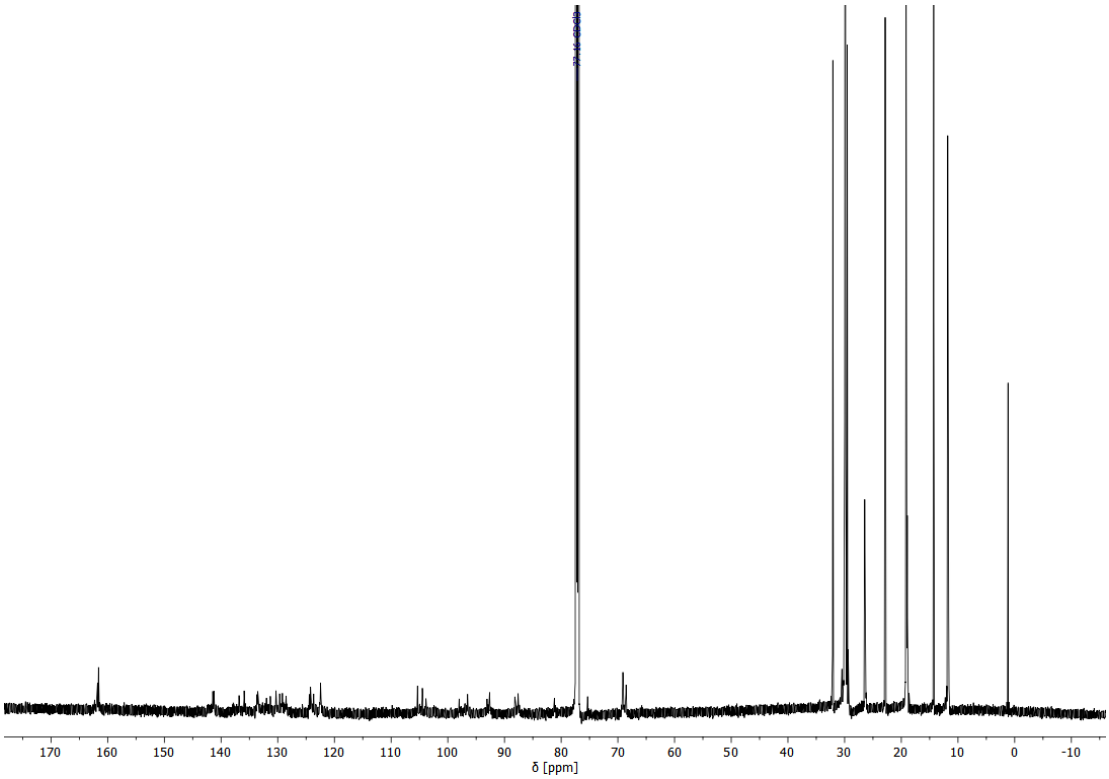

Figure 95: ^{13}C-NMR spectrum of **T₂** (176 MHz, $CDCl_3$, 298 K).

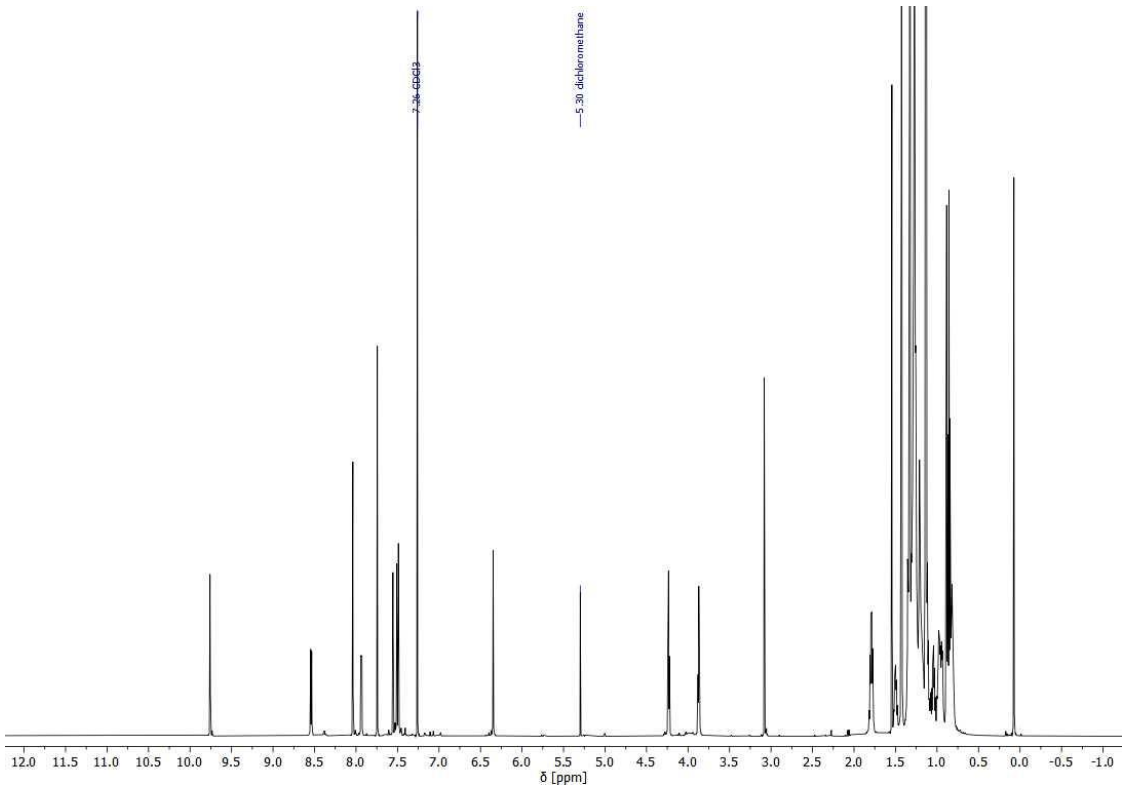

Figure 96: ^{1}H-NMR spectrum of **III** (700 MHz, $CDCl_3$, 298 K).

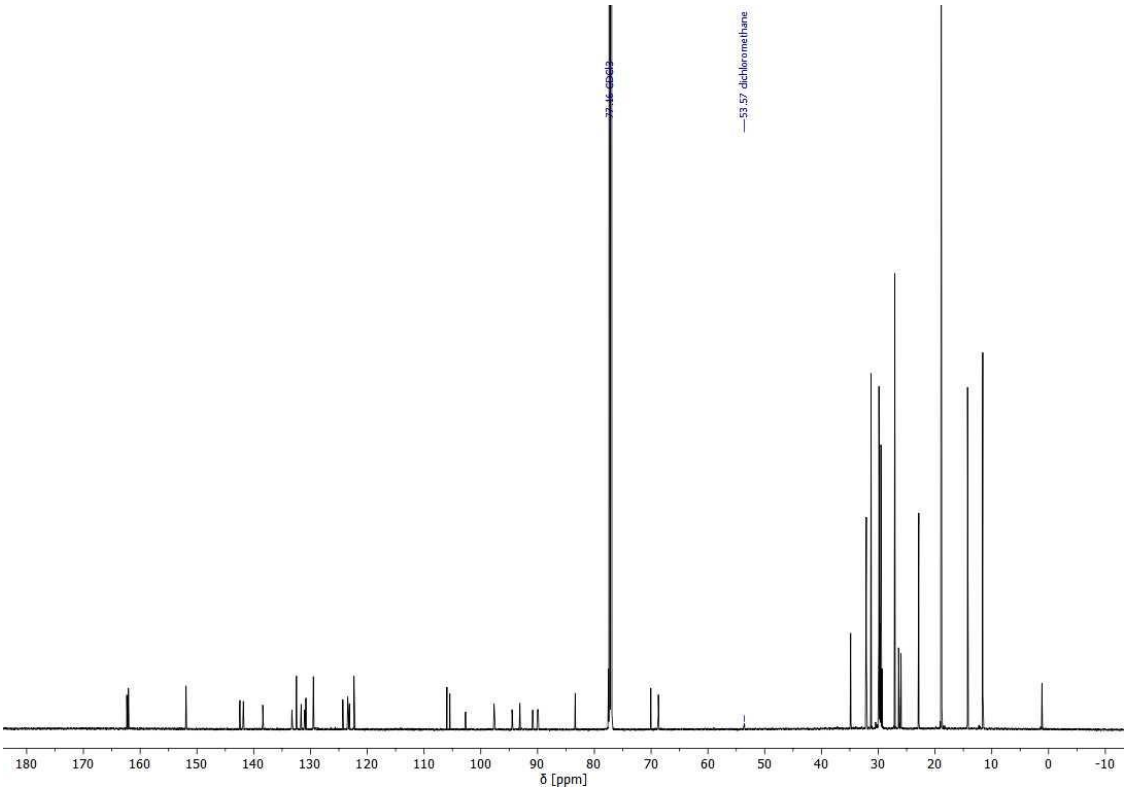

Figure 97: ^{13}C-NMR spectrum of **III** (176 MHz, $CDCl_3$, 298 K).

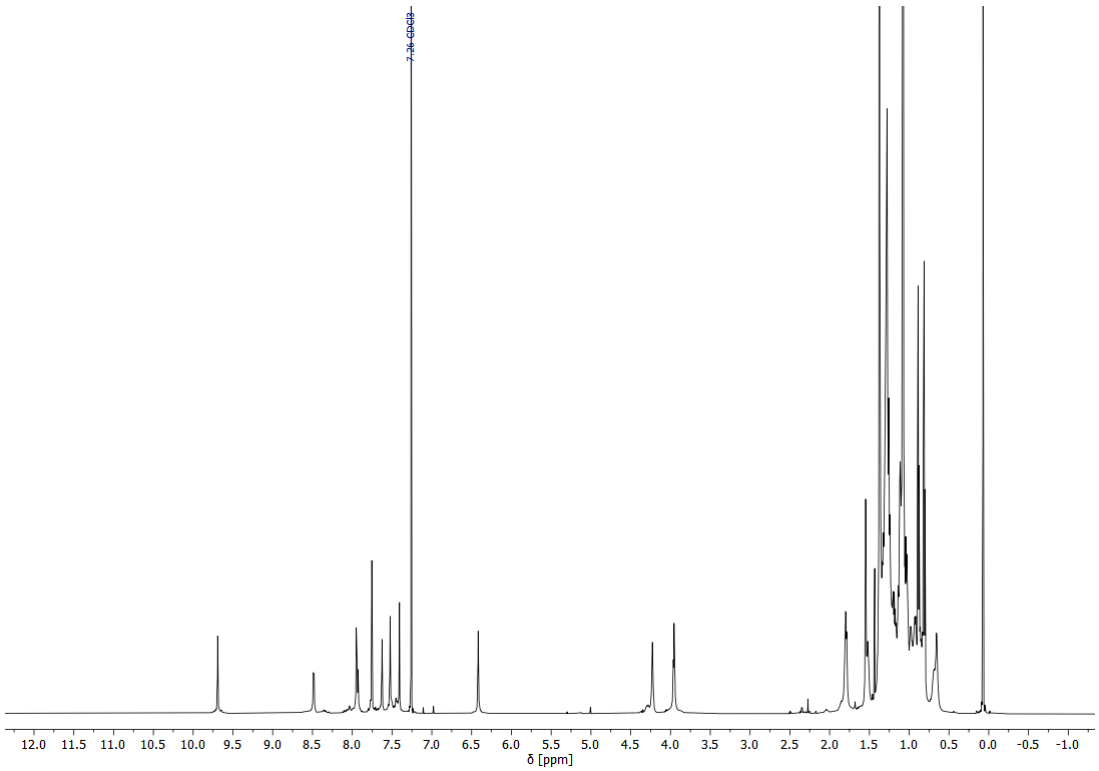

Figure 98: ^{1}H-NMR spectrum of **D3** (700 MHz, $CDCl_3$, 298 K).

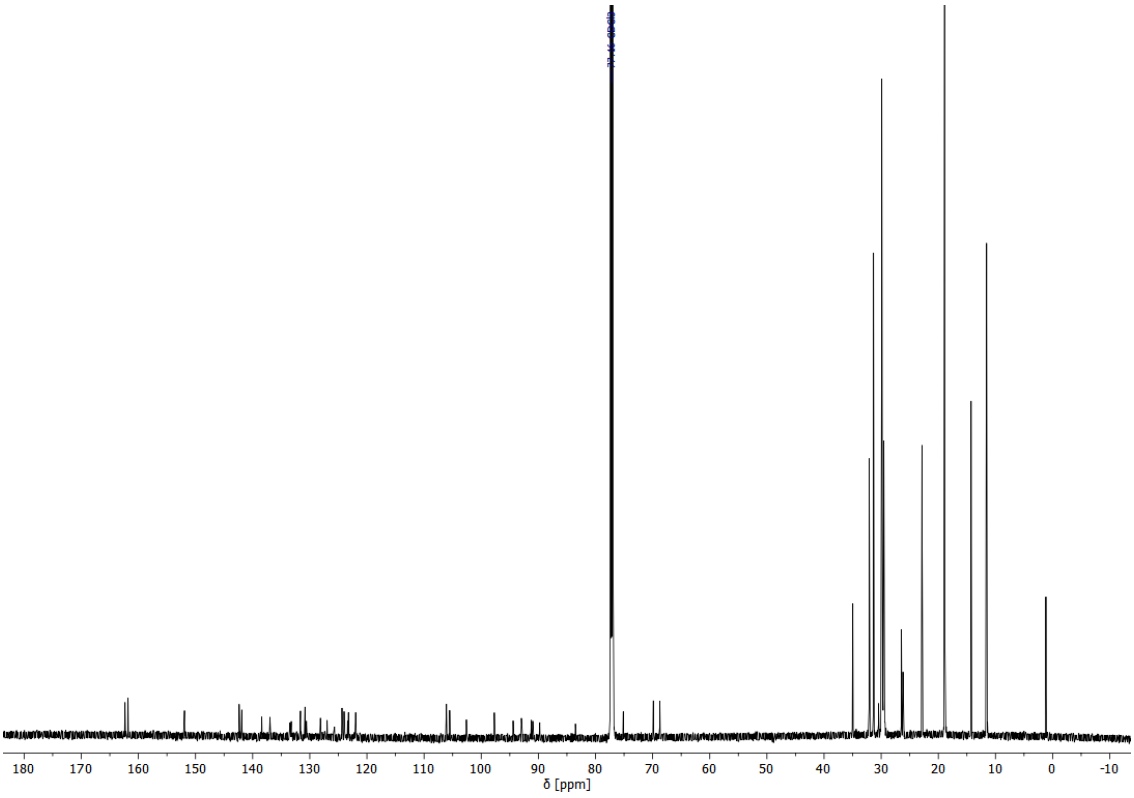

Figure 99: ^{13}C-NMR spectrum of **D3** (176 MHz, $CDCl_3$, 298 K).

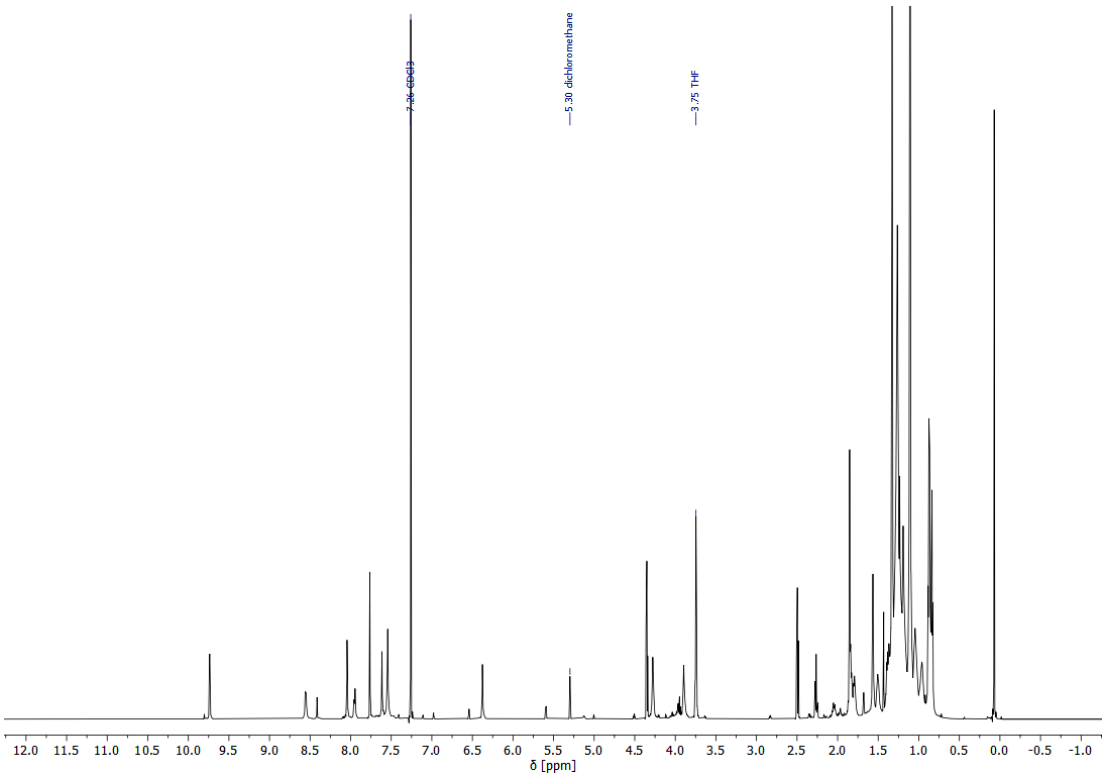

Figure 100: ^{1}H-NMR spectrum of **T$_3$** (700 MHz, $CDCl_3$, 298 K).

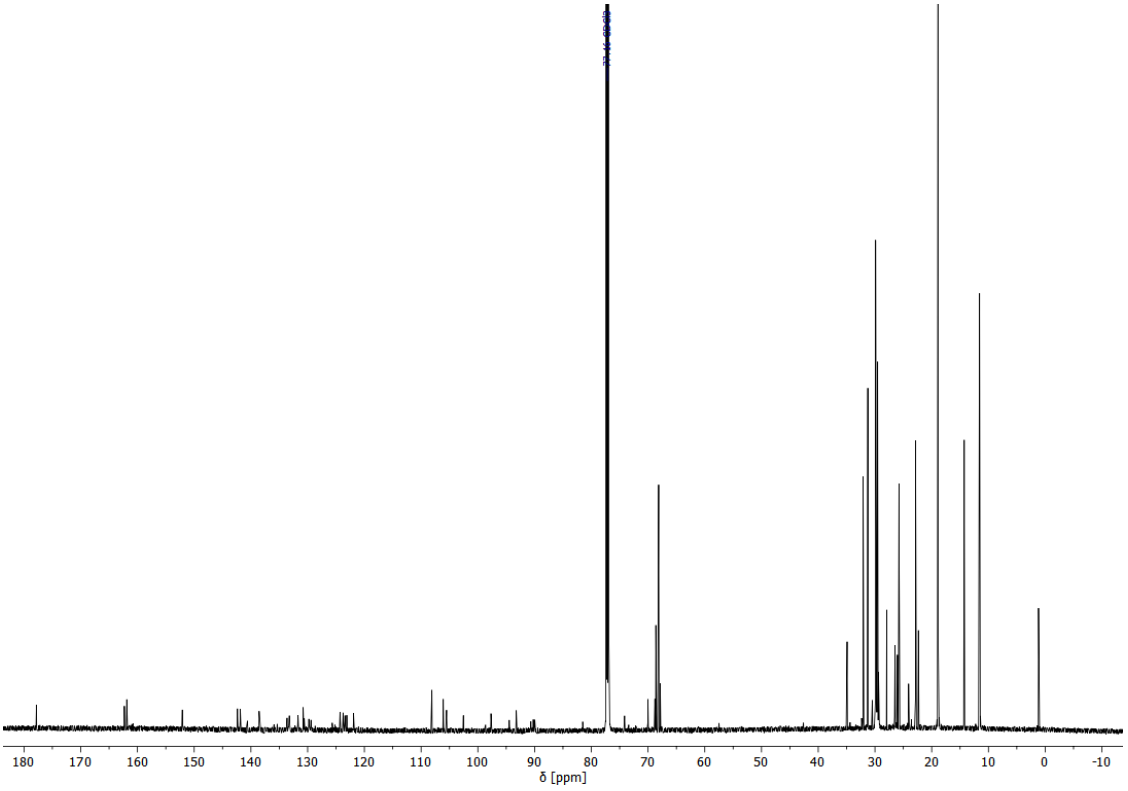

Figure 101: ^{13}C-NMR spectrum of **T$_3$** (176 MHz, $CDCl_3$, 298 K).

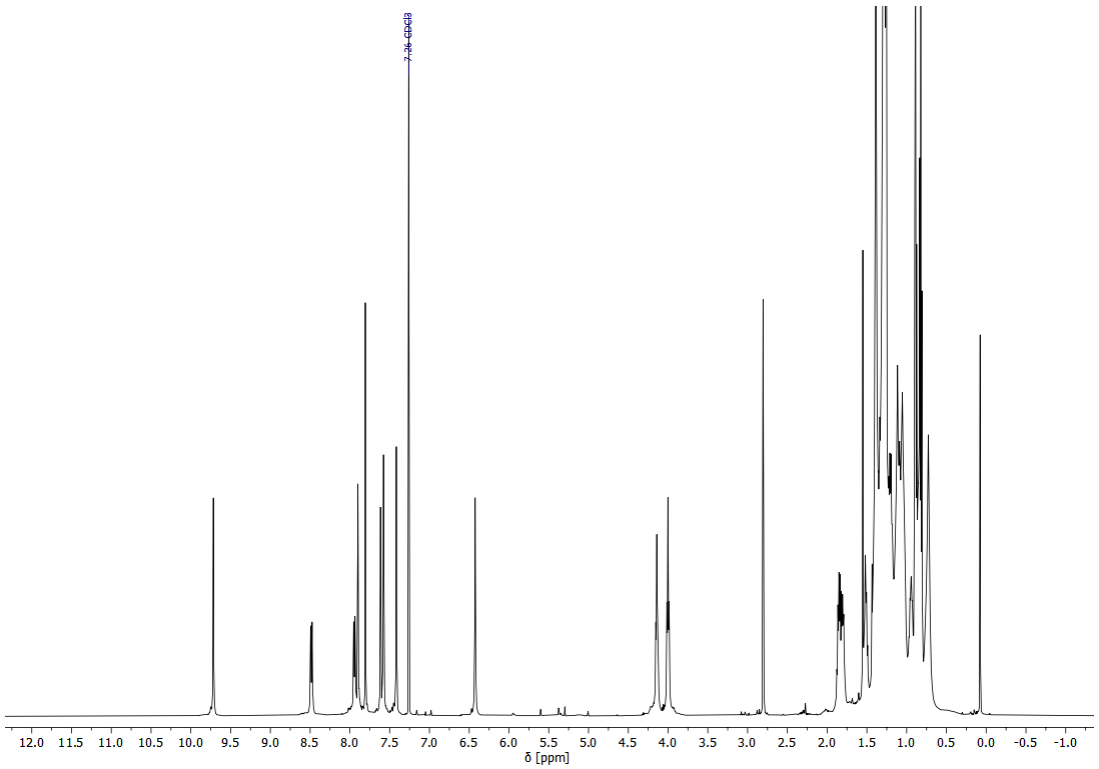

Figure 102: ^{1}H-NMR spectrum of **D$_{3d}$** (500 MHz, $CDCl_3$, 298 K).

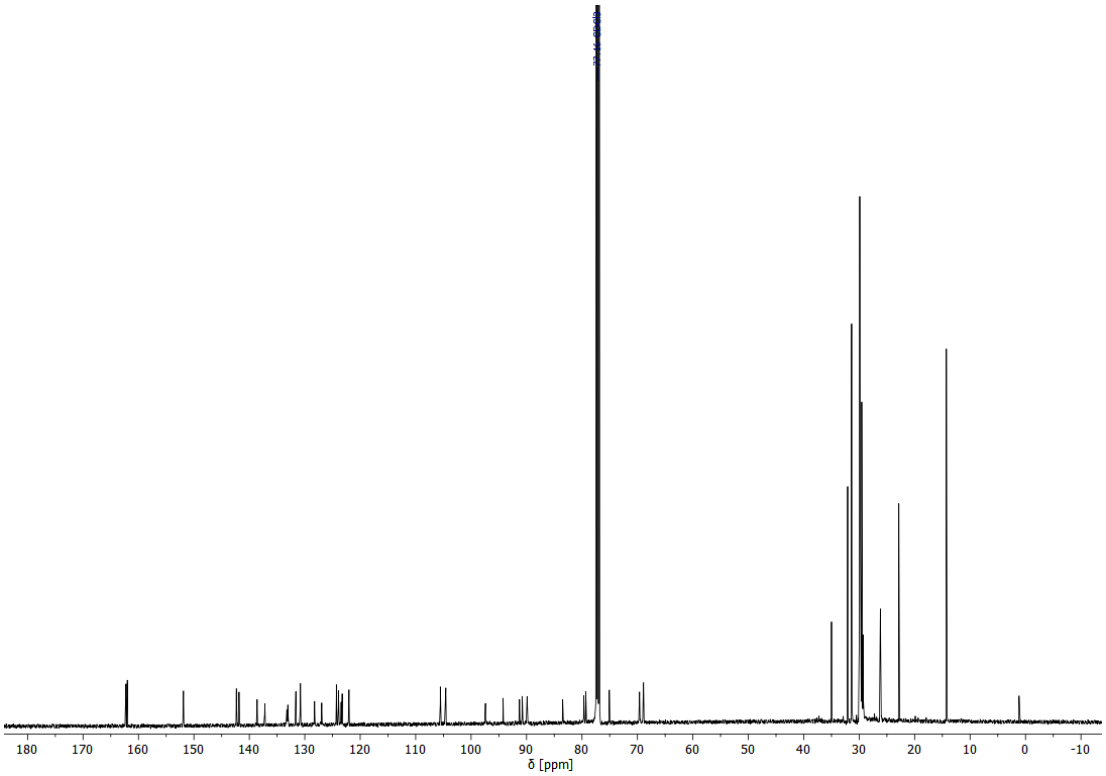

Figure 103: ^{13}C-NMR spectrum of **D$_{3d}$** (126 MHz, $CDCl_3$, 298 K).

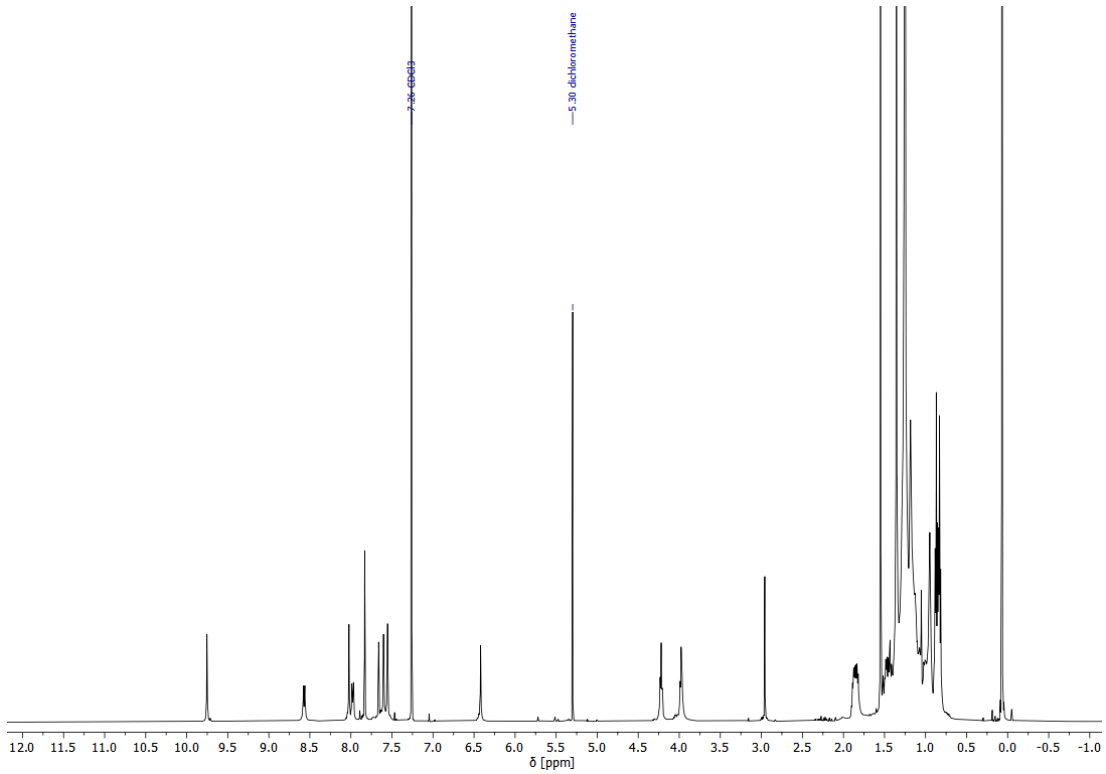

Figure 104: ^{1}H-NMR spectrum of **T$_{3d}$** (500 MHz, $CDCl_3$, 298 K).

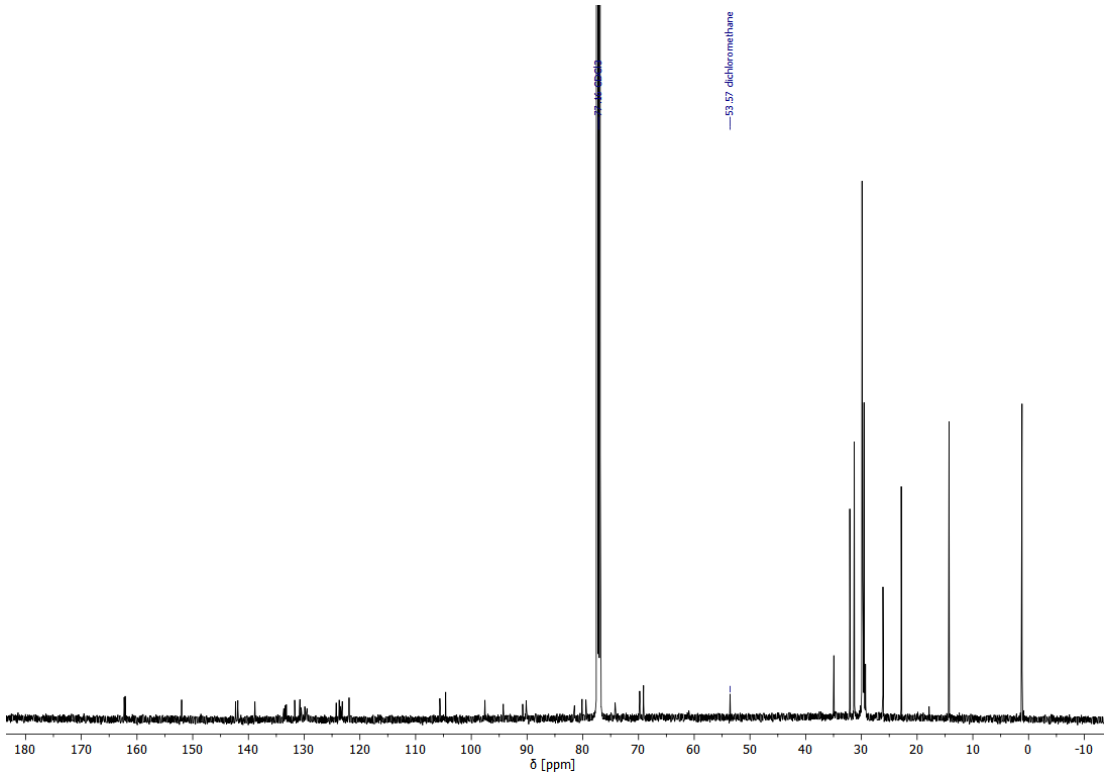

Figure 105: ^{13}C-NMR spectrum of **T$_{3d}$** (126 MHz, $CDCl_3$, 298 K).

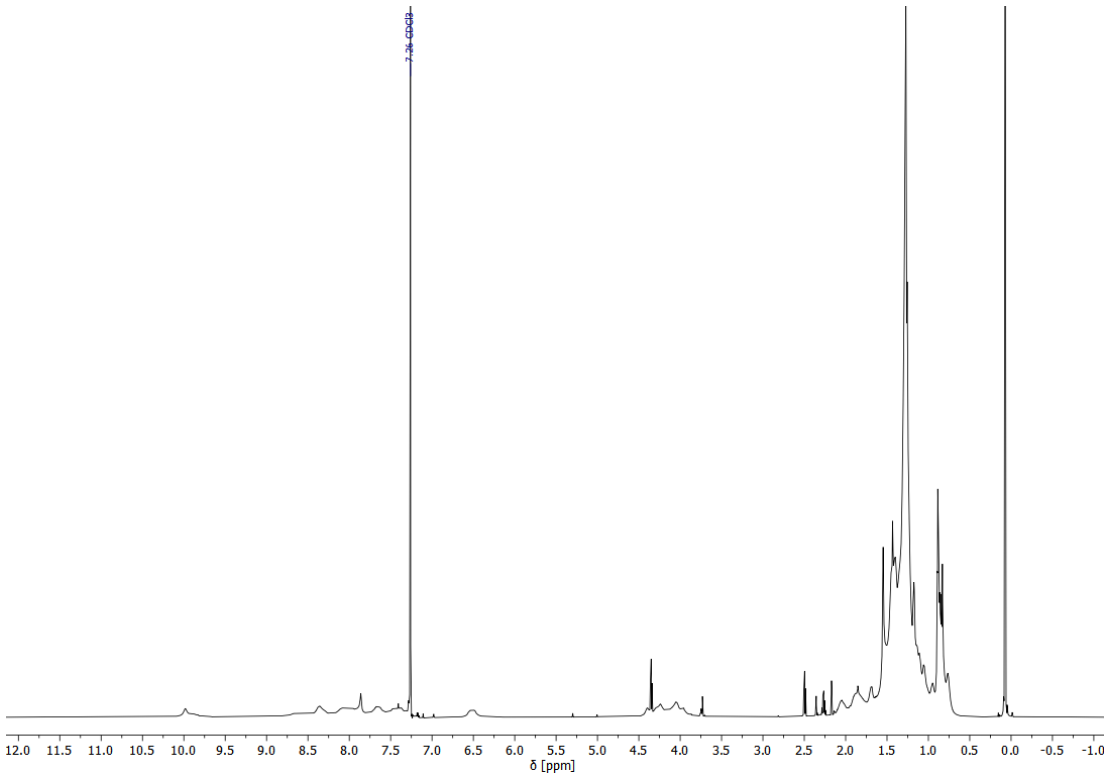

Figure 106: ^{1}H-NMR spectrum of **D$_{3c}$** (700 MHz, $CDCl_3$, 298 K).

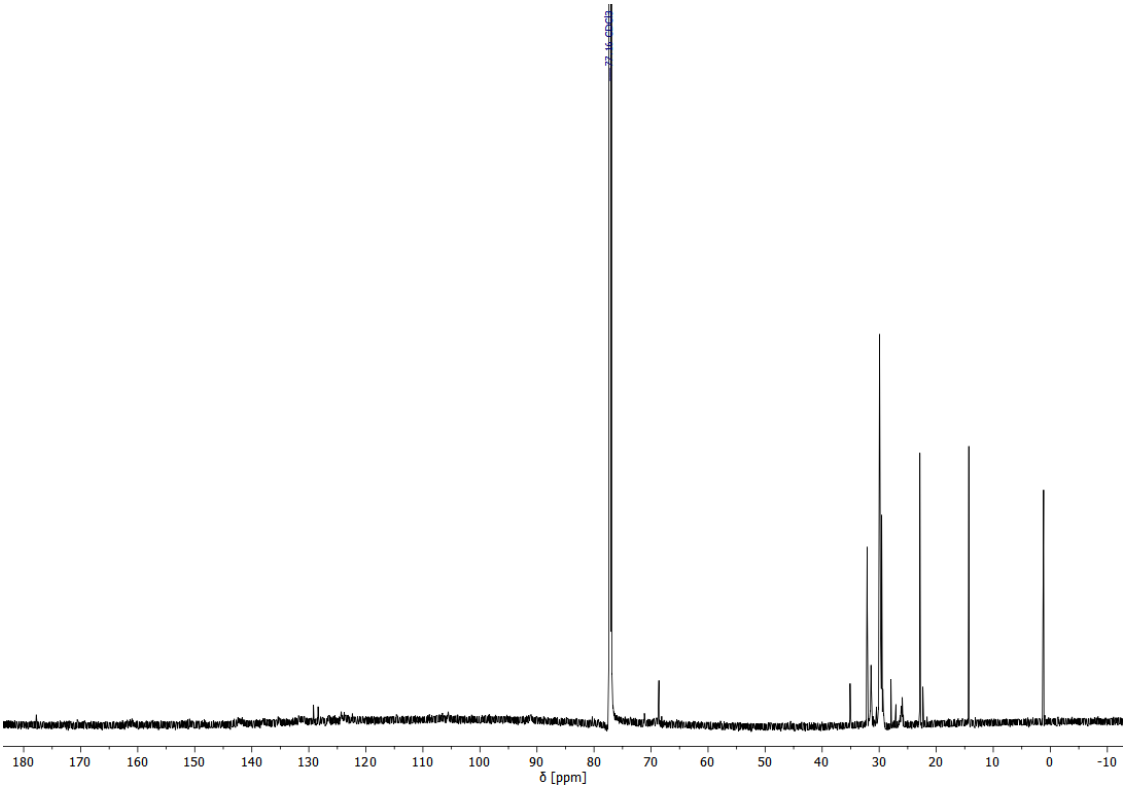

Figure 107: ^{13}C-NMR spectrum of **D$_{3c}$** (176 MHz, $CDCl_3$, 298 K).

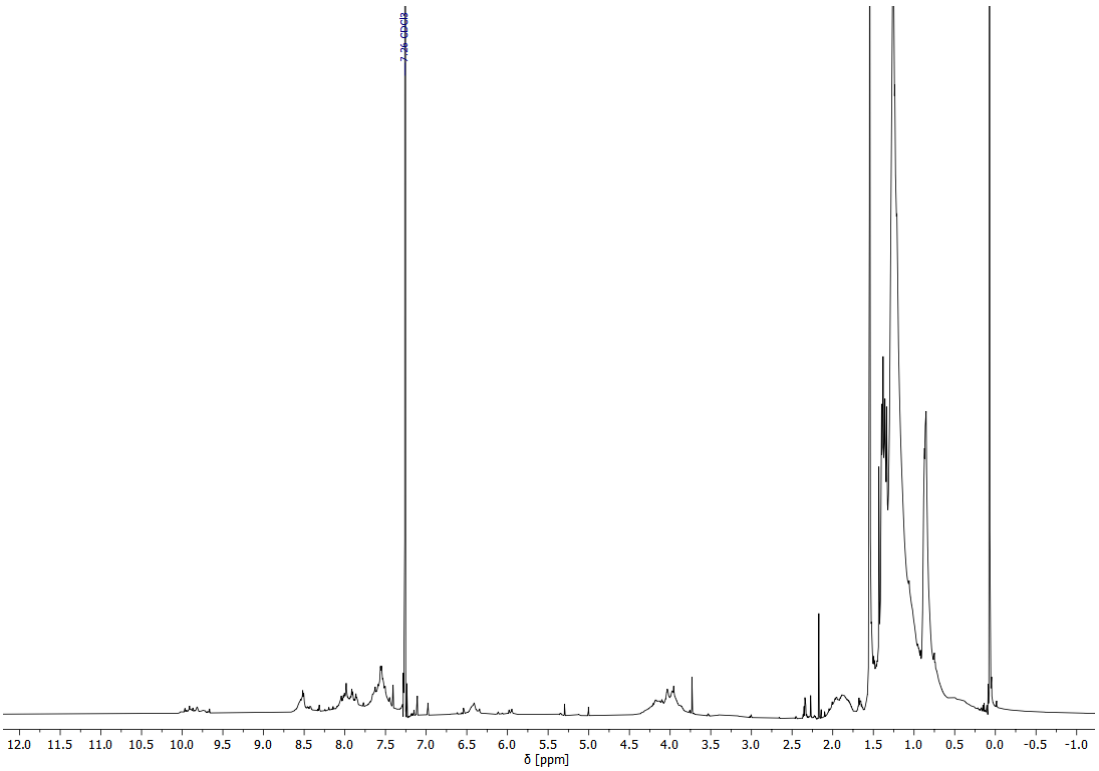

Figure 108: ^{1}H-NMR spectrum of **T$_{3c}$** (700 MHz, $CDCl_3$, 298 K).

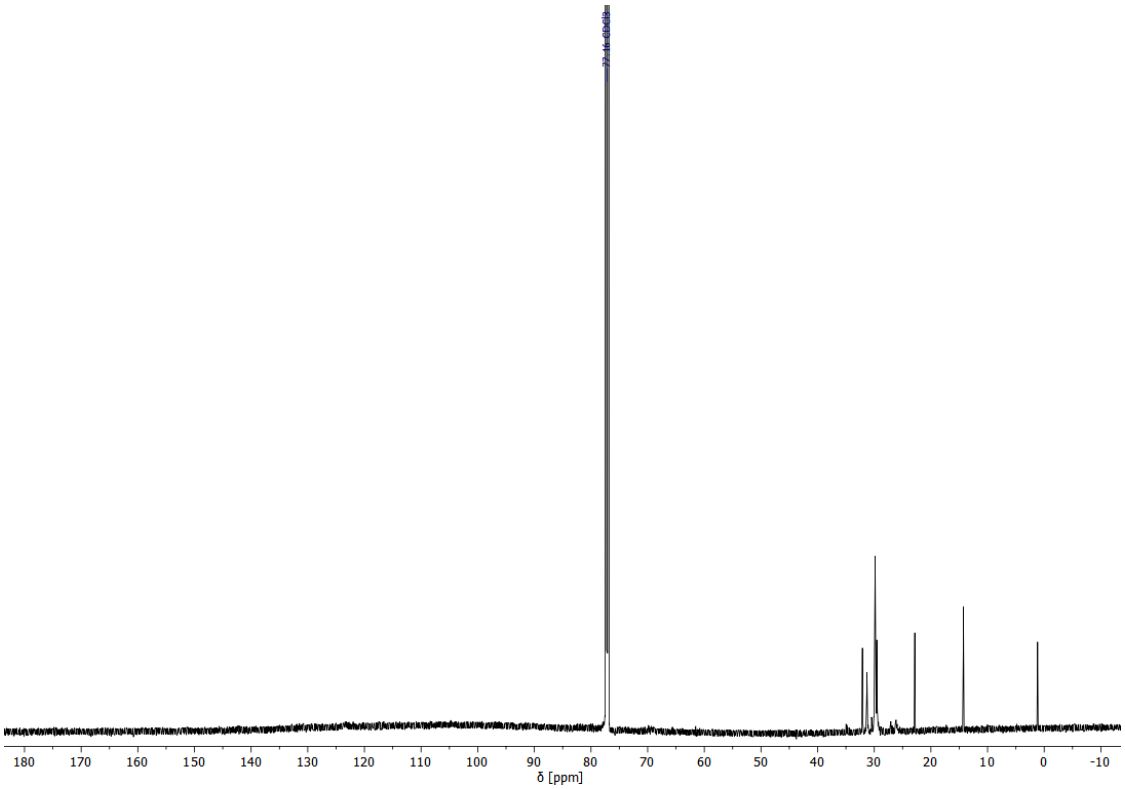

Figure 109: ^{13}C-NMR spectrum of **T$_{3c}$** (176 MHz, $CDCl_3$, 298 K).

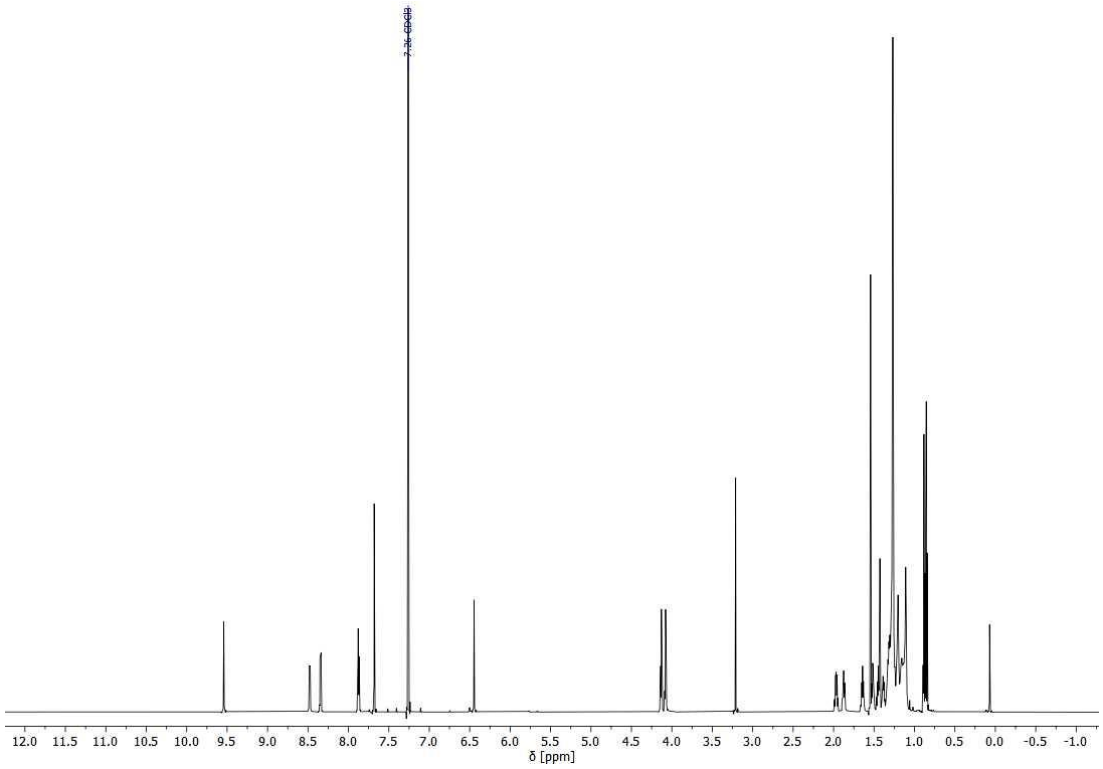

Figure 110: ^{1}H-NMR spectrum of **IV** (700 MHz, $CDCl_3$, 298 K).

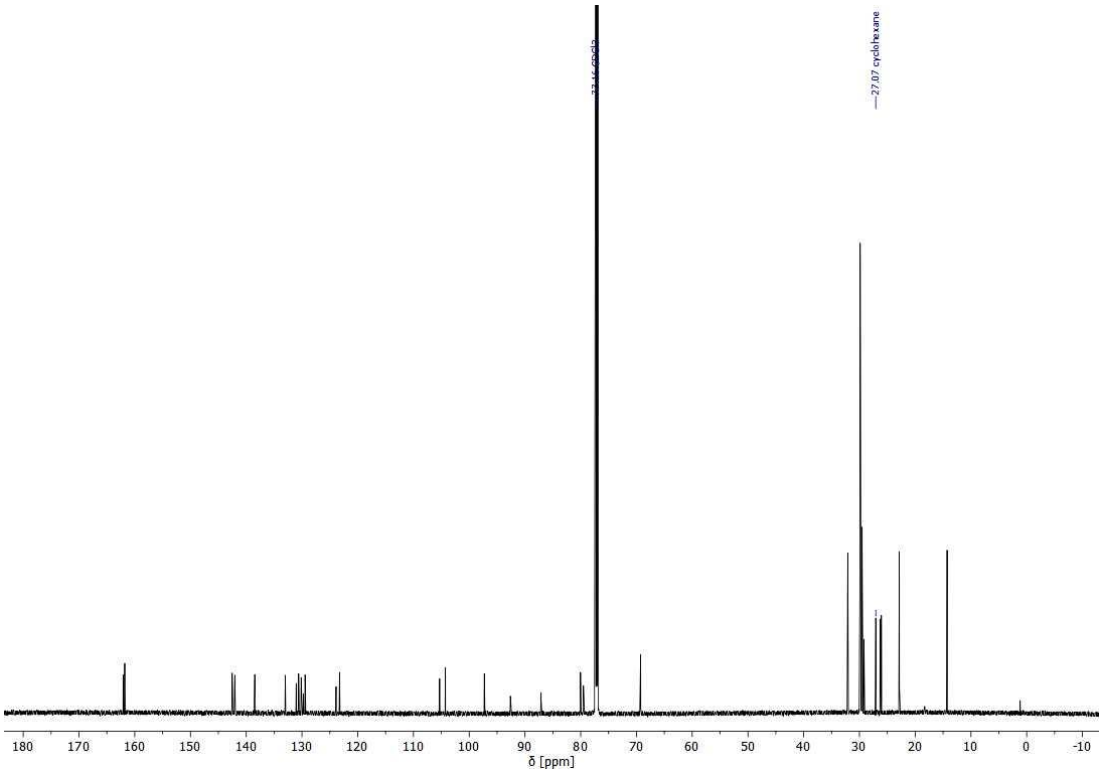

Figure 111: ^{13}C-NMR spectrum of **IV** (176 MHz, $CDCl_3$, 298 K).

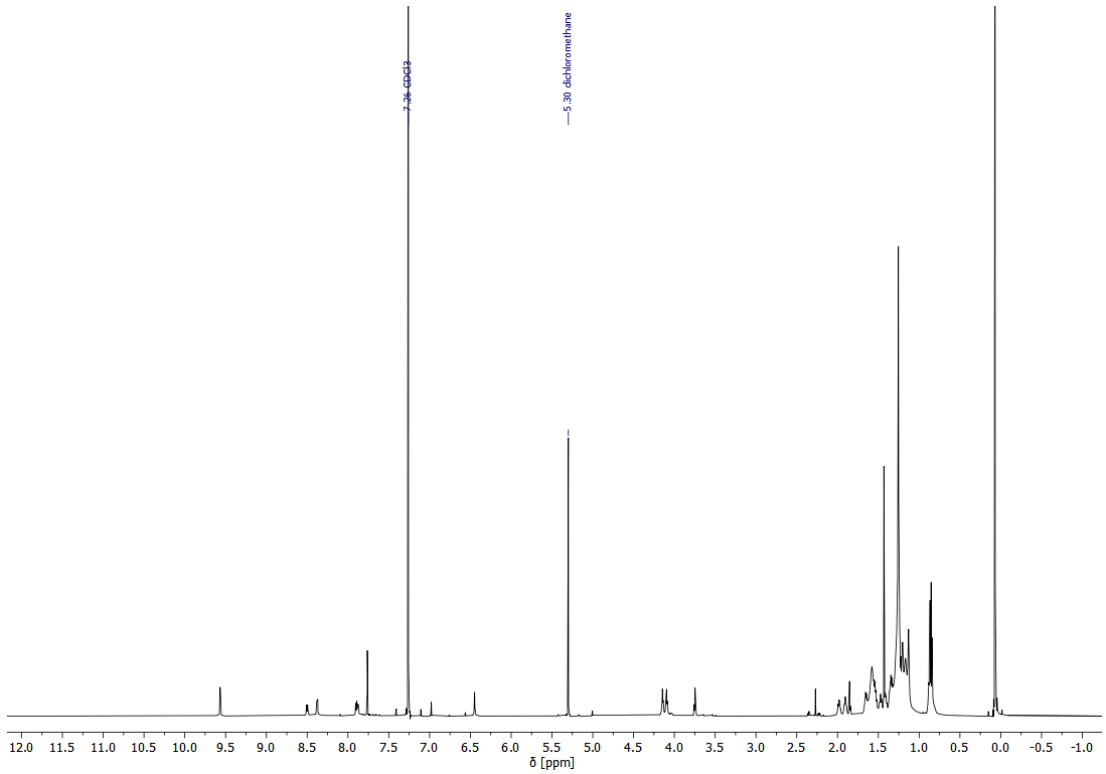

Figure 112: ^{1}H-NMR spectrum of **T₄** (700 MHz, $CDCl_3$, 298 K).

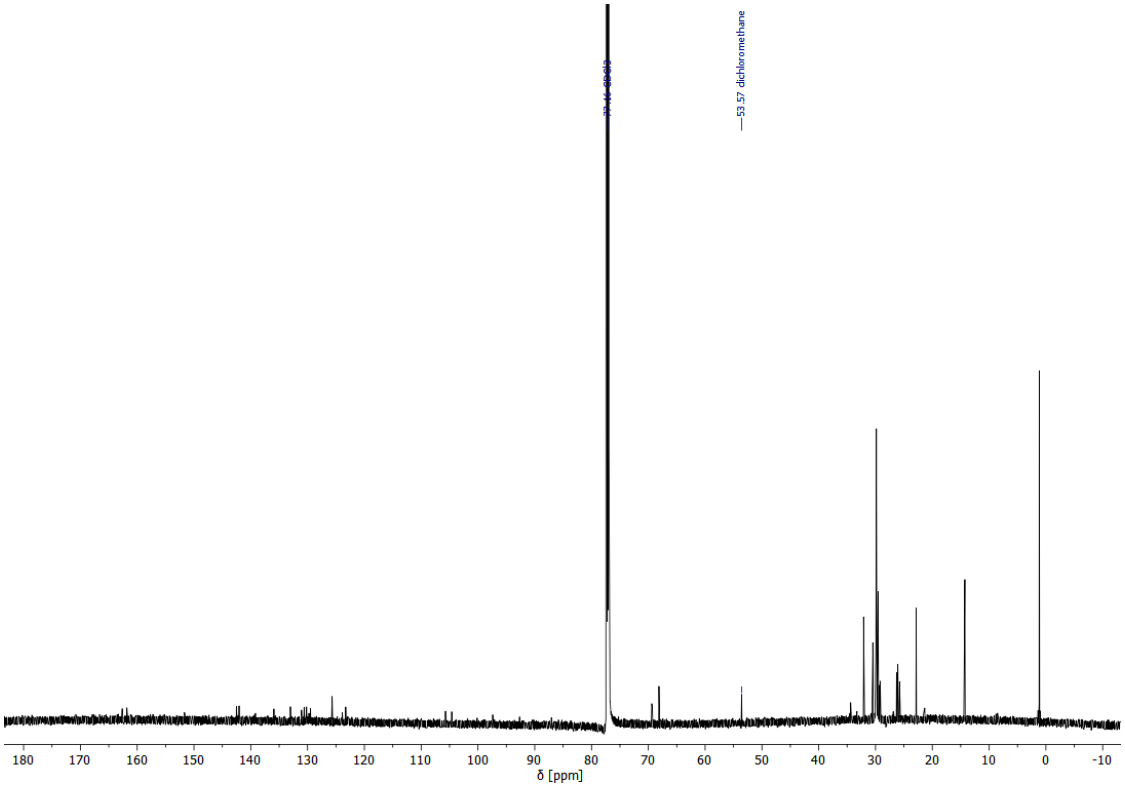

Figure 113: ^{13}C-NMR spectrum of **T₄** (176 MHz, $CDCl_3$, 298 K).

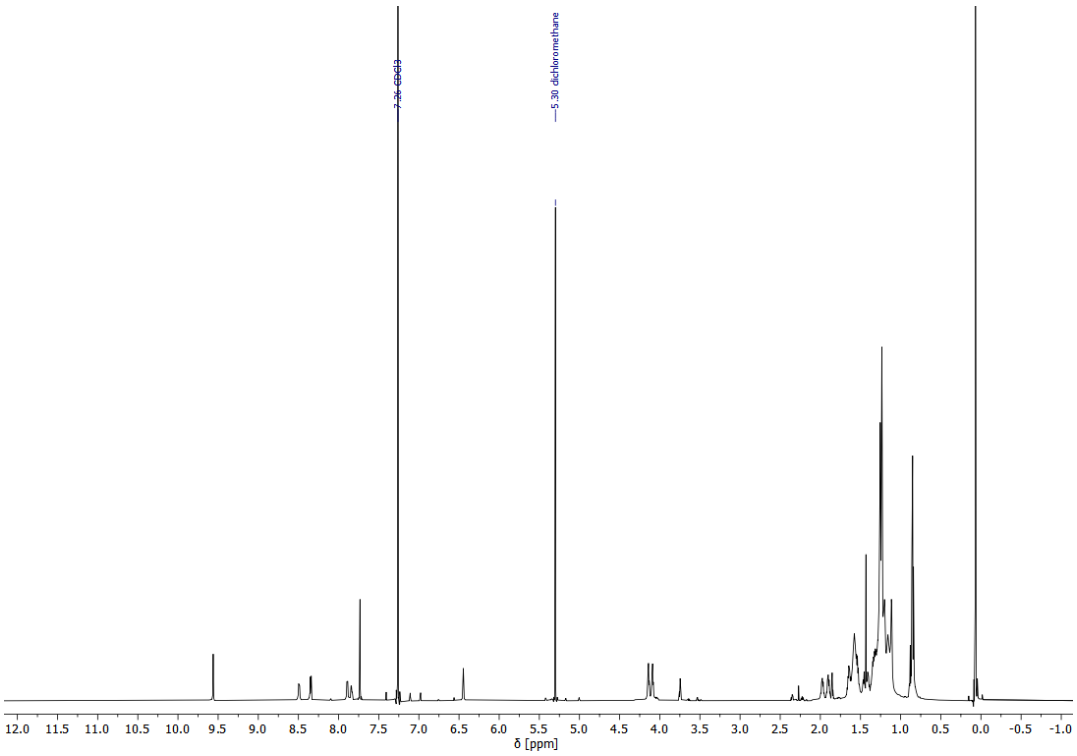

Figure 114: ^{1}H-NMR spectrum of **Tet$_4$** (700 MHz, $CDCl_3$, 298 K).

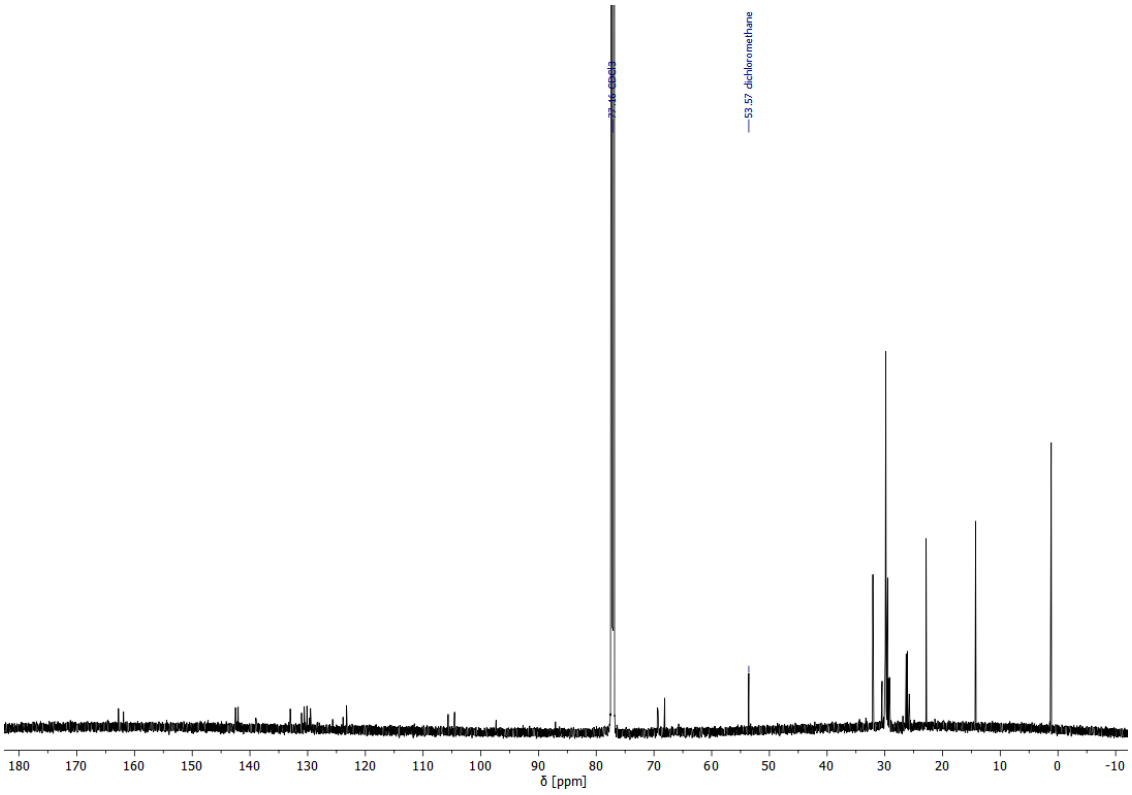

Figure 115: ^{13}C-NMR spectrum of **Tet$_4$** (176 MHz, $CDCl_3$, 298 K).

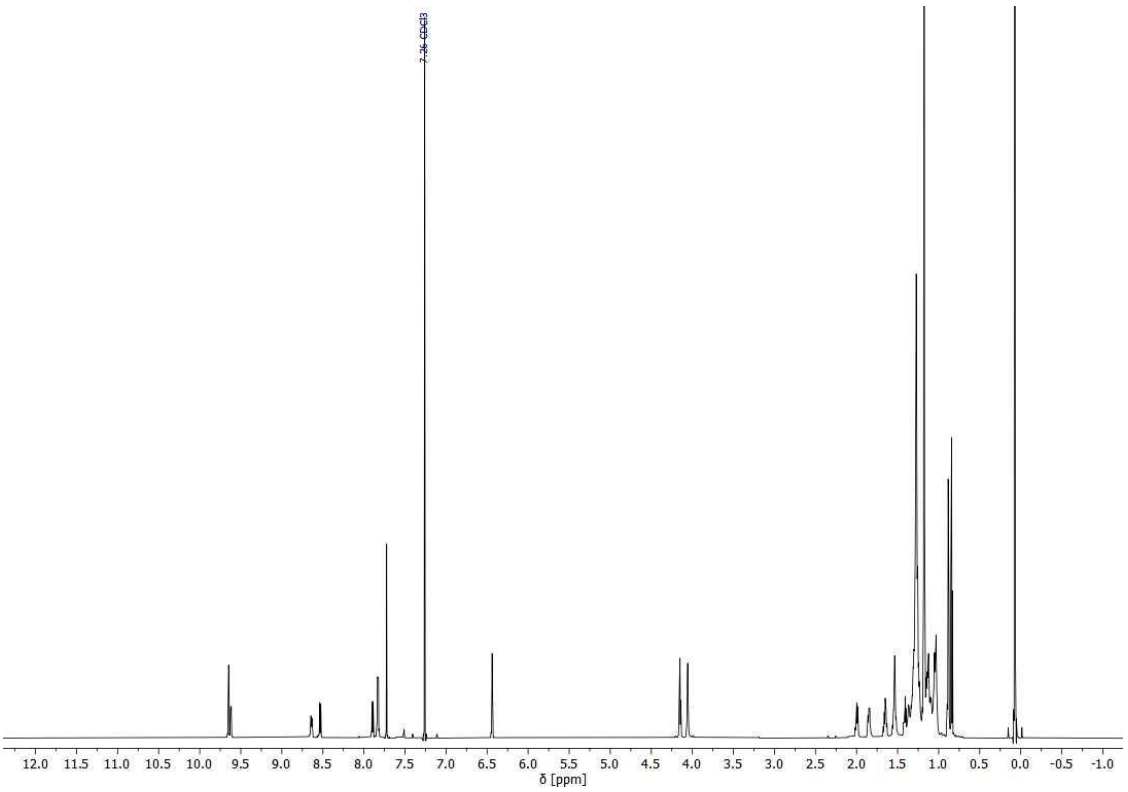

Figure 116: ^{1}H-NMR spectrum of **46** (700 MHz, $CDCl_3$, 298 K).

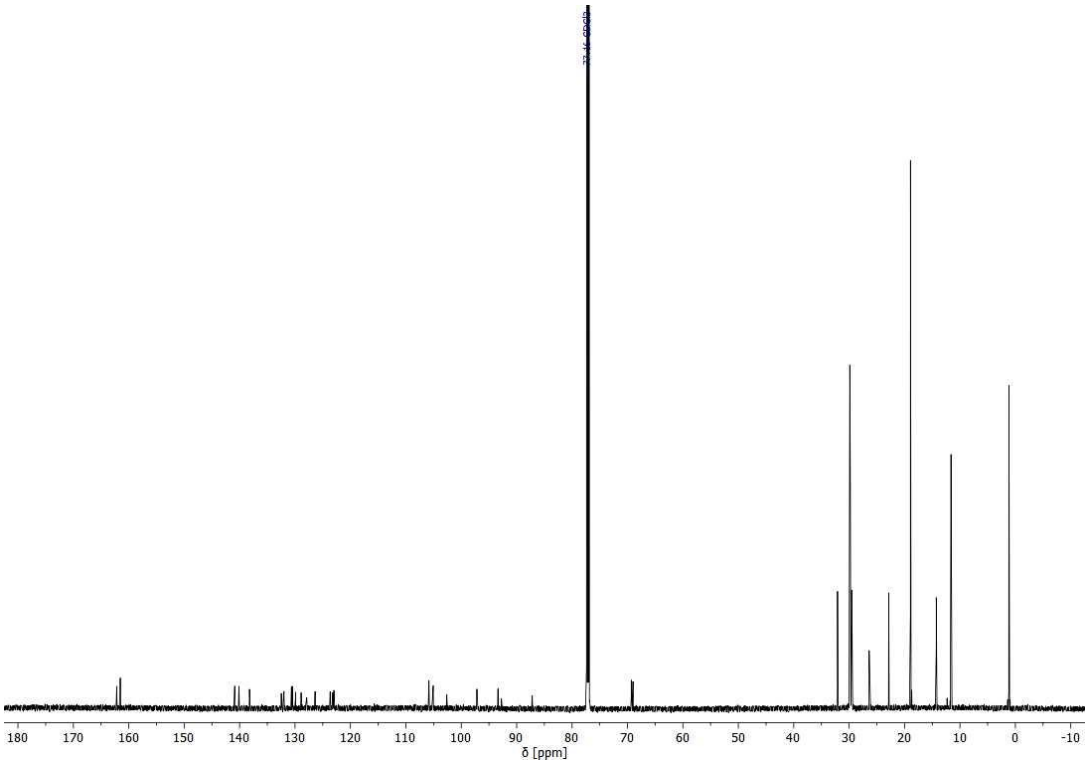

Figure 117: ^{13}C-NMR spectrum of **46** (176 MHz, $CDCl_3$, 298 K).

11.4 MALDI(+) Mass Spectra

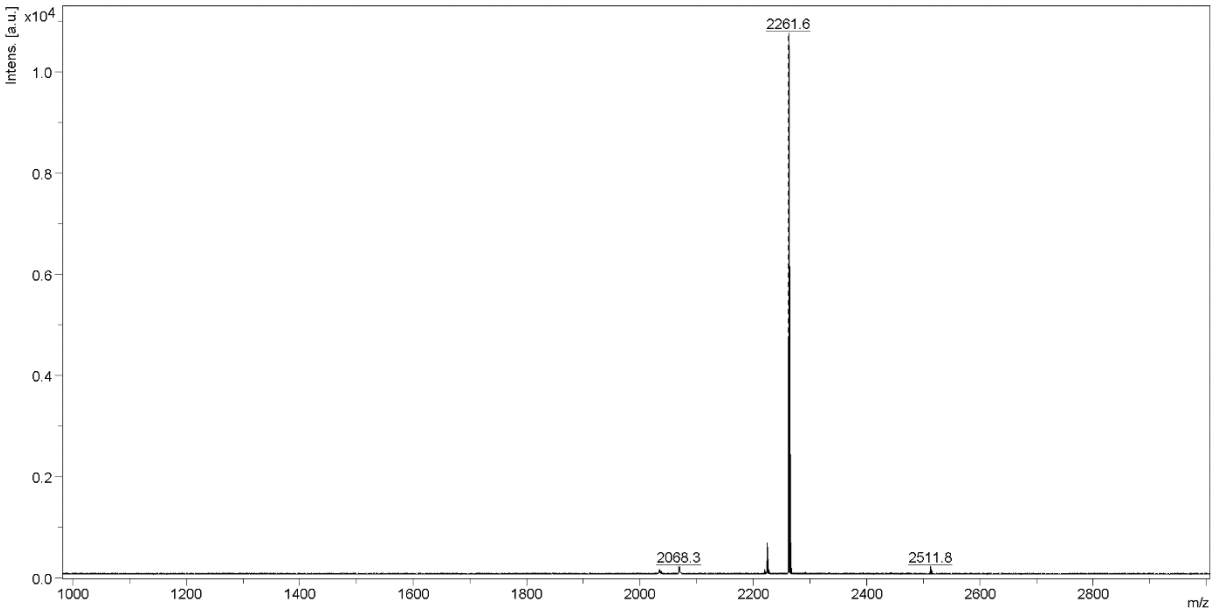

Figure 118: MALDI-TOF mass spectrum of **I** (matrix: DCTB).[102]

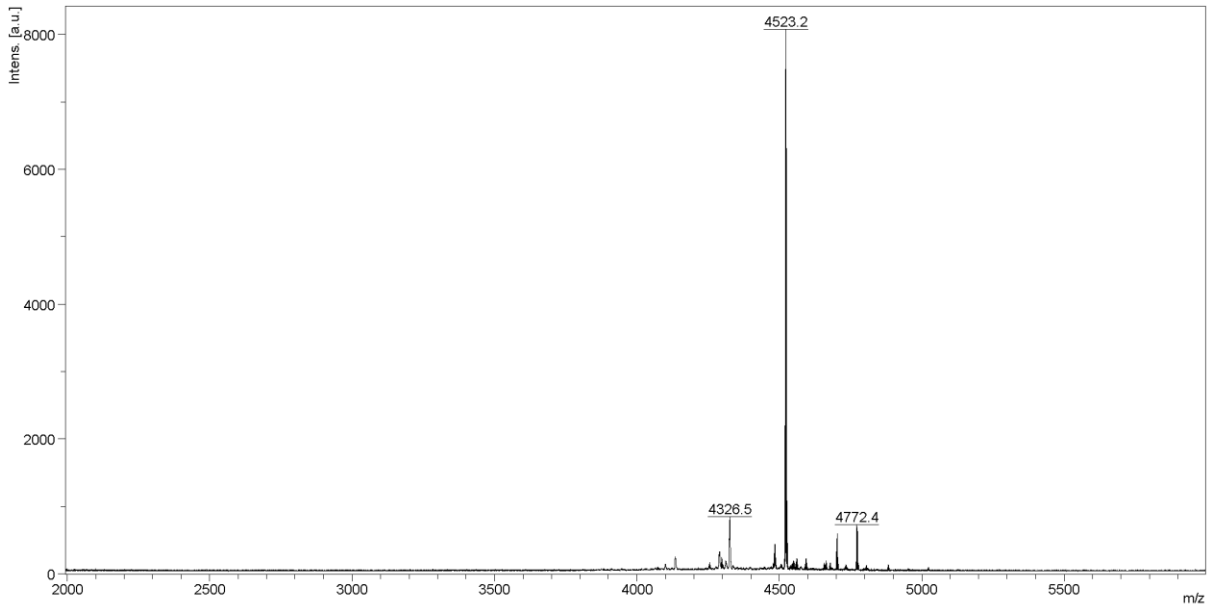

Figure 119: MALDI-TOF mass spectrum of **D_1** (matrix: DCTB).

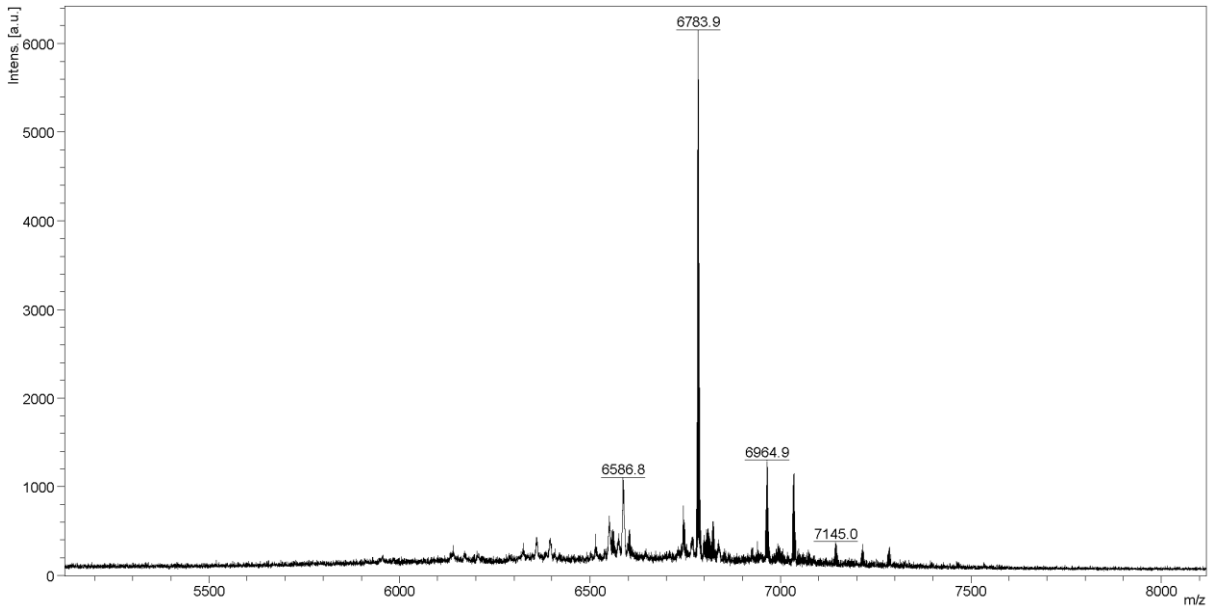

Figure 120: MALDI-TOF mass spectrum of $\mathbf{T_1}$ (matrix: DCTB).

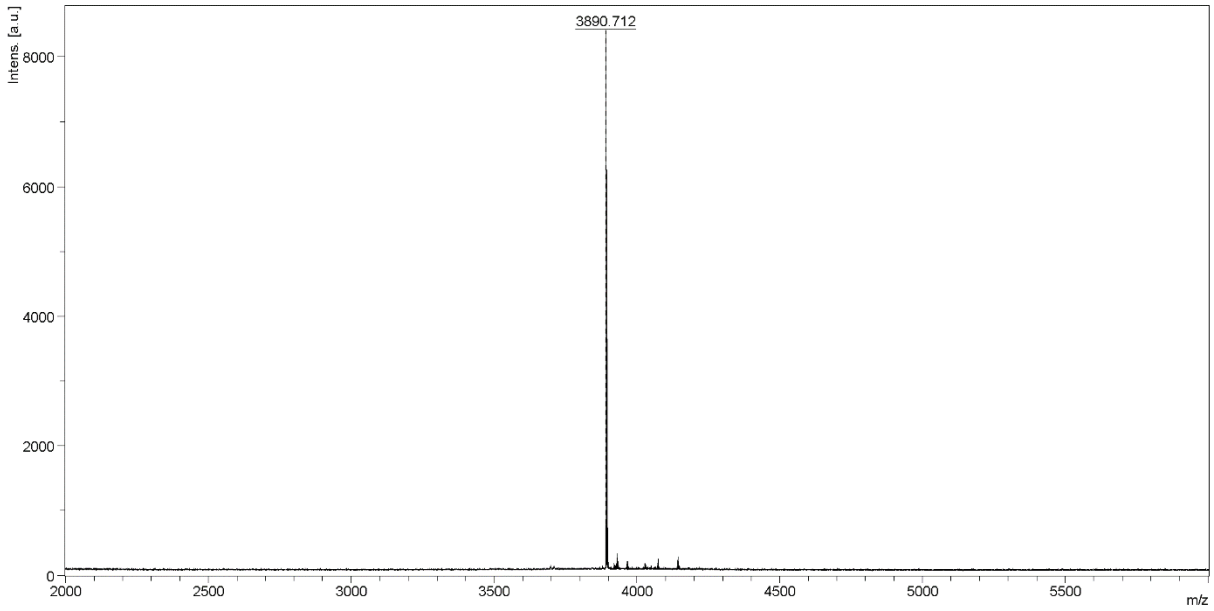

Figure 121: MALDI-TOF mass spectrum of $\mathbf{D_{1c}}$ (matrix: DCTB).[102]

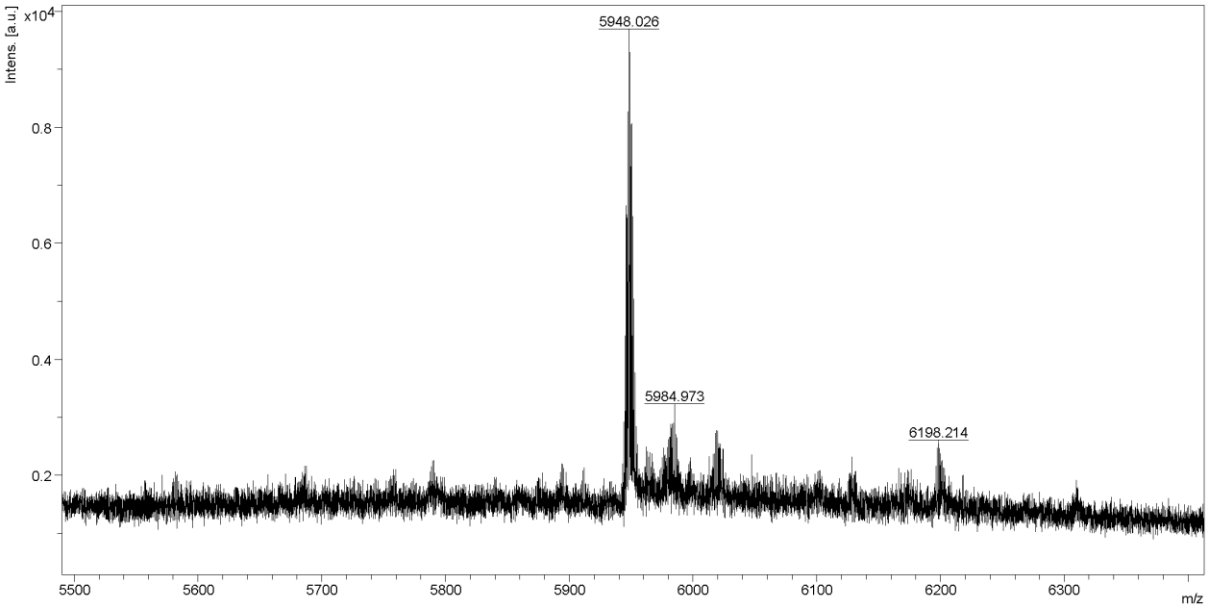

Figure 122: MALDI-TOF mass spectrum of $\mathbf{T_{1c}}$ (matrix: DCTB; added Ag^+-salts).[102]

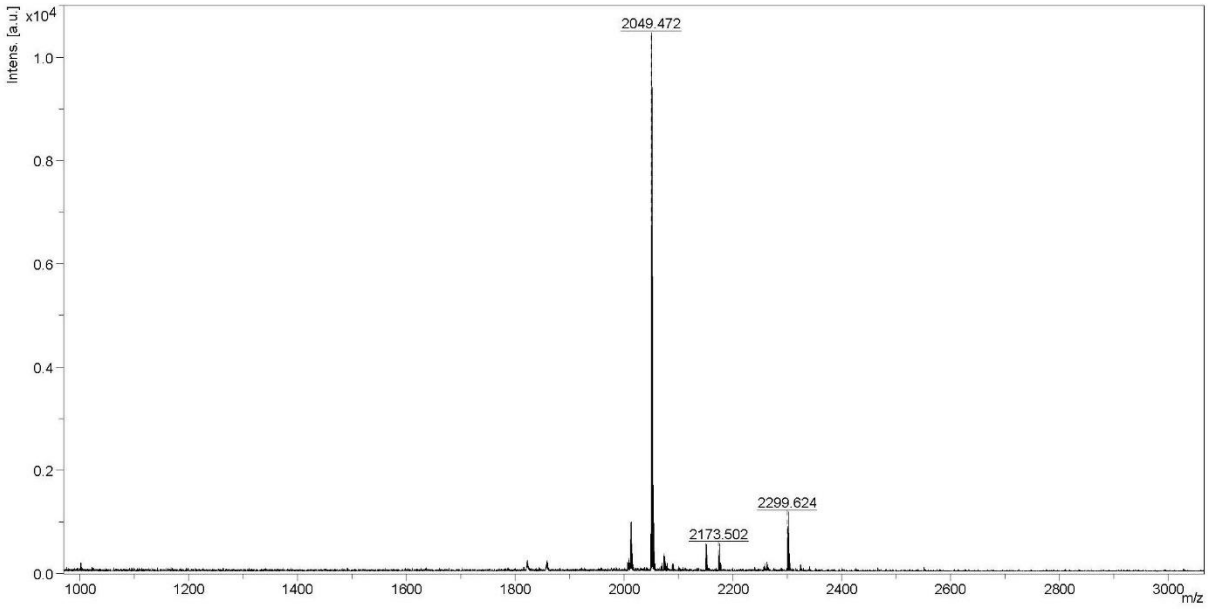

Figure 123: MALDI-TOF mass spectrum of **II** (matrix: DCTB).

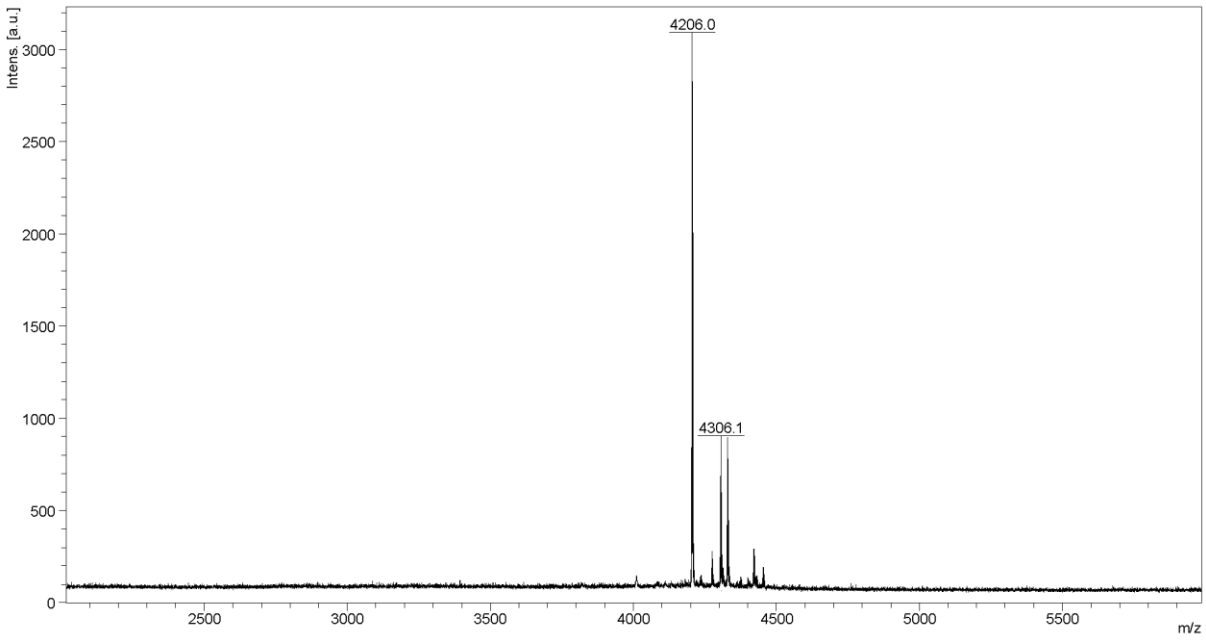

Figure 124: MALDI-TOF mass spectrum of **D_2** (matrix: DCTB; added Ag^+-salts).

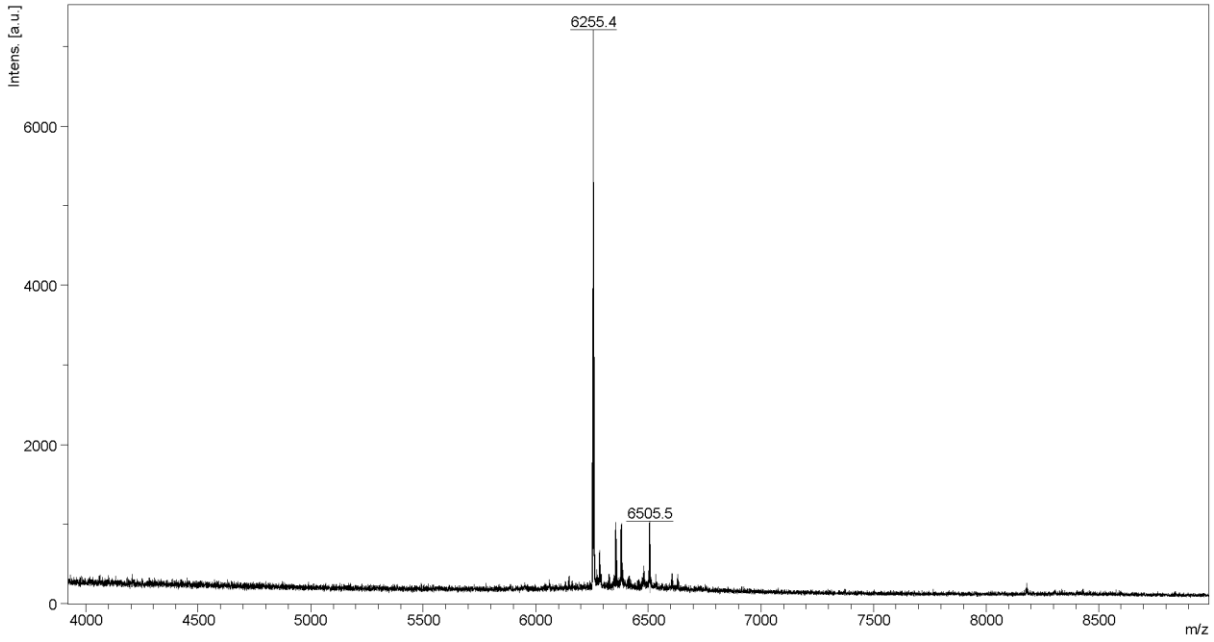

Figure 125: MALDI-TOF mass spectrum of **T_2** (matrix: DCTB; added Ag^+-salts).

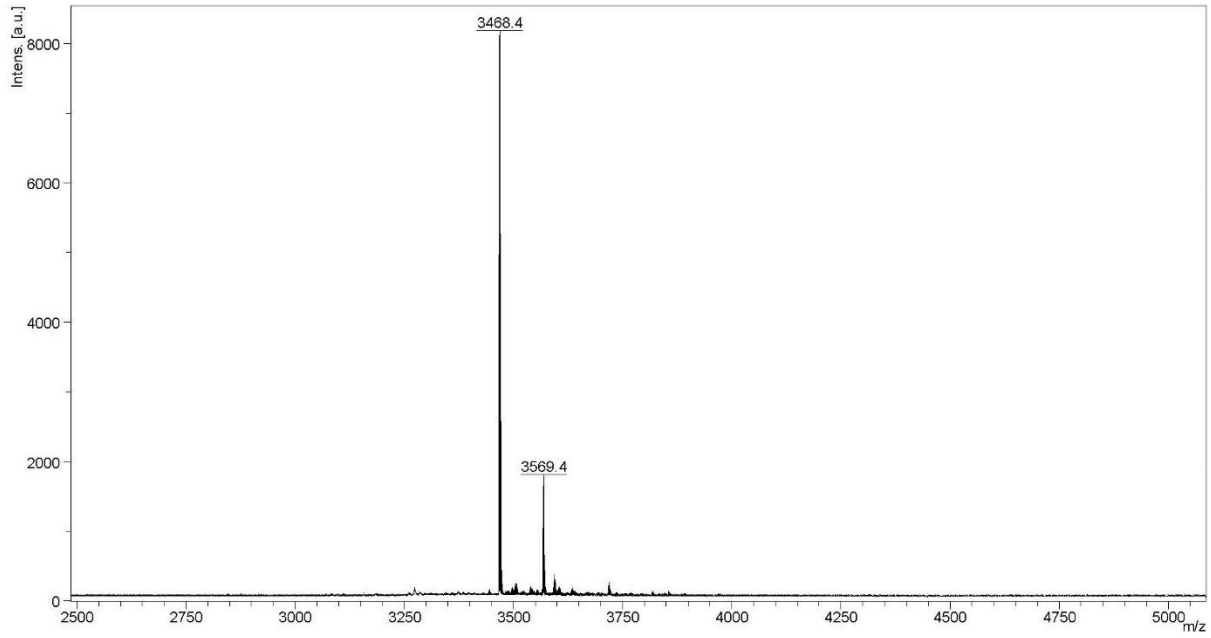

Figure 126: MALDI-TOF mass spectrum of $\mathbf{D_{2c}}$ (matrix: DCTB).

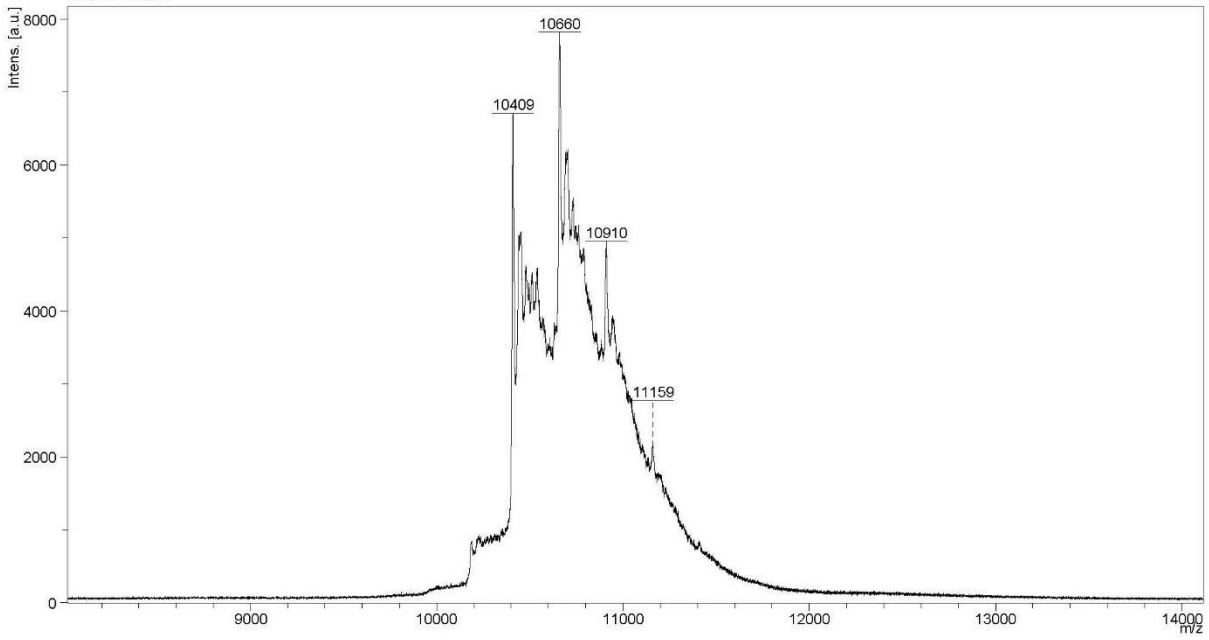

Figure 127: MALDI-TOF mass spectrum of $\mathbf{T_{2c}}$ (matrix: DCTB).

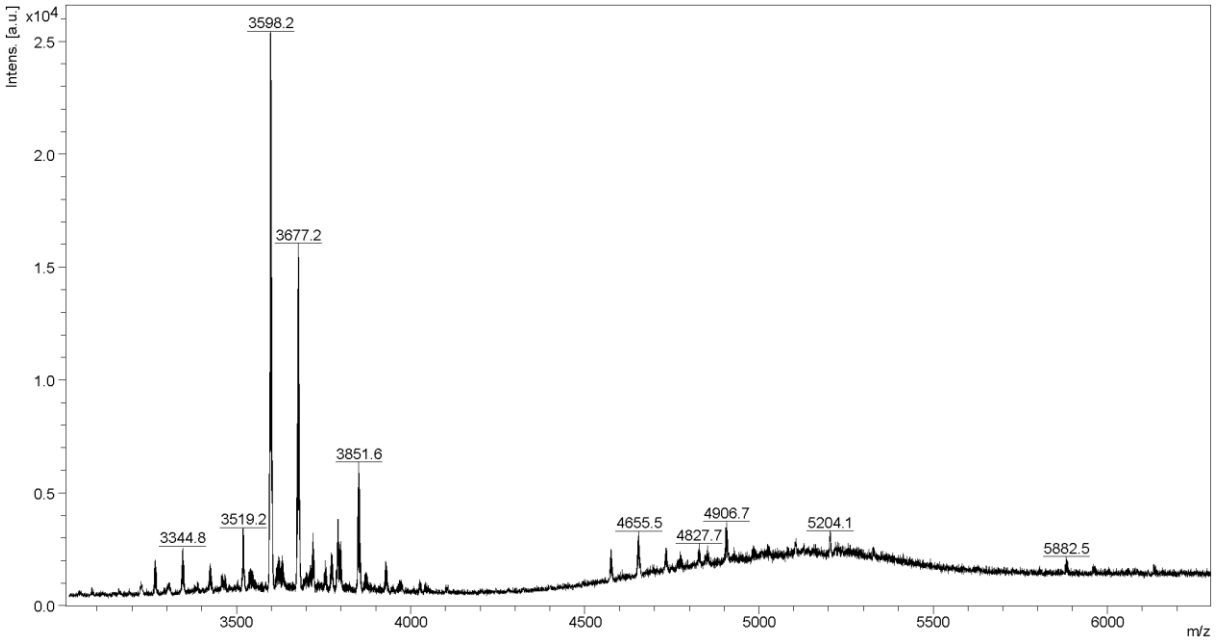

Figure 128: MALDI-TOF mass spectrum of $\mathbf{T_{2c}}$ (matrix: DCTB).

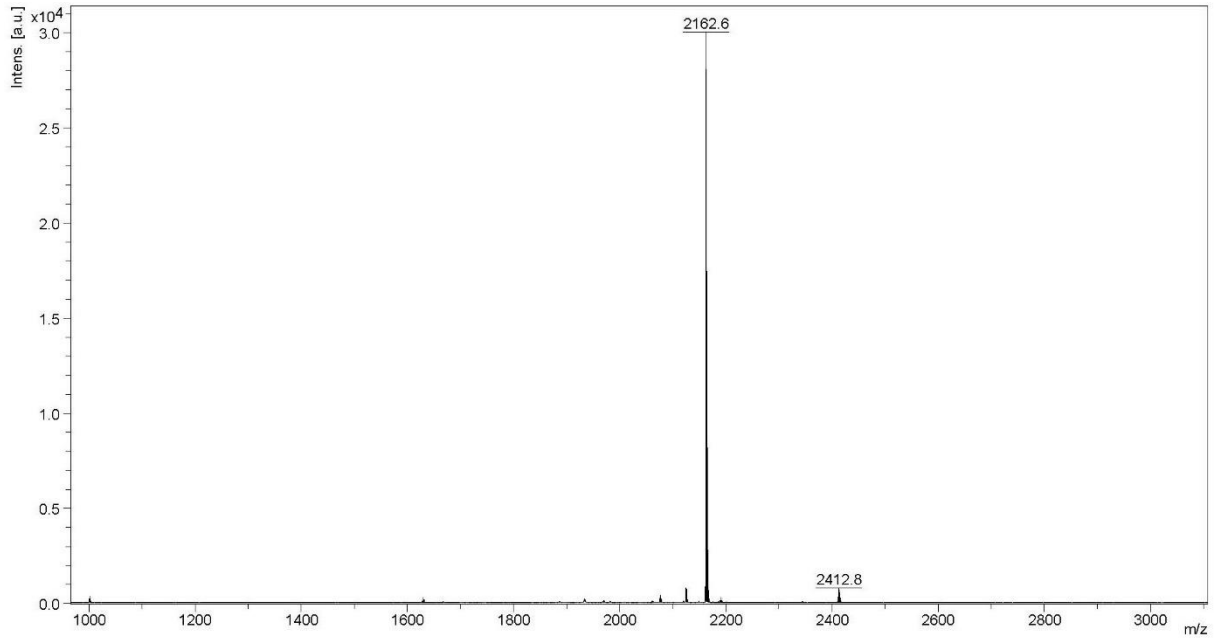

Figure 129: MALDI-TOF mass spectrum of **III** (matrix: DCTB).

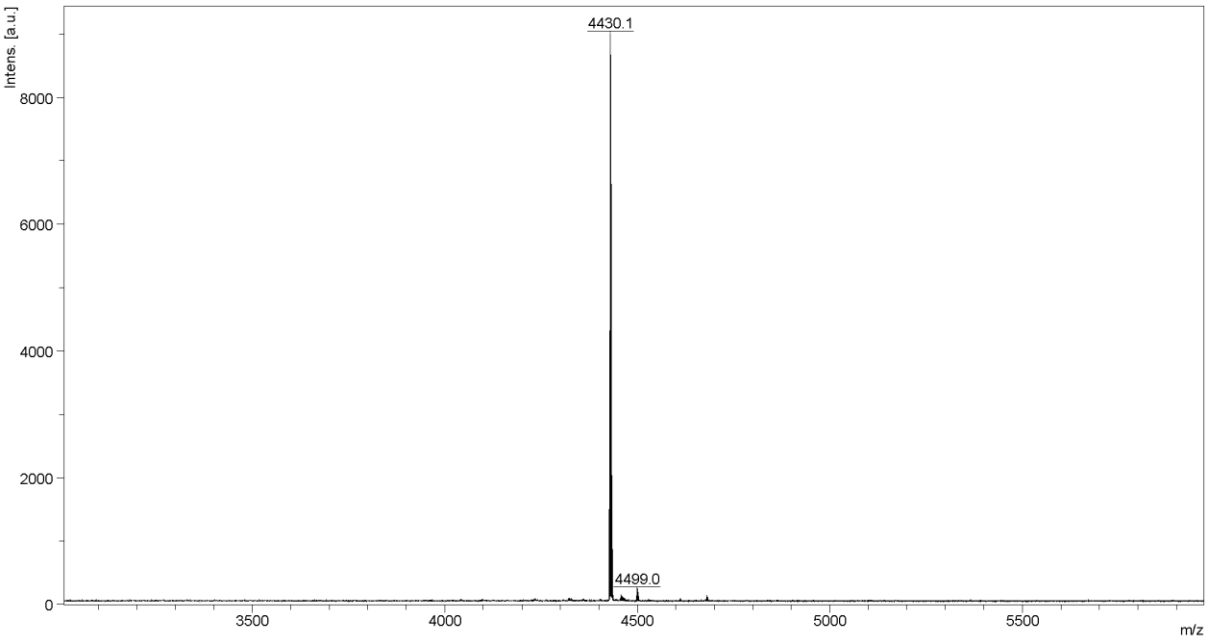

Figure 130: MALDI-TOF mass spectrum of **D_3** (matrix: DCTB; added Ag^+-salts).

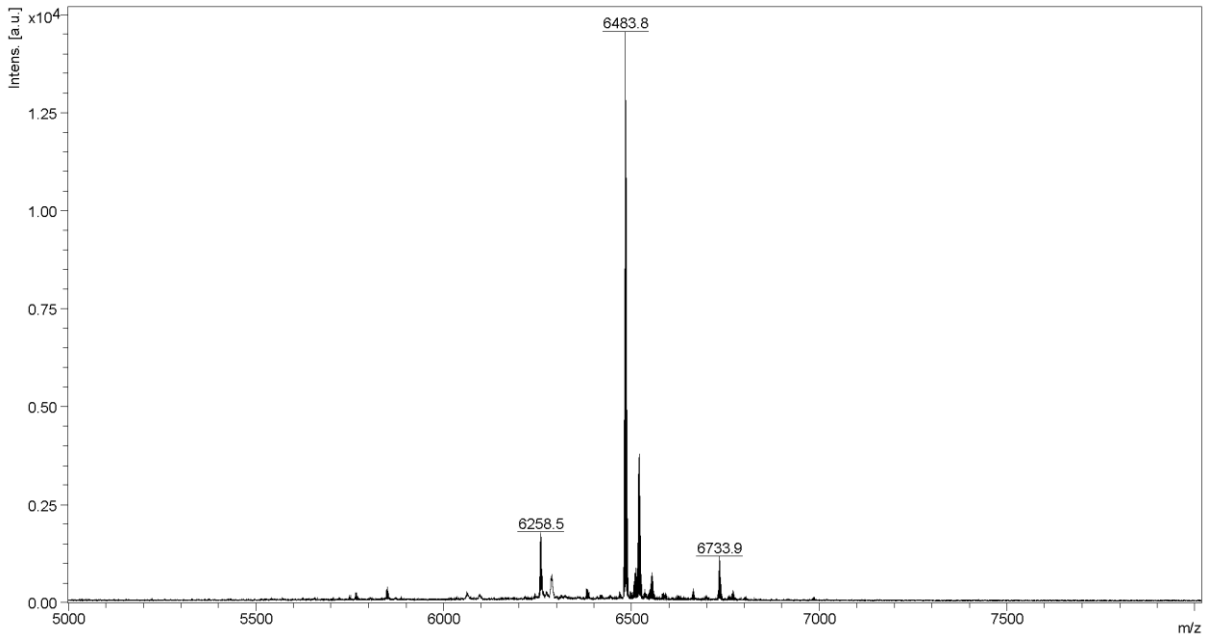

Figure 131: MALDI-TOF mass spectrum of **T_3** (matrix: DCTB).

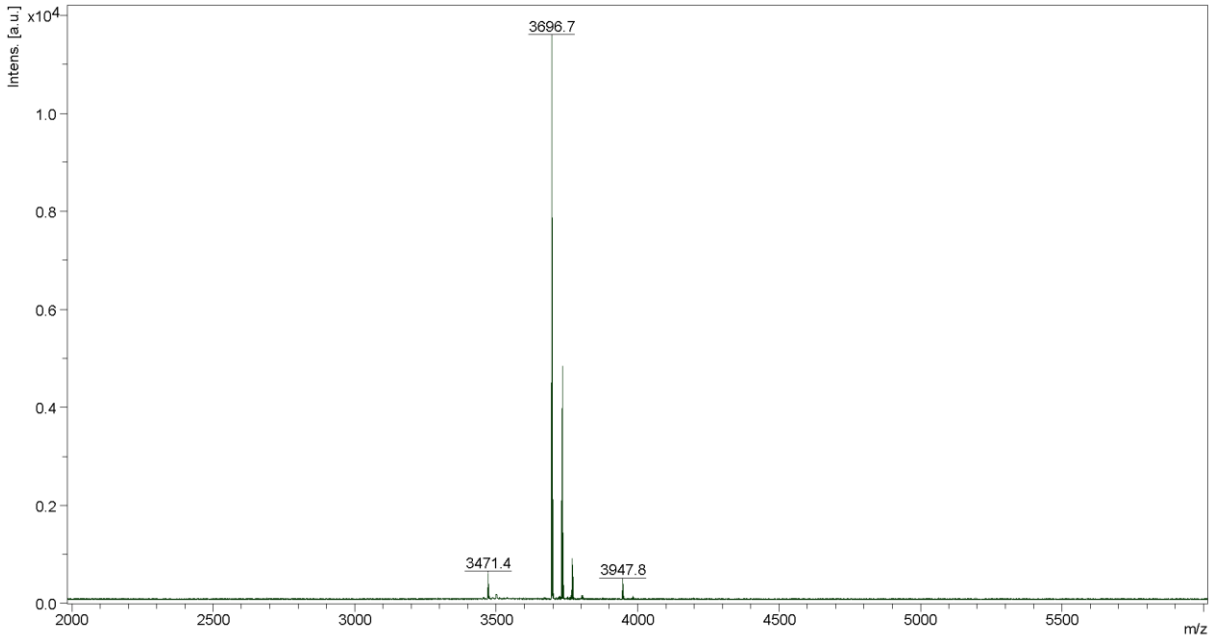

Figure 132: MALDI-TOF mass spectrum of $\mathbf{D_{3d}}$ (matrix: DCTB).

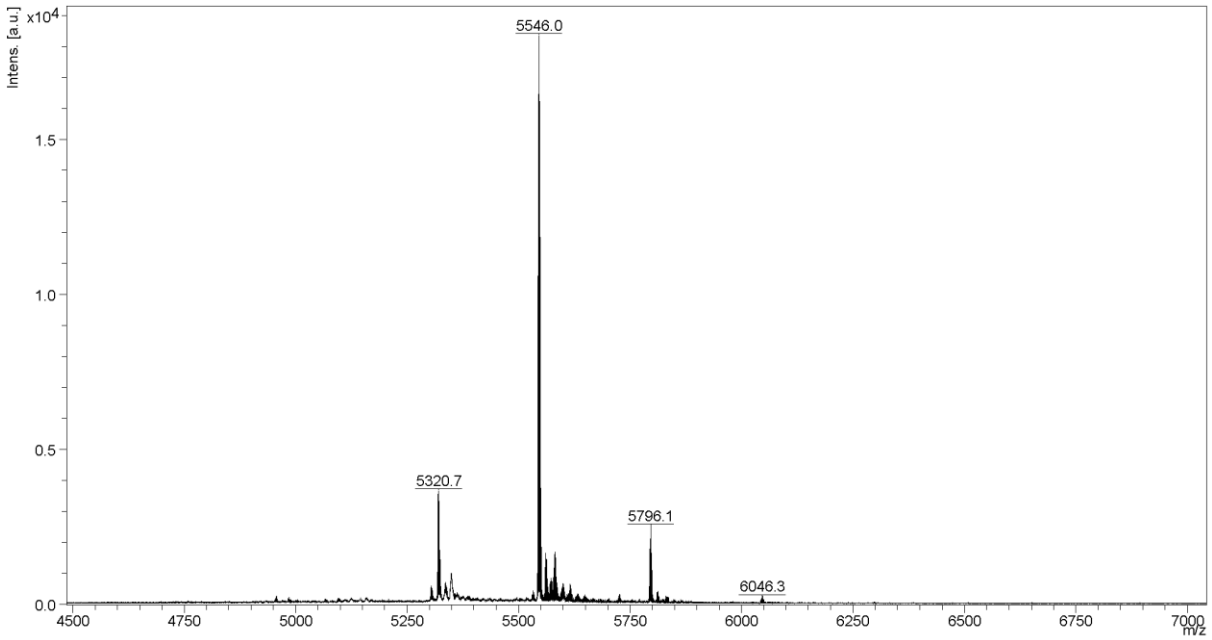

Figure 133: MALDI-TOF mass spectrum of $\mathbf{T_{3d}}$ (matrix: DCTB).

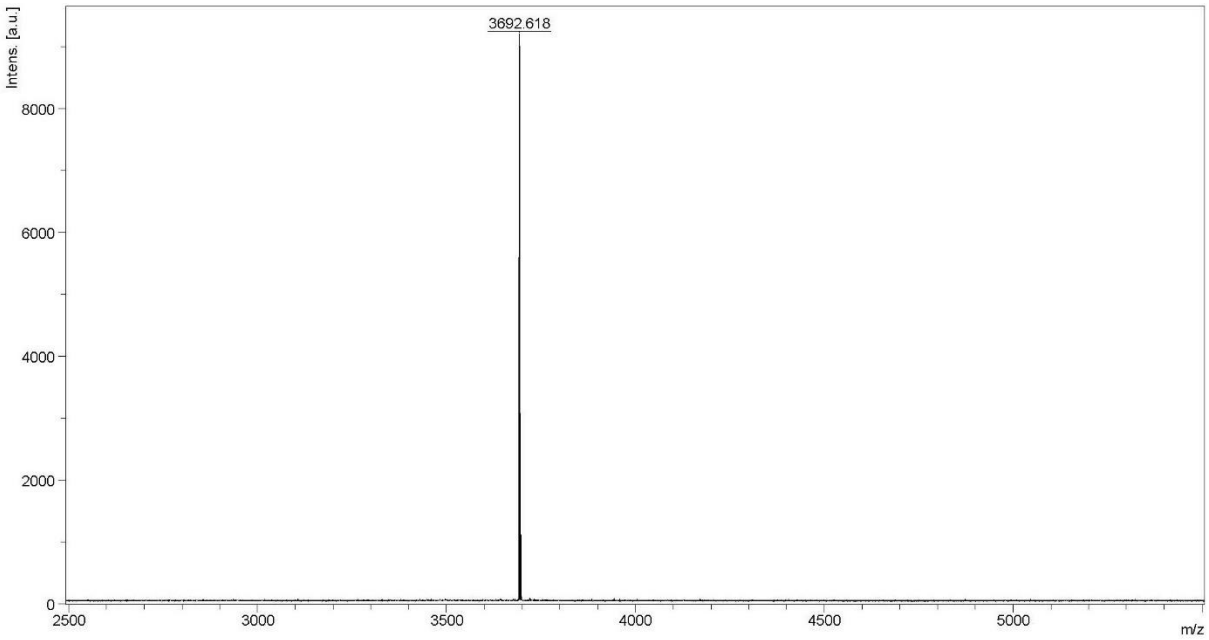

Figure 134: MALDI-TOF mass spectrum of **D_{3c}** (matrix: DCTB).

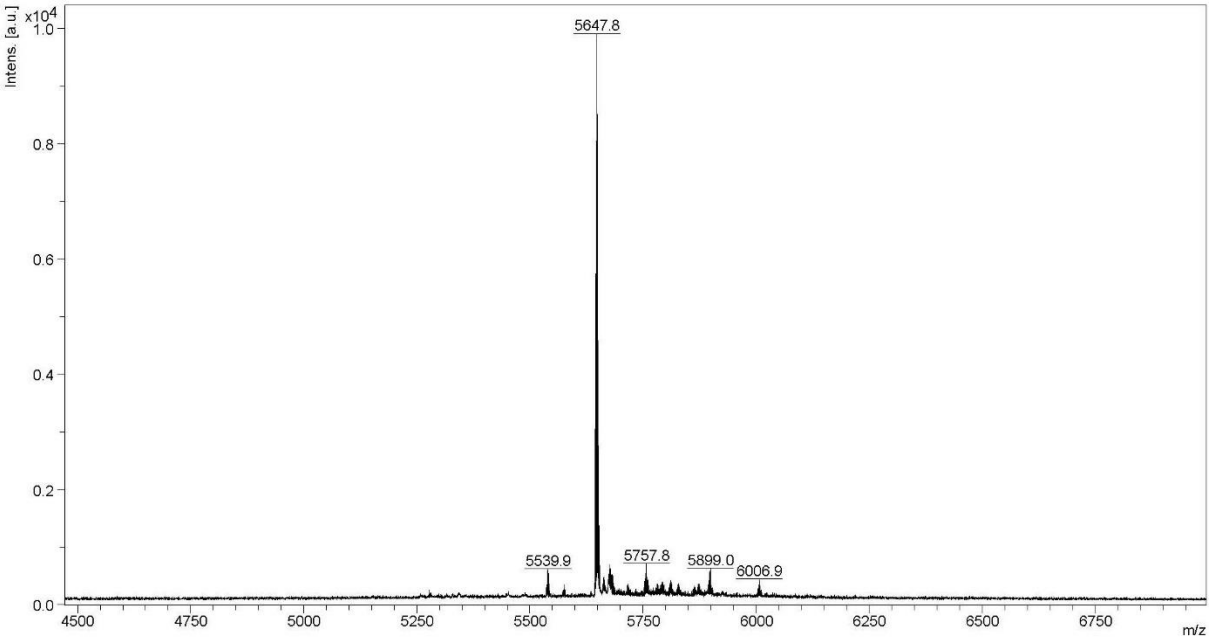

Figure 135: MALDI-TOF mass spectrum of **T_{3c}** (matrix: DCTB; added Ag^+-salts).

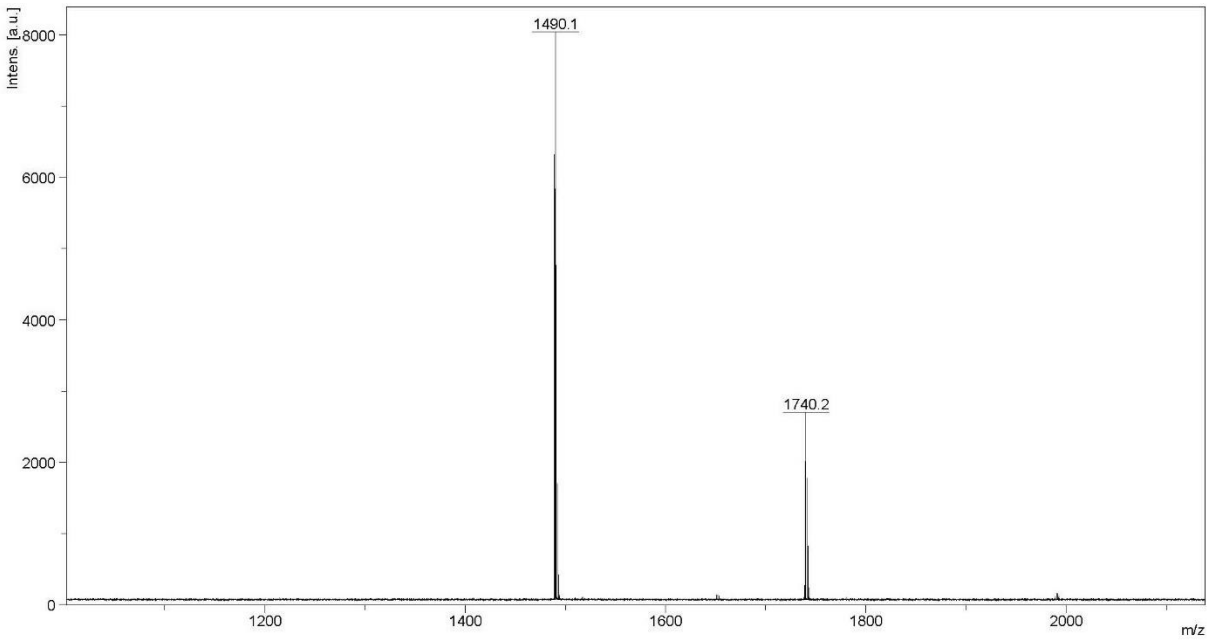

Figure 136: MALDI-TOF mass spectrum of **IV** (matrix: DCTB).

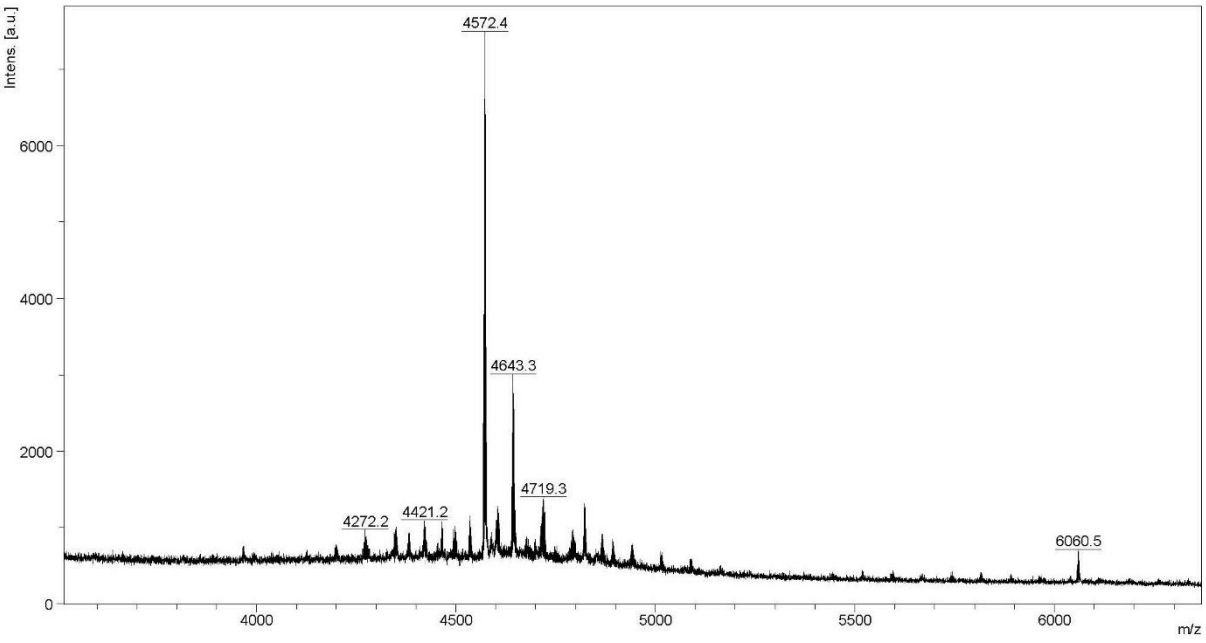

Figure 137: MALDI-TOF mass spectrum of $\mathbf{T_4}$ (matrix: DCTB; added Ag^+-salts).

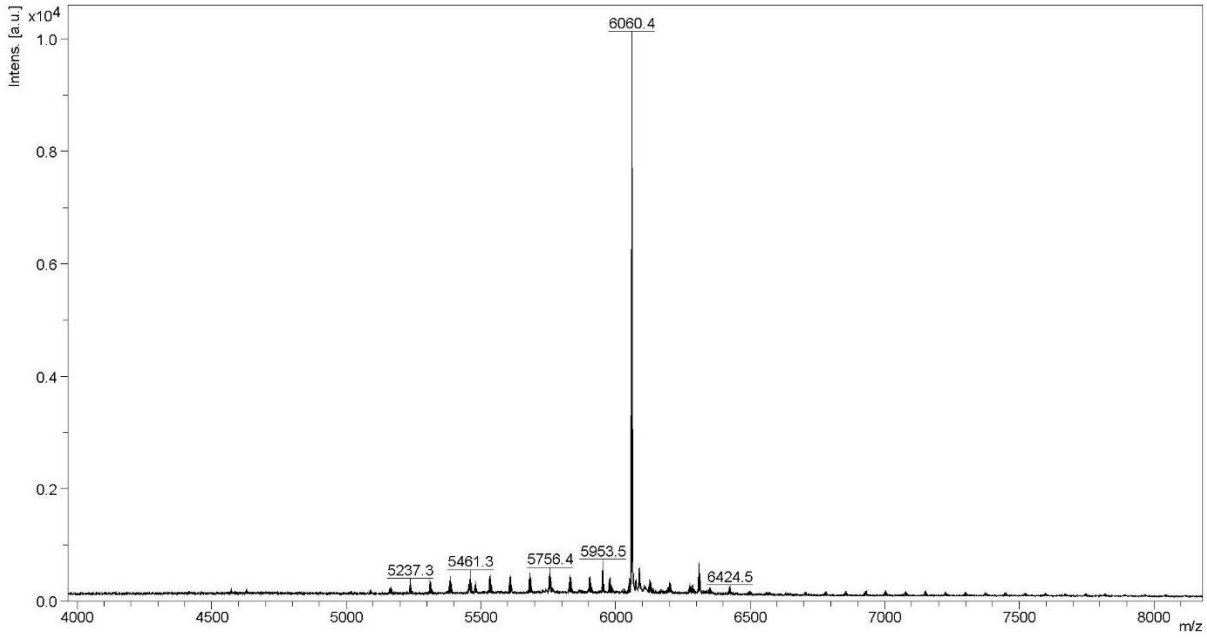

Figure 138: MALDI-TOF mass spectrum of **Tet$_4$** (matrix: DCTB; added Ag^+-salts).

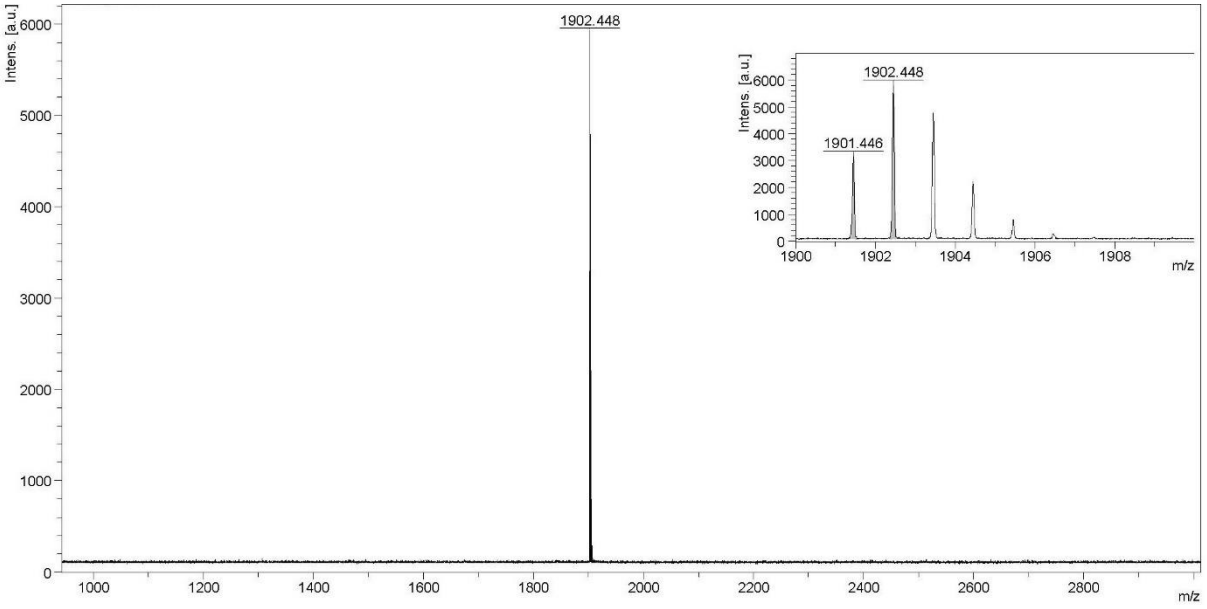

Figure 139: MALDI-TOF mass spectrum of **46** (matrix: DCTB).